Development of hydrogel-based photoluminescent ratiometric detection systems for hydrogen peroxide

Dissertation to obtain a doctoral degree

of the natural sciences (Dr. rer. Nat.)

faculty of chemistry and pharmacy

of the University of Regensburg

Germany

Submitted by

John Josef Galligan

From Regensburg

In the Year 2025

Personal note from the author[a]

Well, this is it. A doctoral thesis… My goodness, *my* doctoral thesis. Which, to be honest still does not feel entirely real. I mean, where did the last four years go? Doing and writing something like this is full of contradictions. You are an expert in the field of what you are doing, but you constantly have the feeling of knowing nothing at all and any day not fighting with imposter syndrome, despite all one's lore as not to be the wretched fool one was before, is a good day. Trying to discover the underlying logic behind the data, which at times can be hard, because there isn't one. Or until you do, all logic is true. You have a lot of time, but you can't seem to find some to do the stuff you want to. You enjoy the full range of academic freedom, but you are restricted in a variety of ways. You love and live for science, but you struggle to find the motivation to go on each day. The emotional high of something working and the devastating realization that the result is not reproducible. The literal and actual excitement[b] of working with luminescence and fluorescence and enjoying every glow around the place but the disappointment of not seeing any of it in the day-to-day work. Going home and expecting not to think about things concerning the thesis and university is like expecting rocks not to think about gravity. The feeling of being so scattered that you have to piece yourself back together from several dimensions and realities just to realize that a rat-sized piece of you is missing. You keep sprinting from project to project but must run the whole thesis marathon. Believing the small lies like: "the experiment will work" or "the data does not look that bad" to make it through the big lies like: "I will manage this" or "only one more experiment". But that is what each and every one of us just has to put up with in the end. You know, *minor* detail(s), like opening your eyes and then opening them again.

[a] Those who will recognize them will understand

[b] I am very sorry (I am of course, not), for the occurrence of such low-key (ground state) photophysical and optical puns.

Personal note from the author

One of the few deeply troubling regrets I can bring to paper here is an issue with the traditional inclusion of a seemingly sophisticated quote of some great scientist or other famous person at the beginning of such work. Generally, it is difficult to find such a single sentence that is not already completely worn out and torn out of context to use as a concise and captivating “bam” beginning. So, where to take it from and not steal/cite it? My favorite method is to be creative and come up with something on my own or hide something in plain sight. Something that has to do with the thesis but is funny and slightly self-mocking. Something that to my shame I will not be able to surpass from my master thesis in a single quote. Recycling is great and is done far too little but just doesn't feel right here. In this sense I have a pln:

The scientist plans, organizes, prepares, tests, experiments and measures.

Chaos laughs.

Adapted old Yiddish proverb

One glow, two glow, red glow, blue glow, some glows are invisible, some glows show. This one shines for ages when lasers blink. That one fades before you think. I like glows that light up bright. They sparkle, twinkle, pure delight! Photoluminescence is its name, it plays the glow and glimmer game. But wait! Oh no! What's this I see? A sneaky glow that should not be! It creeps, it peaks, it makes a mess -It's autofluorescence or maybe Raman! Oh, what stress! It glows when we don't want it to, it hides in green, it hides in blue. It jumps right in our spectrum and fills our hearts with quite a tantrum!

The dissertation was written in the period from February 2021 to May 2025 at the Institute of Analytical Chemistry, Chemo- and Biosensorics at the University of Regensburg.

The dissertation was supervised by:

Prof. Dr. Antje J. Baeumner

Doctoral application submitted on: May 14th 2025

Colloquium on: July 18th 2025

Examination board:

Chairwoman: Prof. Dr. Miriam Breunig

1st referee: Prof. Dr. Antje J. Baeumner

2nd referee: Prof. Dr. Axel Duerkop

3rd referee: Prof. Dr. Patrick Nuernberger

Acknowledgments

This fascinating journey would not have been possible without the support, love and company of so many astonishing and great people along the way, which I will try to name as many as I'll get away with (like, who is going to stop me?).

First and foremost, I want to thank **Prof. Dr. Antje J. Baeumner** for taking me in at a difficult time with the world in turmoil (and busy with coughing) and for allowing me to work on such a fascinating and literally exciting topic, for her much-appreciated support and for her motivational superpower along the way.

I also want to express my heartfelt thanks to **Prof. Dr. Axel Dürkop**, for his guidance, being there for any question and idea I had, no matter how crazy and for giving me the scientific space to explore I needed and the metaphorical nudge now and then that I so very much deserved.

I am very grateful for **Prof. Dr. Miriam Breunig** and **Prof. Dr. Patrick Nürnberger** for agreeing to be the chairwoman and third referee for my defense and for readily taking on all the hassle and efforts involved in the endeavor.

Thanks to:

Dr. Meike "Mutti" Bauer for teaching me everything she knew about EuTc, knife coating and hydrogels;

Dr. Meike Bauer, **Barbara Grotz** and **Iga Malicka** for their work, friendship and the camaraderie throughout my thesis and an entire project that shall not be named;

Dr. Simone "HEXE!" Rink for being on the same wavelength the whole time since my bachelor's thesis way too long ago;

Simon Streif for being my companion in pain with a glorified and very expensive pipetting robot;

Dr. Antonia Perju for the SEM micrographs and **Christoph Bühler** for the TEM micrographs used in this thesis;

Our technical assistants for keeping everything running smoothly on a day-to-day basis for both the practical courses. Namely **Rosi** “the good soul”, “die kleine” **Gisi**, both enjoying their well-deserved retirement, **Vanessa** “the render goddess”, my silver lining with any ordering process chaos, **Silvia** “duu, I häd da amoi a Frage” for helping me with pipette inventory and testing, **Rewi** “the old hairy biker” for teaching and showing me how to solve issues without undue red tape and **Sanja** “de san vom Bugatti oida” for her assistance with nanospotting;

My bachelor students, **Christina-Anna**, **Lea**, and **Luisa** and my “shared parenthood” Master Student **Laura** for achieving excellent science despite my probably incoherent rambling during their theses;

My lab mates **Barbara**, **Kili** and **Ferdi** for a ton of laughs, really messed up music alliteration days and for making even the dreariest day bearable and fun;

All the people in the working group, working alongside the lot of you was a great joy, honor and sometimes a pian fíor i mo thóin. But I would not have it any other way;

Dr. Klaus Huber, for his support genuine interest how it was going with my “Inauguraldissertation” and networking in the clinics in Regensburg which helped me get access to a suitable and sufficiently powerful γ-sterilization source and in identifying relevant drugs and dosages used during heart surgeries;

The blood bank team at the UKR, especially **Marion Posset** for uncomplicated supply with human plasma and for the assistance with γ-sterilization;

All my friends from work, the Wasserwacht, the MuCa Clan Saunamitserclub, and family by blood or choice, who helped me stay more or less sane through this insanity in ways and actions they might not even be aware of;

My **Mother** and **Father** who raised and nurtured this idjit with food and all their love and steeled me for the world with their care, humor and just the right diet of sarcasm and Terry Pratchett, warnings of the Spanish inquisition (really nobody expects it) and for asking how bottomless MTPs can have a bottom;

My siblings **Thomas**, **Ciarán** and **Anna**, without my Broddas and my Sista a lot of fun and joy would not have been had;

My grandparents, **Elfride** and **Josef**, look what your little buawe did!

My **granny** “girly” who would have loved to see this;

My fiancée **Connie**, without whom I couldn't even imagine having made it through the last eight years of my life;

And last, but not least I want to thank you, dear reader, for reading this thesis.

Declaration of collaboration

Most of the theoretical and experimental work shown in this thesis was performed solely by the author. Some or parts of results were gained in collaboration with other researchers, which are stated here in accordance with § 8 Para. 1 Clause 2 No. 7 “Regulations for earning the academic degree Doctor of Natural Sciences (Dr. rer. nat.) at the University of Regensburg” from June 18, 2009 in the version of the resolutions of December 18, 2023.

Summary, Zusammenfassung & Relevance and structure of the thesis (chapter 1)

Literature research and writing of the chapter(s) was solely done by the author.

Recent advances and trends in optical devices and sensors for hydrogen peroxide detection (chapter 2)

Literature research and writing of the original manuscript draft was solely done by the author. Antje J. Baeumner (AJB) and Axel Duerkop (AD) reviewed most of the manuscript and contributed with strategic discussions. The original draft was rewritten by the author based on the review and suggestions of AJB and AD. AD is the corresponding author.

A fluorescent MTP-based detection platform for hydrogen peroxide, glucose, and lactate (chapter 3)

Most of the experimental work was solely done by the author. Antje J. Baeumner (AJB) and Axel Duerkop (AD) reviewed most of the manuscript and contributed with strategic

discussions. The original draft was rewritten by the author based on the review and suggestions of AJB and AD. AD is the corresponding author.

Ratiometric detection of H_2O_2 with Europium(III) Tetracycline as luminescent probe (chapter 4)

Most of the experimental work was solely done by the author. Christina-Anna Senser performed the interference study under supervision as part of her Bachelor Thesis. Meike Bauer (MB), Barbara Grotz (BG), Antje J. Baeumner (AJB) and Axel Duerkop (AD) contributed with strategic discussions. The chapter was written solely by the author. Parts of this chapter have been patented by Terumo Cardiovascular services under the patent WO 2024/059143 A1, 2023.

Conclusion and Outlook (chapter 5)

Conceptualization and writing of the chapter were done solely by the author.

Table of Contents

Zusammenfassung

Der Hauptaspekt dieser Dissertation ist die Entwicklung und Weiterentwicklung von Hydrogel basierten, dünnschichtigen optischen Sensoren und Assay Plattformen für bioanalytische und klinische Detektion von Wasserstoffperoxid (H_2O_2). Unter diesem Gesichtspunkt betrachtet zunächst ein kritischer Review neue und wesentliche Entwicklungen und Methoden von optischen Sensoren für H_2O_2 seit 2018. Bemerkenswert ist hier vor allem die immer stärkere Integration von Smartphones für optische und insbesondere reflektometrische Anwendungen. Während es bei einfach verwendbaren Applikationen eine Vielzahl an neuen und innovativen Matrices, Sensormaterialen und Katalysatoren gibt, werden hier auch oft kommerziell erhältliche Matrices und etablierte und Farbstoffe wie 3,3′,5,5′-Tetramethylbenzidin (TMB) oder Amplex Red™ verwendet. Für semi-reversible und -kontinuierliche Messungen gibt es vornehmlich neue Anwendungen mit chemilumineszenter Fließinjektionsanalyse (FIA). Die aktuell am besten entwickelte Plattform für die (vollkommen) reversible und kontinuierliche Detektion von H_2O_2 basieren auf O_2-Löschung der Phosphoreszenz von Platinporphyrinen. Eine vollkommen ideale optische Detektions- und Messmethode existiert jedoch nach wie vor nicht.

Da bei kommerziell erhältlichen Assays für die Quantifizierung von H_2O_2 oft mehrere und damit zeitaufwändige Vorbereitungs- und Verdünnungsschritte benötigt werden, wurde eine sofort nutzbare (RTU) Mikrotiterplatten (MTP) basierte Plattform für die sehr schnelle Detektion und Einfachmessung von H_2O_2 entwickelt. Grundlage der Plattform ist wie beim kommerziell erhältlichen Amplex Red™ Kit die katalytische und 1:1 stöchiometrische Umwandlung des nicht fluoreszenten und farblosen Stoffes 10-Acetyl-3,7-dihydroxyphenoxazine (ADHP) mit H_2O_2 zu dem fluoreszenten und pink gefärbten Resorufin in Gegenwart des Enzyms Meerrettich Peroxidase (HRP). Da HRP ADHP auch ohne H_2O_2 langsam in Resorufin umwandelt, müssen Enzym und Farbstoff voneinander getrennt aufbewahrt werden. Dafür wird ADHP als gefrorene Stammlösung in DMSO bei -20 °C und HRP in Lösung bei 4 °C gelagert. Um diese Problematik zu umgehen, wurde ADHP zunächst in die kommerziell erhältliche polyurethanbasierte Hydrogelmatrix D640 eingebettet. Das in EtOH/H_2O gelöste D640

mit ADHP ließ sich dabei als µm dünne Schichten und Membranen mittels Streichbeschichtung auf ein klares Beschichtungssubstrat, hier industriell gefertigtes biaxial orientiertes PET auftragen, was den Herstellungsprozess sehr interessant für großtechnische Produktion macht. In diesen getrockneten Membranen war ADHP bei Raumtemperatur und damit um 42° C von der idealen Lagertemperatur von -20 °C entfernt für mindestens 22 Monate stabil. Im Assay wird durch die Zugabe von Lösung oder Probe der Farbstoff mit dem Aufschwellen des Hydrogels in die Lösung freigesetzt. Diese Membranen wurden mit einem Lasercutter ausgeschnitten und auf eine eigens, mit doppelseitigem Klebeband präparierte bodenlose Mikrotiterplatte geklebt. Um die Trennung von Enzym und Farbstoff zu erreichen, wurde konzentrierte HRP als Lösung in 30 nL großen Tröpfchen aufgetropft und damit eine Mischung von Enzym und Farbstoff minimiert. In einem Assay mit H_2O_2 in PBS pH 7.4 konnte mit diesen MTPs bei 37 °C innerhalb von nur drei Minuten Assayzeit H_2O_2 mit einem exzellenten unteren Detektionslimit (LOD) von nur 10 nmol·L^{-1} und einer oberen Grenze von bis zu 2 µmol·L^{-1} in 100 µL Probenvolumen detektiert werden. Der erreichte LOD war damit um eine Größenordnung besser als die Herstellerangabe des kommerziellen Kits (0.1 µmol·L^{-1} angegeben als 10 pmol pro 100 µL). Durch die Verwendung von 50 v% Glycerin als Kälteschutzmittel waren die RTU MTPs bei einer Lagerung bei -20 °C bis zu 13 Wochen ohne signifikanten Aktivitätsverlust und mit einer produktionsbedingten Varianz (cv) von ≈ 9 % verwendbar. Ohne oder mit dem falschen Kälteschutzmittel verursachte die Denaturierung der HRP innerhalb von 4 Wochen den vollständigen Verlust der Detektionskapazität. Glucose Oxidase (GOx) oder Lactat Oxidase (LOx) als H_2O_2-generierende Enzyme zusätzlich zu HRP mit auf die Platte aufgebracht, erlaubte die Detektion von Glucose, bzw. Lactat. Dabei war für Glucose einen LOD von 4 mmol·L^{-1} und nach oben hin bis zu 20 mmol·L^{-1} möglich und damit sehr interessant für die Detektion von milder und schwerer Hyperglykämie. Für Lactat wurde ein LOD von 0.04 mmol·L^{-1} erreicht und ein linearer Bereich von bis zu 0.4 mmol·L^{-1}. Um herstellungsbedingte Schichtdickenunterschiede auszugleichen, wurde die Integration von Polystyrol Nanopartikeln (PSNP), beladen mit einem Cy5 Farbstoff, in die Membran untersucht. Die Einbettung des Farbstoffes in die Partikel war dabei zwingend notwendig, da der Referenzfarbstoff im Assay mit HRP und H_2O_2 ohne diesen Schutz auch abgebaut wurde. Die optimierte Beladung des Hydrogels mit Partikel ermöglichte damit eine ratiometrische Detektion.

Für die (Weiter)Entwicklung von Sensormembranen und die letztendlich angedachte kontinuierliche Detektion von H_2O_2 und in Kombination mit GOx und LOx, Glukose und Laktat, wurde Europium (III) Tetracyclin (EuTc) als lumineszente Sonde verwendet. Diese wurde in eine dafür entwickelte Sensormembran eingebettet. Die Membran

besteht aus einer Sondenschicht aus D4, einem kommerziell erhältlichen Hydrogel auf Polyurethanbasis, das von einer Schutzschicht aus Polyvinylacetat/Celluloseacetat (PVAc/CA) bedeckt wird. Auch hier wurden die jeweiligen Membranen und Schichten auf ein klares Beschichtungssubstrat aus industriell gefertigtem, biaxial orientiertem PET mittels Streichbeschichtung aufgetragen. Die erwähnte Schutzschicht wurde dabei zur Vermeidung des störenden Einflusses von interferierenden Substanzen und für die Unterbindung ungewollter Freisetzung der Sonde benötigt. Diese Schutzschicht limitiert jedoch auch die Diffusion in die darunter liegende Hydrogelschicht und erhöht damit die Zeit, die das System zur initialen Equilibrierung benötigt, drastisch. Um diese Zeit zu verkürzen, wurde die Dicke der Schutzschicht reduziert. Auf der einen Seite wurde das durch die Verdünnung der Beschichtungslösung und auf der anderen Seite durch die mechanische Reduzierung der Streichbeschichtungshöhe erreicht. In beiden Fällen konnte eine signifikante Beschleunigung der initialen Equilibrierung erreicht werden. Um etwaige Schwankungen im Verlauf in der Messung auszugleichen und um in einem finalen Produkt die Kalibrierung zu vereinfachen, wurde auch hier eine ratiometrische Detektion entwickelt. 9,10-Bis(phenylethynyl)anthracene (BPEA) stellte sich dabei als idealer Referenzfarbstoff heraus, da er sowohl wie EuTc mit 405 nm angeregt werden konnte, jedoch einen deutlich kleineren Stokes-shift aufwies, und auch die Überlappung der Peaks der Emissionsspektren von Referenz und Sonde minimal waren. Durch die Einbettung des Referenzfarbstoffes in eine Schicht aus Cycloolefin-Copolymer (COC) konnte die Photostabilität mit einem Faktor von zwei im Vergleich zur Lösung deutlich erhöht werden. Als Alternative zu der Einbettung in eine separate Schicht konnte der Referenzfarbstoff auch in synthetisierte COC-Nanopartikel integriert werden. Da eine chemische und auch thermische Sterilisation des Sensors durch die eingebetteten Enzyme unmöglich war, wurden die separaten Sensorschichten mit γ-Bestrahlung behandelt. BPEA in seiner COC-Schicht und GOx in D4 zeigten dabei eine hervorragende Stabilität. Die Sensormembranen mit EuTc zeigten im Vergleich zur Referenz eine Reduktion der Lumineszenz von ≈ 50 %. Es ist davon auszugehen, dass optimierte temperierte Bedingungen und verkürzte Behandlungszeiten bei höherer Dosis diesen Verlust reduzieren. Die Sensormembranen zeigten keine oder nur minimale Beeinflussung in Gegenwart verschiedener Interferenzsubstanzen. Insbesondere konnten in der Literatur bekannte Interferenzen vermutlich durch die Schutzmembran abgewehrt werden. In verdünntem humanem Plasma zeigten die Sensormembranen eine gute Leistung. Durch die lange Lumineszenzlebenszeit von EuTc war die Detektion von H_2O_2 nicht nur in Lösung, sondern auch in der Membran möglich.

Summary

The main aspect of this dissertation is the development and advancement of hydrogel-based, thin-film optical sensors and assay platforms for bioanalytical and clinical detection of hydrogen peroxide (H_2O_2). From this point of view, a critical review first examines new and significant developments and methods of optical sensors for H_2O_2 since 2018. Of particular note here is the increasing integration of smartphones for optical and especially reflectometric applications. While there are a variety of new and innovative matrices, sensor materials and catalysts for easy-to-use applications, commercially available matrices and established dyes such as 3,3′,5,5′-tetramethylbenzidine (TMB) or Amplex Red™ are also often used here. For semi-reversible and continuous measurements, there are mainly new applications with chemiluminescent flow injection analysis (FIA). The currently best developed platform for the (fully) reversible and continuous detection of H_2O_2 is based on O2-quenching of the phosphorescence of platinum porphyrins. The development of such systems is however, rare. Furthermore, a completely ideal optical detection and measurement method for H_2O_2 does still not exist to this day.

As commercially available assays for the quantification of H_2O_2 often require several and thus time-consuming preparation and dilution steps, a “ready to use” (RTU) microtiter plate (MTP)-based platform was developed for the highly sensitive, single-use detection of H_2O_2. Since commercially available assays for the quantification of H_2O_2 often require several and therefore time-consuming preparation and dilution steps, a “ready to use” (RTU) microtiter plate (MTP)-based platform was developed for the very rapid detection of H2O2. As with the commercially available Amplex Red™ kit, the platform is based on the catalytic and 1:1 stoichiometric conversion of the non-fluorescent and colorless substance 10-acetyl-3,7-dihydroxyphenoxazine (ADHP) with H_2O_2 to the fluorescent and pink-colored resorufin in the presence of the enzyme horseradish peroxidase (HRP). Since HRP slowly converts ADHP into resorufin even without H_2O_2, the enzyme and dye must be stored separately. For this purpose, ADHP is stored as a frozen stock in DMSO at -20 °C and HRP in solution at 4 °C. To avoid this problem, ADHP was first embedded in the commercially available polyurethane-

based hydrogel matrix D640. The D640 with ADHP dissolved in EtOH/H2O could be applied as µm-thin layers and membranes on a clear coating substrate, in this case industrially manufactured biaxially oriented PET, by means of spread coating, which makes the manufacturing process very interesting for large-scale production. In these dried membranes, ADHP was stable for at least 22 months at room temperature, which is 42°C away from the ideal storage temperature of -20°C. In the assay, the addition of solution or sample releases the dye into the solution as the hydrogel swells. These membranes were cut out with a laser cutter and glued to a specially prepared bottomless microtiter plate with double-sided adhesive tape. To achieve separation of enzyme and dye, concentrated HRP was dripped as a solution in 30 nL droplets to minimize mixing of enzyme and dye. In an assay with H_2O_2 in PBS pH 7.4, H_2O_2 could be detected with these MTPs at 37 °C within only three minutes assay time with an excellent lower limit of detection (LOD) of only 10 nmol L^{-1}, which is an order of magnitude better than the manufacturer's specification of the commercial kit (0.1 µmol·L^{-1} given as 10 pmol per 100 µL), and an upper limit of up to 2 µmol·L^{-1} in 100 µL sample volume. By using 50 v% glycerol as cryoprotectant, the RTU MTPs were usable for up to 13 weeks when stored at -20 °C without significant loss of activity and with a production-related variance (cv) of ≈ 9 %. Without or with the wrong cryoprotectant, denaturation of HRP caused complete loss of sensitivity and detection capacity within 4 weeks. Glucose oxidase (GOx) or lactate oxidase (LOx) as H_2O_2-generating enzymes applied to the plate in addition to HRP allowed the detection of glucose and lactate, respectively. For glucose, an LOD of 4 mmol·L^{-1} and up to 20 mmol·L^{-1} was possible, and thus very interesting for the detection of mild and severe hyperglycemia. For lactate, an LOD of 0.04 mmol·L^{-1} was achieved and a linear range of up to 0.4 mmol·L^{-1}. In order to compensate for production-related differences in layer thickness, the integration of polystyrene nanoparticles (PSNP), loaded with a Cy5 dye into the membrane, was investigated. The embedding of the dye in the particles was necessary, as the reference dye was also degraded in the assay with HRP and H_2O_2 without this protection. The optimized loading of the hydrogel with particles thus enabled ratiometric detection.

For the (further) development of sensor membranes and the ultimately planned continuous detection of H_2O_2 and in combination with GOx and LOx, glucose and lactate, europium (III) tetracycline (EuTc) was used as a luminescent probe. This was embedded in a specially developed sensor membrane. The membrane consists of a probe layer of D4, a commercially available polyurethane-based hydrogel, which is covered by a protective layer of polyvinyl acetate/cellulose acetate (PVAc/CA). Here, too, the respective membranes and layers were applied to a clear coating substrate

made of industrially produced, biaxially oriented PET by means of kinfecoating. The protective layer mentioned above was required to avoid the interfering influence of interfering substances and to prevent unwanted leakage of the probe. However, this protective layer also limits diffusion into the underlying hydrogel layer, drastically increasing the time the system needs for initial equilibration. To shorten this time, the thickness of the protective layer was reduced. On the one hand, this was achieved by diluting the coating solution and, on the other, by mechanically reducing the coating height. In both cases, a significant acceleration of the initial equilibration was achieved. In order to compensate for any fluctuations in the course of the measurement and to simplify calibration in a final product, ratiometric detection was also developed here. 9,10-Bis(phenylethynyl)anthracene (BPEA) proved to be the ideal reference dye, as it could be excited at 405 nm like EuTc, but had a significantly smaller Stokes shift, and the overlap of the peaks of the emission spectra of reference and probe was also minimal. By embedding the reference dye in a layer of cycloolefin copolymer (COC), the photostability was significantly increased by a factor of two compared to the solution. Alternatively, BPEA could also be integrated in synthesized COC-nanoparticles. Since chemical as well as thermal sterilization of the sensor was impossible due to the embedded enzymes, the separate sensor layers were treated with γ-irradiation. BPEA in its COC layer and GOx in D4 showed excellent stability. The sensor membranes with EuTc showed a reduction in luminescence of ≈ 50 % compared to the reference. It can be assumed that optimized temperature-controlled conditions and shorter treatment times at higher doses will reduce this loss. The sensor membranes showed no or only minimal influence in the presence of various interference substances. In particular, interferences known in literature could presumably be repelled by the protective membrane. The sensor membranes performed well in diluted human plasma. Due to the long luminescence lifetime of EuTc, the detection of H_2O_2 was possible not only in solution but also in the membrane.

1 Relevance and Structure of the Thesis

The core goals of bioanalytical chemistry are to find answers to the questions of **how much** of **what** (substance/chemical) is **where**. Answers essential not only for healthcare, but also for environmental, product and workplace safety. Answers that often have to be found in spite of difficult samples, matrices and a true host of interfering substances. Answers that are made possible by new and innovative solutions, but often also in combination of previously known concepts and methods.

The development of these, together with the need of finding better, more sensitive and faster detection methods is the driving force and basis of novel (bio)sensors, assays and analytical approaches.

One potential target and thus analyte (**what**) of such assays, sensors and approaches is hydrogen peroxide (H_2O_2). H_2O_2 is used in many industrial and chemical applications as disinfectant and reagent. However, H_2O_2 is not just a dead, inorganic reactive oxygen species (ROS) but is also present in a variety of metabolic processes, both as intermediate and metabolic products. Elevated H_2O_2 levels have been associated with a variety of diseases [1]. But, due to a variety of biological processes functioning as efficient and rapid degradation of H_2O_2, together with the instability of dilute H_2O_2, determining the exact concentrations of such relatively low H_2O_2 concentrations, especially in tissues and bodily fluids, is challenging [2,3]. The issue is also illustrated by the literature data for hydrogen peroxide, which can deviate from each other even by orders of magnitude [4,5]. This in turn makes the development of rapid and sensitive detection a key goal. Furthermore, as several enzymes, primarily oxidases, exist which can produce H_2O_2 [6], the latter is also a very versatile secondary analyte for a variety of other relevant metabolites and biomarkers.

Two examples of such enzyme-metabolite pairs that are accessible to subsequent H_2O_2-quantification are glucose with glucose oxidase (GOx) and lactate with lactate oxidase (LOx).

Glucose is a very important and vital biomarker, as too high blood glucose levels over a long time can lead to a variety of metabolic complications (usually only for diabetic patients), such as hyperglycemic shock, hyperosmolar hyperglycemic coma [7], diabetic angiopathy [8] and, if untreated or treated poorly, death. Short-term, stress hyperglycemia often occurs in critically ill patients and in extreme stress situations. This short-term hyperglycemia is not necessarily a bad thing, but rather an indicator or symptom of a biological response to a far more serios health issue [9]. Unfortunately, the number of people suffering from diabetes has increased in the last two decades and will probably also grow further in the future [10]. With reduced physical activity [11] and sugar still being added excessively to processed foods, despite the benefits of reduced sugar contents [12], and the risks and damage to health of added sugars [13,14], the issue will most likely not get better.

Lactate as an analyte is both relevant in clinical and lifestyle settings. Systemically high lactate levels or lactate acidosis are often an indicator of poor survivability or bad clinical outcomes of patients [15]. After its discovery lactate has often been seen as a mere metabolic byproduct out of necessity or a result from oxygen lack in muscles. The increased production of lactate under anaerobic conditions has also made it a common lifestyle analyte to determine correct training intensity and frequency [16]. However, in the meantime, lactate has been recognized as taking an essential part in several processes, both metabolic under aerobic conditions and in regulatory and signaling functions [17]. Increased lactate levels have also been tied to cancer growth and metabolism [18] with cancer tissue lactate levels rising up to 40 $mmol \cdot L^{-1}$ above the regular 1.5 – 3 $mmol \cdot L^{-1}$ of healthy individuals [19].

The development of sensors capable of detecting glucose and lactate are two major active research areas (Figure 1.1) and markets, with an estimated market size of 9.68 billion USD for glucose biosensors [20] and 370 million USD for lactate meters [21]. Especially for glucose, the measurement with glucometers is widely established and they are fast and indispensable tools for the private healthcare of (diabetic) patients and in emergency medicine. Lactate and glucose are mostly measured via H_2O_2 and subsequent electrochemical [22] or optical detection of the latter.

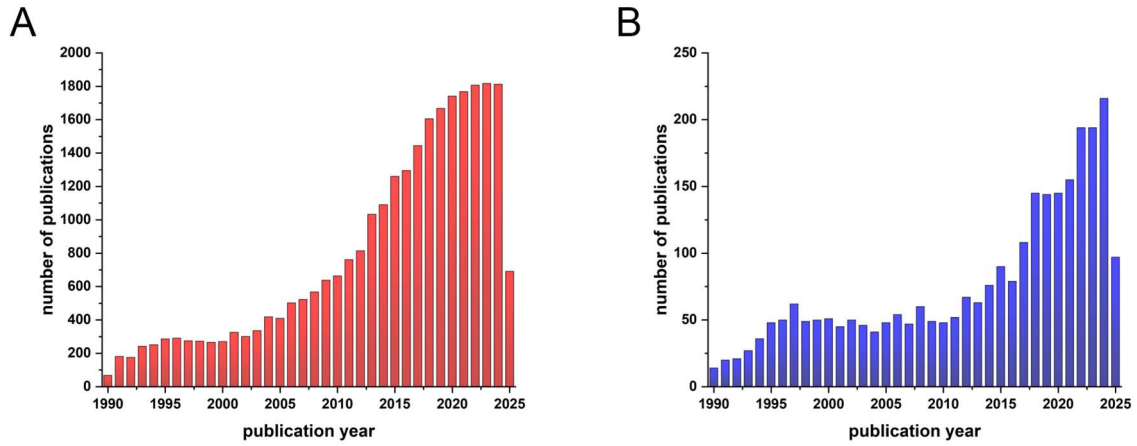

Figure 1.1 Web of science record count for **A** "glucose sensor" and **B** "lactate sensor" between 1990 and 2025. [23]

While electrochemical setups can offer fast and sensitive responses, electrochemical detection can often be hamstrung by a plethora of interfering electroactive substances, electrode fouling [24], and passivation [25], which severely limit the (re)usability of expensive components. Optical detection can offer a (not necessarily metallic) silver[c] lining here. Using light for characterization and quantification of molecules and materials is very exciting, not just on a ground level, but can allow access to information across a wide range of scales across the whole (visible and invisible) spectrum. That the recognition element with the transducer can be decoupled and does not have to be in direct physical contact with the detector, is elegant and practical in terms of wear on the connection to the detector. Furthermore, optical assays and approaches allow for high-throughput screening in microtiter plate formats for the rapid measurement of up to 1536 samples in one run.

Considering the presented versatility and importance of H_2O_2 both as primary and secondary analyte, it is hardly surprising that a variety of innovative sensors, assays and analytical approaches have been developed and are currently being developed. Here, more recent (2018-2024) advances and trends in optical devices for the detection of H_2O_2 are critically reviewed and discussed in chapter 2. One point, which under no circumstances should be overlooked is the **how**[d]. As mentioned before there

[c] Unless of course, we use a silver nanoparticle agglomeration assay [26]…

[d] to detect how much of what and where.

are a variety of possible options. For this thesis the main focus was the development methods for the photoluminescent detection of H_2O_2.

In a nutshell, photoluminescence is the emission of photons or light after excitation of electrons with an external light source. In contrast to this chemi- and bioluminescence are the emission of photons after a chemical reaction, the latter just being chemiluminescence in lifeforms or parts thereof, such as cells, higher organisms or luminescent enzymes and proteins. There are a variety of photoluminescent types, such as fluorescence, phosphorescence, lanthanide and complex photoluminescence and upconversion luminescence. What they all have in common: light goes in, light (of a different wavelength) goes out. In the range of optical detection, photoluminescent approaches can provide superior limits of detection when compared to absorbance- or extinction-based measurements[e].

In the scope of this thesis two photoluminescent systems are used for the detection of H_2O_2 with the development of a single-use assay platform and a continuous sensor. Specifically, 10-Acetyl-3,7-dihydroxyphenoxazine (ADHP) and Europium(III) tetracycline (EuTc) are the assay reagent and probe respectively.

ADHP, also known by its brand name Amplex Red™, is a colorless and non-fluorescent, resorufin-based derivative. Sold as part of assay kits, ADHP is one of the most commonly used fluorophores to detect H_2O_2 [27]. In the assay together with horseradish peroxidase (HRP), ADHP and H_2O_2 are catalytically transformed in a 1:1 stoichiometric reaction to the fluorescent and pink colored resorufin, H_2O and O_2.

An issue commonly observed and known for ADHP in this liquid assay is that the fluorescence intensity decreases with higher H_2O_2 concentrations [28]. The reason often stated, especially in operating instructions of assay manufacturers is that a further oxidation of resorufin to resazurin allegedly takes place. To the author's knowledge, no analytic proof thereof has been published. Spectroscopic data in a well-cited paper from 1997 [28] showing a lack of resazurin emission peaks, and electrochemical data showing the irreversible reduction of resazurin to resorufin [29–31] would suggest that the proposed resazurin formation does not take place. At the time, Haugland [28] and other researchers [32] actually mentioned or proposed a precipitating colorless oxidation product showing no fluorescence. A later paper from

[e] "Measuring the weight of a car by weighing a containership with and without the car", or, as beautifully demonstrated by Uli Stein: "die Katze hat schon wieder zugenommen"

2004 [33] is probably the origin of the resazurin statement, as it cites the earlier paper [28] and another publication of Brotea et al. [32] as source, but neither suggests resazurin forming as oxidative product of resorufin with HRP and H_2O_2. In fact, Brotea et al. mentioned their laboratory working with the resazurin-resorufin system previously, which might have led to the confusion in literature. Unfortunately, to the author's knowledge, these nonfluorescent oxidation compound(s) have not been identified to this day.

Aside from this issue the assay also requires several dilution and (manual) preparation steps, which increases the time required for reagent preparation and thus limits the sample throughput. In fully automated setups and laboratories this makes more sophisticated and elaborate automation necessary. Here, the development of a ready-to-use MTP-based platform, intended to reduce the preparation steps and thus increase sample throughput, is presented in chapter 3.

As previously mentioned, the most advanced method of detecting H_2O_2 is based on the oxygen quenching of the phosphorescence of Pt-porphoryn-complexes following the catalytic decomposition of H_2O_2. Although the response time of the probe to oxygen is only limited by the diffusion of O_2 into the membrane, the catalytic process of H_2O_2 to O_2 and the use of oxygen-harvesting modules to eliminate any previously dissolved oxygen increases the overall response time drastically [34]. As such, those sensors are only of limited use in highly oxygenated samples and media. Furthermore, the flow cells and the attached microfluidics must be very impermeable to any oxygen containing atmosphere. Alternatively, a sensor based on a non-O_2 can be used. Here, EuTc is a very interesting and versatile probe that allows the detection of H_2O_2 based on the Eu(III)-lanthanide transition $^5D_0 \rightarrow {}^7F_2$, detectable at 616 nm [35]. The emission is enhanced by the presence of H_2O_2 due to the displacement of H_2O from coordinating sites. The development and optimization of such an EuTc-based ratiometric sensor is discussed in chapter 4.

Finally, in Chapter 5 the findings of the thesis are summarized and evaluated in a conclusion. Here, the potentials and outlooks of the developed and presented technologies are highlighted.

For such a sensor and platform development, the probes and recognition elements require suitable matrices. With the additional prerequisite of the usage in an optical assay or in an optical sensor the matrix should also be transparent, permeable for the analyte or, when looking for a reagent release, the active assay components. In sensor

development, hydrogels have become highly favorable matrix for probes and dyes [36–38] due to their excellent properties that cover the above-mentioned requirements. A gel is, according to IUPAC, a “non-fluid colloidal network or polymer network that is expanded throughout its whole volume by a fluid”. For a hydrogel the swelling component is water [39]. That in turn means, paraphrasing Herve Thís [40], that we, you and I my reader, are, with around 60 w% water content [41], hydrogels according to IUPAC[f]. (Hydro)gels come in many shapes and synthesis/manufacturing processes. As such, there is a variety of options to produce such membranes and thin films [42]. As the best alternative that can also be used in larger scale mass production knife coating is used as method of hydrogel application. Knife coating is a technique where the coating substance is placed in front of a blade or a coating bar which is then moved across the coating substrate with a defined distance from the latter, resulting in a coated film. There are various designs of knife coaters with the fundamental difference being in the moving part. For smaller production and knife coaters usually the coating substrate is fixed (eg. vacuum, magnets locks, clamps, or tape) and the knife is moved either manually or mechanically over the surface. These setups are very suited for smaller productions and for initial parameter testing. However, the reproducibility and the precision of the layer thickness is strongly affected by any ridges, the slope and the overall roughness of the coating bed. Furthermore, as the knife is usually removed and cleaned between coating steps, the set coating thickness can only be guaranteed to a limited extent, again affecting the in-batch reproducibility. In a larger production line which enables a mass production by roll-to roll fabrication [42], the knife is usually fixed and the coating substrate is moved from roll to roll. Depending on the substrate, the resulting friction over the flat surface can cause damage to the coating substrate or an inhomogeneous coating thickness due to the vibration. With very thin layers where the substrate is moved on a roll or a roller, an unbalance of the rotating cylinder can lead to different (periodic) layer thicknesses.

The mentioned deviation in thickness does of course also impact the reaction overall. As more or less membrane is associated here with the amount of dye and thus substrate, both, the assay precision and the reproducibility, suffer. To a certain extent, these problems can be reduced by the (manufacturing) quality of the devices used for coating and a correspondingly good adjustment and levelling. However, the issue cannot be brought completely under control like this. As a result of this issue with reproducibility, true replicas, i.e. the same concentration with different areas on the

[f] To be read in a lovely Elsassian accent.

membrane/film are rarely measured or published in applications that knife-coat their sensors, especially with very thin layers [34]. Determining the thickness of the membrane e.g. by SEM or other methods is often time-consuming, expensive and not representative for the thickness over larger areas. A ratiometric measurement on the other hand can quickly and easily provide information about the thickness of the membrane and thus the amount of dye per well. Such ratiometric approaches are a common method used in commercial [43] and for development [44] of thin film sensors and applications. Usually ratiometric detection in a system using two independent fluorophores is performed with an analyte-responsive fluorophore with a large Stokes shift, which allows for the use of a reference with a smaller shift [45,46]. This can allow the circumvention of certain optical effects like analyte dependent FRET and reabsorbance/emission of the probe dye emission by the reference dye [47]. With small Stokes shift of probes this strategy of a shorter wavelength emitting reference dye does not work. This in turn means that the reference dye needs to be excitable in the same region as the probe, the spectral overlap should ideally be minimal, and the reference emission should not be affected by an increase of analyte and thus probe emission. With these methods a fast, reliant, efficient and scalable production and development of sensor and detection platforms is feasible.

1.3 References

[1] R. Stolarek, P. Bialasiewicz, M. Krol, D. Nowak, Breath analysis of hydrogen peroxide as a diagnostic tool, Clin. Chim. Acta. 411 (2010) 1849–1861. https://doi.org/10.1016/j.cca.2010.08.031.

[2] J.J. Galligan, A.J. Baeumner, A. Duerkop, Recent advances and trends in optical devices and sensors for hydrogen peroxide detection, TrAC, Trends Anal. Chem. 180 (2024) 117948. https://doi.org/10.1016/j.trac.2024.117948.

[3] H.J. Forman, A. Bernardo, K.J.A. Davies, What is the concentration of hydrogen peroxide in blood and plasma?, Arch. Biochem. Biophys. 603 (2016) 48–53. https://doi.org/10.1016/j.abb.2016.05.005.

[4] B. Frei, Y. Yamamoto, D. Niclas, B.N. Ames, Evaluation of an isoluminol chemiluminescence assay for the detection of hydroperoxides in human blood plasma, Anal. Biochem. 175 (1988) 120–130. https://doi.org/10.1016/0003-2697(88)90369-7.

[5] S.D. Varma, P.S. Devamanoharan, Hydrogen peroxide in human blood, Free Radical Res. Commun. 14 (1991) 125–131. https://doi.org/10.3109/10715769109094124.

[6] Nóra Aányi, Teréz Barna, Tamás Emri, Márton Miskei, István Pósci, Hydrogen Peroxide Producing and Decomposing Enzymes: their Use in Biosensors and other Applications, in: J. Polaina (Ed.), Industrial enzymes: Structure, function and applications, Springer, Dordrecht, 2007, pp. 441–459.

[7] R. van Ness-Otunnu, J.B. Hack, Hyperglycemic crisis, J. Emerg. Med. 45 (2013) 797–805. https://doi.org/10.1016/j.jemermed.2013.03.040.

[8] C.D. Stehouwer, J. Lambert, A.J. Donker, V.W. van Hinsbergh, Endothelial dysfunction and pathogenesis of diabetic angiopathy, Cardiovasc. Res. 34 (1997) 55–68. https://doi.org/10.1016/S0008-6363(96)00272-6.

[9] P.E. Marik, R. Bellomo, Stress hyperglycemia: an essential survival response!, Crit. Care 17 (2013) 305. https://doi.org/10.1186/cc12514.

[10] K.L. Ong, L.K. Stafford, S.A. McLaughlin, E.J. Boyko, S.E. Vollset, A.E. Smith, B.E. Dalton, J. Duprey, J.A. Cruz, H. Hagins, P.A. Lindstedt, A. Aali, Y.H. Abate, M.D. Abate, M. Abbasian, Z. Abbasi-Kangevari, M. Abbasi-Kangevari, S. Abd ElHafeez, R. Abd-Rabu, D.M. Abdulah, A.Y.M. Abdullah, V. Abedi, H. Abidi, R.G. Aboagye, H. Abolhassani, E. Abu-Gharbieh, A. Abu-Zaid, T.D. Adane, D.E. Adane, I.Y. Addo, O.A. Adegboye, V. Adekanmbi, A.V. Adepoju, Q.E.S. Adnani, R.F. Afolabi, G. Agarwal, Z.B. Aghdam, M. Agudelo-Botero, C.E. Aguilera Arriagada, W. Agyemang-Duah, B.O. Ahinkorah, D. Ahmad, R. Ahmad, S. Ahmad, A. Ahmad, A. Ahmadi, K. Ahmadi, A. Ahmed, A. Ahmed, L.A. Ahmed, S.A. Ahmed, M. Ajami, R.O. Akinyemi, H. Al Hamad, S.M. Al Hasan, T.M.A. AL-Ahdal, T.A. Alalwan, Z. Al-Aly, M.T. AlBataineh, J.E. Alcalde-Rabanal, S. Alemi, H. Ali, T. Alinia, S.M. Aljunid, S. Almustanyir, R.M. Al-Raddadi, N. Alvis-Guzman, F. Amare, E.K. Ameyaw, S. Amiri, G.A. Amusa, C.L. Andrei, R.M. Anjana, A. Ansar, G. Ansari, A. Ansari-Moghaddam, A.E. Anyasodor, J. Arabloo, A.Y. Aravkin, D. Areda, H. Arifin, M. Arkew, B. Armocida, J. Ärnlöv, A.A. Artamonov, J. Arulappan, R.T. Aruleba, A. Arumugam, Z. Aryan, M.T. Asemu, M. Asghari-Jafarabadi, E. Askari, D. Asmelash, T. Astell-Burt, M. Athar, S.S. Athari, M.M.W. Atout, L. Avila-Burgos, A. Awaisu, S. Azadnajafabad, D.B. B, H. Babamohamadi, M. Badar, A. Badawi, A.D. Badiye, N. Baghcheghi, N. Bagheri, S. Bagherieh, S. Bah, S. Bahadory, R. Bai, A.A. Baig, O.C. Baltatu, H.R. Baradaran, M. Barchitta, M. Bardhan, N.C. Barengo, T.W. Bärnighausen, M.T.U. Barone, F. Barone-Adesi, A. Barrow, H. Bashiri, A. Basiru, S. Basu, S. Basu, A.-M.M. Batiha, K. Batra, M.T. Bayih, N.S. Bayileyegn, A.H. Behnoush, A.B. Bekele, M.A. Belete, U.I. Belgaumi, L. Belo, D.A. Bennett, I.M. Bensenor, K. Berhe, A.Y. Berhie, S. Bhaskar, A.N. Bhat, J.S. Bhatti, B. Bikbov, F. Bilal, B.S. Bintoro, S. Bitaraf, V.R. Bitra, V. Bjegovic-Mikanovic, V. Bodolica, A. Boloor, M. Brauer, J. Brazo-Sayavera, H. Brenner, Z.A. Butt, D. Calina, L.A. Campos, I.R. Campos-Nonato, Y. Cao, C. Cao, J. Car, M. Carvalho, C.A. Castañeda-Orjuela, F. Catalá-López, E. Cerin, J. Chadwick, E.K. Chandrasekar, G.S. Chanie, J. Charan, V.K. Chattu, K. Chauhan, H.A. Cheema, E. Chekol Abebe, S. Chen, N. Cherbuin, F. Chichagi, S.B. Chidambaram, W.C.S. Cho, S.G. Choudhari, R. Chowdhury, E.K. Chowdhury, D.-T. Chu, I.S. Chukwu, S.-C. Chung, K. Coberly, A. Columbus, D. Contreras, E. Cousin, M.H. Criqui, N. Cruz-Martins, S. Cuschieri, B. Dabo, O. Dadras, X. Dai, A.A.M. Damasceno, R. Dandona, L. Dandona, S. Das, A.M. Dascalu, N.R. Dash, M. Dashti, C.A. Dávila-Cervantes, V. de La Cruz-Góngora, G.R. Debele, K. Delpasand, F.W. Demisse, G.D. Demissie, X. Deng, E. Denova-Gutiérrez, S.V. Deo, E. Dervišević, H.D. Desai, A.T. Desale, A.M. Dessie, F. Desta, S.M.R. Dewan, S. Dey, K. Dhama, M. Dhimal, N. Diao, D. Diaz, M. Dinu, M. Diress, S. Djalalinia, L.P. Doan, D. Dongarwar, dos Santos Figueiredo, Francisco Winter, B.B. Duncan, S. Dutta, A.M. Dziedzic, H.A. Edinur, M. Ekholuenetale, T.C. Ekundayo, I.Y. Elgendy, M. Elhadi, W. El-Huneidi, O.A.A. Elmeligy, M.A. Elmonem, D. Endeshaw, H.L. Esayas, H.B. Eshetu, F. Etaee, I. Fadhil, A.F. Fagbamigbe, A. Fahim, S. Falahi, M.E.M. Faris, H. Farrokhpour, F. Farzadfar, A. Fatehizadeh, G. Fazli, X. Feng, T.Y. Ferede, F. Fischer, D. Flood, A. Forouhari, R. Foroumadi, M. Foroutan Koudehi, A.M. Gaidhane, S. Gaihre, A. Gaipov, Y. Galali, B. Ganesan, M.A. Garcia-Gordillo, R.K. Gautam, M. Gebrehiwot, K.G. Gebrekidan, T.G. Gebremeskel, L. Getacher, F. Ghadirian, S.-H. Ghamari, M. Ghasemi Nour, F. Ghassemi, M. Golechha, P. Goleij, D. Golinelli, S.V. Gopalani, H.A. Guadie, S.-Y. Guan, T.W. Gudayu, R.A. Guimarães, R.A. Guled, R. Gupta, K. Gupta, V.B. Gupta, V.K. Gupta, B. Gyawali, R. Haddadi, N.R. Hadi, T.G. Haile, R. Hajibeygi, A. Haj-Mirzaian, R. Halwani, S. Hamidi, G.J. Hankey, M.A. Hannan, S. Haque, H. Harandi, N.I. Harlianto, S.M.M. Hasan, S.S. Hasan, H. Hasani, S. Hassanipour, M.B. Hassen, J. Haubold, K. Hayat, G. Heidari, M. Heidari, K. Hessami, Y. Hiraike, R. Holla, S. Hossain, M.S. Hossain, M.-S. Hosseini, M. Hosseinzadeh, H. Hosseinzadeh, J. Huang, M.N. Huda, S. Hussain, H.-H. Huynh, B.-F. Hwang, S.E. Ibitoye, N. Ikeda, I.M. Ilic, M.D. Ilic, L.R. Inbaraj, A. Iqbal, S.M.S. Islam, R.M. Islam, N.E. Ismail, H. Iso, G. Isola, R. Itumalla, M. Iwagami, C.C.D. Iwu, I.O. Iyamu, A.N. Iyasu, L. Jacob, A. Jafarzadeh, H. Jahrami, R. Jain, C. Jaja, Z. Jamalpoor, E. Jamshidi, B. Janakiraman, K. Jayanna, S.K. Jayapal, S. Jayaram, R. Jayawardena, R. Jebai, W. Jeong, Y. Jin, M. Jokar, J.B. Jonas, N. Joseph, A. Joseph, C.E. Joshua, F. Joukar, J.J. Jozwiak, B. Kaambwa, A. Kabir, R.H. Kabthymer, V. Kadashetti, F. Kahe, R. Kalhor, H. Kandel, S.D. Karanth, I.M. Karaye, S. Karkhah, P.D. Katoto, N. Kaur, S. Kazemian, S.A. Kebede, Y.S. Khader, H. Khajuria, A. Khalaji, Khan, Moien AB, M. Khan, A. Khan, S. Khanal, M.M. Khatatbeh, A.M. Khater, S. Khateri, F. khorashadizadeh, J. Khubchandani, B.G. Kibret, M.S. Kim, R.W. Kimokoti, A. Kisa, M. Kivimäki, A.-A. Kolahi, S. Komaki, F. Kompani, H.R. Koohestani, O. Korzh, K. Kostev, N. Kothari, A. Koyanagi, K. Krishan, Y. Krishnamoorthy, B. Kuate Defo, M. Kuddus, M.A. Kuddus, R. Kumar, H. Kumar, S. Kundu, M.D. Kurniasari, A. Kuttikkattu, C. La Vecchia, T. Lallukka, B. Larijani, A.O. Larsson, K. Latief, B.K. Lawal, T.T.T. Le, T.T.B. Le, S.W.H. Lee, M. Lee, W.-C. Lee, P.H. Lee, S. Lee, S.W. Lee, S.M. Legesse, J. Lenzi, Y. Li, M.-C. Li, S.S. Lim, L.-L. Lim, X. Liu, C. Liu, C.-H. Lo, G. Lopes, S. Lorkowski, R. Lozano, G. Lucchetti, A.A. Maghazachi, P.W. Mahasha, S. Mahjoub, M.A. Mahmoud, R. Mahmoudi, M. Mahmoudimanesh, A.T. Mai, A. Majeed, P. Majma Sanaye, K.C. Makris, K. Malhotra, A.A. Malik, I. Malik, T.H. Mallhi, D.C. Malta, A.A. Mamun, B. Mansouri, H.R. Marateb, P. Mardi, S. Martini, M. Martorell, R.R. Marzo, R. Masoudi, S. Masoudi, E. Mathews, A. Maugeri, G. Mazzaglia, T. Mekonnen, M. Meshkat, T. Mestrovic, J. Miao Jonasson, T. Miazgowski, I.M. Michalek, H.N. Le Minh, G.K. Mini, J.J. Miranda, R. Mirfakhraie, E.M. Mirrakhimov, M. Mirza-Aghazadeh-Attari, A. Misganaw, K.H. Misgina, M. Mishra, B. Moazen, N.S. Mohamed, E. Mohammadi, M. Mohammadi, A. Mohammadian-Hafshejani, M. Mohammadshahi, A. Mohseni, H. Mojiri-forushani, A.H. Mokdad, S. Momtazmanesh, L. Monasta, M. Moniruzzaman, U. Mons, F. Montazeri, A. Moodi Ghalibaf, Y. Moradi, M. Moradi, M. Moradi Sarabi, N.

Morovatdar, S.D. Morrison, J. Morze, E. Mossialos, E. Mostafavi, U.O. Mueller, F. Mulita, A. Mulita, E. Murillo-Zamora, K.I. Musa, J.C. Mwita, S.P. Nagaraju, M. Naghavi, F. Nainu, T.S. Nair, H.H.R. Najmuldeen, V. Nangia, S. Nargus, A.Y. Naser, H. Nassereldine, Z.S. Natto, J. Nauman, B.P. Nayak, R. Ndejjo, H. Negash, R.I. Negoi, H.T.H. Nguyen, D.H. Nguyen, P.T. Nguyen, T. van Nguyen, H.Q. Nguyen, R.K. Niazi, Y.T. Nigatu, D.N.A. Ningrum, M.A. Nizam, L.A. Nnyanzi, M. Noreen, J.J. Noubiap, O.J. Nzoputam, C.I. Nzoputam, B. Oancea, N.M. Odogwu, O.O. Odukoya, V.A. Ojha, H. Okati-Aliabad, A.P. Okekunle, O.C. Okonji, P.G. Okwute, I.I. Olufadewa, O.E. Onwujekwe, M. Ordak, A. Ortiz, U.L. Osuagwu, A. Oulhaj, M.O. Owolabi, A. Padron-Monedero, J.R. Padubidri, R. Palladino, D. Panagiotakos, S. Panda-Jonas, A. Pandey, A. Pandey, S.R. Pandi-Perumal, A.M. Pantea Stoian, S. Pardhan, T. Parekh, U. Parekh, M. Pasovic, J. Patel, J.R. Patel, U. Paudel, V.C.F. Pepito, M. Pereira, N. Perico, S. Perna, I.-R. Petcu, F.E. Petermann-Rocha, V. Podder, M.J. Postma, G. Pourali, N. Pourtaheri, E.J.S. Prates, M.M.F. Qadir, I. Qattea, P. Raee, I. Rafique, M. Rahimi, M. Rahimifard, V. Rahimi-Movaghar, M.O. Rahman, M.A. Rahman, M.H.U. Rahman, M. Rahman, M.M. Rahman, M. Rahmani, S. Rahmani, V. Rahmanian, S. Rahmawaty, N. Rahnavard, B. Rajbhandari, P. Ram, S. Ramazanu, J. Rana, N. Rancic, Ranjha, Muhammad Modassar Ali Nawaz, C.R. Rao, D. Rapaka, D.P. Rasali, S. Rashedi, V. Rashedi, A.M. Rashid, M.-M. Rashidi, Z.A. Ratan, S. Rawaf, L. Rawal, E.M.M. Redwan, G. Remuzzi, K.R.R. Rengasamy, A.M.N. Renzaho, L.F. Reyes, N. Rezaei, N. Rezaei, M. Rezaeian, H. Rezazadeh, S.M. Riahi, Y.A. Rias, M. Riaz, D. Ribeiro, M. Rodrigues, J.A.B. Rodriguez, L. Roever, P. Rohloff, G. Roshandel, A. Roustazadeh, G.M. Rwegerera, A.M.A. Saad, M.M. Saber-Ayad, S. Sabour, L. Sabzmakan, B. Saddik, E. Sadeghi, U. Saeed, S. Saeedi Moghaddam, S. Safi, S.Z. Safi, A. Saghazadeh, N. Saheb Sharif-Askari, F. Saheb Sharif-Askari, A. Sahebkar, S.S. Sahoo, H. Sahoo, K.M. Saif-Ur-Rahman, M.R. Sajid, S. Salahi, S. Salahi, M.A. Saleh, M.A. Salehi, J.A. Salomon, J. Sanabria, R.K. Sanjeev, F. Sanmarchi, M.M. Santric-Milicevic, M.A. Sarasmita, S. Sargazi, B. Sathian, T. Sathish, M. Sawhney, M.P. Schlaich, M.I. Schmidt, A. Schuermans, A.-A. Seidu, N. Senthil Kumar, S.G. Sepanlou, Y. Sethi, A. Seylani, M. Shabany, T. Shafaghat, M. Shafeghat, M. Shafie, N.S. Shah, S. Shahid, M.A. Shaikh, M. Shanawaz, M. Shannawaz, S. Sharfaei, B.B. Shashamo, R. Shiri, A. Shittu, K.M. Shivakumar, S. Shivalli, P. Shobeiri, F. Shokri, K. Shuval, M.M. Sibhat, Silva, Luís Manuel Lopes Rodrigues, C.R. Simpson, J.A. Singh, P. Singh, S. Singh, M.S. Siraj, A.A. Skryabina, A.A.M. Sohag, H. Soleimani, S. Solikhah, M.S. Soltani-Zangbar, R. Somayaji, R.J.D. Sorensen, A.V. Starodubova, S. Sujata, M. Suleman, J. Sun, J. Sundström, R. Tabarés-Seisdedos, S.M. Tabatabaei, S.-A. Tabatabaeizadeh, M. Tabish, M. Taheri, E. Taheri, E. Taki, J.J.L. Tamuzi, K.-K. Tan, N.Y. Tat, B.T. Taye, W.A. Temesgen, M.-H. Temsah, R. Tesler, P. Thangaraju, K.R. Thankappan, R. Thapa, S. Tharwat, N. Thomas, J.H.V. Ticoalu, A. Tiyuri, M. Tonelli, M.R. Tovani-Palone, D. Trico, I. Trihandini, J.P. Tripathy, S.J. Tromans, G.M. Tsegay, A.R. Tualeka, D.G. Tufa, S. Tyrovolas, S. Ullah, E. Upadhyay, S.M. Vahabi, A.G. Vaithinathan, R. Valizadeh, K.R. van Daalen, P. Vart, S.B. Varthya, T.J. Vasankari, S. Vaziri, M.v. Verma, G.-I. Verras, D.C. Vo, B. Wagaye, Y. Waheed, Z. Wang, Y. Wang, C. Wang, F. Wang, G.T. Wassie, M.Y.W. Wei, A.H. Weldemariam, R. Westerman, N.D. Wickramasinghe, Y. Wu, R.D. Wulandari, J. Xia, H. Xiao, S. Xu, X. Xu, D.Y. Yada, L. Yang, H. Yatsuya, M. Yesiltepe, S. Yi, H.K. Yohannis, N. Yonemoto, Y. You, S.B. Zaman, N. Zamora, I. Zare, K. Zarea, A. Zarrintan, M.S. Zastrozhin, N.G. Zeru, Z.-J. Zhang, C. Zhong, J. Zhou, M. Zielińska, Y.T. Zikarg, S. Zodpey, M. Zoladl, Z. Zou, A. Zumla, Y.M.H. Zuniga, D.J. Magliano, C.J.L. Murray, S.I. Hay, T. Vos, Global, regional, and national burden of diabetes from 1990 to 2021, with projections of prevalence to 2050: a systematic analysis for the Global Burden of Disease Study 2021, Lancet 402 (2023) 203–234. https://doi.org/10.1016/S0140-6736(23)01301-6.

[11] K.A. Bowden Davies, S. Pickles, V.S. Sprung, G.J. Kemp, U. Alam, D.R. Moore, A.A. Tahrani, D.J. Cuthbertson, Reduced physical activity in young and older adults: metabolic and musculoskeletal implications, Ther. Adv. Endocrinol. Metab. 10 (2019) 2042018819888824. https://doi.org/10.1177/2042018819888824.

[12] M. Pfinder, T.L. Heise, M. Hilton Boon, F. Pega, C. Fenton, U. Griebler, G. Gartlehner, I. Sommer, S.V. Katikireddi, S.K. Lhachimi, Taxation of unprocessed sugar or sugar-added foods for reducing their consumption and preventing obesity or other adverse health outcomes, CDSR 4 (2020) CD012333. https://doi.org/10.1002/14651858.CD012333.pub2.

[13] M.B. Vos, J.L. Kaar, J.A. Welsh, L.V. van Horn, D.I. Feig, C.A.M. Anderson, M.J. Patel, J. Cruz Munos, N.F. Krebs, S.A. Xanthakos, R.K. Johnson, Added Sugars and Cardiovascular Disease Risk in Children: A Scientific Statement From the American Heart Association, Circulation 135 (2017) e1017-e1034. https://doi.org/10.1161/CIR.0000000000000439.

[14] Q. Yang, Z. Zhang, E.W. Gregg, W.D. Flanders, R. Merritt, F.B. Hu, Added sugar intake and cardiovascular diseases mortality among US adults, JAMA Intern. Med. (JAMA Internal Medicine) 174 (2014) 516–524. https://doi.org/10.1001/jamainternmed.2013.13563.

[15] J. Villar, J.H. Short, G. Lighthall, Lactate Predicts Both Short- and Long-Term Mortality in Patients With and Without Sepsis, Infect. Dis. 12 (2019) 1178633719862776. https://doi.org/10.1177/1178633719862776.

[16] Aldeam Facey, Rachael Irving, Lowell Dilworth, Overview of Lactate Metabolism and the Implications for Athletes, Am. J. Sports Sci. 1 (2013) 42–46. https://doi.org/10.12691/ajssm-1-3-3.

[17] G.A. Brooks, Lactate as a fulcrum of metabolism, Redox Biol. 35 (2020) 101454. https://doi.org/10.1016/j.redox.2020.101454.

[18] D. Hanahan, R.A. Weinberg, Hallmarks of cancer: the next generation, Cell 144 (2011) 646–674. https://doi.org/10.1016/j.cell.2011.02.013.

[19] V. Pucino, M. Bombardieri, C. Pitzalis, C. Mauro, Lactate at the crossroads of metabolism, inflammation, and autoimmunity, Eur. J. Immunol. 47 (2017) 14–21. https://doi.org/10.1002/eji.201646477.

[20] Grand View Research, Glucose Biosensors Market Size And Share Report, 2030, 2025. https://www.grandviewresearch.com/industry-analysis/glucose-biosensors-market (accessed 4 May 2025).

[21] G. Wani, M. Faizullabhoy, Lactate Meters Market Size & Share Report, 2025 – 2034. https://www.gminsights.com/industry-analysis/lactate-meters-market (accessed 4 May 2025).

[22] K. Rathee, V. Dhull, R. Dhull, S. Singh, Biosensors based on electrochemical lactate detection: A comprehensive review, Biochem. Biophys. Rep. 5 (2016) 35–54. https://doi.org/10.1016/j.bbrep.2015.11.010.

[23] Clarivate Analytics, Web of science glucose and lactate sensor report. www.webofscience.com (accessed May 04th 2025).

[24] B.L. Hanssen, S. Siraj, D.K. Wong, Recent strategies to minimise fouling in electrochemical detection systems, Rev. Anal. Chem. 35 (2016) 1–28. https://doi.org/10.1515/revac-2015-0008.

[25] M. Ingelsson, N. Yasri, E.P.L. Roberts, Electrode passivation, faradaic efficiency, and performance enhancement strategies in electrocoagulation-a review, Water Res. 187 (2020) 116433. https://doi.org/10.1016/j.watres.2020.116433.

[26] H. Haripriya, R.S.R. Isaac, One step synthesis of polyvinylpyrrolidone coated silver nanoparticles for the detection of hydrogen peroxide, AIP Conf. Proc. 2270 (2020) 110016. https://doi.org/10.1063/5.0019359.

[27] S.G. Rhee, T.-S. Chang, W. Jeong, D. Kang, Methods for detection and measurement of hydrogen peroxide inside and outside of cells, Mol. Cells 29 (2010) 539–549. https://doi.org/10.1007/s10059-010-0082-3.

[28] M. Zhou, Z. Diwu, N. Panchuk-Voloshina, R.P. Haugland, A stable nonfluorescent derivative of resorufin for the fluorometric determination of trace hydrogen peroxide: applications in detecting the activity of phagocyte NADPH oxidase and other oxidases, Anal. Biochem. 253 (1997) 162–168. https://doi.org/10.1006/abio.1997.2391.

[29] B. Crane, J.P. Hughes, S.J. Rowley Neale, M. Rashid, P.E. Linton, C.E. Banks, K.J. Shaw, Rapid antibiotic susceptibility testing using resazurin bulk modified screen-printed electrochemical sensing platforms, Analyst 146 (2021) 5574–5583. https://doi.org/10.1039/D1AN00850A.

[30] D. Ibáñez, D. Izquierdo-Bote, A. Pérez-Junquera, M.B. González-García, D. Hernández-Santos, P. Fanjul-Bolado, Raman and fluorescence spectroelectrochemical monitoring of resazurin-resorufin fluorogenic system, Dyes Pigment. 172 (2020) 107848. https://doi.org/10.1016/j.dyepig.2019.107848.

[31] T. Doneux, L. Bouffier, B. Goudeau, S. Arbault, Coupling Electrochemistry with Fluorescence Confocal Microscopy To Investigate Electrochemical Reactivity: A Case Study with the Resazurin-Resorufin Fluorogenic Couple, Anal. Chem. 88 (2016) 6292–6300. https://doi.org/10.1021/acs.analchem.6b00477.

[32] G.P. Brotea, R.J. Thibert, Fluorometric determination of hydrogen peroxide using resorufin and peroxidase, Microchem. J. 37 (1988) 368–376. https://doi.org/10.1016/0026-265X(88)90150-6.

[33] V. Towne, M. Will, B. Oswald, Q. Zhao, Complexities in horseradish peroxidase-catalyzed oxidation of dihydroxyphenoxazine derivatives: appropriate ranges for pH values and hydrogen peroxide concentrations in quantitative analysis, Anal. Biochem. 334 (2004) 290–296. https://doi.org/10.1016/j.ab.2004.07.037.

[34] A.Ø. Tjell, B. Jud, R. Schaller-Ammann, T. Mayr, Optical Hydrogen Peroxide Sensor for Measurements in Flow, Sens. Actuators, B (2023) 134904. https://doi.org/10.1016/j.snb.2023.134904.

[35] G. Dehaen, G. Absillis, K. Driesen, K. Binnemans, T.N. Parac-Vogt, (Tetracycline)europium(III) Complex as Luminescent Probe for Hydrogen Peroxide Detection, Helv. Chim. Acta 92 (2009) 2387–2397. https://doi.org/10.1002/hlca.200900184.

[36] D. Zhai, B. Liu, Y. Shi, L. Pan, Y. Wang, W. Li, R. Zhang, G. Yu, Highly sensitive glucose sensor based on pt nanoparticle/polyaniline hydrogel heterostructures, ACS Nano 7 (2013) 3540–3546. https://doi.org/10.1021/nn400482d.

[37] J. Bae, J. Park, S. Kim, H. Cho, H.J. Kim, S. Park, D.-S. Shin, Tailored hydrogels for biosensor applications, J. Ind. Eng. Chem. 89 (2020) 1–12. https://doi.org/10.1016/j.jiec.2020.05.001.

[38] K. Völlmecke, R. Afroz, S. Bierbach, L.J. Brenker, S. Frücht, A. Glass, R. Giebelhaus, A. Hoppe, K. Kanemaru, M. Lazarek, L. Rabbe, L. Song, A. Velasco Suarez, S. Wu, M. Serpe, D. Kuckling, Hydrogel-Based Biosensors, Gels 8 (2022). https://doi.org/10.3390/gels8120768.

[39] J.V. Alemán, A.V. Chadwick, J. He, M. Hess, K. Horie, R.G. Jones, P. Kratochvíl, I. Meisel, I. Mita, G. Moad, S. Penczek, R.F.T. Stepto, Definitions of terms relating to the structure and processing of sols, gels, networks, and inorganic-organic hybrid materials (IUPAC Recommendations 2007), Pure Appl. Chem. 79 (2007) 1801–1829. https://doi.org/10.1351/pac200779101801.

[40] Hervé This, Molecular Gastronomy: Exploring the Science of Flavor, Columbia University Press, 2006.

[41] E. Jéquier, F. Constant, Water as an essential nutrient: the physiological basis of hydration, Eur. J. Clin. Nutr. (European Journal of Clinical Nutrition) 64 (2010) 115–123. https://doi.org/10.1038/ejcn.2009.111.

[42] M. Bauer, A. Duerkop, A.J. Baeumner, Critical review of polymer and hydrogel deposition methods for optical and electrochemical bioanalytical sensors correlated to the sensor's applicability in real samples, Anal. Bioanal. Chem. 415 (2023) 83–95. https://doi.org/10.1007/s00216-022-04363-2.

[43] C. Schmittlein, R.J. Meier, L. Sauer, G. Liebsch, J. Wegener, Image-Based Monitoring of Oxygenation in Microfluidic Cell Culture, Genet. Eng. Biotechnol. News 39 (2019) 87–89. https://doi.org/10.1089/gen.39.01.18.

[44] Y. Feng, J. Cheng, L. Zhou, X. Zhou, H. Xiang, Ratiometric optical oxygen sensing: a review in respect of material design, Analyst 137 (2012) 4885–4901. https://doi.org/10.1039/c2an35907c.

[45] H.D. Duong, J.I. Rhee, Development of Ratiometric Fluorescence Sensors Based on CdSe/ZnS Quantum Dots for the Detection of Hydrogen Peroxide, Sensors 19 (2019). https://doi.org/10.3390/s19224977.

[46] P. Wu, X. Hou, J.-J. Xu, H.-Y. Chen, Ratiometric fluorescence, electrochemiluminescence, and photoelectrochemical chemo/biosensing based on semiconductor quantum dots, Nanoscale 8 (2016) 8427–8442. https://doi.org/10.1039/C6NR01912A.

[47] M. Schäferling, A. Dürkop, Intrinsically Referenced Fluorimetric Sensing and Detection Schemes: Methods, Advantages and Applications, in: U. Resch-Genger (Ed.), Standardization and Quality Assurance in Fluorescence Measurements I: Techniques (Springer Series on Fluorescence), Springer, Berlin Heidelberg, 2008, pp. 373–414.

2 Recent advances and trends in optical devices and sensors for hydrogen peroxide detection

---

2.3 Abstract

Hydrogen peroxide (H_2O_2) is a critically important, vital biomarker and hence a highly relevant analyte in a broad range of bioanalytical applications. The most recent trends furthering the ability of its reliable, reproducible, and sensitive quantification include the development of non-biological enzyme mimics, the investigation of smartphone cameras as transducers and detectors, and the continued development of semi-reversible and reversible detection strategies. While the non-biological catalysts offer stability-related advantages over enzymes while providing equally good limits of detection, critical questions regarding toxicity, persistence, (bio)accumulation, and overall environmental footprint need to be answered. In the case of heavy metal-based strategies a replacement by non-toxic, renewable alternatives should be an obvious research need. Signal recording has seen a dramatic change toward smartphones, with their ever-improving computing and image-acquisition abilities. Yet, with the sheer number of different camera and phone models progress can be difficult to assess, as reproducibility and comparability of results and experimental set-ups are too often elusive. In the area of semi-reversible sensors flow injection analysis (FIA) coupled with chemiluminescence (CL) remains the most advanced system. In the case of fully reversible sensors, research points toward oxygen-based sensing to be the most reliable. Analyzing publications from 2018-2024, it is not surprising that the important analytical figures of merit of low limits of detection (LODs), broad quantitation ranges, faster response and regeneration times combined with novel (reversible) probes continue and should remain central focus of future developments.

Keywords: H_2O_2, Hydrogen Peroxide, optical detection, optical sensors, single-use devices, HRP, Enzyme mimic, smartphones

2.4 Introduction

Hydrogen peroxide (H_2O_2) plays a significant role in numerous physiological processes including, metabolic functions, apoptosis [1], cell-signaling [2] and immune-cell activation [3–5]. Its significance as an indicator of oxidative stress [6], a defense mechanism, and a contributor to aging is well-established [7,8]. It serves as a vital biomarker for various diseases, such as diabetes [9], cancer and has potential to be used in treatment of the latter [10], Parkinson's [11], cardiovascular diseases [12], Alzheimer's [13], and neurodegenerative disorders [14]. In food safety and quality, H_2O_2 is an important analyte, due to its use as food adulterant for example in milk, in many cases above allowed and thus potentially harmful concentrations [15].

The quantitation of H_2O_2 may be combined with oxidases of the large group of H_2O_2-producing enzymes, such as glucose, cholesterol, lactate, and glutamate oxidases, or with catalase as a H_2O_2-degrading enzyme. These coupled reactions allow for the development of sensors and bioassays that rely on H_2O_2 detection to quantify both enzyme substrates or products, thus widening the scope of probes for H_2O_2 [16–18]. Consequently, the ongoing research in (bio)sensors based on the detection for H_2O_2 has found applications and is of interest in fields including medical diagnostics [19], clinical research, food chemistry [20] and environmental investigations [21]. Furthermore, with the increasing use of peroxide-based explosives, such as triacetone peroxide in terrorist attacks, H_2O_2 as a residual precursor and indicator has unfortunately also become an important analyte to ensure the safety of first responders and security personnel [22].

Electrochemical and optical methods are the two major techniques broadly used for analysis and quantification of H_2O_2. Electrochemical devices are more frequently developed, more commonly published, usually offer fast response times and are in principle also applicable to continuous monitoring. The interfering challenges caused by other electroactive species present in various matrices at higher concentrations, such as vitamin C or uric acid, have long been solved by using a second redox reagent that is oxidized by H_2O_2 acting as a mediator or by using electrodes with selectively active or catalytic electrode surfaces and materials that can then detect specifically H_2O_2 at lower potentials [20]. Especially interesting is the development of reversible electrochemical systems [23]. Yet, electrode fouling is a serious issue not to be underestimated in real samples.

Optical H_2O_2 detection and quantification is often performed with commercially available assay kits, such as the colorimetric 3,3′,5,5′-Tetramethylbenzidin (TMB)/HRP or the fluorometric Amplex red/HRP-assay. However, these assays require several preparation steps with buffer addition, and calibration via dilution series thus increasing assay time and the chance for erroneous data due to human error. Furthermore, sample preparation can require further steps as the dye and the enzyme have to be stored separately and at different temperatures, as it is the case for the Amplex Red assay. While the fluorescent and strongly pink reaction product resorufin that forms upon action of HRP or of other catalysts in presence of H_2O_2, is useful for both fluorometric [24] and colorimetric [25] detection, its applicability is limited due to an autocatalytic degradation of Amplex Red to resorufin when exposed to light [26]. In the past, detection methods based on the interaction of nanomaterials [27] or peroxidase [28] with H_2O_2 and the resulting optical change have also been developed and successfully used.

It is hence not surprising, considering the importance of H_2O_2 detection and the limited optical detection strategies that over the last two decades, a true plethora of H_2O_2-sensitive photoluminescent probes has been developed [29], many of which are in the field of organoboron-based probes [30–32]. These innovative fluorescent probes are applied for assay development and more importantly for cellular imaging, The experimental utilization of these innovative fluorescent probes is typically applied to standard bioassays and more importantly for cellular imaging. Unfortunately, most of the probes show an irreversible reaction with H_2O_2, making them useless for continuous or reversible measurements, and are thus far from the ideal chemical sensor [33]. Yet, they are often referred to as sensors irrespective of the definition IUPAC definition given in 1991 [34] requiring both a receptor and a transducer.

In many application scenarios, simpler and cheaper single-use disposable devices are preferrable over expensive and complex sensors, especially in point-of-care settings where factors like cross-contamination or harsh conditions would affect results negatively. These devices offer easy and cost-effective diagnostic and quantification capabilities, reducing the need for complex laboratory equipment and potentially lowering healthcare costs, such as pregnancy, COVID or glucose tests. Much recent research focuses on developing single-use devices for H_2O_2, which, when combined with H_2O_2 generating enzymes, facilitate the quantification of various biomarkers on-site. At this point, such point-of-care devices complement traditional sensors for H_2O_2, offering simple and rapid determination methods, while the latter may be preferred for

more demanding online quantitation requiring higher instrumental effort over an extended period of time.

An additional challenge researchers will commonly encounter for optical applications when working with complex (biological) media and samples such as whole blood is having to overcome opacity and autofluorescence. Furthermore, the presence of catalases (which, to add to the nuisance are of course not present in the same concentration in every person [35]) and other H_2O_2-degrading species make the quantification of H_2O_2 both time sensitive and thus unreliable, which to some degree could explain the concentration discrepancy and range reported in literature [36].

This critical review provides insight into the trends of recent (2018 – mid 2024) optical sensing devices and sensors for the detection of H_2O_2 focusing on colorimetric, chemiluminescent, photoluminescent detection and surface plasmon resonance approaches. In analyzing the trends, the authors decided that papers exclusively reliant on liquid assays conducted within cuvettes and microtiter plates, or applications restricted solely to imaging or (surface enhanced) Raman spectroscopy, were deliberately excluded from the article, with the latter having been reviewed recently [37]. Instead, focus is on studies encompassing a broader spectrum of novel, innovative methodologies and applications, ensuring a more diverse and comprehensive examination of the subject matter. Based on our literature analysis and the IUPAC definition of sensors and their possible classifications [34] we have categorized applications and devices into three groups:

- Single-use sensors and systems featuring a non-reusable detection/sensing module, exemplified by paper-based devices.
- Intermediate sensors and semi-reversible systems, in accordance with the classification by Moßhammer et al. [36], encompassing devices and sensing applications capable of semi-continuous detection. This involves the consistent introduction of reagents, akin to flow injection analysis (FIA), or relying on reactions reversible by external factors such as light, temperature, addition of redox reagents, or potential cycling to facilitate the regeneration of sensing capability.
- Fully reversible sensors.

Herein, we highlight innovative devices and sensors employing novel (enzymatic and enzyme mimicking) enhancement strategies and materials, (smartphone) detection and (semi) reversible and continuous sensors.

2.5 Single-use sensors and systems for quantitation of H2O2

2.5.1 Novel (enzymatic) enhancement strategies and materials

2.5.1.1 Enzymatic detection

Detection of H_2O_2 with HRP as a catalyst/recognition element is a classical way of signal generation. The commercial availability of this reasonably inexpensive enzyme has resulted in an abundance of published protocols demonstrating its rapid reaction kinetics under mild reaction conditions ideal for biological and bioanalytical applications. Standard protein chemistry allows conjugation to various (bio)molecules, immobilization and its use as a signal enhancement strategy. However, similar to most enzymatic applications it is susceptible to inhibition by interferences. In the case of HRP, cyanide, azide, hydroxylamine, and some heavy metal ions are most known for reaction inhibition. Furthermore, a higher background signal due to non-specific enzymatic conversion in the absence of H_2O_2, a high pH dependent activity, a poor stability when exposed to higher temperatures and organic solvents limit HRP's application and calls for more research [38].

In order to increase the stability of HRP and reduce the experimental assay complexity some research focuses on the encapsulation or immobilization of HRP in a suitable matrix such as a polydimethylsiloxane (PDMS) layer with a GPT linker [39], in a carbon dot-doped hydrogel sensor array [40], as enzyme-inorganic nanoflowers made from EDTA, $CaHPO_4$ and HRP [41], gold nanoparticle(AuNP)-enzyme [42] or HRP-BSA AuNP nanoclusters [43]. The respective approaches hone in on providing a reusable and simple CL-platform by Bocanegra-Rodríguez et al. [39] to achieve an LOD of 0.02 $\mu mol \cdot L^{-1}$ range 0.06 - 10 $\mu mol \cdot L^{-1}$ (see table 1), a multiplexing, PDMS-housed sensing array for H_2O_2 mediated colorimetric detection of wound related biomarkers such as glucose and uric acid and non-H_2O_2 mediated like pH, total protein and urea with good accuracy by Zheng et al. [40], enabling colorimetric H_2O_2 detection with TMB was developed by Tian et al. whose nanoflowers maintained 90% activity over 30 days at -20°C, offering potential in applications like prostate cancer screening and water quality monitoring and achieving an LOD of 1 $\mu mol \cdot L^{-1}$ and an analytical range of 2 – 100 $\mu mol \cdot L^{-1}$ [41], integration of luminescent HRP-Au nanoclusters into a microfluidic droplet device for single-cell secreted H_2O_2 detection by Shen et al. [42] or

the encapsulation of advanced HRP-BSA AuNP nanoclusters [43] into a glass-based microfluidic device limited to visual detection and an LOD of 0.5 $nmol \cdot L^{-1}$ and a reasonably broad analytical range of 0.5 – 50 $nmol \cdot L^{-1}$ in cuvette-measurements (Figure 2.1). However, for a better comparability of the performance in the cuvette and of the microfluidic device, a signal data acquisition of the HRP-encapsulated fluorescent bio-nanoparticles (HEFBNPs) beyond mere detection with eye-vision, especially considering the impressively low LOD and analytical range, would have been desirable.

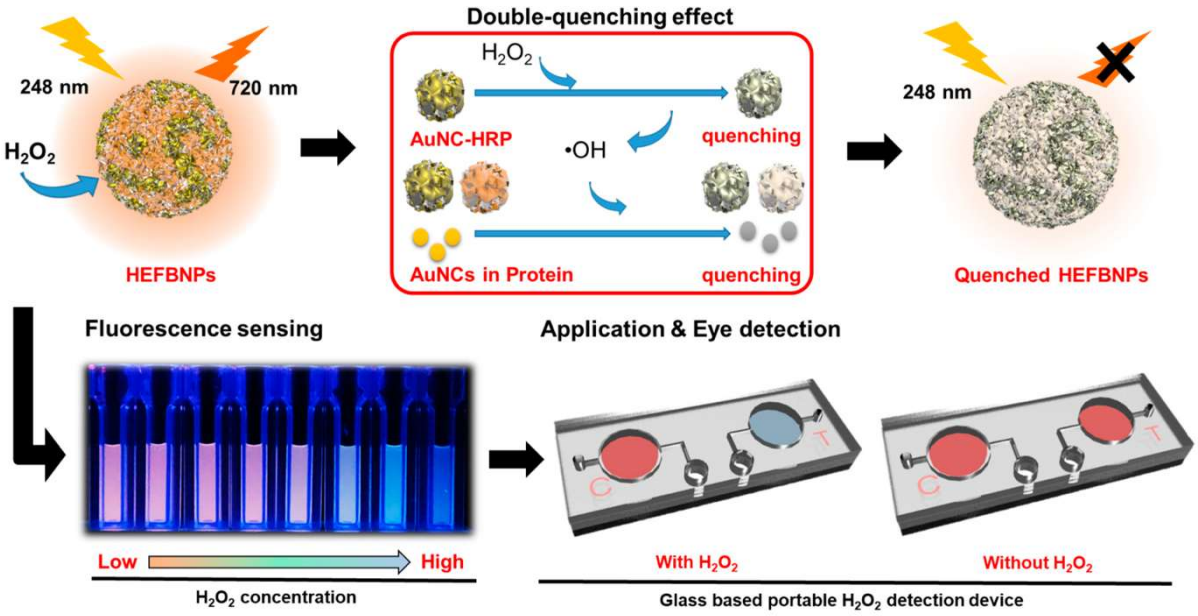

Figure 2.1: Schematic illustration of the quenching mechanism of the innate Au-nanoclusters HEFBNPs fluorescence by addition of H2O2 and its applications. Reprinted with permission from [43]. ©MDPI

Goicoechea et al. [44] developed a self-referenced optical fiber sensor for H_2O_2 detection based on localized surface plasmon resonance (LSPR) of metallic nanoparticles in layer-by-layer (LbL) films. The sensor utilizes a LbL nanoassembly technique to fabricate sensitive nanocoatings on the optical fiber core. The nanocoatings incorporate both silver nanoparticles (AgNPs) and gold nanoparticles (AuNPs), which exhibit different sensitivities to H_2O_2. The LOD of the sensor is estimated to be 2.7 ppm and allowed for compensation of light source fluctuations, sensor drift and measurements of a total of 40 min. Unfortunately, the signal from the LSPR absorption bands was noisy impacting signal quality, in the current setup, presumably due to dipping of the sensor into solutions, instead of using a flow-system, which would have been desirable. While the sensor did show no to very little signal change in presence of interferents such as Hanks' Balanced Salt Solution (HBSS),

glucose and ascorbic acid, a measurement in a real 'live' cell culture or any other complex matrix to see the effect of cell matter and proteins on the sensor would have been interesting.

Main focus on paper-based colorimetric enzyme-based devices using HRP take advantage of smartphones for signal recording. For Galbán [25], Amplex red provided significantly better LODs as demonstrated for the precise and reproducible detection of histamine/tyramine and H_2O_2 than using TMB or ABTS, as their approach avoids the issue of lateral reactions such as the oxidation of the dye by the aldehyde forming in the oxidation step of histamine. Yet, as indicated in the introduction, both Amplex Red and the respective peroxide-generating enzymes require refrigeration for storage inhibiting the applicability in the field. In the case of Hosu et al. [45] a poly(aniline-co-anthranilic acid) (ANI-co-AA) composite film was used as substrate. It was applied in a multiplexing platform reaching LODs of 34.6 $\mu mol \cdot L^{-1}$ by spectrophotometric detection and 51 $\mu mol \cdot L^{-1}$ with the smartphone, thus not providing the most sensitive device, an acceptable trade-off for its simplicity in use, a 2 min assay time, the multiplexing assay and the accessibility of the smartphone readout. The advantage of the of the film material was, that it could not just act as carrier/immobilization membrane for the enzyme, but also as chromogenic reagent. Lima et al. [46] used guaiacol in a paper-based device with wax-printed wells together with self-extracted peroxidase from zucchini for the detection and quantification of H_2O_2 in milk. With a linear calibration between 1.25 $mmol \cdot L^{-1}$ and 15 $mmol \cdot L^{-1}$ they were able to achieve an LOD of 0.354 $mmol \cdot L^{-1}$ and an LOQ of 1.18 $mmol \cdot L^{-1}$ respectively. In spiked milk samples, they were able to achieve recovery values between 92.2 % - 108 % whilst maintaining relative standard deviations below 6.5 %. Guaiacol is hence an interesting substrate as it delivers appropriate detection limits while being much cheaper than other colorimetric substrates.

2.5.2 Enzyme mimic-based and catalysis-enhanced sensing

Synthetic enzyme mimics or nanozymes have proven to be a true gamechanger in the field of optical sensing of hydrogen peroxide. In the last 15 years, the development of synthetic materials with alleged peroxidase activity has been increasingly successful [47] with their use being reported in several electrochemical sensors [48]. Initial papers describe the use of Fe_3O_4-NPs and graphene derivatives. Currently, other nanomaterials dominate the research landscape. Such studies are e.g. based on the structural and surface modification of already existing mimics, of new metal organic frameworks (MOFs) including their surface activation/increase, and the search for

more sustainable synthesis and precursors/educts. So called enzyme mimics or nanozymes are supposed to overcome issues such as storage & temperature stability, limitations of pH dependent activity; and can provide a tunable activity [49,50]. As with any nanomaterial, one of the major issues is the reproducibility of their synthesis, size, homogeneity, and batch-to-batch variations. Crucial questions regarding toxicity have to be addressed before moving to *in-vivo* or clinical applications. Of equal importance is the environmental impact where release into the environment is possible, a consideration that is unfortunately rather rare in literature.

Also in optical assay strategies these peroxidase mimicking artificial enzymes are increasingly employed [51,52]. Major advances made over the last years include the development gel-based matrices with peroxidase-mimicking ability and the integration of novel synthetic enzyme surrogates in paper-based devices. In the first case, the list of such novel gel-based devices include, a capillary array-based colorimetric platform to detect H_2O_2 in milk with sodium alginate coated Fe_3O_4-NPs and TMB showing an enhanced catalytic activity [53] in comparison to 'naked' NPs, a Cu(II)/Co(II) bimetallic organic gel with enhanced peroxidase-like activity, requiring 20 min at 45 °C [54], a dual-use $PtNi_3$ hydrogel with high stability, selectivity and reproducibility as electrocatalyst for electrochemical and as peroxide-like nanozyme with TMB for the colorimetric detection of H_2O_2 secreted from HELA cells in a custom-made portable colorimetric sensor [55] or the development of a chemiluminescent glucose POC device with a peroxidase-like hemin containing guanosine hydrogel loaded with luminol in analytical cartridges for smartphone detection [56] (Figure). In all of these assays the used mimics showed competitive catalytic activity in comparison to HRP or were able to provide catalytic activity in HRP-adverse conditions.

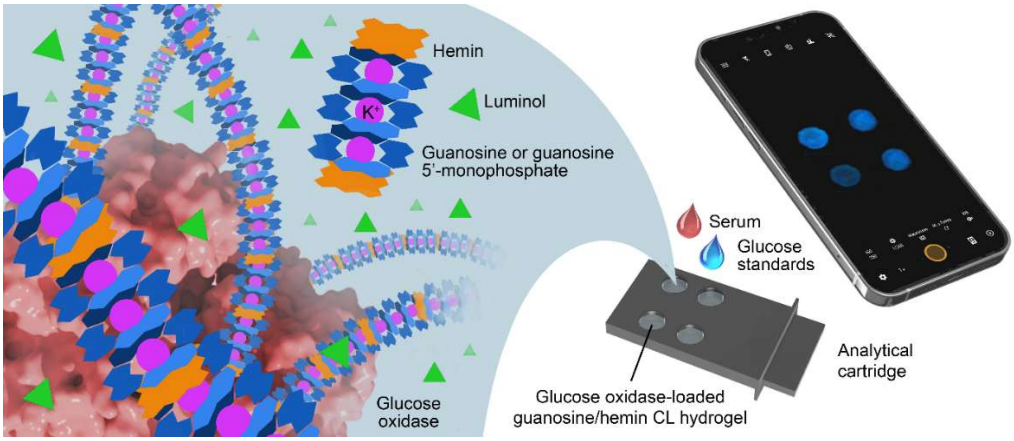

Figure 2.2: Illustration of the peroxidase-mimicking G-quadruplex guanosine-derived hydrogel loaded in analytical cartridges for chemiluminescent detection of glucose and H2O2 for smartphone-based detection as developed by Calabria et al. Reprinted with permission from [56]. ©2023 MDPI.

In the case of paper-based strategies, innovation afforded through an enzyme mimic is paired with the unique advantages of the simplistic, yet adaptable assay format. Listed here are a few especially interesting publications that have demonstrated applicability in real matrices in all cases. For example, sericin-capped AgNPs were integrated into a paper-based origami folding device whereby folding the paper-based device the sample flows through the enzyme layer (for the glucose device) or the enzyme mimic layer before reaching the TMB reagent (Figure). This origami layout allowed for both, the separation of the reagents and catalysts/enzymes and showed improved assay speed in comparison to 'classical' paper-based devices [57].

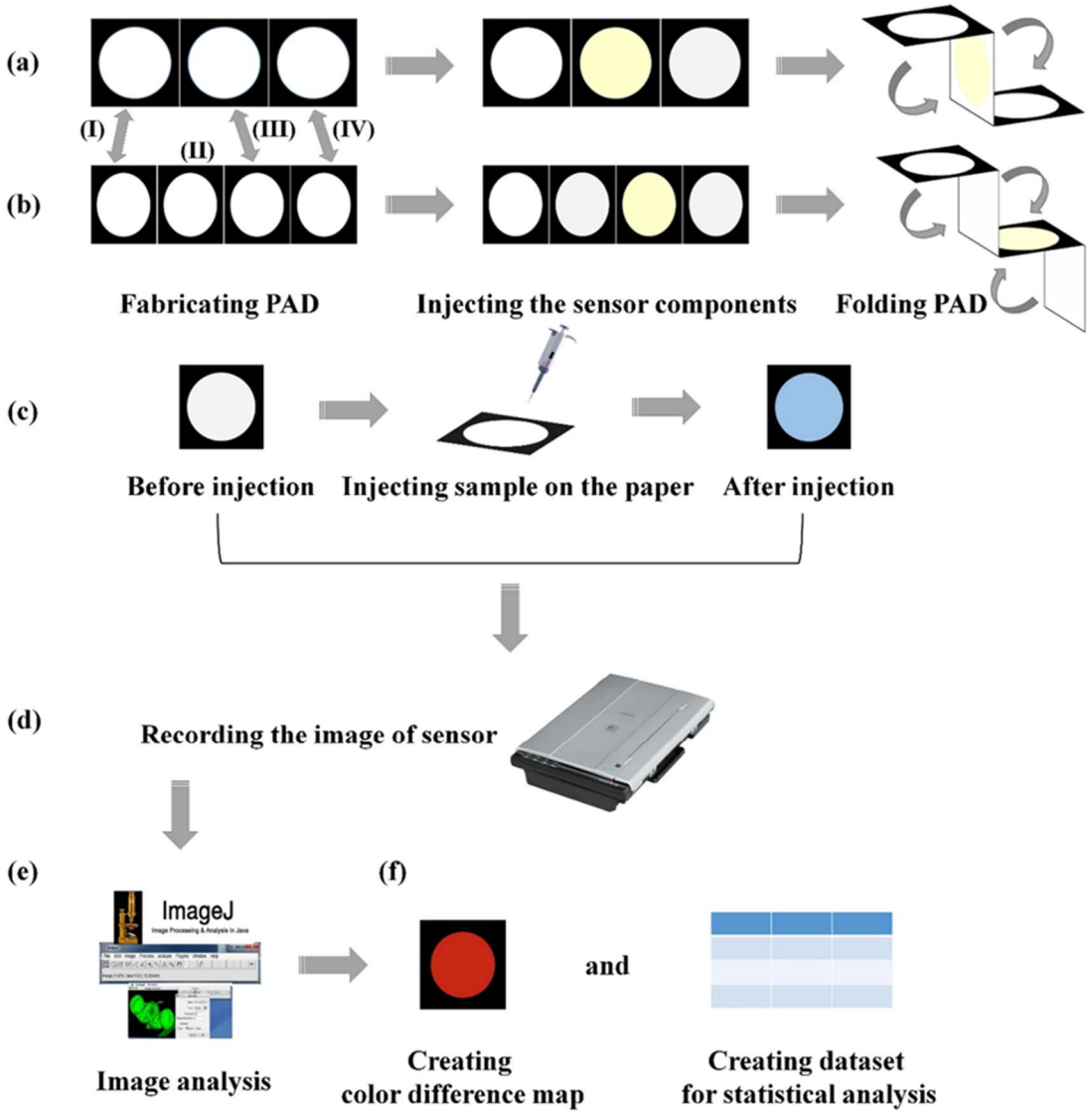

Figure 2.3: Mirzaei et al developed a paper-based origami folding device for the detection of glucose and H2O2. Layout and design of the devices for (a) H2O2 and (b) glucose detection. With (I) injection, (II) GOx (glucose-detection exclusive), (III) nanozyme and (IV) detection layer). (c) Assay procedure and colorimetric change. (d) Recording the image of sensor before and after exposing to analyte. (e) Image analysis in ImageJ, (f) evaluation of color difference map. Reprinted with permission from [57]. ©2023 Springer.

Cheng et al utilized mesoporous CuO hollow sphere nanozymes in a paper-based device for a smartphone-based readout [53]. However, the authors fail to mention any specifics regarding, lighting and camera settings and how the smartphone was held in position. Cellulose membranes with immobilized Au nanoclusters acting as peroxidase mimic for the detection of H_2O_2 and uric acid were proposed by Wei et al. [58]. Peroxidase mimicking MoS_2-$SrTiO_3$ [59] and alginate-gel stabilized MoS_2@$CoTiO_3$ [60] nanocomposites for colorimetric detection of H_2O_2 with TMB were applied in paper-based formats. Research on cellulose nanofibrils/Fe-doped carbon dot composite nanopapers for the smartphone-based colorimetric detection of H_2O_2 and glucose was published by Bandi et al. [61]. Most notably, the group was able to recycle and reuse the test strips with the enzyme mimic with treatment of 0.1 mol·L^{-1} ascorbic acid, followed by washing steps up to 10 times without a significant loss of activity. The group of Qui [62] used self-assembled nanocomposite Pd-Pt@hemin-rGO/CNTs-COOH in paper-based indicator strips with TMB for the detection of H_2O_2. Beng et al. synthesized carbon dots co-doped with B, N, and S for smartphone-based colorimetric detection of H_2O_2 in samples like milk and mouthwash [63]. Another group [64] used molybdenum oxide quantum dots (MoOx QDs) showing peroxidase-like activity on a microfluidic paper-based analytical device for the rapid colorimetric detection of H_2O_2 released from PC12 cells with ABTS as dye. The paper-based device was able to detect H_2O_2 with an LOD of 0.175 µmol·L^{-1} after an assay time of 10 min.

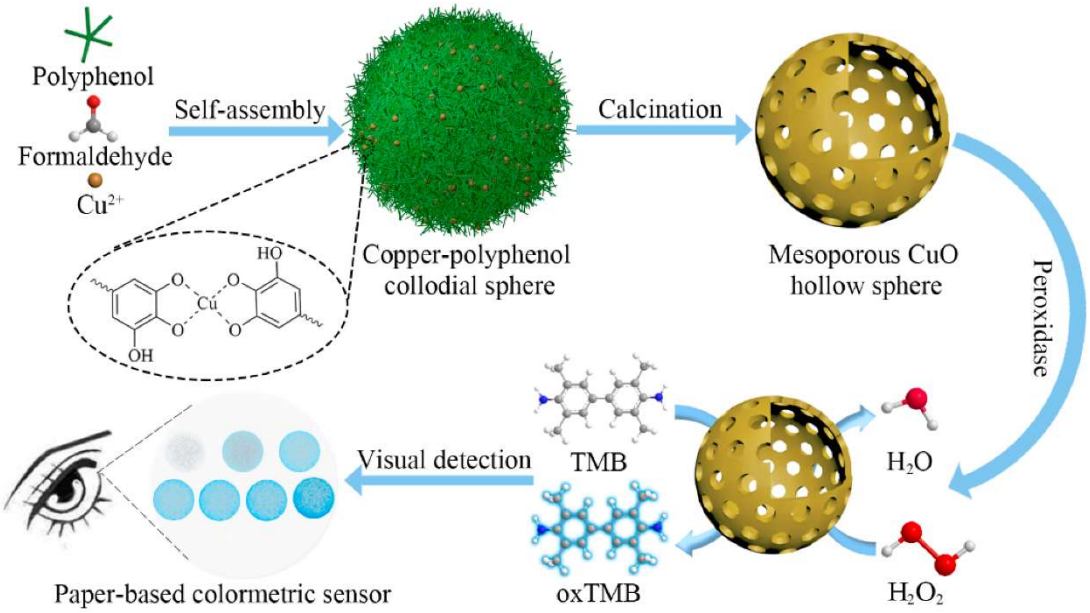

Figure 2.4: Cheng et al. developed a paper-based platform with mesoporous CuO hollow sphere nanozymes as peroxidase mimic for the colorimetric detection of H2O2. Reprinted with permission from [65]. ©2021 MDPI

Overall enzyme mimics can provide an innovative and intriguing alternative to classical enzymatic catalysis in H_2O_2 detection. Aside from the general limitations and issues aforementioned, it is crucial to see more benchmark experiments with HRP in place of the mimic. Only this would allow for true comparability and as proof of an actual improvement or advantage of the mimics over the enzyme. Few researchers spend time and resources on such often enough tedious comparison studies since assay parameters for enzymes and mimics differ. Thus, such parameter misalignment when done poorly, will potentially compromise comparability once more. Furthermore, the terms or rather neologisms nanozyme and enzyme mimics are often coined to new catalysts with improved surface structures or combinations of metals employed in reactions that result in the same detectable product as with an enzymatic reaction, i.e. TMB in a Fenton-type reaction without the peroxidase-typical two-electron process. Often Michaelis-Menten kinetics for single-enzyme, single-substrate [66] systems are used despite the often-encountered two-substrate mechanism [53] where other kinetic models, such as Langmuir-Hinselwood [67] are better suited to describe the observed reaction time course. Furthermore, a sufficient saturation with substrate or the amount of catalytically active surface or centers in comparison to the used weight is often ignored. That raises the question if the employed substances qualify for the term nanozyme or enzyme mimic and, if needed in excessive amounts 600 $\mu g \cdot mL^{-1}$ of Fe_3O_4 QDs vs 500 $\mu g \cdot mL^{-1}$ TMB [53], even as a catalyst or just as a stochiometric reagent [68].

In the field of catalytically enhanced H_2O_2-sensing, next-generation probes have provided much advancement in the detection of H_2O_2. Huang et al. developed a biocompatible GelMA hydrogel with encapsulated Mn-containing bioactive glass and $CePO_4$:Tb (CPT-MnBG-Gel) for wound monitoring and H_2O_2 scavenging capabilities for faster wound healing [69] Through chemical modification of luminol, m-carboxyluminol demonstrated an enhanced CL-signal [70] and was successfully integrated in µ-pads with the option of a smartphone-based readout [71] where H_2O_2 was detectable with an LOD of 13 µmol·L^{-1} with a range of up to 2000 µmol·L^{-1} and lactate with an LOD of 0.03 mmol·L^{-1} with an analytical range of up to 100 mmol·L^{-1}.

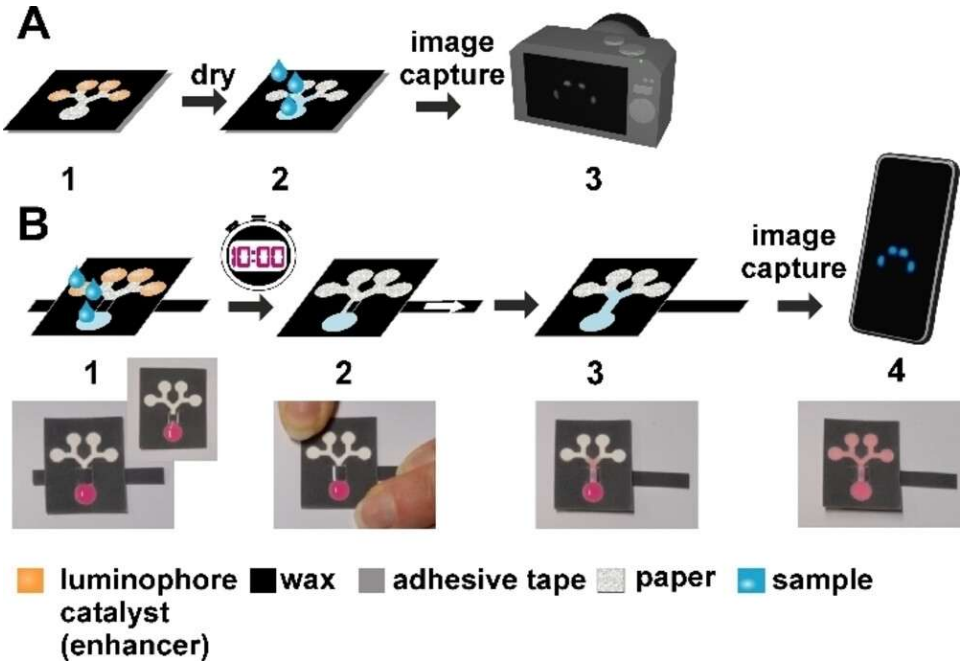

Figure 2.5: Rink et al. present a wax-printed µ-pad with the enhanced CL-reagent carboxyluminol for the smartphone- or CCD-camera based detection of H2O2. Stepwise illustration of the assay procedure in (A) for H2O2 detection and luminophore detection with (1) applying sample to sample zone, (2) signal development and (3) taking images with a CCD camera and in (B) for the L-lactate assay with (1) applying sample to sample zone, incubation for 10 min, (2) opening sample chamber (3) signal development and (4) taking images with either a smartphone or CCD camera, schematic illustration, and real images with sulforhodamine B dye solution for better illustration of liquid flow. Reprinted with permission from [71]. ©Wiley 2023.

The integration of previously known catalysts and reagents into paper-based or miniaturized 3D-printed devices are other innovations seen in literature. For chemiluminescent quantification of H_2O_2 in milk, featuring a dedicated variable gain amplification system, and disposable wells with a hydroxyethyl cellulose-based detection membrane, miniaturized 3D-printed devices with disposable cartridges and flow-systems were developed by Vasconelos et. al. [72]. They allowed detection of H_2O_2 down to an LOD of 9 µmol·L^{-1} and a linear range of approximately 30 - 270 µmol·L^{-1}.

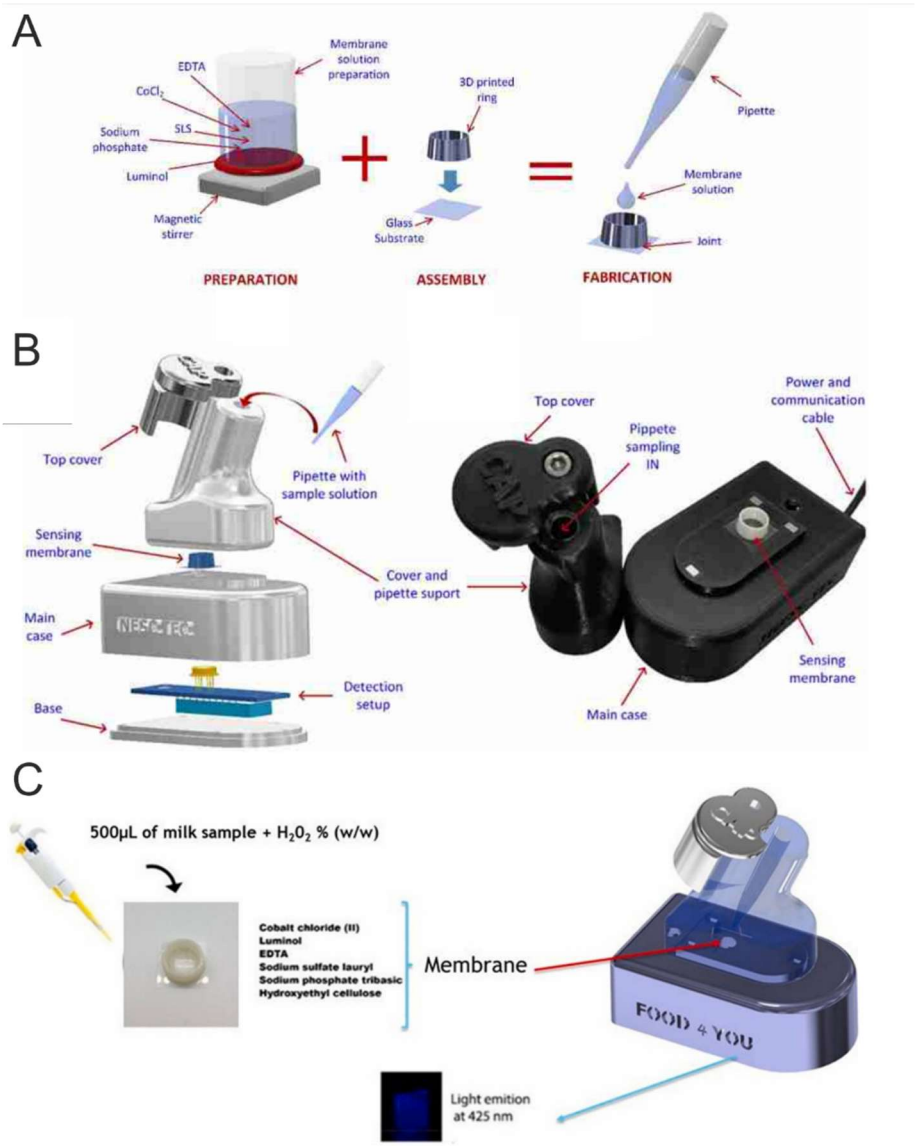

Figure 2.6: A miniaturized 3D-printed device for chemiluminescent quantification of H2O2 in milk developed by Vasconelos et. al. A) Scheme of the sensing membrane fabrication; B) exploded view of the integrated detection module. C) Image of the sensing module and chemiluminescence at 425 nm. Reprinted with permission from [72]. © 2023 Elsevier

Upconverting nanoparticles (UCNPs) have shown to be a valuable approach to work with or in complex biological matrices. Here, the efficiency and reliability of traditional probes and sensors are often challenged by many interfering substances as well as physical, chemical, and biological barriers. UCNPs are nanoparticles based on a nanocrystalline host e.g., $NaYF_4$ or $LiYF_4$ that have the ability to convert low energy NIR light into visible light with higher energy by serial multiphoton excitation steps. The various (and complex) mechanisms of upconversion and the design and variety of upconverting nanoparticles are highly interesting and literally exciting topics that has been reviewed thoroughly elsewhere [73,74]. When doped with Yb^{3+} as sensitizer and

Er^{3+} as acceptor, UCNPs have the capability to be excited close to the optical window of tissue allowing a deep tissue penetration. Moreover, UCNPs offer great optical properties among low autofluorescence, high signal-to-noise ratios, exceptional photostability and non-blinking emission. Despite some issues with UCNPs such as the susceptibility to water quenching and the significantly lower quantum yield and overall brightness in comparison to organic dyes, UCNPs have become an increasingly popular choice and powerful tool for photodynamic therapy approaches as well as sensor and probe development [73,74]. Their applicability for H_2O_2 detection was beautifully demonstrated by Wang et al.'s [75] device with an integrated pump for long-term monitoring of H_2O_2 in ovarian cancer peritoneal metastasis (Figure). Good sensitivity and real-time detection capabilities show promise, yet challenges remain regarding *in-vivo* applicability and long-term stability. Unfortunately, the device is being hamstrung by its detection method with the irreversible oxidation of the used IR820 dye by •OH produced in a Fenton-type reaction, making replacement of the sensing membrane necessary for longer measurements underscoring the need for further research and refinement in this field.

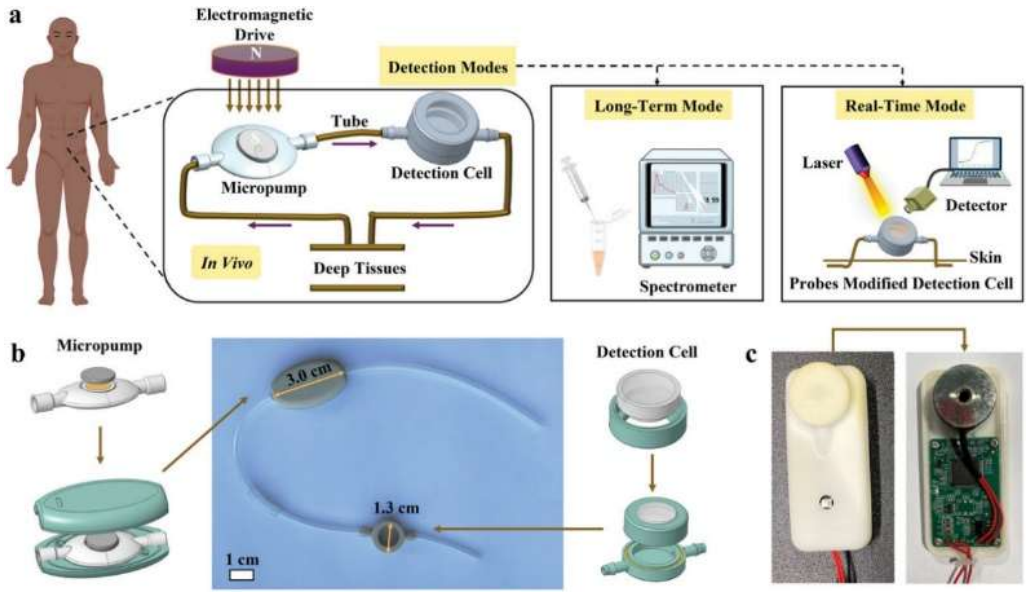

Figure 2.7: Detection modes and devices using UCNP-luminescence as developed by Wang et al. a) Scheme of the developed detection modes for H2O2 via implantable devices. b) Structural schemes and photographs of the fabricated micropump and detection cell. c) Photographs of the electromagnetic-driven device before and after dismantling of the shell. Reprinted from [75] with permission. © 2023 Wiley.

Wu et al. [76] developed a portable dual mode sensing chip combined containing *o*-phenylenediamine (OPD) as colorimetric reagent together with facet-engineered iron-based MOFs as enhanced Fenton-type catalysts and fluorometric agents. In their chip the sample would first be exposed to the MOFs producing •OH and quenching the

MOF fluorescence with a simultaneous emission color shift from blue to yellow. The produced •OH could then be washed to the second pad containing OPD resulting in a colorimetric change. This change in MOF emission and dye color change could be captured with a smartphone. Based on the evaluation of the image with a network model the differentiation between different oxidizing agents, such as permanganate, dichromate, and TATP was possible. In cuvette-based experiments and the ratiometric emission 572 / 447 nm of the MOFs allowed for an LOD of 2.06 nmol·L^{-1}.

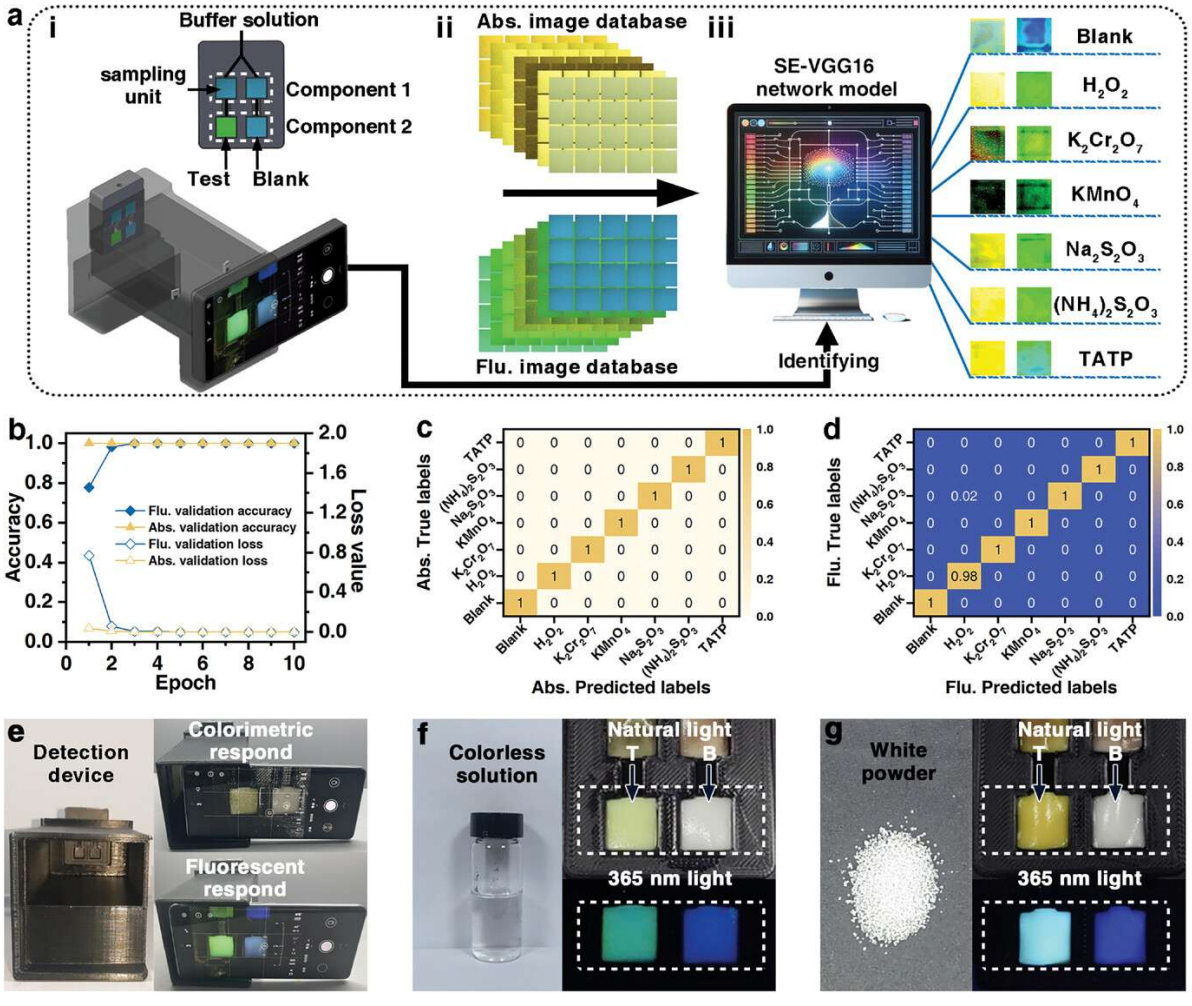

Figure 2.8: Portable dual detection sensing chip by Wu et al. a) Schematic representation of the sensing chip design and image-based network model analysis. B) validation accuracy and loss values of the fluorescent and colorimetric detection modes. Confusion matrices of the c) colorimetric and d) fluorescent detection with different analytes. e) image of the 3D printed chip/smartphone holder and colorimetric and fluorescent response on screen. f) response to colorless analyte solution with 0.3 w% H_2O_2 and g) white powder with 5 w% TATP. Reprinted with permission from [76] © 2024 Wiley

2.5.3 Noncatalytic sensing of H_2O_2

Non-catalytic detection approaches of H_2O_2 are leaner and are often more straightforward than those requiring an additional, catalytic assay component. Typical and recent examples for the detection of H_2O_2 are probes with a boronic-ester group as a recognition element, (quenching of) aggregation-induced emission, sonochemiluminescence, and fluorescence quenching. Obviously, the lack of an enzyme or catalyst as recognition element leads to reduced selectivity as unwanted (faster) reactions with other (oxidizing) reagents occur, such as boronic-ester groups reacting non-specifically also with peroxynitrite, hypochlorous acid and peroxymonophosphate [36]. Also, the lack of a catalyst and hence increased activation energy barrier suggests that additional energy input is needed, or increased assay times occur, possibly limiting the practical application of such devices. That is the case for Dutta and Maitra's [77] paper-based approach utilizing a cholate hydrogel with the deboronation of a sensitizer ligand to then allow the energy transfer of UV-excitation light to the lanthanides Eu^{3+} or Tb^{3+}, respectively. With an incubation time of 1 h and a required temperature of 50 °C the method is both time-consuming and requires an additional heating element to work. Surprisingly, the method shows reasonably good reproducibility and disc to disc variation despite the ‘simple’ drop coating preparation.

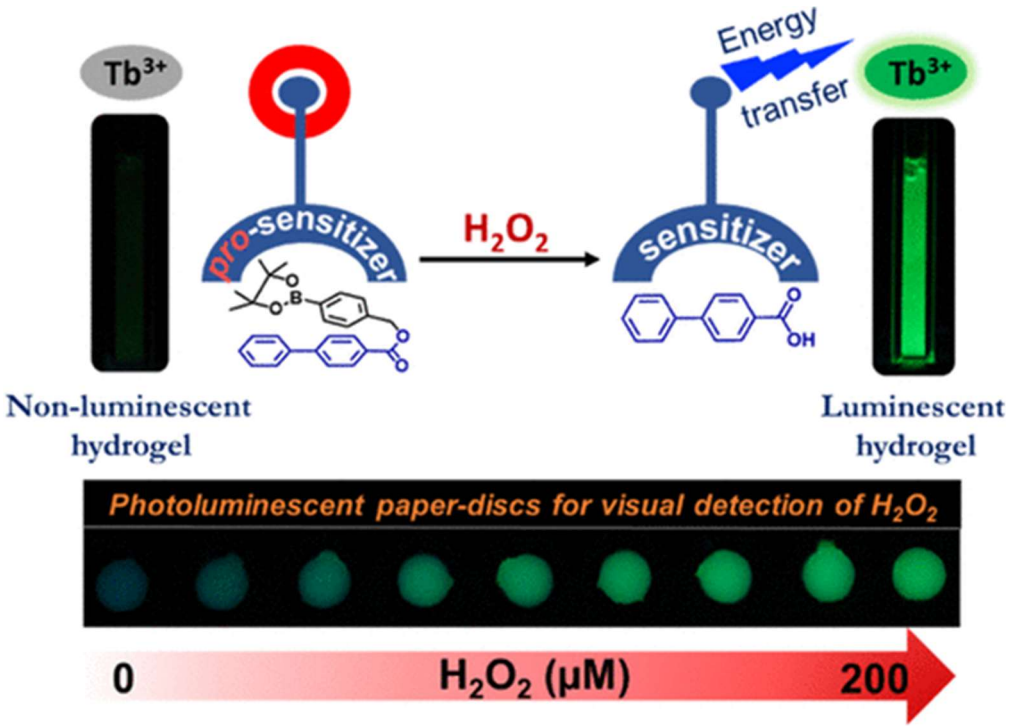

Figure 2.9: Schematic representation of the sensitization of the Tb^{3+} lanthanide hydrogel and images of photoluminescent paper discs with different concentrations of H_2O_2. Reprinted with permission from [77]. ©2022 American Chemical Society.

Cheng et al. [78] used a naphtalimide-based dye with a hexyl backbone and an aryl boronic ester moiety (C6NIB) on an aluminum foil-based silica gel plate sensing platform for the detection of H_2O_2 in vapor. They were able to detect H_2O_2 down to an LOD of 2 ppb with a detection time of only 70 s. For higher concentrations such as 30% H_2O_2, a detection/ response time of 0.5 s could be achieved. However, presumably due to difficulties regarding reproducibility in the production of the films and the and the construction-related measuring time, the authors did not carry out multiple determinations. Similarly, the group of Zhang [79] used pyrene/fluorene-based probes DB-WCZ (with two carbazole groups) forming porous microstructures enhancing the diffusion of H_2O_2 in vapor and DB-W with two aryl boronic-ester moieties, one on the pyrene and the fluorene moiety each, for the fluorometric detection of H_2O_2 and triacetone peroxide (TATP) in vapor. The spin-coated films could detect 2.2 ppb of H_2O_2 with a reasonably good reproducibility.

Xu et al. [80] integrated a fluorescent ratiometric probe for smartphone-based detection of H_2O_2 into a paper-based device or a miniaturized portable 3D printed testing system with an integrated UV light excitation source. They used a flavonoid dye with an organoboron H_2O_2-reactive moiety that can bind or coordinate to the hydrophobic drug reception sites in albumin in a 1:1 ratio resulting in both, an enhancement and a blue shift of the observed fluorescence reaching an emission maximum after about 5 min assay time. In a titration assay, the flavonoid/albumin probe (HFPQ@ALB) could reach an LOD of approximately 3.5 $\mu mol \cdot L^{-1}$ and a linear range of up to 50 $\mu mol \cdot L^{-1}$. With the smartphone application Color Desk a good linear relationship up to 200 $\mu mol \cdot L^{-1}$ H_2O_2 was achieved (Figure). Here, the general disadvantages of the non-catalytic approach are overcome through the favorable hydrophobic environment in the albumin. As is true for most reactions in organic chemistry, the oxidative cleavage of boronic ester moieties and their kinetic is strongly influenced by electronic and steric coordination effects. This results in the stabilization of transition steps as a result of solvent cages other groups from the boronated molecule. These factors could explain some of the variations seen in the required reaction times and temperatures of the aforementioned probes and assays.

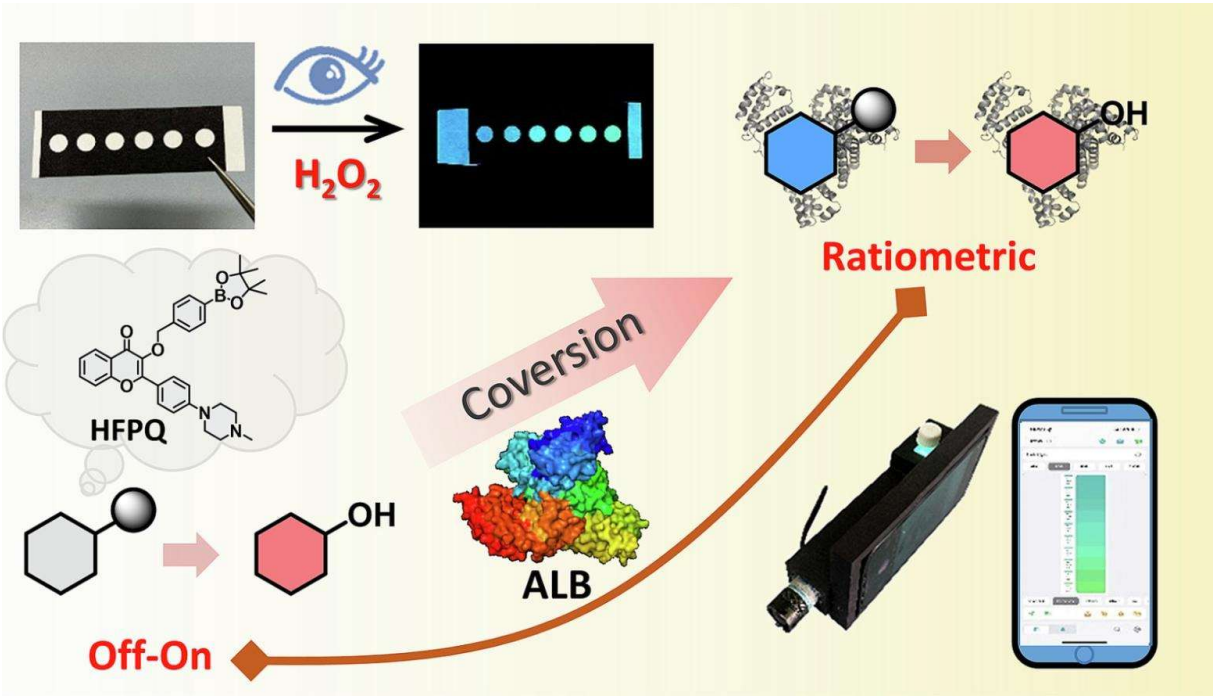

Figure 2.10: Xu et al. [80] present the integration of an advanced flavonoid dye with a boronate group as recognition element embedded in albumin in a paper-based device or cuvette-based assay for smartphone readout. Reprinted with permission from [80]. ©2023 Elsevier.

Chang et. al. [81] published a strategy for the detection of H_2O_2 and glucose on a paper-based system using an AIE fluorogen-based sensing. The proposed AIE fluorogen-based sensing strategy shows high sensitivity for H_2O_2 detection in both, solution state and on a paper-based fluorescence sensor. The paper-based assay has an LOD of 2.5 $\mu mol \cdot L^{-1}$ and a range up to 5 $mmol \cdot L^{-1}$ for H_2O_2 and 50 $nmol \cdot L^{-1}$ for glucose. An obvious disadvantage is the incubation time of 30 min at 37°C and, if human serum is applied the need to dilute the sample 1:10 to avoid a reduction of the fluorescence intensity (Figure). The paper-based device of Mei et al. [82] detects H_2O_2 via the quenching of the aggregation-induced emission (AIE) of Cu nanoclusters with Ce^{3+}. The detection of H_2O_2 is possible with an LOD of 3 $\mu mol \cdot L^{-1}$ and a linear range of 14 – 140 $\mu mol \cdot L^{-1}$. Combined with GOx, the device could be used for the detection of glucose in human serum with an LOD of 2.4 $\mu mol \cdot L^{-1}$ and a linear range of 8 - 48 $\mu mol \cdot L^{-1}$ showing high sensitivity and selectivity for glucose detection. The authors also claimed that glucose concentrations from 16 – 3200 $\mu mol \cdot L^{-1}$ could be discerned by eye-vision based on the color change under a 365 nm UV lamp, making rapid clinical or POC diagnostics possible. However, with a total incubation/reaction time of 40 min, the term ‘rapid’ diagnostics is questionable especially compared with commercially available electrochemical glucose sensors, that can provide data from whole blood within seconds.

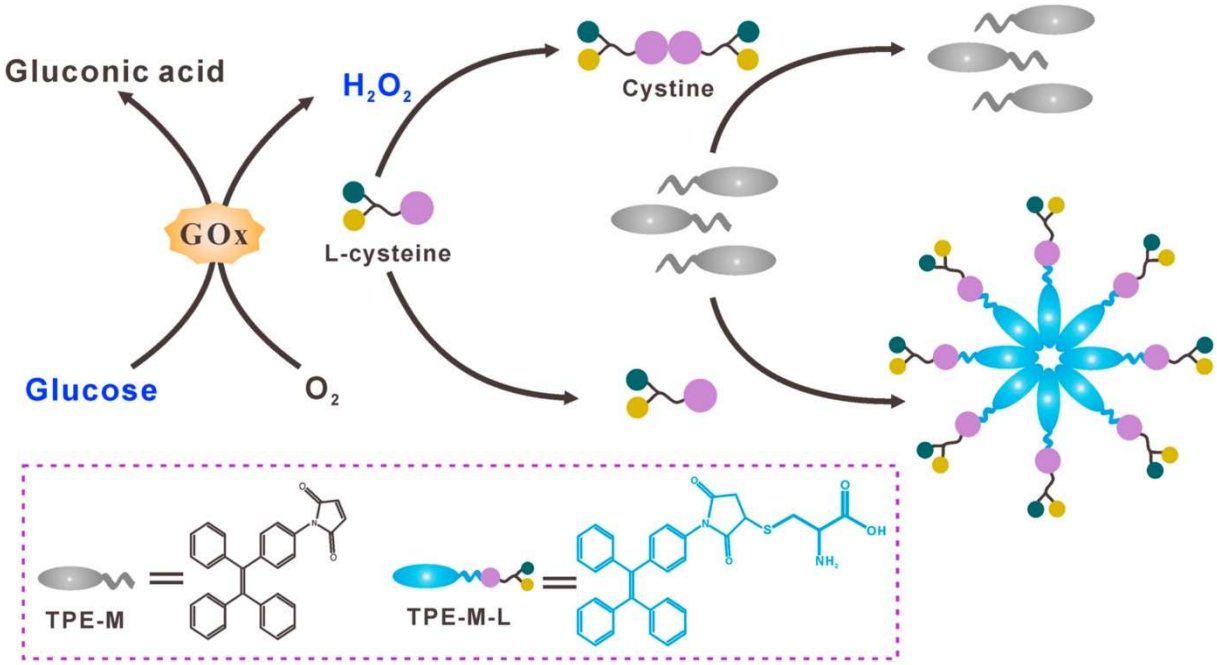

Figure 2.11: Schematic illustration of the principle for H_2O_2 and glucose detection based on AIEgens. Reprinted with permission from [81]. ©2018 Elsevier.

Providing an apparative improvement the sonochemiluminescence (SCL) approach of Meng et al. [83] features an apertureless ultrasonic spray-based photoacoustic sensing platform for the detection of H_2O_2, glucose, and GOx activity. The apertureless USB-piezoelectric ultrasonic transducer (USB-PUT) overcomes the limitations of the previously established mesh-type USB-PUT, such as solution leakage and atomization, and enhances the sensitivity and intensity of the detection.

Sharma et al. [84] modified the surface of a paper-based device with a silver nanoparticle alginate composite (AgNPs@alg) for the smartphone-based colorimetric detection of H_2O_2 in a custom-made 3D printed photobox suitable for multiple smartphone models and form factors. With only 5 s of assay time (dipping into solution), detection is simple and fast, but with an LOD of 0.1 mmol·L^{-1} not the most sensitive approach.

He et al. [85] developed a paper-based fluorescent device for the rapid early screening of oral squamous cell carcinoma by detecting lactate and choline via the generation of H_2O_2 by GOx and LOx. H_2O_2 was detected by the fluorescence decrease of porphin-grafted composite fluorescent polymer colloids (PF-PDMTP/HQ) (Figure). The signal could be detected by a grayscale value analysis of a smartphone image of the paper-based device allowing for the quantification of H_2O_2 with an LOD of 9.4 µmol·L^{-1} and a range up to 200 µmol·L^{-1}. The linear detection ranges of the grayscale value were

10 – 200 µmol·L^{-1} for lactic acid and 10 – 100 µmol·L^{-1} for choline, with LODs of 5.7 µmol·L^{-1} and 8.9 µmol·L^{-1} respectively. With the need for an UV-lamp for detection the device is not the most convenient, but with a very short assay time of only 5 min and the smartphone-based readout the method offers an intriguing and powerful opportunity for POC-care.

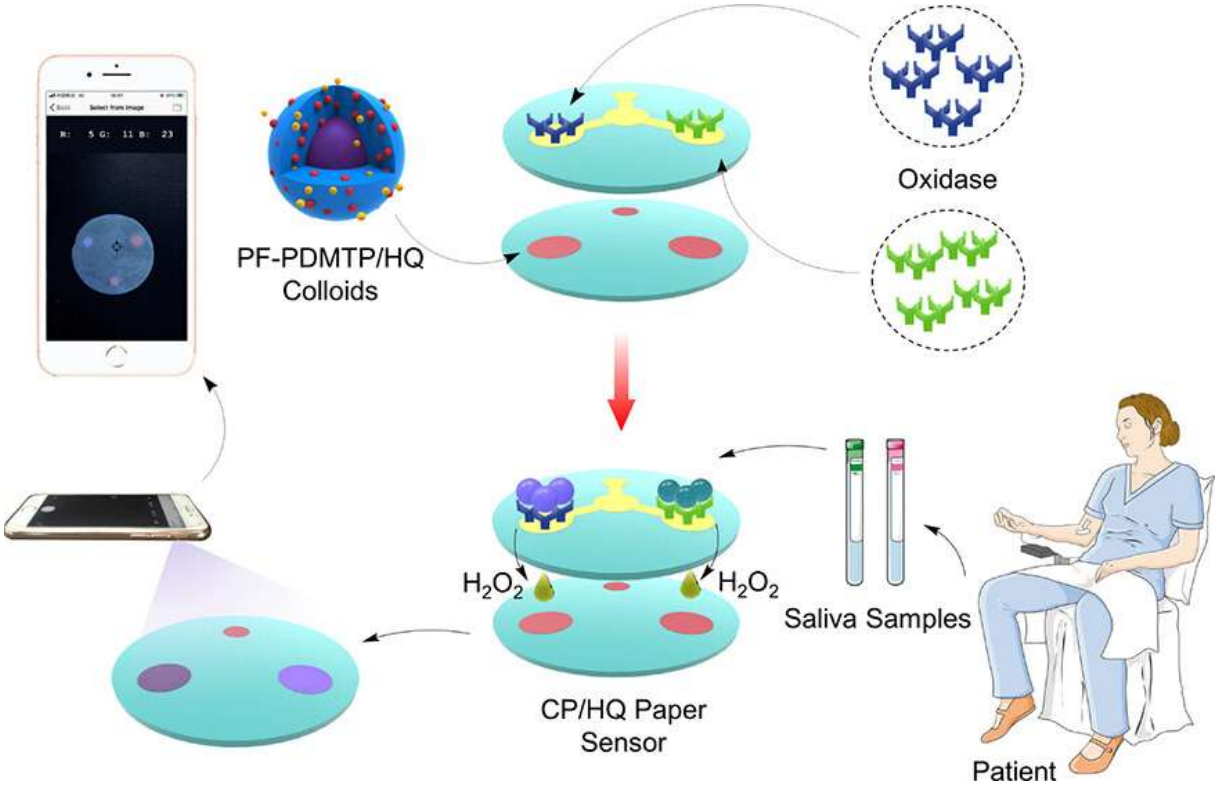

Figure 2.12: Design and detection methods of CP/HQ paper-based device as presented by He et al. Reprinted with permission from [85]. ©2023 ACS.

Unfortunately, with a few positive exceptions, many publications of single-use devices do not examine important analytical measurement parameters such as the reproducibility of the production process or the precision and accuracy of the results. Layer thickness variation for (thin)films, coated and printed devices [86], the coffee-ring effect [87] or dispensing volume variations for drop coated and similar applications or variations from the probe carrier material or catalyst can negatively affect performance to name a few. Unfortunately, such considerations and measurements receive too little attention although they are direly needed to evaluate the production process and all measurements. Yet, since manual preparation in the lab cannot provide the precision provided by mass-produced devices, and since additional significant effort is needed to produce such results, too many academic scientists shy away from presenting such potentially difficult data.

2.5.4 The complexity of smartphone-based optical data acquisition

With several groups using smartphones in previously mentioned publications, one cannot and should not avoid addressing the issue here. The dramatic improvement of camera and imaging technology of smartphones enables researchers to use them for data recording of sensor signals [88–90] and in general as transducers and photon detectors for optical applications. Smartphones can represent a compact and user-friendly detection system for performing various chemical assays, enabling real-time, on-site, and point-of-care testing. This shift from traditional laboratory-based analyses to portable, smartphone-integrated approaches broadens the accessibility of chemical testing away from the lab toward the general public. In contrast to photoluminescence, chemiluminescent [56,71] and colorimetric applications [25,40,63,91] generally require no additional external light source, making the latter two the preferred detection methods in the readout of analyte concentrations with smartphones.

The constant evolution of smartphone cameras and the variation between models brings forth a substantial challenge for standardization and hence universal applicability in analytical systems. While the ongoing advancements enable more sensitive and sophisticated detection methods, the plethora of choices in the smartphone market makes it challenging to create detection cabinets and protocols that can seamlessly integrate with every model. Each smartphone model possesses unique features, dimensions, camera specifications, positioning of the camera on the smartphone, software (availability & compatibility) and sensor configurations, leading to variations in light detection performance and potentially compromising the reliability of analytical results, a factor typically overlooked or ignored in papers featuring smartphones as detection platform. Specifically, most researchers are content to demonstrate the feasibility of their studies with one specific smartphone model and one operating system and do not provide general applicability. Moreover, the abundance and widespread availability of smartphones are often touted as major selling points and primary reasons for utilizing them in analytical applications. However, the very characteristic that makes smartphones attractive for widespread use becomes a double-edged sword. The allure of accessibility can lead to a lack of thorough consideration for the challenges posed by the diversity of smartphones.

With regard to the measurement setup or measurement design, one should ask oneself in many publications why, if a simple and portable low-effort system is to be developed for ‘everyone’, the complex and time-consuming calibrations should not also be simplified. Especially for colorimetric and reflectometric measurements, the addition

or rather integration of a calibration color-bar or code (as is already used in a variety of indicator and test strips [92]) should do the trick. Thinking onward: With the current developments and interest in machine-learning and image analyzing AI, future applications in detection and analysis with smartphone based apps could also greatly benefit from that development with some groups already applying that to basic colorimetric systems [93].

The lack of standardized reporting of operational parameters used in smartphone-based detection in publications exacerbates this issue. Without comprehensive information on the specific parameters and settings used in experiments, the reproducibility of results becomes a daunting task. Researchers aiming to replicate or build upon these studies may face difficulties in achieving consistent outcomes without a clear understanding of the operational intricacies tied to specific smartphone models. Ideally, parameters that would be published are (if available) used aperture, shutter speed, white balance, ISO-value, color space, data format (e.g. JPEG, RAW, TIFF, etc.; with only RAW files representing real image data unbiased by the camera software), type of (CCD)sensor, software version of image-capturing software and used automated image processing routines by the camera software (if so), and the used illumination source. Such datasets should become standard or at least be a standard to that should be striven for to warrant replicability of analytical detection with smartphones and contribute to let them become a more accepted means of detection rather than a trendy additional detection system.

The need for adaptability across different smartphones and operating systems is crucial for the advancement and acceptance of smartphone-based analytical systems. Collaborative efforts within the scientific community, involving researchers, developers, and industry stakeholders, are essential to establish guidelines for reporting operational parameters and creating adaptable detection cabinets. Such guidelines would ensure a more systematic approach to smartphone-based analytical research, fostering standardization and improving the overall robustness and reliability of these systems. This issue is gaining attention, with different groups on the scientific side proposing such standards for reproducible reporting and data acquisition [94,95], open source software for image analysis [96], digital color analysis [97], color correction algorithms [98] and positive influences arising from microscopy applications [99].

Table 2.1: Single-use sensors and systems for the detection of H_2O_2 presented in this review. LOD's and ranges in italics represent data collected in ideal laboratory conditions such as cuvette measurements in a cuvette spectrometer and not in the proposed sensor design, the latter are given in non-italics. Excitation and emission wavelengths given are either the used wavelengths in the publication or the respective excitation/emission maxima of the respective dye(s) (the latter is indicated by a *). For colorimetric measurements the maximum absorbance wavelength is given. For CL measurements the detection wavelength of the emission in the publication is given. [a]: only visual quantification

Probe / recognition element	Detected signal	$\Lambda_{exc}/_{em}$	Device type	(LOD) Analytical Range of H_2O_2	Real world sample type	Comments	Ref
			Enzymatic detection				
Luminol / HRP	HRP/Luminol chemiluminescence	424*	Reaction tube	(0.03 µmol·L^{-1}) 0.06 - 10 µmol·L^{-1}		reusable	[39]
Amplex Red / HRP	HRP/H_2O_2 oxidation of Amplex red to resorufin	572*	colorimetric readout with a smartphone, cellulose based carrier material	(3.4 µmol·L^{-1}) 10 - 100 µmol·L^{-1}	Histamine and tyramine in PBS, tuna sample	For simultaneous detection of histamine and tyramine	[25]
ABTS, 4-Aminoantipyrene / HRP	Colorimetric oxidation of ABTS and 4-Aminoantipyrene	415, 510*	Colorimetric readout with a smartphone, carbon dot doped hydrogel in microfluidic PDMS sensor array		pH, glucose, urea, uric acid and total protein from rat wound fluid		[40]
TMB / HRP	HRP catalysed oxidation of TMB	652*	Paper-based smartphone readout	(1 µmol·L^{-1}) 2 - 100 µmol·L^{-1}	H_2O_2 in Liquor and water	Can also detect salicylic acid	[41]
HRP-AuNCs	Luminescence quenching	542 / 620	Microfluidic	(1 nmol·L^{-1}) up to 40 nmol·L^{-1}	H_2O_2 secreted from single cells		[42]
protein-stabilized gold nanoclusters HEFBNPs	Luminescence quenching	248 / 720	Microfluidic	*(500 pmol·L^{-1}) 500 pmol·L^{-1} - 50 mmol·L^{-1}*	River water	Microfluidic sensor only with visual readout	[43]
Layer-by-layer embedded AGNPs + AuNPs	LSPR		LSPR Flow Cell	(2.7 ppm)			[44]
poly(aniline-co-anthranilic acid) (ANI-co-AA) composite film / HRP	Colorimetric change of composite film	655*	Film-based colorimetric readout with a smartphone	(*35.6 µmol·L^{-1},* 51.2 µmol·L^{-1}) *25 - 200 µmol·L^{-1}*	H_2O_2, glucose and catechol in diluted juice samples	For simultaneous detection of H_2O_2, glucose and catechol	[45]
Guaiacol / HRP	Colorimetric change of Guaiacol to Tetraguaiacol		Paper-based	(0.354 mmol·L^{-1}) 1.25 - 15 mmol·L^{-1}	H_2O_2 in Milk		[46]

Probe / recognition element	Detected signal	$\Lambda_{exc}/_{em}$	Device type	(LOD) Analytical Range of H_2O_2	Real world sample type	Comments	Ref
Enzyme mimic and catalysis enhanced sensing							
TMB / Fe_3O_4 QD	Colorimetric oxidation of TMB	652	Capillary based array	(4.5 µmol·L^{-1}) 10 - 100 µmol·L^{-1}	Milk		[53]
TPA / Cu(II)/Co(II) organic gel	Oxidation of TPA to 2-hydroxyTPA with Cu(II)/Co(II) organic gel in presence of H_2O_2	315 / 446	Hydrogel-based	(81 nmol·L^{-1}) 0 - 120 µmol·L^{-1}	H_2O_2 and glucose in PBS (pH 7.0)	Metal-organic gel with peroxidase activity	[54]
Luminol / Guanosine/hemin hydrogel	Chemiluminescence	424*	Smartphone readout of GOx-loaded guanosine/hemin CL hydrogel cartridge	(7 µmol·L^{-1})	Glucose in artificial serum		[56]
TMB / $PtNi_3$	Colorimetric oxidation of TMB	652*	Paper-based with custom-made portable colorimeter	(0.03 µmol·L^{-1}) 0.1 - 10 µmol·L^{-1}	H_2O_2 secreted from HELA cells	Fast 3 min assay speed. Catalyst/nanozyme also usable in electrochemical detection	[55]
TMB / sericin modified silver nanozyme	Colorimetric oxidation of TMB	652*	Paper-based origami pad	(0.15 mg·dL^{-1}) 0.5 - 240.0 mg·dL^{-1}	H_2O_2 and Glucose in saliva		[57]
TMB / cellulose membranes with immobilized Au nanoclusters	Colorimetric oxidation of TMB	652*	Paper-based	(7 mmol·L^{-1}[a])			[58]
TMB / MoS_2-$SrTiO_3$ nanocomposite	Colorimetric oxidation of TMB	652*	Paper-based	(80 nmol·L^{-1}) 0.1 - 5 µmol·L^{-1}			[59]
TMB / MoS_2@$CoTiO_3$ nanocomposite	Colorimetric oxidation of TMB	652*	Paper-based	(*0.01 µmol·L^{-1}*)	H_2O_2 in milk and tap water		[60]
TMB / Pd-Pt@hemin-rGO/CNTs-COOH	Colorimetric oxidation of TMB	652*	Paper-based	(*0.01 µmol·L^{-1}*)			[62]
TMB / Cellulose nanofibrils/Fe-doped carbon dot composite nanopapers	Colorimetric oxidation of TMB	652*	Paper-based with smartphone readout	(0.93 µmol·L^{-1}) 6 - 42 µmol·L^{-1}		Reusable enzyme mimic strips after cleaning/regeneration with ascorbic acid	[61]

Probe / recognition element	Detected signal	$\Lambda_{exc}/_{em}$	Device type	(LOD) Analytical Range of H_2O_2	Real world sample type	Comments	Ref
Enzyme mimic and catalysis enhanced sensing							
TMB / Pd-Pt@hemin-rGO/CNTs-COOH	Colorimetric oxidation of TMB	652*	Paper-based	(*0.01 µmol·L^{-1}*)			[62]
TMB / B, N, and S co-doped carbon dots (BNS-CDs) peroxidase mimic	Colorimetric oxidation of TMB	652*	Smartphone RGB readout	(0.8 µmol·L^{-1}) 3 - 30 µmol·L^{-1}	Mouthwash and Milk		[63]
ABTS / MoOx QDs	Colorimetric oxidation of ABTS	420*	Paper-based	(0.175 µmol·L^{-1})	H_2O_2 released from PC12 cells		[64]
TMB / CuO hollow Sphere Nanozyme	Colorimetric oxidation of TMB	652*	Paper-based	(2.1 µmol·L^{-1}) 2.4 - 150 µmol·L^{-1}			[65]
CPT-MnBG-Gel	Luminescence quenching	254 / 544	Hydrogel-based wound dressing	(10.35 µmol·L^{-1}) up to 200 µmol·L^{-1}	Diabetic wound	H_2O_2 scavenging for diabetic wound treatment	[69]
Carboxyluminol / Hemin	Chemiluminescence	430	µpad based point-of care device for lactate readout with smartphone or CCD-camera	(13 µmol·L^{-1}) up to 2000 µmol·L^{-1}		Can also detect lactate	[71]
Luminol/$CoCl_2$	Chemiluminescence	424*	miniaturized 3D-printed device	($3.0\cdot10^{-5}$ %w/w / 9 µmol·L^{-1}) $1.0\cdot10^{-4}$ - $9.0\cdot10^{-3}$ %w/w 30 – 270 µmol·L^{-1}	H_2O_2 in milk		[72]
IR820 Core-shell UCNP	Inhibition of ET to UCNP by oxidation of IR820 with OH in Fenton-type reaction	808+980 / 525+540	Flow-cell based	(0.1 nmol·L^{-1}) 0.5-100 nmol·L^{-1}			[75]
Fe-based MOFs / OPD	Dual-mode ratiometric fluorescence quenching with colorimetric change	365 / 447 +572; 450	3D printed chip holder and chip with machine learning smartphone image evaluation	*2.06 nmol·L^{-1}*			[76]

Probe / recognition element	Detected signal	$\Lambda_{exc}/_{em}$	Device type	(LOD) Analytical Range of H_2O_2	Real world sample type	Comments	Ref
			Nonenzymatic detection				
Tb^{3+}/Eu^{3+} [1,1′-Biphenyl]-4-carboxylic acid Deboraontion	Ligand energy transfer luminescence	270 / 545	Hydrogel-drop-caoted paper discs	(2 μmol·L^{-1}) 2 - 200 μmol·L^{-1}	H_2O_2 in hand sanitizer		[77]
C6NIB Deboronation	Fluorescence	270 / 617 458 / 522	aluminum foil-based silica gel plate	2 ppb	H_2O_2 vapor	Very fast response time of <0.5 s for high concentrations of H_2O_2 possible	[78]
pyrene/fluorene-based probes DB-WCZ DB-W Deboronation	Fluorescence	370 / 449	Thin film	(2.2 ppb)	H_2O_2 vapor		[79]
HFPQ@ALB Deboronation	Ratiometric fluorescence	365 / 515 +484	Paper-based / miniaturized measurement chamber + Smartphone readout	Up to 200 μmol·L^{-1} paper-based Up to 100 μmol·L^{-1} miniaturized chamber	H_2O_2 in milk		[80]
maleimide-functionalized tetraphenylethene (TPE-M) and cysteine	Aggregation induced emission/quenching	365 / 460	Paper-based	(2.5 μmol·L^{-1} paper-based 10 nmol·L^{-1} in solution) up to 20 μmol·L^{-1}	H_2O_2 and glucose in PBS (pH 7.0)		[81]
Cu nanoclusters with Ce^{3+}	AIE quenching	350 / 650	Paper based	(3 μmol·L^{-1}) 14 - 140 μmol·L^{-1}			[82]
Luminol	Ultrasonic/H_2O_2 induced SCL of Luminol	424	apertureless stainless steel substrate USB piezoelectric ultrasonic transducer	(0.32 μmol·L^{-1}) 0.5-50 μmol·L^{-1}	Glucose/GOx in PBS (pH 7.4)		[83]
Ag NPs-alginate composite	colorimetric change	400	Paper-based with a smartphone readout	(0.1 mmol·L^{-1}) 0.1 – 10 mmol·L^{-1}		Photobox dimensions suitable for multiple smartphone models	[84]
PF-PDMTP/HQ	Fluorescence quenching	365 / 420 +650	Paper-based with smartphone greyscale readout	(9.4 μmol·L^{-1}) up to 200 μmol·L^{-1}	Human salivia		[85]

2.6 Sensors, Intermediate and semi-reversible sensing systems for quantitation of H_2O_2

Many applications including environmental analysis, process, biomedical and general cell culture monitoring, will greatly benefit from a constant monitoring of H_2O_2 or precursor analytes [100]. Overall, development of such continuous and fully reversible optical sensors has been slow since their tasks are significantly more challenging. The well-known interferences and problems such as (bio)fouling [101], photobleaching, general changes in the composition of the analyte matrix including variations in pH, ionic strength, leakage of probe molecules and temperature are all dramatically enhanced challenges for continuous sensors. Intermediate and semi-reversible strategies can in some instances provide a sufficient solution through the help of an appropriate engineering and assay design.

2.6.1 Intermediate and semi-reversible sensing systems for quantitation of H_2O_2

Intermediate and semi-reversible systems represent the steppingstone between discontinuous single-use sensors and continuous fully reversible sensors. These systems allow semi-continuous detection by repeated sample injection with irreversible reactions, with steadily or repeated input of reagents, such as flow injection analysis (FIA) or external factors such as light, temperature, addition of redox reagents or cycling by an applied potential to allow (sufficiently fast) regeneration of the sensing capability.

2.6.1.1 FIA systems

Due to the in-flow addition of buffer and reagents, FIA systems can work with a variety of sample types and concentration ranges with a broad range of pH values, assuming a sufficient dilution and buffering can be reached. The noteworthy recently developed FIA-protocols are mostly CL-based. Aside from the advantage of not requiring an excitation lamp, thus reducing the required number of optical components, CL reactions often show rapid to seemingly instantaneous kinetics, the temporal resolution therefore being mostly defined by instrumental limitations. However, requiring a certain level of instrumentation with pumps, waste disposal, reagents, buffers and the like combined with a temperature dependence of CL reactions, such FIA systems are not the preferred choice for remote or POC applications. As the injected samples are being

'contaminated' with reagents and buffers such systems are also not applicable to 'closed loop' systems and are not ideal for very small sample volumes.

Advances both in instrumental nature and on the basis of reagent additives were key to the work by Moßhammer et al. [102] (Table 2.2) who developed a versatile FIA system coupled with microdialysis probes allowing an initial size exclusion to avoid contamination of the system with larger molecules for the sensitive detection of H_2O_2 with an acridinium ester as CL reagent. Their protocol and setup offers customizable calibration ranges and exhibits enhanced selectivity, especially with the addition of EDTA to prevent commonly occurring interference from metal ions such as Fe(II) and Fe(III) [103] (Figure 2.13).

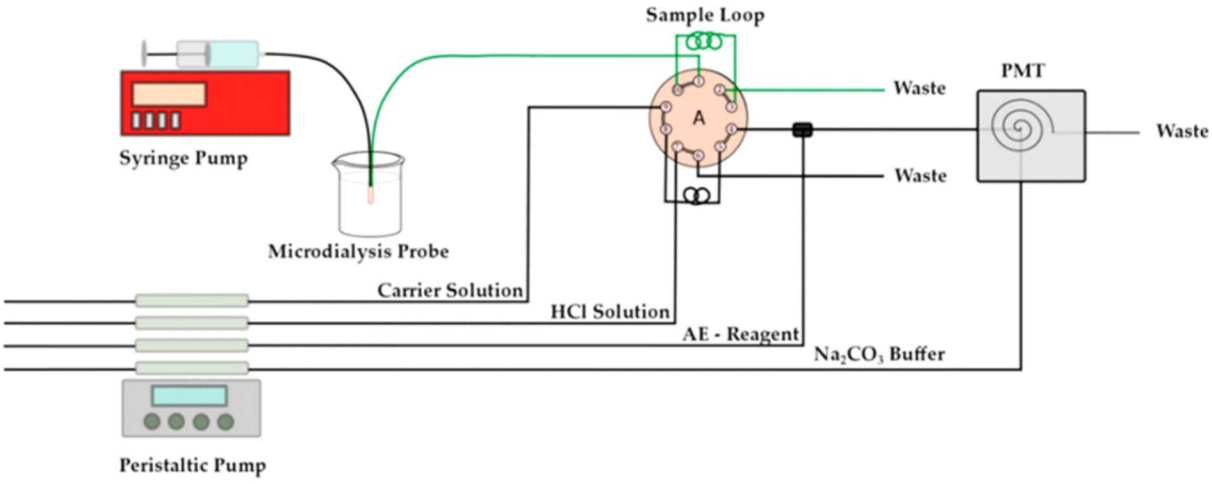

Figure 2.13: Schematic of the FIA setup developed by Moßhammer et al. with microdialysis probe for sample uptake with a syringe pump. The reagent and buffer additions are achieved with a with peristaltic pump. Reprinted from with permission [102]. ©2018 Elsevier.

As with single-use devices, also enzyme mimics are seeing their use in FIA systems. For example Li et al. developed a [104] CL FIA protocol using a Fe-porphyrin covalent organic framework (Fe-PorCOF) as peroxidase mimic combined with luminol for H_2O_2 detection and a broad linear range of 0.01 to 10.0 µmol·L^{-1} and an LOD of 5.3 nmol·L^{-1} in carbonate buffer pH 10.5. Aside from the use of the enzyme mimic the FIA protocol and setup was standard.

Yuan et al. [105] realized a CL FIA approach through a sulfonated polyaniline decorated copper-based metal organic frame composite (SPAN/HKUST-1@Luminol). This composite has a significantly enhanced CL quantum yield of 136 times higher than luminol and showed good signal intensities not only in basic conditions, but also at physiological pH of 7.4. In a PBS pH 7.4 running buffer, they were able to detect

H_2O_2 with an LOD of 60 nmol·L^{-1} with a linear range of 0.1 – 30 µmol·L^{-1} and in 0.1 mol·L^{-1} NaOH down to 25 pmol·L^{-1} with a linear range of 30 – 600 pmol·L^{-1}. Thus, combining their system with an autosampling setup would make a very interesting setup for monitoring H_2O_2 in cell cultures (Figure 2.14). In another study, Shen et al. [106] published a FIA protocol integrating carbon nanodots (CDs) and bis(2,4,6-trichlorophenyl) oxalate (TCPO) for sensitive quantification of H_2O_2 and glucose with an LOD of 11.7 µmol·L^{-1} and a wide linear range up to 15 mmol·L^{-1} with the option for an exponential fit extending the quantitation range up to 50 mmol·L^{-1}. Most notably, the CL quantum yield of the CDs reached (8.22 ± 0.30) × 10^{-3} which the authors claim is among the best values reported for a CL nanomaterial used in chemical analysis. New in their system is the use of these enhanced CL-carbon dots, whereas the FIA protocol itself is a traditional strategy.

In the case of Sun et al. [107] a chemiluminescence resonance energy transfer (CRET) platform is proposed that utilizes WS_2 quantum Dots (QDs) for assessing H_2O_2 during photocatalytic processes, achieving a low LOD of 38 nmol·L^{-1} and a linear range from 0.14 – 14 µmol·L^{-1}. This is especially interesting for future applications on the analysis and evaluation of disinfectant properties of photocatalytic species.

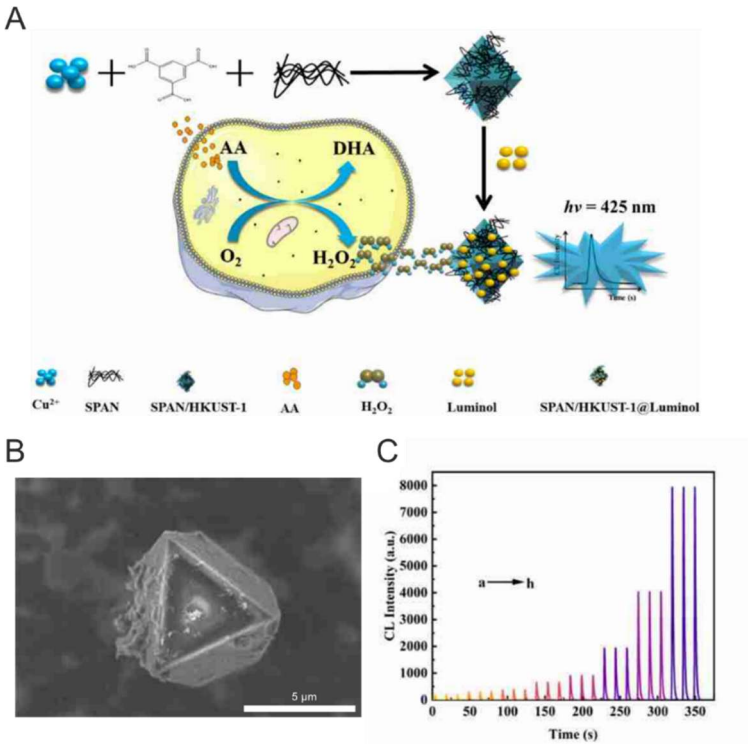

Figure 2.14: **A** Schematic diagram of synthesis of SPAN/HKUST-1@Luminol composite and the mechanism of the CL detection of H_2O_2. **B** SEM image of SPAN/HKUST-1@Luminol **C** CL responses of the SPAN/HKUST-1@Luminol in PBS (pH 7.4) toward different concentrations of H_2O_2 (from a to h, 0.1, 0.7, 1, 2, 3, 7, 15, 30 µmol·L^{-1}). Reprinted with permission from [105]. © 2023 Elsevier.

A unique strategy to overcome problems with both the autofluorescence/color of erythrocytes and the time-factor of measuring H_2O_2 from whole blood samples is proposed by Sen et al. [108]. By using an acoustics-based blood plasma separation module in their microfluidic setup they were able to remove interfering and H_2O_2-degrading contents and quantify H_2O_2 from fresh whole blood samples in one setup in flow. The separated plasma was then mixed in the microfluidic chip with HRP, buffer and Amplex red which could be measured on-chip and off-chip in their setup. In the on-chip separated plasma the group was able to detect H_2O_2 in a range of 0 – 49 µmol·L^{-1} and with an LOD of 0.05 µmol·L^{-1} within a total response time of 15 min. For healthy individuals the group reported H_2O_2 values in the range of 0.8 – 6 µmol·L^{-1} in whole blood. While microfluidic systems do allow a miniaturization of the actual mixing and measurement modules, and in this case also makes centrifugation obsolete the previously mentioned same restrictions as for the other FIA systems apply, but by using a microfluidic system they were able to reduce the required sample, buffer and reagent volume in comparison with a larger FIA setup. By choosing a photoluminescent reagent, the setup naturally also requires an excitation light source or laser, respectively. The results suggest that the setup could be applied also to rapid blood screening (Figure).

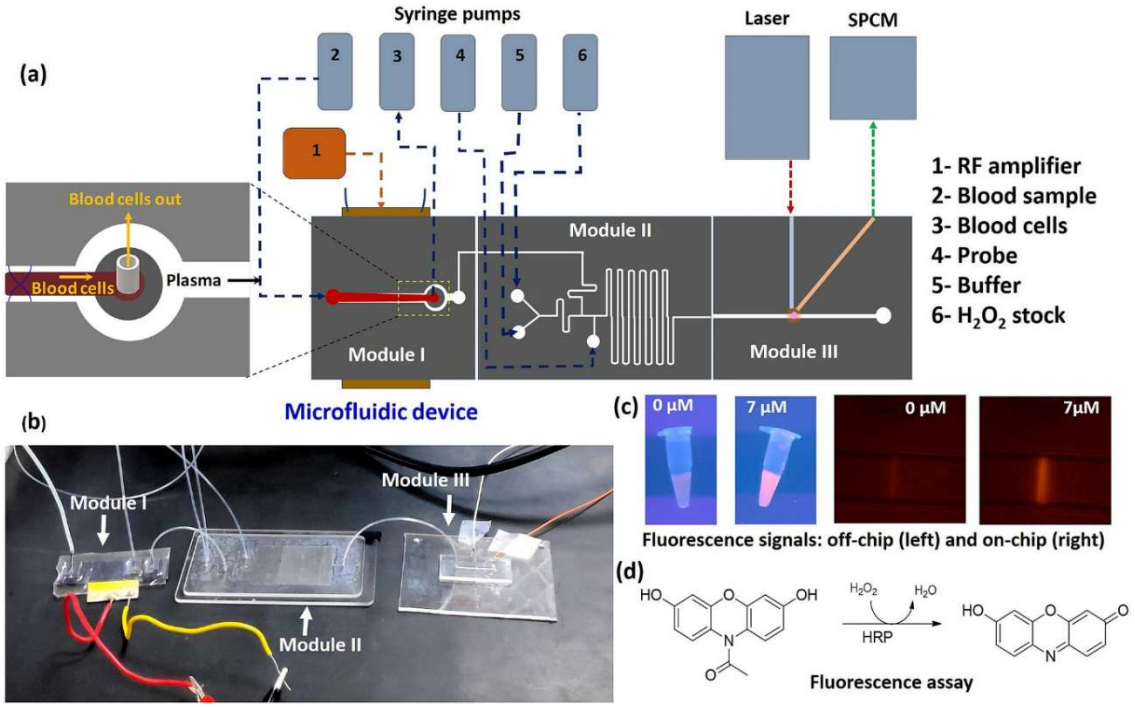

Figure 2.15: Sen et al developed a microfluidic FIA-device for the detection of H_2O_2 in whole blood with a blood separation device on-chip. (**a**) Schematic of the microfluidic device with blood separation (module I) reagent and buffer addition and mixing (module II) and detection (module III) (**b**) photograph of the microfluidic device and the respective modules, (**c**) images of the fluorescence in a reaction cup and in the channel (**d**) Amplex Red reaction with H_2O_2 in presence of HRP. Reprinted with permission from [108]. © 2021 Springer.

2.6.1.2 Regeneration of the detection system by external factors

Reversibility of a detection strategy was proposed by Malyukin et al. using CeO_{2-x} NPs [109]. These NPs can detect H_2O_2 by oxidation of Ce^{3+} to Ce^{4+}. This is accompanied by quenching of Ce^{3+} luminescence of the nanoceria at 430 nm by a Fenton-type reaction as the nanoceria particles also show a peroxidase-like activity. However, the long regeneration time of the nanoparticles of up to 120 h at 22 °C or 24 h at 37 °C for : the smaller, 2 nm nanoparticle species, with the larger 10 nm nanocrystals taking even longer for their regeneration required faster conversion to make this approach competitive to other methods. Later, Seminko et al. [110] discovered, that by simultaneously increasing the temperature and continuous irradiation with UV light, they were able to reduce the regeneration time for the H_2O_2 detection of CeO_{2-x} and CeO_{2-x}:Eu^{3+} NPs from 180 h and 4 h down to 36 min at 52 °C respectively. These reduced regeneration times might not be sufficient for applications that require constant monitoring but could be suitable for applications where a high temporal resolution is not required. In combination with a currently severely limited capability of quantitation this technology requires further development and improvement before being implemented into a functional sensing device.

Cobalt(II)-hexacyanoferrate (CoHCF) was used as an advanced Prussian white substitute by Virbickas et al. [111] as an optical indicator for H_2O_2 which is electrochemically regeneratable as a layer on an ITO/glass substrate. This unique system shows high stability of CoHCF's thermochromic properties after voltammetric cycling and also resistance to air exposure. The needed constant temperature of 25 °C for photometric detection seems to be a minor disadvantage that can be overcome with a simple chip-controlled temperature module (Figure).

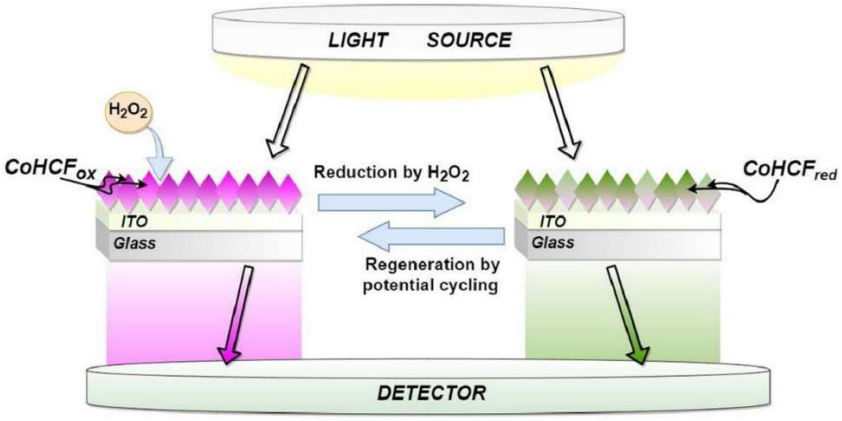

Figure 2.16: Scheme of the semi-reversible Cobalt(II)-hexacyanoferrate (CoHCF) sensor as published by Virbickas et al. Reprinted with permission from [111]. ©2020 Elsevier.

Table 2.2: intermediate and semi-reversible sensors for the detection of H_2O_2 presented in this review. LOD's and ranges in italics represent data collected in ideal laboratory conditions such as cuvette measurements in a cuvette spectrometer and not in the proposed sensor design, the latter are given in non-italics.

Probe / recognition element	**Detected signal**	**(LOD) Analytical/calibration Range(s) of H_2O_2**	**conditions**	**Regeneration condition / cycle time & condition**	**Ref**
acridinium ester	CL	0 - 1000 nmol·L^{-1}; 0 - 10 µmol·L^{-1}; 1 - 100 µmol·L^{-1}		FIA	[102,103]
Luminol / Fe-PorCOF	CL	(5.3 nmol·L^{-1}) 0.01 - 10.0 µmol·L^{-1}	carbonate buffer pH 10.5	FIA	[104]
SPAN/ HKUST-1@Luminol	CL	(60 nmol·L^{-1}) 0.1 - 30 µmol·L^{-1} (25 pmol·L^{-1}) 30 - 600 pmol·L^{-1}	pH 7.4 PBS; 0.1 mol·L^{-1} NaOH.	FIA	[105]
TCPO / Carbon nanodots	CL	(11.7 µmol·L^{-1}) up to 15 mmol·L^{-1} (linear) up to 50 mmol·L^{-1} (exponential fit)		FIA	[106]
WS_2 QD NaCLO	CRET	(38 nmol·L^{-1}) 0.14 – 14 µmol·L^{-1}.		FIA	[107]
Amplex Red / HRP	HRP/H_2O_2 oxidation of Amplex red to resorufin	(0.05 µmol·L^{-1}) 0 – 49 µmol·L^{-1}	1/6 dilution with buffer	FIA, washing with buffer 15 min	[108]
CeO_{2-x} NPs	Luminescence quenching	n.a.		36 min UV light + 52 °C	[110]
CoHCF	Absorbance	1.5 - 20 mmol·L^{-1}		Redox Cycle	[111]

2.6.2 Continuous and fully reversible sensors for quantitation of H_2O_2

The interplay between signal response, recovery, interferences, calibration, and long-term signal drift distinguishes continuous and fully reversible sensors from discontinuous or single-use sensors. In the case of H_2O_2 detection, sensors should show rapid response times, allowing for real-time detection of concentration changes in a dynamic environment as this timely information enhances safety, efficiency, and overall process optimization. For all new concepts proposed, it is hence very important to understand the mechanisms underlying the reversibility as only this will allow smart optimization of the sensor performance ensuring their longevity in demanding applications.

Publications over the last five years have proposed valuable new concepts and probes for continuous and reversible optical sensors for H_2O_2. Such concepts address photobleaching, leakage, internal referencing, reduction of interferences and background signals.

2.6.2.1 Ratiometric fluorescence

Dung and Rhee [112] (Table 2.3) immobilized HRP on the surface of a sol-gel glycidoxypropyl trimethoxysilane and aminopropyl trimethoxysilane membrane containing carboxyl group functionalized-CdSe/ZnS quantum dots (QDs) and aminofluorescein (AF)-encapsulated polymer particles as probe and reference material, respectively. The membranes were excited at 400 nm and measured at 500 nm for the reference and at 560 nm for the QDs, respectively. In presence of H_2O_2, the luminescence of the QDs was quenched allowing a detection of H_2O_2 with a calculated LOD of 11 µmol·L^{-1} and a linear range of 0.1 -1 mmol·L^{-1} with a response time of 5.5 - 8.5 min. The membrane also showed an acceptable reusability and stability of the signal after 60 test runs for concentrations up to 1 mmol·L^{-1} whereas for higher concentrations (up to 10 mmol·L^{-1}) the response of the membranes was reduced. The authors attribute this reduction in sensitivity to the polymer backbone degradation. By using QDs, the sensor eliminates the issue of photobleaching if one ignores the photobleaching of the reference (AF)-encapsulated polymer particles. On the negative side, QDs innately also show a blinking emission, an issue usually easily remedied by longer integration time of the signal. With the rather long response time and a limited usable analytical range further research in the field is required (Figure).

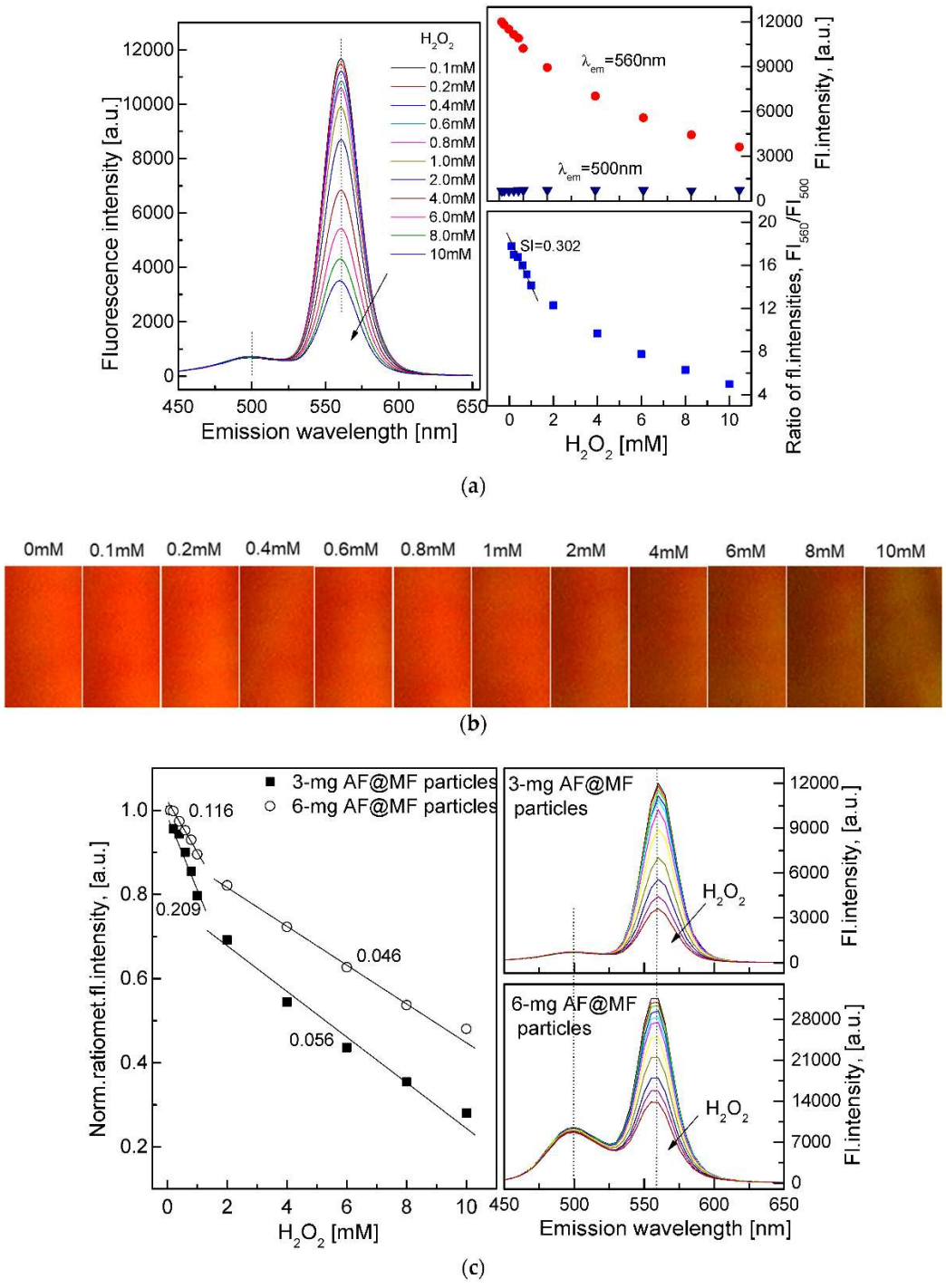

Figure 2.17: (a) Emission spectra of QD–AF membrane at different concentrations of H_2O_2 and its calibration curve for H_2O_2 determined by normalization of the fluorescence intensities (FI560/FI500). (b) Images of fluorescence quenching of the QD–AF membrane after exposure to increasing H_2O_2 concentrations. (c) Calibration curves and response of the QD–AF membranes in H_2O_2 at concentration ranges of 0.1 – 1 mmol·L^{-1} and 1 – 10 mmol·L^{-1} using a small (3 mg) or large (6 mg) amount of reference dye particles. Reprinted with permission from [112]. © 2019 MDPI

2.6.2.2 SPR-based detection

The label-free SPR technique has long been used in flow-systems making it applicable for in-situ measurements. It enables very fast response times and depending on the setup it may only require small sample volumes. As label-free strategy that monitors activity at the sensor surface, it obviously suffers from non-specific interactions and adsorption processes [113]. Gupta and Semwal [114] proposed an enzymatic decomposition of H_2O_2 to O_2 and H_2O, where the latter interacts with graphene oxide (GO) nanosheets in the GO/gold wafer interface. This interaction causes a change in the refractive index and a shift in the resonance wavelength of the SPR curve. Unfortunately, the authors opted for discontinuous FIA-style operation and did not take advantage of an in principle possible continuous measurement set-up. Nonetheless, the sensor showed a response time of 30 s, an LOD of 55 µmol·L^{-1} and a quantitation range up to 1000 µmol·L^{-1} (Figure).

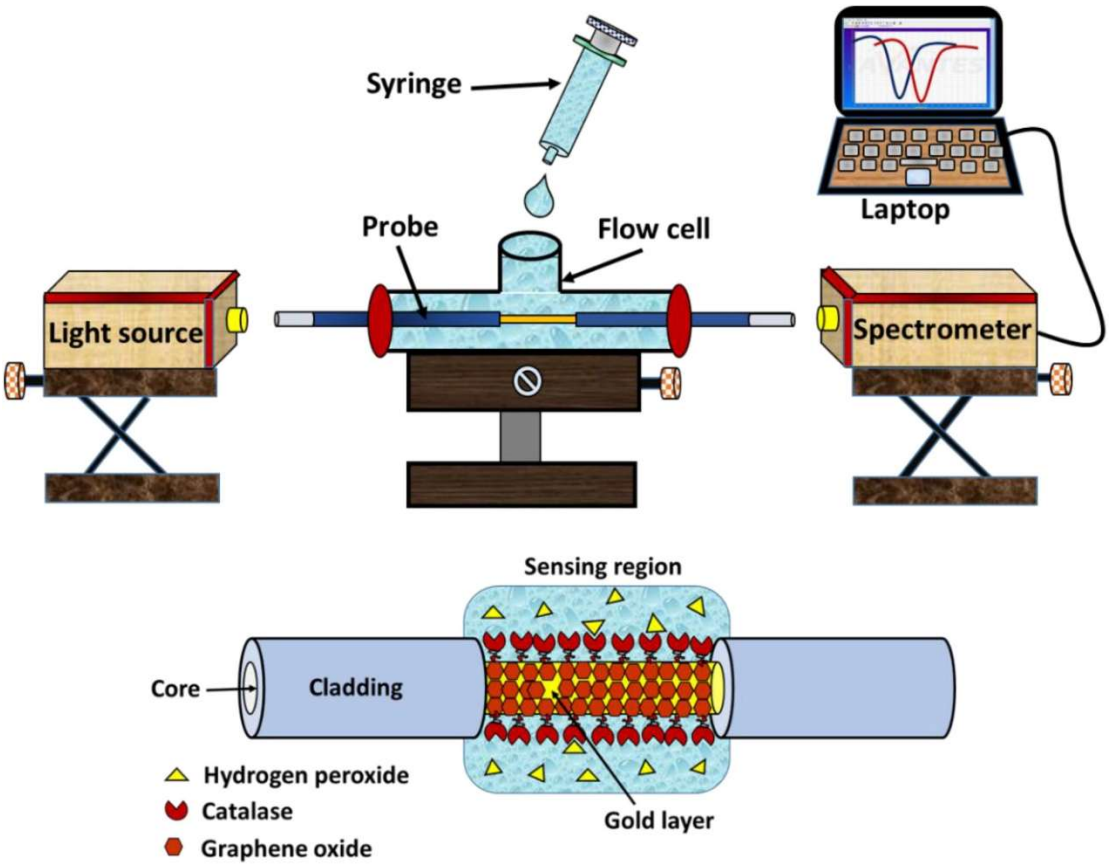

Figure 2.18: Schematic diagram of SPR sensing setup and probe design as proposed by Gupta and Semwal. Reprinted with permission from [114]. © 2021 Elsevier

2.6.2.3 Oxygen-based H_2O_2 detection

The well-known and well-published concept of quantifying H_2O_2 through catalytically or enzymatically generated oxygen followed by quenching of fluorescence or phosphorescence [115] allows the use of several well-established oxygen-sensitive dyes and complexes as probes, such as Ru-bipyridines, Ru-Phenanthrolines and Pt- and Pd-porphyrins [116]. Major advantages of this approach include probe response time and regeneration time with the quenching mechanism being primarily diffusion limited. Obviously, residual oxygen or oxygen concentration changes within the samples can severely impact measurement quality, reproducibility, and precision and must be taken into consideration. Ding et al. [117] present a sensor employing Pt NPs within fibrous silica particles embedded in a hydrogel matrix, demonstrating promising detection capabilities and requiring only very small sample volumes. Unfortunately, they noticed a luminescence decrease of 12% after the first calibration cycle, which they attributed to leakage. Aside from that, they also observed concentration-dependent response times and, while acknowledging the issue of interference from residual oxygen and temperature in principle only briefly suggested possible solutions, i.e. the integration of an oxygen and temperature control sensing spots. The work of Torsten Mayr's group [118] which they were recently also able to use as detection element for at-line monitoring of H_2O_2 released from a photocatalytic synthesis [119] offers an innovative flow-cell-based sensor with an additional oxygen sensing element and an upstream deoxygenation module to mitigate such baseline issues and sensory drifts based on oxygen changes as in their previously published glucose sensor [120]. While achieving enhanced LODs, extended linear ranges, full reversibility, stable hysteresis, and stability over 9 h of measurement, the sensor's response/equilibration time of 5 minutes, the batch-to-batch variation and complexity associated with the experimental setup underscore the need for further refinement and consideration of practical application challenges.

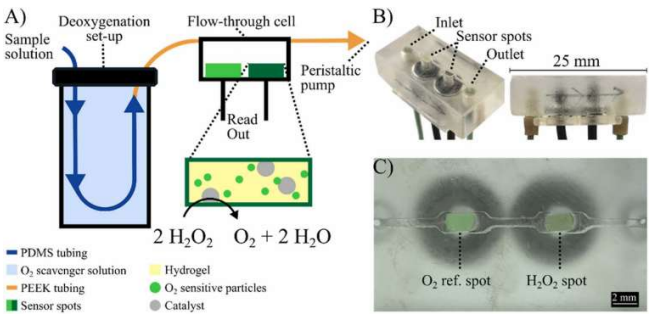

Figure 2.19: A) Schematic and B) picture of the flow cell of the oxygen sensor with C) O_2-reference and H_2O_2 detection spot developed by Torsten Mayr's group. Reprinted with permission from [118]. ©2023 Elsevier.

Table 2.3: Reversible sensors for the detection of H_2O_2 presented in this review. LOD's and ranges in italics represent data collected in ideal laboratory conditions such as cuvette measurements in a cuvette spectrometer and not in the proposed sensor design, the latter are given in non-italics.

Probe/recognition element	Detected signal	Sensor type	(LOD) Analytical Range of H_2O_2	Conditions	Response time	Ref
carboxyl group functionalized-CdSe/ZnS	Ratiometric fluorescence / fluorescence quenching	GPTMS / APTMS hydrogel membrane	(11 µmol·L^{-1}) 0.1 - 1 mmol·L^{-1}			[112]
GO nanosheets/catalase	SPR curve shift	SPR Flow Cell	(55 µmol·L^{-1}) up to 1000 µmol·L^{-1}		30 s	[114]
PtTFPP in D4 membrane KCC-1-PEI/PtNPs in D4 membrane	Oxygen quenching of PTFPP emission by catalase-like mimic degradation of H_2O_2	Hydrogel membrane based	(15 µmol·L^{-1}) 1 µmol·L^{-1} - 10 m mol·L^{-1}		< 1 min for 3 mmol·L^{-1} H_2O_2 up to 6 min for other concentrations	[117]
PtTPTBPF/PdTPTBPF	RuO_2 / PtNP catalyzed degradation of H_2O_2 with O_2-quenching of PtTPTBPF and PdTPTBPF phosphorescence	Flow-cell based	(0.17 µmol·L^{-1}) (0.16 µmol·L^{-1}) Up to 1000 µmol·L^{-1}	PtNP spots RuO_2 spots	4.6 min total, ≈2.5 min retention time; 5 min equilibration	[118]

2.7 Conclusion and Outlook

The development of optical H_2O_2 sensors shows a clear trend toward implementing synthetic enzyme mimics and nanozymes as tunable and efficient replacements for peroxidases. Although some aspects, regarding catalytic activity, issues with the vague interpretation of the definitions and wording are under scrutiny the hope is that these nanomaterials can provide a better long-term and assay stability in addition to desirably low LOD's. Nevertheless, benchmark experiments and closer comparison to enzyme activities and nanozyme weight- or amount-based turnover rates should be included in publications for better classification. The next steps towards their possibly broad-based use in analytical systems are the comprehensive design of studies investigating their effect on the environment including toxicity, persistence, (bio)accumulation, and overall environmental impact [121]. In fact, some of the heavy metal-based systems may be far from any sustainable use. It is therefore of great interest that some efforts are made searching for renewable sources of educts for the synthesis of certain enzyme mimics [122–124].

For colorimetric applications, TMB continues to be the most common indicator, despite the availability of other valid options such as Amplex red, nanomaterials or ABTS. This increased use is likely due to its commercial availability, comparably low price, and an abundance of protocols for enzymes and synthetic enzyme mimics. However, finding a replacement for colorimetric substrates with a broader dynamic range, lower background signal and lower environmental impact would be highly desirable. Considering the vast number of published enzyme mimics, there may be a possibility of new developments and applications on this front in the future.

The dramatic improvement of cameras integrated in smartphones has made those an easy transducer for sensor development as signals can easily be taken and processed through appropriate apps. This clearly is a significant and growing, but not entirely unproblematic trend in the field of analytical chemistry [90]. The paradigm shift from lab-based detectors to smartphone cameras is driven by the widespread use, computational power, and portability of modern smartphones, which have transformed these handheld devices into versatile tools for quantitative chemical analysis. Smartphone-based detection is also commonly used with paper-based sensors combining low-cost and weight disposable sensors and broadly available smartphone devices. However, standardization of smartphone optical data acquisition and its software conversion to work with smartphones from any producer still remains an

unsolved task. Specifically, comprehensive reporting of experimental parameters regarding image capture and data/software processing, is necessary for reproducibility and reliability in smartphone-based detection. The diversity of smartphone models does pose a challenge for standardization and universal applicability in analytical systems. Efforts to adapt measurement setups to accommodate different models and operating systems are crucial. In combination, performing control experiments with different smartphones are needed to show the robustness and versatility of sensing platforms. The implementation or integration of simplified calibration processes such as standard color bars or codes into measurement designs to facilitate ease-of-use for a wide range of users in different lighting and (smartphone) camera situations could also improve sensing accuracy and accessibility.

Overall, such collaborative efforts within the scientific community are needed and are being actively pursued [92,94–99] to establish guidelines for reporting operational parameters and creating adaptable detection systems. This would promote standardization and improve the reliability of smartphone-based analytical research. Such standards from researchers for researchers will help development and innovation and serve as a benchmark, as well as provide regulatory institutions with helpful examples for developing operational guidelines and requirements.

The current rise of machine-learning algorithms and AI-tools could also provide a massive enhancement for image and data analysis for both smartphone-based mobile and more classical laboratory-based applications. This trend leans on early research in the 1990s using neural networks for pattern recognition [125]. A main hurdle will always be the sheer amount of data that is needed to feed such digital learning tools but considering current trends and openness from funding agencies to go along this developmental route, the integration of AI in sensors and sensing technology will become not only feasible but also useful.

Although an abundance of novel photoluminescent probes is developed and published, the number of sensors based on new probes is limited. Literature surveys show that over 1152 papers alone are found in the Web of Science since 2018 when searching for ‘fluorescence detection hydrogen peroxide’. Yet, these are seldomly picked up by researchers developing optical sensors, who tend to use established probes. One may ask why this disconnect exists. Don’t the new probes address challenges hampering optical sensors? Or do sensors lag behind probe development? Obviously, there should be more interaction between these two research fields. If there was more

cooperation here, great sensors would surely come to or rather emit light (with a higher wavelength).

For the semi-reversible/continuous systems FIA methods, especially in combination with CL reagents, have seen improvement and have shown to be powerful tools. With the developments based on newer, brighter CL reagents, microfluidics, portable systems usable for more remote work [126] and the improved sampling systems, new innovations and better systems are just around the corner.

Clearly, fully reversible and continuous optical H_2O_2 sensors remain a rarity where to-date no fully satisfying solution exists. Yet, the development of probes or recognition or catalytic elements alone is not sufficient. It is also necessary to develop new, sustainable membrane coatings that protect optical probes from fouling and leaking. Self-referencing or ratiometric probes are needed to avoid extensive calibration and sensory drifts. Novel probes with a truly reversible detection mechanism that work not only in cuvettes but can be used in sensor membranes and for continuous detection are required. We thus think that this should motivate the leading minds in sensor and optical probe development to enhance collaboration towards the advancement of superior optical sensors addressing the critical issues here described that are beyond each single lab’s expertise.

2.8 References

[1] X. Liu, C.N. Kim, J. Yang, R. Jemmerson, X. Wang, Induction of apoptotic program in cell-free extracts: requirement for dATP and cytochrome c, Cell 86 (1996) 147–157. https://doi.org/10.1016/s0092-8674(00)80085-9.

[2] E.A. Veal, A.M. Day, B.A. Morgan, Hydrogen peroxide sensing and signaling, Mol. Cell 26 (2007) 1–14. https://doi.org/10.1016/j.molcel.2007.03.016.

[3] P.M. Vanhoutte, H. Shimokawa, M. Feletou, E.H.C. Tang, Endothelial dysfunction and vascular disease – a 30th anniversary update, Acta Physiol. 219 (2017) 22–96. https://doi.org/10.1111/apha.12646.

[4] E.W. Miller, O. Tulyathan, E.Y. Isacoff, C.J. Chang, Molecular imaging of hydrogen peroxide produced for cell signaling, Nat. Chem. Biol. 3 (2007) 263–267. https://doi.org/10.1038/nchembio871.

[5] M. Sundaresan, Z.X. Yu, V.J. Ferrans, K. Irani, T. Finkel, Requirement for generation of H2O2 for platelet-derived growth factor signal transduction, Science 270 (1995) 296–299. https://doi.org/10.1126/science.270.5234.296.

[6] H. Sies, Role of metabolic H2O2 generation: redox signaling and oxidative stress, J. Biol. Chem. 289 (2014) 8735–8741. https://doi.org/10.1074/jbc.R113.544635.

[7] J.A. Bolduc, J.A. Collins, R.F. Loeser, Reactive oxygen species, aging and articular cartilage homeostasis, Free Radical Biol. Med. 132 (2019) 73–82. https://doi.org/10.1016/j.freeradbiomed.2018.08.038.

[8] S.I. Liochev, Reactive oxygen species and the free radical theory of aging, Free Radical Biol. Med. 60 (2013) 1–4. https://doi.org/10.1016/j.freeradbiomed.2013.02.011.

[9] W.-X. Wang, W.-L. Jiang, G.-J. Mao, M. Tan, J. Fei, Y. Li, C.-Y. Li, Monitoring the Fluctuation of Hydrogen Peroxide in Diabetes and Its Complications with a Novel Near-Infrared Fluorescent Probe, Anal. Chem. 93 (2021) 3301–3307. https://doi.org/10.1021/acs.analchem.0c05364.

[10] S. Galadari, A. Rahman, S. Pallichankandy, F. Thayyullathil, Reactive oxygen species and cancer paradox: To promote or to suppress?, Free Radical Biol. Med. 104 (2017) 144–164. https://doi.org/10.1016/j.freeradbiomed.2017.01.004.

[11] C. Chinopoulos, V. Adam-Vizi, Mitochondria deficient in complex I activity are depolarized by hydrogen peroxide in nerve terminals: relevance to Parkinson's disease, J. Neurochem. 76 (2001) 302–306. https://doi.org/10.1046/j.1471-4159.2001.00060.x.

[12] G.J. Harrison, L.R. Jordan, R.J. Willis, Deleterious effects of hydrogen peroxide on the function and ultrastructure of cardiac muscle and the coronary vasculature of perfused rat hearts, Can. J. Cardiol. 10 (1994) 843–849.

[13] N.G.N. Milton, Role of hydrogen peroxide in the aetiology of Alzheimer's disease: implications for treatment, Drugs Aging 21 (2004) 81–100. https://doi.org/10.2165/00002512-200421020-00002.

[14] Y.M. Lee, W. He, Y.-C. Liou, The redox language in neurodegenerative diseases: oxidative post-translational modifications by hydrogen peroxide, Cell Death Dis. 12 (2021) 58. https://doi.org/10.1038/s41419-020-03355-3.

[15] M.E. Abbas, W. Luo, L. Zhu, J. Zou, H. Tang, Fluorometric determination of hydrogen peroxide in milk by using a Fenton reaction system, Food Chem. 120 (2010) 327–331. https://doi.org/10.1016/j.foodchem.2009.10.024.

[16] S.B. Bankar, M.V. Bule, R.S. Singhal, L. Ananthanarayan, Glucose oxidase--an overview, Biotechnol. Adv. 27 (2009) 489–501. https://doi.org/10.1016/j.biotechadv.2009.04.003.

[17] M. Seki, K. Iida, M. Saito, H. Nakayama, S. Yoshida, Hydrogen peroxide production in Streptococcus pyogenes: involvement of lactate oxidase and coupling with aerobic utilization of lactate, J. Bacteriol. 186 (2004) 2046–2051. https://doi.org/10.1128/JB.186.7.2046-2051.2004.

[18] J. MacLachlan, A. Wotherspoon, R.O. Ansell, C. Brooks, Cholesterol oxidase: sources, physical properties and analytical applications, J. Steroid Biochem. Mol. Biol. 72 (2000) 169–195. https://doi.org/10.1016/S0960-0760(00)00044-3.

[19] J. Meier, E. M Hofferber, J. A Stapleton, N. M Iverson, Hydrogen Peroxide Sensors for Biomedical Applications, Chemosensors 7 (2019) 64. https://doi.org/10.3390/chemosensors7040064.

[20] L. Xing, W. Zhang, L. Fu, J.M. Lorenzo, Y. Hao, Fabrication and application of electrochemical sensor for analyzing hydrogen peroxide in food system and biological samples, Food Chem. 385 (2022) 132555. https://doi.org/10.1016/j.foodchem.2022.132555.

[21] Z. Li, Y. Jiang, C. Liu, Z. Wang, Z. Cao, Y. Yuan, M. Li, Y. Wang, D. Fang, Z. Guo, D. Wang, G. Zhang, J. Jiang, Emerging investigator series: dispersed transition metals on a nitrogen-doped carbon nanoframework for environmental hydrogen peroxide detection, Environ. Sci.: Nano 5 (2018) 1834–1843. https://doi.org/10.1039/C8EN00498F.

[22] F.S. Romolo, S. Connell, C. Ferrari, G. Suarez, J.-J. Sauvain, N.B. Hopf, Locating bomb factories by detecting hydrogen peroxide, Talanta 160 (2016) 15–20. https://doi.org/10.1016/j.talanta.2016.06.033.

[23] J.E. Giaretta, H. Duan, F. Oveissi, S. Farajikhah, F. Dehghani, S. Naficy, Flexible Sensors for Hydrogen Peroxide Detection: A Critical Review, ACS Appl. Mater. Interfaces 14 (2022) 20491–20505. https://doi.org/10.1021/acsami.1c24727.

[24] J.G. Mohanty, Jonathan S. Jaffe, Edward S. Schulman, Donald G. Raible, A highly sensitive fluorescent micro-assay of H_2O_2 release from activated human leukocytes using a dihydroxyphenoxazine derivative, J. Immunol. Methods (1997) 122–141. https://doi.org/10.1016/S0022-1759(96)00244-X.

[25] I. Sanz-Vicente, I. Rivero, L. Marcuello, M.P. Montano, S. de Marcos, J. Galbán, Portable colorimetric enzymatic disposable biosensor for histamine and simultaneous histamine/tyramine determination using a smartphone, Anal. Bioanal. Chem. 415 (2023) 1777–1786. https://doi.org/10.1007/s00216-023-04583-0.

[26] B. Zhao, F.A. Summers, R.P. Mason, Photooxidation of Amplex Red to resorufin: implications of exposing the Amplex Red assay to light, Free Radical Biol. Med. 53 (2012) 1080–1087. https://doi.org/10.1016/j.freeradbiomed.2012.06.034.

[27] N. Burmistrova, O. Kolontaeva, A. Duerkop, New Nanomaterials and Luminescent Optical Sensors for Detection of Hydrogen Peroxide, Chemosensors 3 (2015) 253–273. https://doi.org/10.3390/chemosensors3040253.

[28] V. Sanz, S. de Marcos, J. Galbán, A reagentless optical biosensor based on the intrinsic absorption properties of peroxidase, Biosens. Bioelectron. 22 (2007) 956–964. https://doi.org/10.1016/j.bios.2006.04.008.

[29] D.-J. Zheng, Y.-S. Yang, H.-L. Zhu, Recent progress in the development of small-molecule fluorescent probes for the detection of hydrogen peroxide, TrAC, Trends Anal. Chem. 118 (2019) 625–651. https://doi.org/10.1016/j.trac.2019.06.031.

[30] J.-W. Chen, T.-C. Wu, W. Liang, J.-J. Ciou, C.-H. Lai, Boronates as hydrogen peroxide-reactive warheads in the design of detection probes, prodrugs, and nanomedicines used in tumors and other diseases, Drug Delivery Transl. Res. 13 (2023) 1305–1321. https://doi.org/10.1007/s13346-022-01248-w.

[31] E. Saxon, X. Peng, Recent Advances in Hydrogen Peroxide Responsive Organoborons for Biological and Biomedical Applications, Chembiochem 23 (2022) e202100366. https://doi.org/10.1002/cbic.202100366.

[32] L. Wang, X. Hou, H. Fang, X. Yang, Boronate-Based Fluorescent Probes as a Prominent Tool for H2O2 Sensing and Recognition, Curr. Med. Chem. 29 (2022) 2476–2489. https://doi.org/10.2174/0929867328666210902101642.

[33] O.S. Wolfbeis, Probes, sensors, and labels: why is real progress slow?, Angew. Chem. Int. Ed. 52 (2013) 9864–9865. https://doi.org/10.1002/anie.201305915.

[34] A. Hulanicki, S. Glab, F. Ingman, Chemical sensors: definitions and classification, Pure Appl. Chem. 63 (1991) 1247–1250. https://doi.org/10.1351/pac199163091247.

[35] Márta Vitai, László Góth, Reference ranges of normal blood catalase activity and levels in familial hypocatalasemia in Hungary, Clin. Chim. Acta 261 (1997) 35–42. https://doi.org/10.1016/S0009-8981(97)06514-5.

[36] M. Moßhammer, M. Kühl, K. Koren, Possibilities and Challenges for Quantitative Optical Sensing of Hydrogen Peroxide, Chemosensors 5 (2017) 28. https://doi.org/10.3390/chemosensors5040028.

[37] S. Ruan, W. Liu, W. Wang, Y. Lu, Research Progress of SERS Sensors Based on Hydrogen Peroxide and Related Substances, Crit. Rev. Anal. Chem. (2023) 1–22. https://doi.org/10.1080/10408347.2023.2255901.

[38] K. Chattopadhyay, S. Mazumdar, Structural and conformational stability of horseradish peroxidase: effect of temperature and pH, Biochemistry 39 (2000) 263–270. https://doi.org/10.1021/bi990729o.

[39] S. Bocanegra-Rodríguez, N. Jornet-Martínez, C. Molins-Legua, P. Campíns-Falcó, New Reusable Solid Biosensor with Covalent Immobilization of the Horseradish Peroxidase Enzyme: In Situ Liberation Studies of

Hydrogen Peroxide by Portable Chemiluminescent Determination, ACS Omega 5 (2020) 2419–2427. https://doi.org/10.1021/acsomega.9b03958.

[40] X.T. Zheng, Y. Zhong, H.E. Chu, Y. Yu, Y. Zhang, J.S. Chin, D.L. Becker, X. Su, X.J. Loh, Carbon Dot-Doped Hydrogel Sensor Array for Multiplexed Colorimetric Detection of Wound Healing, ACS Appl. Mater. Interfaces 15 (2023) 17675–17687. https://doi.org/10.1021/acsami.3c01185.

[41] X. Yang, C. Jin, J. Zheng, F. Chai, M. Tian, Portable intelligent paper-based sensors for rapid colorimetric and smartphone-assisted analysis of hydrogen peroxide for food, environmental and medical detection applications, Sens. Actuators, B 394 (2023) 134417. https://doi.org/10.1016/j.snb.2023.134417.

[42] R. Shen, P. Liu, Y. Zhang, Z. Yu, X. Chen, L. Zhou, B. Nie, A. Żaczek, J. Chen, J. Liu, Sensitive Detection of Single-Cell Secreted H2O2 by Integrating a Microfluidic Droplet Sensor and Au Nanoclusters, Anal. Chem. 90 (2018) 4478–4484. https://doi.org/10.1021/acs.analchem.7b04798.

[43] M.-J. Lee, J.-A. Song, J.-H. Choi, J.-H. Shin, J.-W. Myeong, K.-P. Lee, T. Kim, K.-E. Park, B.-K. Oh, 2023. Horseradish Peroxidase-Encapsulated Fluorescent Bio-Nanoparticle for Ultra-Sensitive and Easy Detection of Hydrogen Peroxide. Biosensors (Basel) 13, 289. https://doi.org/10.3390/bios13020289.

[44] J. Goicoechea, P.J. Rivero, S. Sada, F.J. Arregui, Self-Referenced Optical Fiber Sensor for Hydrogen Peroxide Detection based on LSPR of Metallic Nanoparticles in Layer-by-Layer Films, Sensors 19 (2019). https://doi.org/10.3390/s19183872.

[45] O. Hosu, M. Lettieri, N. Papara, A. Ravalli, R. Sandulescu, C. Cristea, G. Marrazza, Colorimetric multienzymatic smart sensors for hydrogen peroxide, glucose and catechol screening analysis, Talanta 204 (2019) 525–532. https://doi.org/10.1016/j.talanta.2019.06.041.

[46] L.S. Lima, E.L. Rossini, L. Pezza, H.R. Pezza, Bioactive paper platform for detection of hydrogen peroxide in milk, Spectrochim. Acta, Part A 227 (2020) 117774. https://doi.org/10.1016/j.saa.2019.117774.

[47] Waris, A. Hasnat, S. Hasan, S. Bano, S. Sultana, A.O. Ibhadon, M.Z. Khan, Development of nanozyme based sensors as diagnostic tools in clinic applications: a review, J. Mater. Chem. B 11 (2023) 6762–6781. https://doi.org/10.1039/d3tb00451a.

[48] L. Tong, L. Wu, E. Su, Y. Li, N. Gu, Recent Advances in the Application of Nanozymes in Amperometric Sensors: A Review, Chemosensors 11 (2023) 233. https://doi.org/10.3390/chemosensors11040233.

[49] N.S. Heo, H.P. Song, S.M. Lee, H.-J. Cho, H.J. Kim, Y.S. Huh, M.I. Kim, Rosette-shaped graphitic carbon nitride acts as a peroxidase mimic in a wide pH range for fluorescence-based determination of glucose with glucose oxidase, Microchim. Acta 187 (2020) 286. https://doi.org/10.1007/s00604-020-04249-z.

[50] S. Zhuo, J. Fang, C. Zhu, J. Du, Preparation of palladium/carbon dot composites as efficient peroxidase mimics for H2O2 and glucose assay, Anal. Bioanal. Chem. 412 (2020) 963–972. https://doi.org/10.1007/s00216-019-02320-0.

[51] S. Zhang, Q. Pu, X. Deng, L. Zhang, N. Ye, Y. Xiang, A ratiometric fluorescence sensor for determination of choline based on gold nanoclusters and enzymatic reaction, Microchem. J. 187 (2023) 108402. https://doi.org/10.1016/j.microc.2023.108402.

[52] Y. Gao, Y. Wang, Y. Wang, P. Magaud, Y. Liu, F. Zeng, J. Yang, L. Baldas, Y. Song, Nanocatalysis meets microfluidics: A powerful platform for sensitive bioanalysis, TrAC, Trends Anal. Chem. 158 (2023) 116887. https://doi.org/10.1016/j.trac.2022.116887.

[53] P. Li, S. Zhang, C. Xu, L. Zhang, Q. Liu, S. Chu, S. Li, G. Mao, H. Wang, Coating Fe3O4 quantum dots with sodium alginate showing enhanced catalysis for capillary array-based rapid analysis of H2O2 in milk, Food Chem. 380 (2022) 132188. https://doi.org/10.1016/j.foodchem.2022.132188.

[54] T.T. Zhao, Z.W. Jiang, S.J. Zhen, C.Z. Huang, Y.F. Li, A copper(II)/cobalt(II) organic gel with enhanced peroxidase-like activity for fluorometric determination of hydrogen peroxide and glucose, Microchim. Acta 186 (2019) 168. https://doi.org/10.1007/s00604-019-3290-3.

[55] G. Li, Y. Chen, F. Liu, W. Bi, C. Wang, D. Lu, D. Wen, Portable visual and electrochemical detection of hydrogen peroxide release from living cells based on dual-functional Pt-Ni hydrogels, Microsyst. Nanoeng. 9 (2023) 152. https://doi.org/10.1038/s41378-023-00623-y.

[56] D. Calabria, A. Pace, E. Lazzarini, I. Trozzi, M. Zangheri, M. Guardigli, S. Pieraccini, S. Masiero, M. Mirasoli, Smartphone-Based Chemiluminescence Glucose Biosensor Employing a Peroxidase-Mimicking, Guanosine-Based Self-Assembled Hydrogel, Biosensors (Basel) 13 (2023). https://doi.org/10.3390/bios13060650.

[57] Y. Mirzaei, A. Gholami, A. Sheini, M.M. Bordbar, An origami-based colorimetric sensor for detection of hydrogen peroxide and glucose using sericin capped silver nanoparticles, Sci. Rep. 13 (2023) 7064. https://doi.org/10.1038/s41598-023-34299-1.

[58] Y. Wei, J. Lu, Y. Xu, X. Song, Y. Yu, H. Zhang, X. Luo, Nanozyme-immobilized cellulose membranes designed by a simple hydrogen bond-dominated for colorimetric detection of hydrogen peroxide and uric acid, Microchem. J. 193 (2023) 109113. https://doi.org/10.1016/j.microc.2023.109113.

[59] M. Farooq, A. Hayat, M.H. Nawaz, M.S. Hassan, M. Nasir, H. Ajab, Tuning the structure and properties of MoS2-SrTiO3 nanocomposite and its enzyme mimic behavior for enhanced optical sensing and measurement of H2O2 in biological samples, Measurement 216 (2023) 112901. https://doi.org/10.1016/j.measurement.2023.112901.

[60] I. Ullah, A. Yaqub, M.Z.U. Haq, H. Ajab, A.T. Jafry, M.K. Khan, Sensitive and cost-effective colorimetric sensor based on enzyme mimic MoS2@CoTiO3 nanocomposite for detection of hydrogen peroxide in milk and tap water, J. Food Compos. Anal. 124 (2023) 105689. https://doi.org/10.1016/j.jfca.2023.105689.

[61] R. Bandi, M. Alle, C.-W. Park, S.-Y. Han, G.-J. Kwon, N.-H. Kim, J.-C. Kim, S.-H. Lee, Cellulose nanofibrils/carbon dots composite nanopapers for the smartphone-based colorimetric detection of hydrogen peroxide and glucose, Sens. Actuators, B 330 (2021) 129330. https://doi.org/10.1016/j.snb.2020.129330.

[62] Y. Li, X. Zhang, J. Shen, W. Qi, 2023. A Colorimetric Paper Sensor Based on Self-assembled Nanocomposite Pd−Pt@hemin-rGO/CNTs-COOH for the Detection of H 2 O 2. ChemNanoMat 9, e202200569. https://doi.org/10.1002/cnma.202200569.

[63] B. Peng, J. Xu, M. Fan, Y. Guo, Y. Ma, M. Zhou, Y. Fang, Smartphone colorimetric determination of hydrogen peroxide in real samples based on B, N, and S co-doped carbon dots probe, Anal. Bioanal. Chem. 412 (2020) 861–870. https://doi.org/10.1007/s00216-019-02284-1.

[64] M.-M. Liu, S.-H. Li, D.-D. Huang, Z.-W. Xu, Y.-W. Wu, Y. Lei, A.-L. Liu, MoOx quantum dots with peroxidase-like activity on microfluidic paper-based analytical device for rapid colorimetric detection of H2O2 released from PC12 cells, Sens. Actuators, B 305 (2020) 127512. https://doi.org/10.1016/j.snb.2019.127512.

[65] D. Cheng, J. Qin, Y. Feng, J. Wei, Synthesis of Mesoporous CuO Hollow Sphere Nanozyme for Paper-Based Hydrogen Peroxide Sensor, Biosensors (Basel) 11 (2021). https://doi.org/10.3390/bios11080258.

[66] S. Schnell, Validity of the Michaelis-Menten equation--steady-state or reactant stationary assumption: that is the question, FEBS J. 281 (2014) 464–472. https://doi.org/10.1111/febs.12564.

[67] S. Gu, S. Risse, Y. Lu, M. Ballauff, Mechanism of the Oxidation of 3,3',5,5'-Tetramethylbenzidine Catalyzed by Peroxidase-Like Pt Nanoparticles Immobilized in Spherical Polyelectrolyte Brushes: A Kinetic Study, ChemPhysChem 21 (2020) 450–458. https://doi.org/10.1002/cphc.201901087.

[68] A. Robert, B. Meunier, How to Define a Nanozyme, ACS Nano 16 (2022) 6956–6959. https://doi.org/10.1021/acsnano.2c02966.

[69] J. Huang, Y. Zheng, H. Niu, J. Huang, X. Zhang, J. Chen, B. Ma, C. Wu, Y. Cao, Y. Zhu, A Multifunctional Hydrogel for Simultaneous Visible H_2O_2 Monitoring and Accelerating Diabetic Wound Healing, Adv. Healthcare Mater. (2023) e2302328. https://doi.org/10.1002/adhm.202302328.

[70] M. Mayer, S. Takegami, M. Neumeier, S. Rink, A. Jacobi von Wangelin, S. Schulte, M. Vollmer, A.G. Griesbeck, A. Duerkop, A.J. Baeumner, Electrochemiluminescence Bioassays with a Water-Soluble Luminol Derivative Can Outperform Fluorescence Assays, Angew. Chem. Int. Ed. 57 (2018) 408–411. https://doi.org/10.1002/anie.201708630.

[71] S. Rink, A. Duerkop, A.J. Baeumner, Enhanced Chemiluminescence of a Superior Luminol Derivative Provides Sensitive Smartphone-Based Point-of-Care Testing with Enzymatic µPAD, Anal. Sens. (2023). https://doi.org/10.1002/anse.202200111.

[72] H. Vasconcelos, A. Matias, J. Mendes, J. Araújo, B. Dias, P.A. Jorge, C. Saraiva, J.M.M. de Almeida, L.C. Coelho, Compact biosensor system for the quantification of hydrogen peroxide in milk, Talanta 253 (2023) 124062. https://doi.org/10.1016/j.talanta.2022.124062.

[73] A. Schroter, T. Hirsch, Control of Luminescence and Interfacial Properties as Perspective for Upconversion Nanoparticles, Small (2023) e2306042. https://doi.org/10.1002/smll.202306042.

[74] G. Chen, H. Qiu, P.N. Prasad, X. Chen, Upconversion nanoparticles: design, nanochemistry, and applications in theranostics, Chem. Rev. 114 (2014) 5161–5214. https://doi.org/10.1021/cr400425h.

[75] X. Wang, J. Fu, C. Jiang, X. Liao, Y. Chen, T. Jia, G. Chen, X. Feng, Specific and Long-Term Luminescent Monitoring of Hydrogen Peroxide in Tumor Metastasis, Adv. Mater. 35 (2023) e2210948. https://doi.org/10.1002/adma.202210948.

[76] Y. Wu, Da Lei, J. Li, Y. Luo, Y. Du, S. Zhang, B. Zu, Y. Su, X. Dou, Controlled Synthesis of Preferential Facet-Exposed Fe-MOFs for Ultrasensitive Detection of Peroxides, Small (2024) e2401024. https://doi.org/10.1002/smll.202401024.

[77] A. Dutta, U. Maitra, Naked-Eye Detection of Hydrogen Peroxide on Photoluminescent Paper Discs, ACS Sens. 7 (2022) 513–522. https://doi.org/10.1021/acssensors.1c02322.

[78] Q. Chen, L. Yang, K. Guo, J. Yang, J.-M. Han, Expedite Fluorescent Sensor Prototype for Hydrogen Peroxide Detection with Long-Life Test Substrates, ACS Omega 6 (2021) 11447–11457. https://doi.org/10.1021/acsomega.1c00471.

[79] Y. Zhang, Y. Feng, Z. Zhang, M. Zhang, Highly efficient fluorescent film probe of hydrogen peroxide vapor, Microchem. J. 158 (2020) 105290. https://doi.org/10.1016/j.microc.2020.105290.

[80] Z. Xu, C. Zeng, Y. Zhao, M. Zhou, T. Lv, C. Song, T. Qin, L. Wang, B. Liu, X. Peng, Smartphone-based on-site detection of hydrogen peroxide in milk by using a portable ratiometric fluorescent probe, Food Chem. 410 (2023) 135381. https://doi.org/10.1016/j.foodchem.2022.135381.

[81] J. Chang, H. Li, T. Hou, W. Duan, F. Li, Paper-based fluorescent sensor via aggregation induced emission fluorogen for facile and sensitive visual detection of hydrogen peroxide and glucose, Biosens. Bioelectron. 104 (2018) 152–157. https://doi.org/10.1016/j.bios.2018.01.007.

[82] H. Mei, Y. Ma, H. Wu, X. Wang, Fluorescent and visual assay of H2O2 and glucose based on a highly sensitive copper nanoclusters-Ce(III) fluoroprobe, Anal. Bioanal. Chem. 413 (2021) 2135–2146. https://doi.org/10.1007/s00216-021-03181-2.

[83] C. Meng, F. Du, A. Abdussalam, A. Wang, D. Snizhko, W. Zhang, G. Xu, Sonochemiluminescence Using Apertureless USB Piezoelectric Ultrasonic Transducer and Its Applications for the Detection of Hydrogen Peroxide, Glucose, and Glucose Oxidase Activity, Anal. Chem. 93 (2021) 14934–14939. https://doi.org/10.1021/acs.analchem.1c03834.

[84] L. Sharma, S. Gouraj, P. Raut, C. Tagad, Development of a surface-modified paper-based colorimetric sensor using synthesized Ag NPs-alginate composite, Environ. Technol. 42 (2021) 3441–3450. https://doi.org/10.1080/09593330.2020.1732471.

[85] Z. He, J. Huang, W. Shen, X. Lei, Y. Zhang, L. Zhu, X. Shen, D. Zhang, D. Yu, M. Zhou, A Paper-Based Fluorescent Sensor for Rapid Early Screening of Oral Squamous Cell Carcinoma, ACS Appl. Mater. Interfaces 15 (2023) 24913–24922. https://doi.org/10.1021/acsami.3c03545.

[86] J. Noh, M. Jung, Y. Jung, C. Yeom, M. Pyo, G. Cho, Key Issues With Printed Flexible Thin Film Transistors and Their Application in Disposable RF Sensors, Proc. IEEE 103 (2015) 554–566. https://doi.org/10.1109/JPROC.2015.2410303.

[87] D. Mampallil, H.B. Eral, A review on suppression and utilization of the coffee-ring effect, Adv. Colloid Interface Sci. 252 (2018) 38–54. https://doi.org/10.1016/j.cis.2017.12.008.

[88] Y. Shen, Y. Wei, C. Zhu, J. Cao, D.-M. Han, Ratiometric fluorescent signals-driven smartphone-based portable sensors for onsite visual detection of food contaminants, Coord. Chem. Rev. 458 (2022) 214442. https://doi.org/10.1016/j.ccr.2022.214442.

[89] D. Zhang, Q. Liu, Biosensors and bioelectronics on smartphone for portable biochemical detection, Biosens. Bioelectron. 75 (2016) 273–284. https://doi.org/10.1016/j.bios.2015.08.037.

[90] G. Ross, Y. Zhao, A.J. Bosman, A. Geballa-Koukoula, H. Zhou, C.T. Elliott, M. Nielen, K. Rafferty, G. Salentijn, Best practices and current implementation of emerging smartphone-based (bio)sensors – Part 1: Data handling and ethics, TrAC, Trends Anal. Chem. 158 (2023) 116863. https://doi.org/10.1016/j.trac.2022.116863.

[91] P. Rai, S. Verma, S. Mehrotra, S.K. Sharma, A QR code-integrated chromogenic paper strip for detection of hydrogen peroxide in aqueous samples, Anal. Methods 15 (2023) 5286–5293. https://doi.org/10.1039/d3ay01584j.

[92] R. Meng, Z. Yu, Q. Fu, Y. Fan, L. Fu, Z. Ding, S. Yang, Z. Cao, L. Jia, Smartphone-based colorimetric detection platform using color correction algorithms to reduce external interference, Spectrochim. Acta, Part A 316 (2024) 124350. https://doi.org/10.1016/j.saa.2024.124350.

[93] V. Doğan, E. Yüzer, V. Kılıç, M. Şen, Non-enzymatic colorimetric detection of hydrogen peroxide using a µPAD coupled with a machine learning-based smartphone app, Analyst 146 (2021) 7336–7344. https://doi.org/10.1039/d1an01888d.

[94] P. Cebrián, L. Pérez-Sienes, I. Sanz-Vicente, Á. López-Molinero, S. de Marcos, J. Galbán, Solving Color Reproducibility between Digital Devices: A Robust Approach of Smartphones Color Management for Chemical (Bio)Sensors, Biosensors (Basel) 12 (2022). https://doi.org/10.3390/bios12050341.

[95] A. García, M.M. Erenas, E.D. Marinetto, C.A. Abad, I. de Orbe-Paya, A.J. Palma, L.F. Capitán-Vallvey, Mobile phone platform as portable chemical analyzer, Sens. Actuators, B 156 (2011) 350–359. https://doi.org/10.1016/j.snb.2011.04.045.

[96] J. Schindelin, I. Arganda-Carreras, E. Frise, V. Kaynig, M. Longair, T. Pietzsch, S. Preibisch, C. Rueden, S. Saalfeld, B. Schmid, J.-Y. Tinevez, D.J. White, V. Hartenstein, K. Eliceiri, P. Tomancak, A. Cardona, Fiji: an open-source platform for biological-image analysis, Nat. Methods 9 (2012) 676–682. https://doi.org/10.1038/nmeth.2019.

[97] N.Y. Tiuftiakov, A.V. Kalinichev, N.V. Pokhvishcheva, M.A. Peshkova, Digital color analysis for colorimetric signal processing: Towards an analytically justified choice of acquisition technique and color space, Sens. Actuators, B 344 (2021) 130274. https://doi.org/10.1016/j.snb.2021.130274.

[98] Y. Zhang, Y. Wu, Y. Zhang, A. Ozcan, Color calibration and fusion of lens-free and mobile-phone microscopy images for high-resolution and accurate color reproduction, Sci. Rep. 6 (2016) 27811. https://doi.org/10.1038/srep27811.

[99] A. Skandarajah, C.D. Reber, N.A. Switz, D.A. Fletcher, Quantitative imaging with a mobile phone microscope, PLoS One 9 (2014) e96906. https://doi.org/10.1371/journal.pone.0096906.

[100] M. Moßhammer, M. Kühl, K. Koren, Possibilities and Challenges for Quantitative Optical Sensing of Hydrogen Peroxide, Chemosensors 5 (2017) 28. https://doi.org/10.3390/chemosensors5040028.

[101] K. Koren, C.M. McGraw, Let's Talk about Slime; or Why Biofouling Needs More Attention in Sensor Science, ACS Sens. 8 (2023) 2432–2439. https://doi.org/10.1021/acssensors.3c00961.

[102] M. Moßhammer, V. Schrameyer, P.Ø. Jensen, K. Koren, M. Kühl, Extracellular hydrogen peroxide measurements using a flow injection system in combination with microdialysis probes - Potential and challenges, Free Radical Biol. Med. 128 (2018) 111–123. https://doi.org/10.1016/j.freeradbiomed.2018.05.089.

[103] M. Moßhammer, K. Koren, M. Kühl, 2. Flow Injection Analysis with Microdialysis Probes Enable Minimally Invasive and Dynamic H2O2 Measurements. Proceedings 2018, 992. https://doi.org/10.3390/proceedings2130992.

[104] F. Li, J. Liu, L. Guo, J. Wang, K. Zhang, J. He, H. Cui, High-resolution temporally resolved chemiluminescence based on double-layered 3D microfluidic paper-based device for multiplexed analysis, Biosens. Bioelectron. 141 (2019) 111472. https://doi.org/10.1016/j.bios.2019.111472.

[105] S. Yuan, R. Yu, Y. Tu, Y. Du, X. Feng, F. Nie, An enhanced chemiluminescence hybrids of luminol by sulfonated polyaniline decorated copper-based metal organic frame composite applicable to the measurement of hydrogen peroxide in a wide pH range, Talanta 254 (2023) 124183. https://doi.org/10.1016/j.talanta.2022.124183.

[106] C.-L. Shen, G.-S. Zheng, M.-Y. Wu, J.-Y. Wei, Q. Lou, Y.-L. Ye, Z.-Y. Liu, J.-H. Zang, L. Dong, C.-X. Shan, Chemiluminescent carbon nanodots as sensors for hydrogen peroxide and glucose, Nanophotonics 9 (2020) 3597–3604. https://doi.org/10.1515/nanoph-2020-0233.

[107] T. Sun, Y. Su, M. Sun, Y. Lv, Homologous chemiluminescence resonance energy transfer on the interface of WS2 quantum dots for monitoring photocatalytic H2O2 evaluation, Microchemical Journal 168 (2021) 106344. https://doi.org/10.1016/j.microc.2021.106344.

[108] R. Gaikwad, P.R. Thangaraj, A.K. Sen, Direct and rapid measurement of hydrogen peroxide in human blood using a microfluidic device, Sci. Rep. 11 (2021) 2960. https://doi.org/10.1038/s41598-021-82623-4.

[109] Y. Malyukin, V. Seminko, P. Maksimchuk, E. Okrushko, O. Sedyh, Y. Zorenko, Hydrogen peroxide sensing using Ce3+ luminescence of cerium oxide (CeO2-x) nanoparticles, Opt. Mater. 85 (2018) 303–307. https://doi.org/10.1016/j.optmat.2018.08.063.

[110] V. Seminko, P. Maksimchuk, V. Klochkov, Y. Neuhodov, L. Demchenko, S. Yefimova, Reversible CeO_{2-x} and CeO_{2-x}:Eu^{3+} Luminescent Hydrogen Peroxide Sensors with Recovery Rates Controlled by Temperature and UV Irradiation, J. Phys. Chem. C 127 (2023) 10662–10669. https://doi.org/10.1021/acs.jpcc.3c02637.

[111] P. Virbickas, G. Kavaliauskaitė, A. Valiūnienė, V. Plaušinaitienė, A.I. Rekertaitė, A. Ramanavičius, Cobalt hexacyanoferrate based optical sensor for continuous optical sensing of hydrogen peroxide, Electrochim. Acta 362 (2020) 137202. https://doi.org/10.1016/j.electacta.2020.137202.

[112] H.D. Duong, J.I. Rhee, Development of Ratiometric Fluorescence Sensors Based on CdSe/ZnS Quantum Dots for the Detection of Hydrogen Peroxide, Sensors 19 (2019). https://doi.org/10.3390/s19224977.

[113] C. Liu, F. Hu, W. Yang, J. Xu, Y. Chen, A critical review of advances in surface plasmon resonance imaging sensitivity, TrAC, Trends Anal. Chem. 97 (2017) 354–362. https://doi.org/10.1016/j.trac.2017.10.001.

[114] V. Semwal, B.D. Gupta, Highly selective SPR based fiber optic sensor for the detection of hydrogen peroxide, Sens. Actuators, B 329 (2021) 129062. https://doi.org/10.1016/j.snb.2020.129062.

[115] H.E. Posch, O.S. Wolfbeis, Optical sensor for hydrogen peroxide, Microchim. Acta 97 (1989) 41–50. https://doi.org/10.1007/BF01197282.

[116] X. Wang, O.S. Wolfbeis, Optical methods for sensing and imaging oxygen: materials, spectroscopies and applications, Chem. Soc. Rev. 43 (2014) 3666–3761. https://doi.org/10.1039/C4CS00039K.

[117] L. Ding, S. Chen, W. Zhang, Y. Zhang, X. Wang, Fully Reversible Optical Sensor for Hydrogen Peroxide with Fast Response, Anal. Chem. 90 (2018) 7544–7551. https://doi.org/10.1021/acs.analchem.8b01159.

[118] A.Ø. Tjell, B. Jud, R. Schaller-Ammann, T. Mayr, Optical Hydrogen Peroxide Sensor for Measurements in Flow, Sens. Actuators, B (2023) 134904. https://doi.org/10.1016/j.snb.2023.134904.

[119] A.Ø. Tjell, L.-E. Meyer, B. Jud, S. Kara, T. Mayr, At-line monitoring of hydrogen peroxide released from its photocatalytic and continuous synthesis, React. Chem. Eng. 9 (2024) 777–781. https://doi.org/10.1039/D3RE00659J.

[120] S. Fuchs, V. Rieger, A.Ø. Tjell, S. Spitz, K. Brandauer, R. Schaller-Ammann, J. Feiel, P. Ertl, I. Klimant, T. Mayr, Optical glucose sensor for microfluidic cell culture systems, Biosens. Bioelectron. 237 (2023) 115491. https://doi.org/10.1016/j.bios.2023.115491.

[121] P.M. Nowak, R. Wietecha-Posłuszny, J. Pawliszyn, White Analytical Chemistry: An approach to reconcile the principles of Green Analytical Chemistry and functionality, TrAC, Trends Anal. Chem. 138 (2021) 116223. https://doi.org/10.1016/j.trac.2021.116223.

[122] M. Buzdar, A. Yaqub, A. Hayat, M.Z. Ul Haq, A. Khan, H. Ajab, Paper based colorimetric sensor using novel green magnetized nanocomposite of pinus for hydrogen peroxide detection in water and milk, Food Biosci. 55 (2023) 103014. https://doi.org/10.1016/j.fbio.2023.103014.

[123] S. Vijayaram, H. Razafindralambo, Y.-Z. Sun, S. Vasantharaj, H. Ghafarifarsani, S.H. Hoseinifar, M. Raeeszadeh, Applications of Green Synthesized Metal Nanoparticles - a Review, Biol. Trace Elem. Res. (2023) 1–27. https://doi.org/10.1007/s12011-023-03645-9.

[124] Le Dong, R. Li, L. Wang, X. Lan, H. Sun, Y. Zhao, L. Wang, Green synthesis of platinum nanoclusters using lentinan for sensitively colorimetric detection of glucose, Int. J. Biol. Macromol. 172 (2021) 289–298. https://doi.org/10.1016/j.ijbiomac.2021.01.049.

[125] J. Seemann, F.-R. Rapp, A. Zell, G. Gauglitz, Classical and modern algorithms for the evaluation of data from sensor-arrays, Fresenius J. Anal. Chem. 359 (1997) 100–106. https://doi.org/10.1007/s002160050543.

[126] W. Yu, X. Zheng, M. Tan, J. Wang, B. Wu, J. Ma, Y. Pan, B. Chen, C. Chu, Field Quantification of Hydroxyl Radicals by Flow-Injection Chemiluminescence Analysis with a Portable Device, Environ. Sci. Technol. 58 (2024) 2808–2816. https://doi.org/10.1021/acs.est.3c09140.

3 A fluorescent MTP-based Detection Platform for Hydrogen Peroxide, Glucose, and Lactate

---

3.1 Abstract

Hydrogen Peroxide (H_2O_2) is an important small metabolite often quantified with commercially available multi-step fluorescence-based assays. We developed a new microtiter plate (MTP) based platform that allows a rapid, one-step assay with a ratiometric readout function. Specifically, we embedded 10-Acetyl-3,7-dihydroxyphenoxazine (ADHP) in a polyurethane-based hydrogel sensor membrane. For a ratiometric set-up the membranes were loaded with polystyrene nanoparticles containing a Cy5-based reference which allowed for the compensation for variations in membrane thickness. These knife-coated µm-thin films were mounted onto bottomless MTPs with double-sided adhesive tape. Optimized membranes provided measurement times of 3 minutes upon sample addition and an LOD that was 10x lower than that of the ADHP-using Amplex Red® commercial kit of 100 nmol·L^{-1} H_2O_2. These ADHP hydrogels could be stored at room temperature for at least 22 months. Horseradish peroxidase (HRP) was nanospotted alone or together with either lactate oxidase or glucose oxidase for the detection of H_2O_2, lactate and glucose, respectively. With 50 v% glycerol as cryoprotectant in the spotting solution the HRP ADHP platform was stable for at least 13 weeks at – 20 °C. Enhanced simplicity and comparable performance to multi-step assays suggest that the platform can simplify MTP-based assays in the future.

Keywords: H_2O_2, Hydrogen Peroxide, Hydrogel, Amplex Red, Sensor, HRP

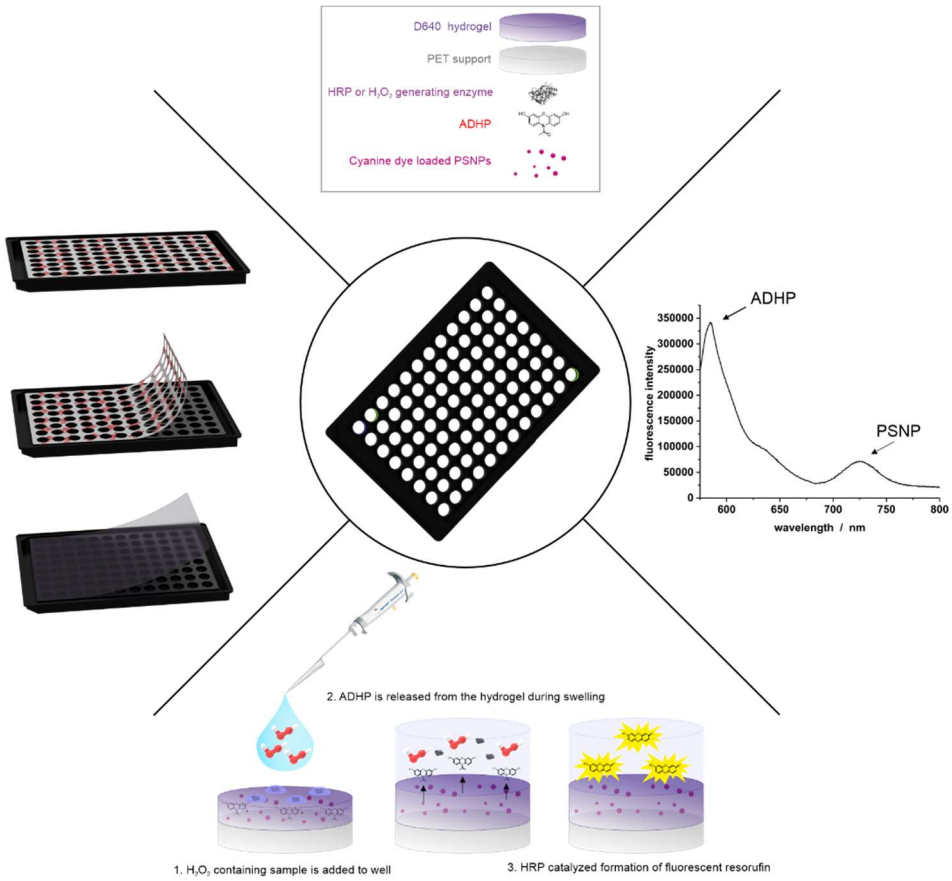

Figure 3.1: Graphical abstract

3.2 Introduction

Hydrogen peroxide (H_2O_2) is a compound found in a variety of applications as reagent, disinfectant, or metabolite in numerous enzyme-catalyzed reactions. In the first cases, the analysis is important in order to determine concentrations beyond the desired or permitted limit values and thus to avert any harmful effects [1]. In case of the latter, H_2O_2 is a particularly interesting analyte as a marker for a variety of diseases [2] and due to the availability of a range of H_2O_2-generating enzymes that provide access to concentrations of multiple precursor analytes [3].

Electrochemical [4] and optical [5] methods are the two most commonly developed approaches to detect H_2O_2. Depending on the setup, electrochemical approaches either monitor the oxidation or reduction of H_2O_2. To overcome the high potentials needed, a plethora of approaches both for novel materials and surface modifications for electrodes and new electrocatalysts for the electrochemical detection of H_2O_2 has been developed making electrochemical detection a viable option for rapid and on-site tests [4,6,7].

In a non-automated setting, optical H_2O_2-quantification is often achieved with commercially available colorimetric or fluorescent assays in microtiter plates (MTPs) with desirably low LODs [8]. In case of colorimetry, TMB [9] or ABTS [10] are typically applied, for fluorescent approaches, although also usable for colorimetric [11] and electrochemical detection [12], the predominant dye is 10-Acetyl-3,7-dihydroxyphenoxazine (ADHP) better known by its commercial name Amplex Red™ [13]. In presence of H_2O_2 and a suitable catalyst or enzyme, here horseradish peroxidase (HRP), a 1:1 stoichiometric, irreversible reaction takes place from colorless and non-fluorescent ADHP to pink-colored resorufin, which shows a fluorescence emission peak at 585 nm with a 572 nm excitation maximum [14] (Figure 3.2).

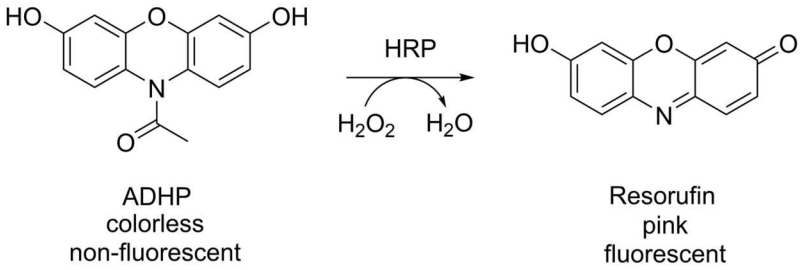

Figure 3.2: HRP-catalyzed reaction of colorless, non-fluorescent ADHP to pink, fluorescent Resorufin in presence of H_2O_2

ADHP is ideally stored at -20 °C, light protected [15] and separately from horseradish peroxidase (HRP) which is preferably stored at 4 °C, due to the slow oxidation to resorufin occurring in presence of HRP, even without any H_2O_2 present which makes the development of one-step biosensors and assays difficult [11]. Hence the combination of the ADHP-HRP couple results in additional thawing, dilution and mixing steps for any assay that takes more time and in turn reduces the amount of sample throughput and considerably increases the chance for human error. However, considering the instability of dilute H_2O_2 [16] the quantification of low concentrations is time-critical to avoid an underestimation of H_2O_2.

In the past, hydrogel membranes have shown to be the ideal environment for the storage of (bio-)recognition probes [17]. Hydrogels have also been used for a variety of applications in the development of detection methods, such as containing the catalytically active component [18], as H_2O_2 scavenger [19] or for housing the probe [20]. Hydrogels and polymers that do not require chemical or physical crosslinking can usually be easily applied onto surfaces by knife coating, also known as doctor blade coating [21] to form versatile sensor membranes of µm-thickness.

We therefore investigated an approach towards an all-in-one ratiometric fluorescent H_2O_2 MTP detection platform that is simple to produce and is based on the fast and efficient release of ADHP from a thin film of commercially available polyurethane hydrogel after a single sample-addition step. By nanospotting HRP together with H_2O_2 generating enzymes, we achieve sufficient separation of enzyme and dye to combine assay times of few minutes with LODs for H_2O_2 down to 10 nmol·L^{-1}. To extend the stability of the spotted enzyme for storage we used 50 v% glycerol as cryoprotectant to investigate the stability for a duration of 13 weeks.

3.3 Material and Methods

Detailed protocols on membrane production, the used devices and all the measurements performed can be found in the SI. Bidistilled water was used for any aqueous solutions, if not stated otherwise. All organic solvents used were of analytical grade or better quality and used without further purification.

3.3.1 Chemicals

HydroMed D640 was supplied from AdvanSource biomaterials, Mitsubishi Chemical America Inc. (Wilmington, USA), H_2O_2-solution (34.5-36.5 %), glycerol (≥ 99 %), Polystyrene (average Mw ≈ 280000 g·mol^{-1}), horseradish peroxidase and glucose oxidase were obtained from Sigma-Aldrich, Merck KGaA (Darmstadt, Germany), lactate oxidase was purchased from Sorachim SA (Lausanne, Switzerland), 10-Acetyl-3,7-dihydroxyphenoxazine (ADHP, 99.5%) was purchased from Synchem UG & Co KG (Felsberg-Altenburg, Germany). S0982, 4,5:4',5'-Dibenzo-1,1'-dibutyl-3,3,3',3'-tetramethylindadicarbocyanine hexafluorophosphate was supplied by FEW-chemicals GmbH (Bitterfeld-Wolfen, Germany), Sodium dodecyl sulfate (SDS, ≥ 99.0%) was obtained from AppliChem GmbH (Darmstadt, Germany)

Phosphate buffered saline (PBS, pH 7.4) was prepared from NaCl (p.A), KCl (p.a.) from Carl Roth GmbH + Co. KG (Karlsruhe, Germany), Na_2HPO_4 (p.a.), and KH_2PO_4 (p.a.) from Merck KGaA (Darmstadt, Germany). The pH was adjusted to 7.4 with NaOH-solution (1 mol·L^{-1}, Titripur®) also from Merck KGaA.

3.3.2 Special labware

Non-sterile black bottomless 96-well MTPs were purchased from Greiner Bio-One GmbH (www.gbo.com). 3M Double-sided adhesive tape with polyester backing GPT-020F, transparent, 100 mm x 50 m, 0.202 mm was obtained from SKS GmbH (www.shop-sks.com). Biaxially oriented PET-membrane roll with a thickness of 125 µm was purchased from goodfellow GmbH (www.goodfellow.com). Spectra/Por® 4 dialysis membrane tubing MWCO:12-14 kD was obtained from Carl Roth GmbH & Co KG (www.carlroth.com). Life science sealing films for storage and automation, aluminum, self-adhesive were bought from Brand GmbH && Co KG (www.brand.de).

3.3.3 Dye-loaded polystyrene nanoparticle (PSNP) synthesis

Dye loaded PSNPs were synthesized following a modified protocol published by Bartoš et al. [22], which is a polymerization free version of the surfactant-enabled microemulsion method [23,24]. In short, aqueous sodium lauryl sulfate (SDS)-solution (14.0 mL, 1.00 mg·mL^{-1}, 48.5 mmol), PS in toluene (average Mw ≈ 280000, 1800 µL, 96.6 mg·mL^{-1}, 174 mg) and S0982 in toluene (100.0 µL, 17.29 mg·mL^{-1}, 1.729 mg) were filled in a glass vial with snap cap. Under vigorous stirring, the solution was sonicated with a sonication tip at 60 W with 60 one-second pulses a total of three times. In between each sonication procedure, the emulsion was stirred with a sealed lid for 1 h. Afterwards, the solvent was allowed to evaporate at RT with an open lid under stirring for 48 h. The residual aqueous phase was then dialyzed over 72 h with bidistilled water (800 mL). The dialysate was exchanged five times. Particle suspensions were stored light-protected in ambient conditions. Particles were analyzed with fluorescence spectroscopy, DLS and TEM.

3.3.4 Membrane production

For a typical membrane, ADHP-stock in DMSO (20 µL, 50 mmol·L^{-1}, 1 µmol) was added to D640 (6 g 10 w%, in EtOH/H_2O 9:1 v/v). The solution was vigorously stirred light-protected for 10 min. Precleaned dust-free 15 x 34 cm PET-substrate was fixed to a vacuum bed and the D640-ADHP cocktail (spacer was set to a thickness of 30 µm) was knife-coated on top. The film was then dried for 2 h at 37 °C, laser-cut (SI figure) and fixed to the underside of a self-made sticky MTP (Figure 3.3 + SI figure 3.1).

3.3.5 Spotting procedure

Nanospotting was done with a scienion nanospotter (www.scienion.com) equipped with a coated NDC-M nozzle. Following a standard startup and priming procedure, the required spotting volume (25 – 50 nL) is set by adjusting pressure and valve-opening time (i.e. 8% pressure ≙ 37 kPa, 350 µs pulse time results in ≈ 30 nL spots, SI figure 3.18). The solution to be nanospotted is aspirated (in PBS pH 7.4: HRP 22.5 U·mL^{-1}, GOx 0.2 U·mL^{-1}, LOx 0.4 U·mL^{-1}) the tip subsequently dipped into water to remove enzyme-solution contaminating the outside of the tip and 20 jets are ejected to remove any water aspirated by capillary forces. The corresponding number of spots is then dispensed into each selected well on the MTP-mounted membrane following the production as described in section 3.8.13. For further functionalization, additional enzyme (GOx, LOx) was spotted in a second step following the same procedure as for HRP.

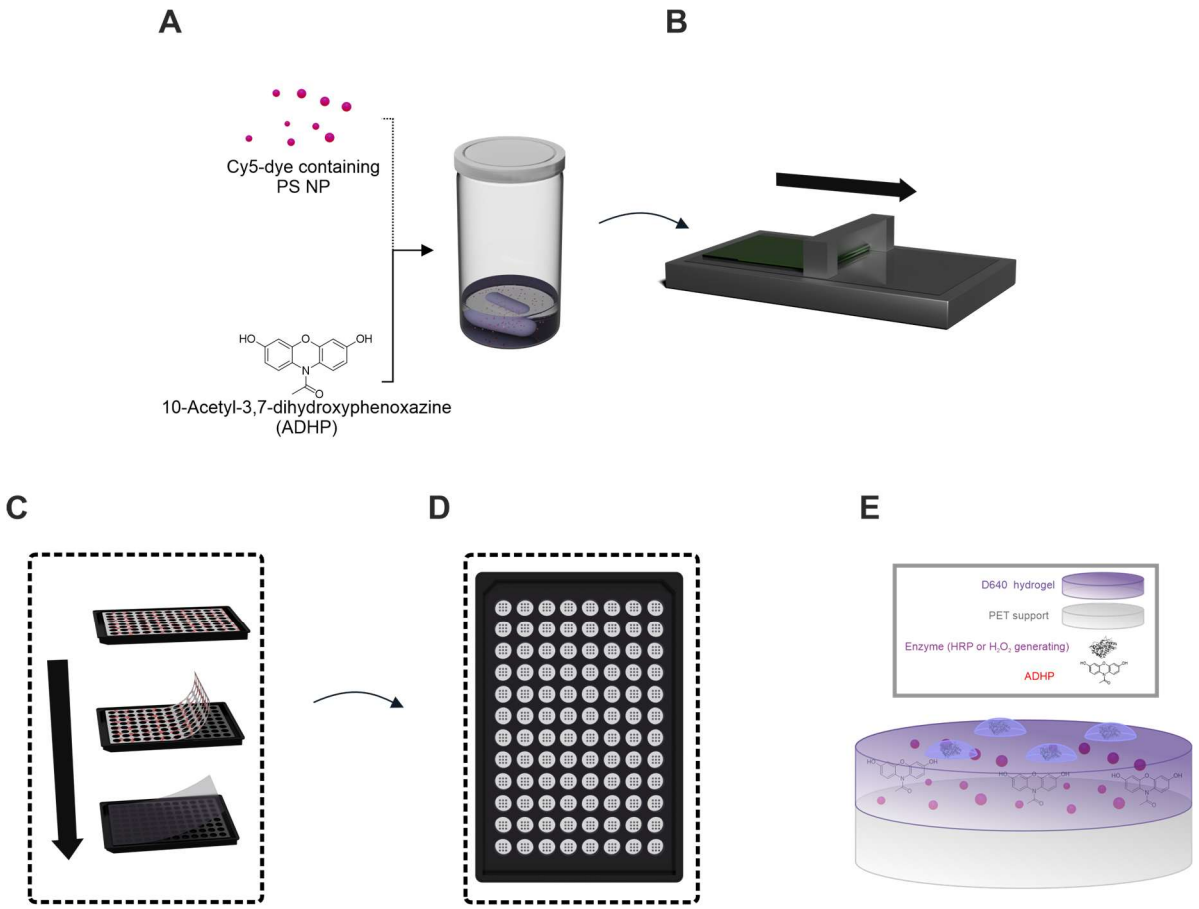

Figure 3.3: A Luminescent HP probe & reference dye particles are dissolved in hydrogel B from which membranes are knife-coated and dried on PET. C Sensing membranes are laser cut and stuck onto the underside of in-house made sticky bottom MTPs. D Enzyme is spotted on top of the sensing membrane in the wells. E Schematic cross-section of stacked sensor membrane with support, hydrogel, dye NPs and the probe ADHP.

3.4 Results and Discussion

3.4.1 MTP design and knife coating

The necessity of several predilution and preparation steps before measurement with commercial ADHP tests makes the usage of the latter time and cost-intensive, and in case of automation, requires more sophisticated procedures and extra steps. In designing the new platform technology, the goal was to reduce this to ideally one step, in which the sample is prediluted in buffer for pH adjustment and then just added to an MTP containing all the other required reagents and catalysts. Key to the new platform is the use of a hydrogel membrane in which the assay reagents can be embedded and simultaneously separated from each other. Thus, a fluorescent detection probe and polystyrene nanoparticles with an integrated reference dye were added into a hydrogel matrix, and enzymes were simply nanospotted on the dried film. Thus, all three components are stored with sufficient separation and the system can easily be mass-produced providing increased stability of all components in the dried state and in the correct concentration for the desired assay. Upon addition of sample or buffer, the enzymes are dissolved, the fluorescent probe is released, and the reference dye remains protected from exposure to the analyte.

While there are a variety of methods to apply hydrogels and polymers for the development of sensors [21] we decided to use knife-coating, also known as doctor blade coating, as it enables both fast prototyping and parameter screening on small scale coaters but is also accessible to large-scale industrial roll-to-roll production. For this approach we also developed and prepared sticky MTPs from bottomless MTPs with double-sided adhesive tape stuck to the underside of the well walls by laser-cutting double-sided adhesive tape to fit the wall of the wells (compare 3.8.11). The knife-coated membranes can then be laser-cut and mounted on the underside of these in-house modified bottomless 96-well MTPs, allowing a fast, simple and streamlined production of a detection platform for a widespread system. The transparent coating substrate and hydrogel allow for the detection with both top optics, and, if available, bottom optics measurement in an MTP-reader.

Looking for a suitable polymer or hydrogel as matrix, we tested several polymer/solvent combinations. We primarily focused on commercially available polymers that do not require chemical or photocatalytic crosslinking or curing, but only solvent evaporation after coating. For this study, we investigated polyvinyl acetate/cellulose acetate (PVAc/CA), LRP t 7016®, D4 and D640.

PVAc/CA has been used in literature as coating for enzymatic sensors [25], we investigated both DMF/H_2O and cyclohexanone (Chon) as solvent candidates. PVAc/CA 10w% DMF/H_2O 9:1 v/v (SI figure 3.4 G, SI figure 3.5 G) shows very little fluorescence intensity increase over time with no clear dependence of H_2O_2 concentration, which suggests very little and insufficient release of ADHP. The kinetic curve of the PVAc/CA 10w% Chon/H_2O 99:1 v/v-membranes indicate a better reagent release of ADHP (SI figure 3.4 F, SI figure 3.5 F), however no specificity towards the concentration of H_2O_2 making this polymer combination unsuitable.

LRP t 7016, which is an amorphous poly(L-lactide-co-D,L-lactide-co-PEG) triblock-polymer dissolved in THF/H_2O 99:1 has the disadvantage of no release of ADHP (SI figure 3.4 H, SI figure 3.5 H). D4 and D640 are both polyurethane-based hydrogels, whereby D4 in particular is often used as matrix for the development of optical sensors [26–29]. In comparison to D4, D640 exhibits a larger pore size, due to its increased maximum water content. Both can be dissolved in a variety of solvents. However, using aqueous-ethanolic mixtures as solvents is particularly interesting as toxic, cancerogenic and high-boiling solvents can be avoided. In this context, alcohols in the 9:1 mix were tested with D4 as solvent component to determine the effect of the type of alcohol on the response. We investigated the effect of different alcohols (ethanol, isopropanol and tert-butanol) and dimethyl formamide (DMF) as polar aprotic solvent in the coating mix toward the release of the dye. In general, D4 shows a good reagent release and response time/kinetic curve. There was however no major difference in the response time for the different solvents, with the last concentration reaching the equilibrium after about 10 min (SI figure 3.4 A-D, SI figure 3.5 A-D). Isopropanol as co-solvent seems to reduce the background signal (SI figure 3.4 C, SI figure 3.5 C) but has no other positive effect apart from that. However, as it is known to form light-induced peroxides under ambient conditions [30] it would not be the optimal choice in this platform set-up. D640 shows both a very fast response time of only around 3 min (SI figure 3.4 E, SI figure 3.5 E) and linear response range up to 5 µmol·L^{-1} H_2O_2 with a calculated LOD of 0.09 µmol·L^{-1} ($3 \cdot \sigma_{blank} \cdot slope^{-1}$ compare Figure 3.4 A) and a linear range up to 5 µmol·L^{-1} already surpassing the given LOD of the Thermo Fisher commercial kit of 0.1 µmol·L^{-1} (reported as 10 pmol per 100 µL in the manual). As a result, we chose D640 as thin-film matrix for the storage and application of ADHP over D4 here because of the fast and effective reagent release.

An issue commonly observed and known for ADHP in the classical liquid assay that also impacts the membrane set-up, is a fluorescence intensity decrease with higher H_2O_2 concentrations as a nonfluorescent product is formed [13]. This formation can

result in an incorrect determination and thus underestimation of high H_2O_2 concentrations. To broaden the dynamic range in that higher concentration, thicker membranes were studied as these could host overall more dye. However, too thick membranes show a slower release of the dye (SI figure 3.7). Also, the amount of dye in the membrane was optimized, as with too high concentrations the gel becomes overloaded with dye and DMSO affecting the drying process and thus performance. In the end, the best overall results were achieved with 20 µL of ADHP-stock (containing 50 mmol·L^{-1} ADHP) per 6 g of hydrogel-solvent mix. Below this concentration the analytical range is reduced, above the hydrogel becomes overloaded and cannot release the dye as efficiently and fast after drying.

Deviations in membrane thickness led to deviations in H_2O_2 detection as the ADHP concentration varies accordingly. This is especially apparent in manual lab-based knife coating processes and likely less so in a commercial roll-to-roll manufacturing process. Nonetheless, ratiometric detection approaches can avoid any problems caused by changes in membrane height of dye distribution. A group of cyanine dyes was identified as a good match for ADHP. They can still be excited with the 560 nm excitation wavelength useful for resorufin but show emission at around 700 nm which is far enough away from the 585 nm resorufin emission. To avoid their oxidation by H_2O_2 and HRP, a hydrophobic cyanine without sulfo-moieties, 4,5:4',5'-Dibenzo-1,1'-dibutyl-3,3,3',3'-tetramethylindadicarbocyanine was used. Since it could not be dissolved in the dye membrane cocktail it was loaded into polystyrene nanoparticles (PSNPs) (SI figure 3.19) which protected it from oxidation. This enabled ratiometric detection of H_2O_2, both in a purely liquid assay in cuvettes (Figure 3.4 B) and membrane-based in the MTP (Figure 3.4 C). The increased reliability afforded by this ratiometric approach also enabled an LOD of 0.05 µmol·L^{-1} surpassing the previous LOD even further ($3 \cdot \sigma_{blank} \cdot slope^{-1}$).

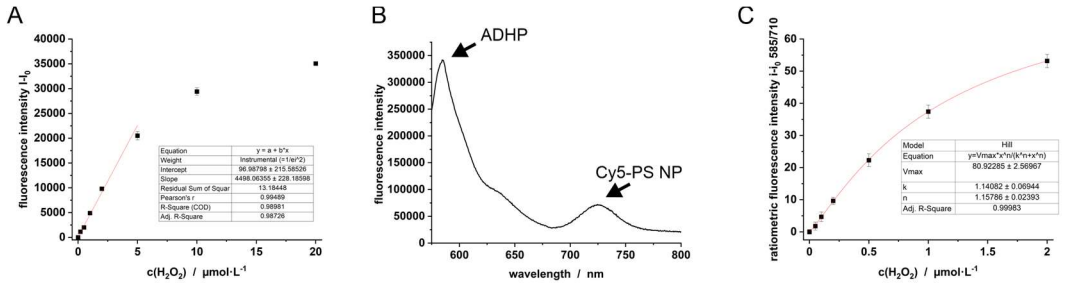

Figure 3.4: A Dose response curve of ADHP in D640 towards increasing concentrations of H_2O_2 with linear fit. B cuvette-based emission spectrum of ADHP with H_2O_2, HRP and S0982-loaded PSNPs in PBS pH 7.4 showing the emission maxima of ADHP at 585 nm and the dye-loaded PSNP at 725 nm. C dose-response curve of the ratiometric signal of ADHP in sensor membrane composed of D640 with dye-loaded PSNPs, 10 mU HRP per well and increasing concentrations of H_2O_2.

3.4.2 Development of nanospotted enzyme-based assays

For a one-step assay, it was investigated how enzymes could be integrated with the membrane platform. Integration of the enzyme in a membrane layer works well, but it requires very high amounts of 80 $U \cdot g^{-1}$ or more enzyme in the coating solution (SI figure 3.8) which indicates the enzyme not being released from the membrane as efficiently as the dye. The amount of enzyme could be dramatically reduced via nanospotting. A 3x3 matrix fitting 9 spots can easily be achieved per well (Figure 3.5 A). The small volume of ≈ 30 nL per spot or ≈ 270 nL per well reduces hydrogel swelling and thus interaction of the enzyme and the dye. This approach can easily be adapted to co-spot more than one enzyme or modify the hydrogel surface with other molecules. The amount of HRP spotted was optimized to avoid increased background due to unspecific oxidation of ADHP or slowed response. Optimal conditions included 4 HRP spots (≈ 30 nL, 22.5 $U \cdot mL^{-1}$, SI figure 3.10) leaving place for 5 extra spots containing other enzymes like GOx or LOx. With the 4 spots of HRP a very good spectral intensity distinction between the background fluorescence caused by the unspecific oxidation of ADHP by HRP and with 0.1 $\mu mol \cdot L^{-1}$ H_2O_2 added is clearly possible (Figure 3.5 B). With a full dose-response curve accessible after only 3 min assay time (Figure 3.5 C), in the smaller concentration range below 0.1 $\mu mol \cdot L^{-1}$ (Figure 3.5 D) a distinction between the blank and 0.02 $\mu mol \cdot L^{-1}$ is clearly possible. The linear regression in this area even results in a calculated LOD of 0.01 $\mu mol \cdot L^{-1}$ H_2O_2.

Secondly, the enzymes GOx or LOx were co-spotted into the wells for the detection of glucose and lactate, respectively. The concentration of the enzymes and the number of spots per well were optimized with respect to detecting within the physiological range. Here the best results were achieved with 4 spots (≈ 30 nL) of GOx with 0.2 $U \cdot mL^{-1}$ (SI figure 3.11 A) and 0.4 $U \cdot mL^{-1}$ LOx (SI figure 3.11 B). The entire system was then applied for glucose and lactate detection in buffer. Glucose could be detected in the range from 4 -20 $mmol \cdot L^{-1}$ (Figure 3.5 E), lactate in the range of 0.04 - 0.4 $mmol \cdot L^{-1}$ (Figure 3.5 F). Considering the reported successful use of ADHP together with HRP and H_2O_2 producing enzymes in a variety of challenging biological matrices [31–34], application of the platform in such systems should be possible.

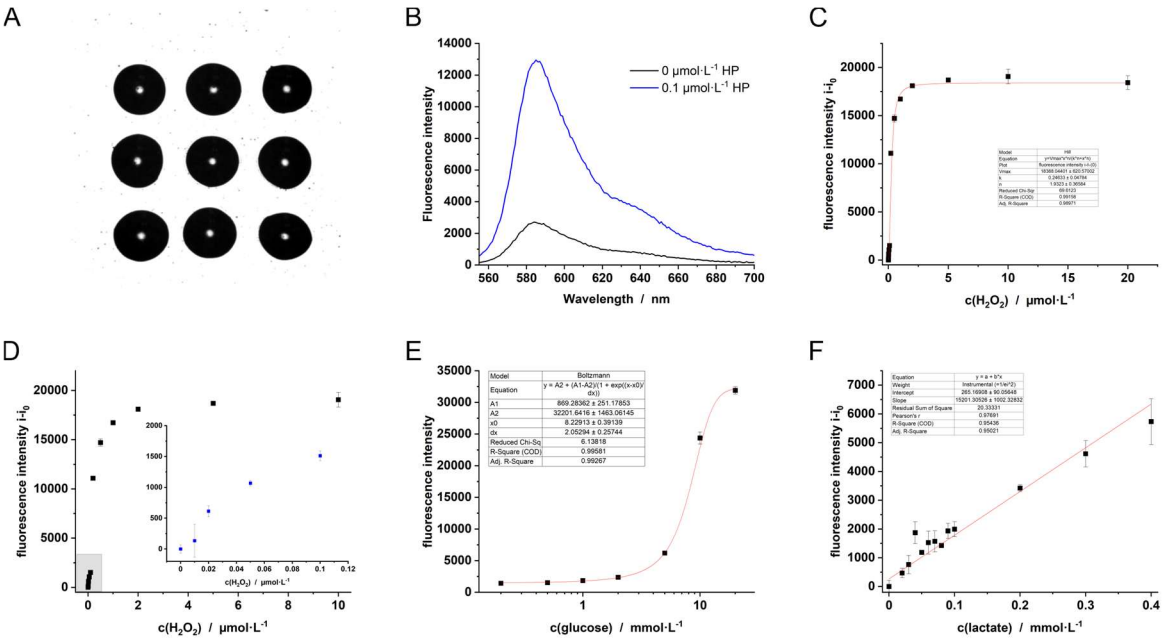

Figure 3.5: A top head image of 9 50 nL HRP spots in a MTP well. B Fluorescence spectra of of ADHP in D640 (λex = 550-10 nm) and HRP (4 spots, 30 nL per spot, 22.5 U·mL·L^{-1}) spotted with 0 µmol·L^{-1} (black) and 0.1 µmol·L^{-1} H_2O_2 in PBS pH 7.4. C dose-response curve with Hill fit of ADHP in D640 (λex = 560-10 nm, T = 37 °C, λem = 585-10 nm, N = 4) and HRP (4 spots, 30 nL per spot, 22.5 U·mL·L^{-1}) spotted with increasing concentrations of H_2O_2 in PBS pH 7.4 after 3 min assay time. D enlarged section (blue squares 0 – 0.1 µmol·L^{-1}) dose-response curve section of ADHP in D640 (λex = 560-10 nm, λem = 585-10 nm, N = 4) and HRP (4 spots, 30 nL per spot, 22.5 U·mL^{-1}) spotted with increasing concentrations of H_2O_2 in PBS pH 7.4 LOD = 0.01 µmol·L^{-1}. E dose-response curve of ADHP in D640 (λex = 560-10 nm, T = 37 °C, λem = 585-10 nm, N = 4) and HRP (4 spots, 30 nL per spot, 22.5 U·mL^{-1}) / GOx (4 spots, 30 nL per spot, 0.2 U·mL^{-1}) spotted with increasing concentrations of glucose in PBS pH 7.4 LOD = 4 mmol·L^{-1}. F dose-response curve of ADHP in D640 (λex = 560-10 nm, T = 37 °C, λem = 585-10 nm, N = 4) and HRP (4 spots, 30 nL per spot, 22.5 U·mL^{-1}) / LOx (4 spots, 30 nL per spot, 0.4 U·mL·L^{-1}) spotted with increasing concentrations of lactate in PBS pH 7.4 LOD = 0.04 mmol·L^{-1}.

3.4.3 Stability

Initial experiments of ADHP-membranes with spotted HRP in PBS showed complete oxidation of ADHP at 4 °C and declines of the activity over a course of 4 weeks at RT and -20 °C (SI figure 3.14). In the case of the latter two, the addition of fresh enzyme allowed for the assay to proceed, which indicates the degradation of the enzyme. It is assumed that at RT, both the increased temperature and the lacking humidity causes denaturation. At -20 °C the denaturation is either caused by the formation of ice crystals or the slow evaporation of H_2O from structurally important coordination positions within the active center of the enzyme [35]. At 4 °C the enzyme can still catalyze the unspecific oxidation of ADHP, albeit slowly. Furthermore, it is assumed that the humidity present allowed some hydrogel swelling and interaction of dye and enzyme leading to the formation of resorufin over time. To improve on storage stability of the enzyme known additives (50 v% glycerol, 10 w% dextran and 500 mmol·L^{-1} sucrose) were added to the spotting solution ensuring that good dispensibility or the

spotting solution was maintained. The composition of 50 v% glycerol in the spotting solution decreases the freezing point to about -40 °C [36] preventing damage caused by the formation of ice crystals [37]. Dextran has been used as alternative to glycerol in literature to prevent hemolysis of red blood cells during freezing [38] and sucrose is a common cryoprotectant used for the cryopreservation by vitrification [39]. Surprisingly, dextran, sucrose and PBS fail in long-term stability protection as about 50 % of signal response is lost within the first week of storage at -20 °C and are in fact hardly discernable from the unspecific oxidation of ADHP by HRP without H_2O_2 (SI figure 3.16). In contrast, HRP spotted with 50 v% glycerol showed a good stability over a course of 13 weeks with a coefficient of variance of 9 %. Considering the random distribution of data the variance is likely caused by membrane thickness variation in production or the variation in spotted HRP-stock and not by significant reduction in enzyme activity (Figure 3.6). The facts that standalone membranes containing ADHP could still be used after 22 months with fresh HRP (SI figure 3.15) and no significant reduction of signal intensity of HRP with glycerol as cryoprotectant suggest the possibility of extended long-term storage, which will be studied further in the future.

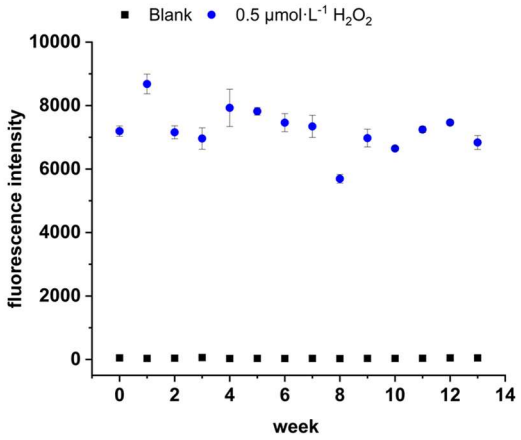

Figure 3.6: stability of ADHP membranes with spotted HRP (3 spots, 30 nL per spot, 22.5 U·mL^{-1}) in 50v% glycerol stored at - 20 °C (λex = 560-10 nm, T = 37 °C, λem = 585-10 nm, N = 3).

3.4.4 Material Cost of Production

Currently commercially available ADHP assay kits retail in Europe at around 500 € or USD for 500 tests or about 1 € or USD per test. Material required for the production of the developed MTP-based platform only costs 7.29 € per MTP (96 tests) or about 0.08 € per test, despite the small-scale purchase of production materials (SI table), suggesting significantly lower material prices in case of large-scale production.

3.5 Conclusion

An MTP-based hydrogel sensor membrane platform was developed containing ADHP, reference particles and nanospotted enzymes for the ratiometric fluorometric detection of H_2O_2. When coupled with H_2O_2-generating enzymes, detection of glucose in physiologically relevant range and lactate in a 1:10 dilution thereof was demonstrated. The presented platform drastically reduces assay preparation steps, with only sample addition after predilution in buffer which is very attractive for automation setups. Depending on the membrane quality, thickness, dye and enzyme load, very fast H_2O_2 assays of 3 min are possible with LODs one order of magnitude lower than published for the commercial assay in solution. At low material costs of 0.08 € per test, this platform technology can provide a drastically simplified analysis strategy for high throughput screening of all assays in which H_2O_2 is produced.

Key design criteria were the separation of ADHP and HRP to avoid non-specific reactions, the pore sizes of the membrane to enable a rapid release of the dye, the implementation of a reference dye to increase reliability, and nanospotting of the enzymes involved to obtain fast response times and low material consumption. Considering the release mechanism of the hydrogel membrane, the platform might also be suitable to host a variety of other responsive dyes and probes.

3.6 Acknowledgements

The author would like to thank Christoph Bühler for the TEM-images of the PSNPs and Prof. Dr. Reiner Müller for giving us access to the rheology measurement equipment.

3.7 References

[1] A. S. Ivanova, A. D. Merkuleva, S. V. Andreev, K. A. Sakharov. Method for determination of hydrogen peroxide in adulterated milk using high performance liquid chromatography., Food Chem. 2019, 283, 431–436, https://doi.org/10.1016/j.foodchem.2019.01.051.

[2] Rezende F, Brandes RP, Schröder K. Detection of Hydrogen Peroxide with Fluorescent Dyes., Antioxid. Redox Signaling 2018, 6 (20), 585–602, https://doi.org/10.1089/ars.2017.7401.

[3] J. J. Galligan, A. J. Baeumner, A. Duerkop. Recent advances and trends in optical devices and sensors for hydrogen peroxide detection., TrAC, Trends Anal. Chem. 2024, 180, 117948, https://doi.org/10.1016/j.trac.2024.117948.

[4] W. Chen, S. Cai, Q.-Q. Ren, W. Wen, Y.-D. Zhao. Recent advances in electrochemical sensing for hydrogen peroxide: a review., Analyst 2012, 137 (1), 49–58, https://doi.org/10.1039/C1AN15738H.

[5] M. Moßhammer, M. Kühl, K. Koren. Possibilities and Challenges for Quantitative Optical Sensing of Hydrogen Peroxide., Chemosensors 2017, 5 (4), 28, https://doi.org/10.3390/chemosensors5040028.

[6] J. E. Giaretta, H. Duan, F. Oveissi, S. Farajikhah, F. Dehghani, S. Naficy. Flexible Sensors for Hydrogen Peroxide Detection: A Critical Review., ACS Appl. Mater. Interfaces 2022, 14 (18), 20491–20505, https://doi.org/10.1021/acsami.1c24727.

[7] K. Dhara and D. R. Mahapatra. Recent advances in electrochemical nonenzymatic hydrogen peroxide sensors based on nanomaterials: a review., J. Mater. Sci. 2019, 54 (19), 12319–12357, https://doi.org/10.1007/s10853-019-03750-y.

[8] M.-J. Lee, J.-A. Song, J.-H. Choi, J.-H. Shin, J.-W. Myeong, K.-P. Lee, T. Kim, K.-E. Park, B.-K. Oh. Horseradish Peroxidase-Encapsulated Fluorescent Bio-Nanoparticle for Ultra-Sensitive and Easy Detection of Hydrogen Peroxide., Biosensors 2023, 13 (2), https://doi.org/10.3390/bios13020289.

[9] Paul E. Thomas, Dene Ryan, Wayne Levin. An improved staining procedure for the detection of the peroxidase activity of cytochrome P-450 on sodium dodecyl sulfate polyacrylamide gels., Anal. Biochem. 1976, 75 (1), 168–176, https://doi.org/10.1016/0003-2697(76)90067-1.

[10] R. E. Childs and W. G. Bardsley. The steady-state kinetics of peroxidase with 2,2'-azino-di-(3-ethyl-benzthiazoline-6-sulphonic acid) as chromogen., Biochem. J. 1975, 145 (1), 93–103, https://doi.org/10.1042/bj1450093.

[11] I. Sanz-Vicente, I. Rivero, L. Marcuello, M. P. Montano, S. de Marcos, J. Galbán. Portable colorimetric enzymatic disposable biosensor for histamine and simultaneous histamine/tyramine determination using a smartphone., Anal. Bioanal. Chem. 2023, 415 (9), 1777–1786, https://doi.org/10.1007/s00216-023-04583-0.

[12] N. Gajovic-Eichelmann and F. F. Bier. Novel Electrochemical Assay for H2O2 Determination in Aqueous Solutions: A Non Time-Critical Method for H2O2 Trace Level Detection., Electroanalysis 2005, 17 (12), 1043–1050, https://doi.org/10.1002/elan.200403212.

[13] M. Zhou, Z. Diwu, N. Panchuk-Voloshina, R. P. Haugland. A stable nonfluorescent derivative of resorufin for the fluorometric determination of trace hydrogen peroxide: applications in detecting the activity of phagocyte NADPH oxidase and other oxidases., Anal. Biochem. 1997, 253 (2), 162–168, https://doi.org/10.1006/abio.1997.2391.

[14] D. Dębski, R. Smulik, J. Zielonka, B. Michałowski, M. Jakubowska, K. Dębowska, J. Adamus, A. Marcinek, B. Kalyanaraman, A. Sikora. Mechanism of oxidative conversion of Amplex® Red to resorufin: Pulse radiolysis and enzymatic studies., Free Radical Biol. Med. 2016, 95, 323–332, https://doi.org/10.1016/j.freeradbiomed.2016.03.027.

[15] B. Zhao, F. A. Summers, R. P. Mason. Photooxidation of Amplex Red to resorufin: implications of exposing the Amplex Red assay to light., Free Radical Biol. Med. 2012, 53 (5), 1080–1087, https://doi.org/10.1016/j.freeradbiomed.2012.06.034.

[16] M. Ventura, in 41st AIAA/ASME/SAE/ASEE Joint Propulsion Conference & Exhibit. 41st AIAA/ASME/SAE/ASEE Joint Propulsion Conference & Exhibit, Tucson, Arizona. American Institute of Aeronautics and Astronautics, Reston, Virigina 2005.

[17] D. Zhai, B. Liu, Y. Shi, L. Pan, Y. Wang, W. Li, R. Zhang, G. Yu. Highly sensitive glucose sensor based on pt nanoparticle/polyaniline hydrogel heterostructures., ACS nano 2013, 7 (4), 3540–3546, https://doi.org/10.1021/nn400482d.

[18] D. Calabria, A. Pace, E. Lazzarini, I. Trozzi, M. Zangheri, M. Guardigli, S. Pieraccini, S. Masiero, M. Mirasoli. Smartphone-Based Chemiluminescence Glucose Biosensor Employing a Peroxidase-Mimicking, Guanosine-Based Self-Assembled Hydrogel., Biosensors 2023, 13 (6), https://doi.org/10.3390/bios13060650.

[19] J. Huang, Y. Zheng, H. Niu, J. Huang, X. Zhang, J. Chen, B. Ma, C. Wu, Y. Cao, Y. Zhu. A Multifunctional Hydrogel for Simultaneous Visible H_2O_2 Monitoring and Accelerating Diabetic Wound Healing., Adv. Healthcare Mater. 2023, e2302328, https://doi.org/10.1002/adhm.202302328.

[20] A. Dutta and U. Maitra. Naked-Eye Detection of Hydrogen Peroxide on Photoluminescent Paper Discs., ACS Sens. 2022, 7 (2), 513–522, https://doi.org/10.1021/acssensors.1c02322.

[21] M. Bauer, A. Duerkop, A. J. Baeumner. Critical review of polymer and hydrogel deposition methods for optical and electrochemical bioanalytical sensors correlated to the sensor's applicability in real samples., Anal. Bioanal. Chem. 2023, 415 (1), 83–95, https://doi.org/10.1007/s00216-022-04363-2.

[22] D. Bartoš, L. Wang, A. S. Anker, M. Rewers, O. Aalling-Frederiksen, K. M. Ø. Jensen, T. J. Sørensen. Synthesis of fluorescent polystyrene nanoparticles: a reproducible and scalable method., PeerJ Mater. Sci. 2022, 4, e22, https://doi.org/10.7717/peerj-matsci.22.

[23] K. Landfester. Miniemulsion polymerization and the structure of polymer and hybrid nanoparticles., Angew. Chem. Int. Ed. 2009, 48 (25), 4488–4507, https://doi.org/10.1002/anie.200900723.

[24] K. Landfester. Synthesis of colloidal particles in miniemulsions., Annu. Rev. Mater. Res. 2006, 36 (1), 231–279, https://doi.org/10.1146/annurev.matsci.36.032905.091025.

[25] T. Tsuchida and K. Yoda. Multi-enzyme membrane electrodes for determination of creatinine and creatine in serum., Clin. Chem. 1983, 29 (1), 51–55, https://doi.org/10.1093/clinchem/29.1.51.

[26] L. Ding, S. Chen, W. Zhang, Y. Zhang, X. Wang. Fully Reversible Optical Sensor for Hydrogen Peroxide with Fast Response., Anal. Chem. 2018, 90 (12), 7544–7551, https://doi.org/10.1021/acs.analchem.8b01159.

[27] A. Ø. Tjell, B. Jud, R. Schaller-Ammann, T. Mayr. Optical Hydrogen Peroxide Sensor for Measurements in Flow., Sens. Actuators, B 2023, 134904, https://doi.org/10.1016/j.snb.2023.134904.

[28] S. Bidmanova, M.-S. Steiner, M. Stepan, K. Vymazalova, M. A. Gruber, A. Duerkop, J. Damborsky, Z. Prokop, O. S. Wolfbeis. Enzyme-Based Test Strips for Visual or Photographic Detection and Quantitation of Gaseous Sulfur Mustard., Anal. Chem. 2016, 88 (11), 6044–6049, https://doi.org/10.1021/acs.analchem.6b01272.

[29] M. Moßhammer, M. Strobl, M. Kühl, I. Klimant, S. M. Borisov, K. Koren. Design and Application of an Optical Sensor for Simultaneous Imaging of pH and Dissolved O2 with Low Cross-Talk., ACS Sens. 2016, 1 (6), 681–687, https://doi.org/10.1021/acssensors.6b00071.

[30] C. E. Redemann. Peroxides in Isopropanol., Journal of the American Chemical Society 1942, 64 (12), 3049–3050, https://doi.org/10.1021/ja01264a512.

[31] R. Gaikwad, P. R. Thangaraj, A. K. Sen. Direct and rapid measurement of hydrogen peroxide in human blood using a microfluidic device., Sci. Rep. 2021, 11 (1), 2960, https://doi.org/10.1038/s41598-021-82623-4.

[32] M. F. Santillo and Y. Liu. A fluorescence assay for measuring acetylcholinesterase activity in rat blood and a human neuroblastoma cell line (SH-SY5Y)., J. Pharmacol. Toxicol. Methods 2015, 76, 15–22, https://doi.org/10.1016/j.vascn.2015.07.002.

[33] Z. Zou, C. Bouchereau-De Pury, A. K. Hewavitharana, S. S. Al-Shehri, J. A. Duley, D. M. Cowley, P. Koorts, P. N. Shaw, N. Bansal. A sensitive and high-throughput fluorescent method for determination of oxidase activities in human, bovine, goat and camel milk., Food Chem. 2021, 336, 127689, https://doi.org/10.1016/j.foodchem.2020.127689.

[34] A. H. Palamakumbura and P. C. Trackman. A fluorometric assay for detection of lysyl oxidase enzyme activity in biological samples., Anal. Biochem. 2002, 300 (2), 245–251, https://doi.org/10.1006/abio.2001.5464.

[35] B. Darbyshire. The results of freezing and dehydration of horseradish peroxidase., Cryobiology 1975, 12 (3), 276–281, https://doi.org/10.1016/0011-2240(75)90026-7.

[36] L. B. Lane. Freezing Points of Glycerol and Its Aqueous Solutions., Ind. Eng. Chem. 1925, 17 (9), 924, https://doi.org/10.1021/ie50189a017.

[37] H. H. Gorris and D. R. Walt. Mechanistic Aspects of Horseradish Peroxidase Elucidated through Single-Molecule Studies., Journal of the American Chemical Society 2009, 131 (17), 6277–6282, https://doi.org/10.1021/ja9008858.

[38] C. Pellerin-Mendes, L. Million, M. Marchand-Arvier, P. Labrude, C. Vigneron. In vitro study of the protective effect of trehalose and dextran during freezing of human red blood cells in liquid nitrogen., Cryobiology 1997, 35 (2), 173–186, https://doi.org/10.1006/cryo.1997.2038.

[39] G. D. Elliott, S. Wang, B. J. Fuller. Cryoprotectants: A review of the actions and applications of cryoprotective solutes that modulate cell recovery from ultra-low temperatures., Cryobiology 2017, 76, 74–91, https://doi.org/10.1016/j.cryobiol.2017.04.004

3.8 Supplementary Material

3.8.1 Non-measurement software

The following software instances were run on a Windows 10 Pro 64-bit-version. General data management and calculations of general nature or concerning mean values, standard deviations and error propagations were done with Excel Version 2402 (www.microsoft.com) Graph plotting, peak picking, peak analysis, particle size distribution histograms and mean particle size with standard deviation calculations were done in Origin 2024 (www.originlab.com). Graphical analysis of TEM images was performed with ImageJ version 1.53f (https://imagej.nih.gov/ij/). 3D images were designed and rendered using Blender 4.1.1 (www.blender.org). Schematics, laser cutting patterns and non-plotted graphs were designed and drawn in CorelDraw® 2023 v. 24.3.0.571 (www.coreldraw.com).

3.8.2 Instruments

Knife-coater with knife (in-house made device with adjustable film thickness in lower µm-range), K control coater K101 with a micrometer adjustable applicator “variocoater” and an aluminum vacuum bed “type B” from RK PrintCoat Instruments Ltd. (www.rkprint.com, Litlington, UK). The Coater was purchased from Coesfeld GmbH & Co KG (www.coesfeld.com, Dortmund, Germany). The applicator and the vacuum bed were purchased from Erichsen GmbH & Co. KG (www.erichsen.de).

For laser cutting sticky tape and membranes, a VLS2.30 laser cutter from Universal Laser Systems (www.ulsinc.com) with a 30 W CO_2 Laser and a 2” lens was used. In both cases, the respective substrate was placed on the template or the cutting table and fixed with masking tape if necessary.

All transmission electron microscopy (TEM) was performed using a 120 kV Philips cm12 microscope by Christoph Bühler. Samples were prepared by dropping 10 µL of 1.1 $mg \cdot mL^{-1}$ nanoparticle solutions on a carbon coated 400 mesh copper grid from Plano GmbH, Wetzlar.

Graphical analysis of the received TEM images was performed with ImageJ. After setting the scaling of the image to the given scale bar, the color values of the TEM images were set to binary, followed by noise removal processing and, if particle silhouettes were in contact, an internal function called water shedding was processed. The Feret diameter of the particles was automatically analyzed using an image specific

scaling. Size distribution and the corresponding histogram was calculated and plotted in origin. The particles mean size together with its standard deviation was calculated by a gaussian fit of the histograms.

All dynamic light scattering (DLS) of particle solutions were measured using a Zetasizer Nano ZS from Malvern Panalytical (www.malvernpanalytical.com). Particle dispersions were measured in disposable 1.5 mL semi-micro PMMA cuvettes from Brand (www.brand.de). Measurements were repeated three times, and the size distribution was calculated by the signal intensity.

Rheology was measured with a Bohlin Instruments CVO rheometer equipped with a 4 cm cone-plate setup and a humidity trap. 1.5 mL of each sample was injected, the gap was set to 150 µm and thermostatted to 25 °C for 60 s. Measurement runs were set to 400 s with a linear increase of the shear rate of 1 s^{-2}.

MTP-based kinetic and spectral fluorescence measurements were performed in a Biotek Synergy Neo2 MTP reader (www.agilent.com) with 100 µL sample per well diluted or prepared in PBS pH 7.4. The assay was performed at 37°C and the kinetic curve was measured for 15 – 20 min. The fluorescence was excited at 560 nm with a 10 nm bandwidth and measured at 585 nm with a 10 nm bandwidth for the ADHP emission and at 710 nm with a 10 nm bandwidth for the emission of the S0982 PSNPs. Cuvette-based excitation/emission spectroscopy was done in an Edinburgh Instruments FS5 spectrofluorometer.

Any shown standard deviations and variances are reported in accordance with DIN 1333.

3.8.3 PBS pH 7.4

NaCl (8.00 g, 137 mmol), KCl (0.20 g, 2.7 mmol), Na_2HPO_4 (1.44 g, 10 mmol) and KH_2PO_4 (0.245 g, 1.8 mmol) were dissolved in water (800 µL) under stirring. The pH was adjusted with NaOH (1 $mmol \cdot L^{-1}$) to pH 7.4 and the solution was filled up with water (to 1 L). The buffer was then filtered through a 0.2 µm nylon membrane filter and stored at 4 °C light protected. The volume required for the respective assays was previously removed from storage and brought to room temperature before use.

3.8.4 D640 Cocktail

Hydromed D640 (10 g) is dissolved in a mixture of ethanol and water (9:1 v/v, 90 g) in an airtight glass flask under strong stirring with a magnetic stirring bar until no lumps are visible.

3.8.5 D640 ratiometric Cocktail

Hydromed D640 (10 g) is dissolved in a mixture of ethanol and PSNP solution (9:1 v/v, 90 g) in an airtight glass flask under strong stirring with a magnetic stirring bar until no lumps are visible.

3.8.6 Coating cocktail

ADHP stock (2.5 µL, 50 mmol·L^{-1} or 25 µL, 5 mmol·L^{-1}) is added to D640 in EtOH/H_2O (1 g, 10 w%, 9:1 v/v) in a snap-cap vial and is stirred for 10 min protected from light. The coating cocktail is used within 1 h after production.

3.8.7 Ratiometric coating cocktail

ADHP stock (2.5 µL, 50 mmol·L^{-1} or 25 µL, 5 mmol·L^{-1}) is added to D640 in EtOH/PSNP-solution (1 g, 10 w%, 9:1 v/v) in a snap-cap vial and is stirred for 10 min protected from light. The coating cocktail is used within 1 h after production.

3.8.8 Knife coating membrane (small coater)

The membranes coated on the small knife coater were primarily used for screening of concentrations, doping amounts and polymer types. 30 µm stacked on the 125 µm spacers are placed in the knife-coater at both sides. PET film is cut (11.5 x 5.5 cm), cleaned with acetone, dried and fixed to the coating bed with vacuum. Dust or remaining contaminants are removed with acetone and wiping. 250 µL of the coating cocktail is pipetted as a homogeneous line on the starting point of the Mylar substrate. The knife is pulled slowly to the end of the substrate to obtain an even film. The applicator is removed and the film with the wet membrane is placed on a pre-heated 1 mm steel plate in an oven (37°C) and dried for 2 h.

3.8.9 Knife coating membrane (large coater)

PET film is cut (34 x 15 cm), cleaned with acetone, dried and fixed to the coating bed with vacuum. Dust or remaining contaminants are removed with acetone and wiping. The leveled and adjusted applicator (30 - 40 µm) is placed on the film and the coating cocktail (650 µL) is applied in a line in front of the knife. The applicator is moved along the coating area (10 x 24.5 cm) with a set speed of 3 (approx. 2.8 $cm \cdot s^{-1}$). The applicator is removed and the film with the wet membrane is placed on a pre-heated 1 mm steel plate in an oven (37°C) and dried for 2 h.

3.8.10 Laser cutting

All shown laser cutting templates (SI figure 3.1 A, SI figure 3.2 A+B) were engraved into 300 x 400 mm 1 mm thick stainless-steel plates to ensure more reproducible cutting as well as easier and faster piece alignment.

3.8.11 Sticky Plate production

Double-sided adhesive tape (36 x 10 cm) is placed on the cutting template (SI figure 3.1 A) and fixed with masking tape. The mounted tape with the cutting template is placed on the laser work surface and the focus is adjusted accordingly (1 mm for the cutting template, 0.1 mm for the tape). First the wells (black lines) are cut out and removed before the outer edge is cut (2” lens, 5 % power, 40 %speed, red lines). The received cutout is placed on the underside of bottomless 96-well MTPs and pressed on firmly. The shelf-life depends mainly on the adhesive strength (and the loss thereof over time) of the adhesive tape used. In the context of this work MTPs that were up to 3 years old stored at RT could still be used without restrictions.

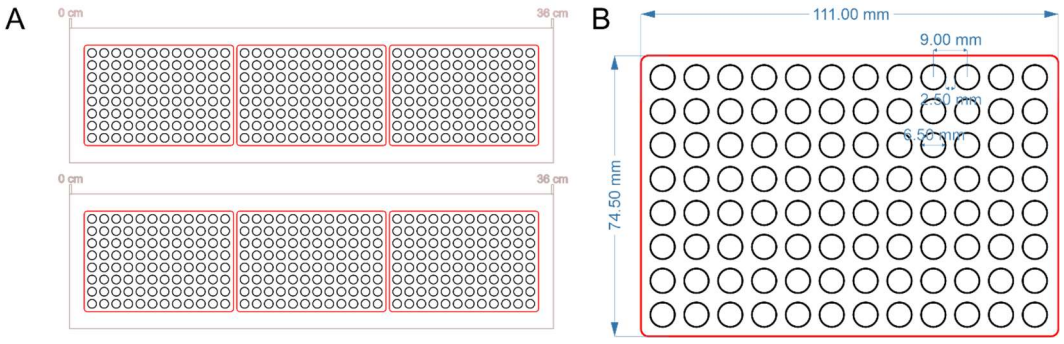

SI figure 3.1: **A** cutting template scheme for the production of double-sided adhesive tape cutout. **B** Scheme of a single MTP cutout. The dimensions of each of the 6 cutouts is 111 x 74.5 mm. Each well cutout has a diameter of 6.5 mm and the distance between each well is 2.5 mm from the edge or 9 mm from each well center respectively. Laser cutting settings: 2” lens, 5 % power, 40 %speed.

3.8.12 Membrane cutting

The knife-coated and dried membranes were placed on the respective cutting template (SI figure 3.2 A and B respectively). For the membranes coated on the small coater a total of 12 strips was cut from 12 coated foils per full MTP (2" lens, 5 % power/1.5 W, 60% speed). These laser-cut membranes can be stored at 25 °C to -20 °C light and humidity protected for at least a year.

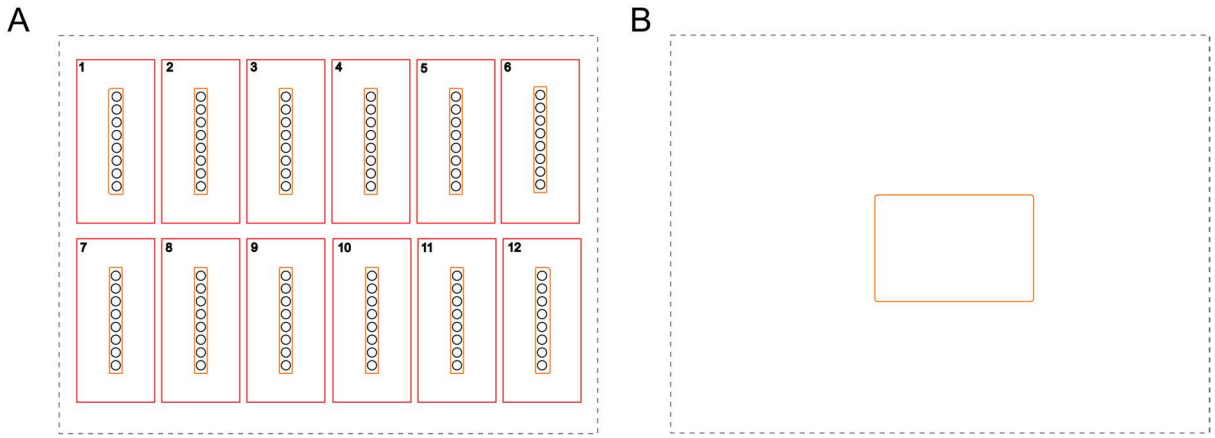

SI figure 3.2: Cutting template schemes for lasercutting membrane strips and sheets. **A** Template layout for small substrate foils 55 x 115 mm from the "small coater". **B** Template layout for large substrate foils 150 x 340 mm from the "large coater". Edges of the steel plates indicated by grey dashed lines.

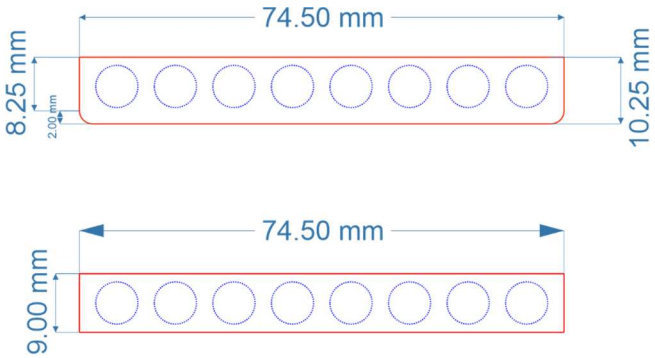

SI figure 3.3: cutting templates for membrane strips of 55 x 115 mm coated membranes. Top: Edge pieces column 1 & 12, bottom: center pieces MTP column 2 - 11. Laser cutting lines (red) well positions in the MTP indicated by blue circles.

3.8.13 Membrane application

First, the protective layer of the sticky tape is removed. Then the laser cut sheet or strips are stuck to the underside of the MTP and firmly pressed on by hand with the hydrogel membrane facing towards the MTP.

3.8.14 Hydrogel/solvent dependence

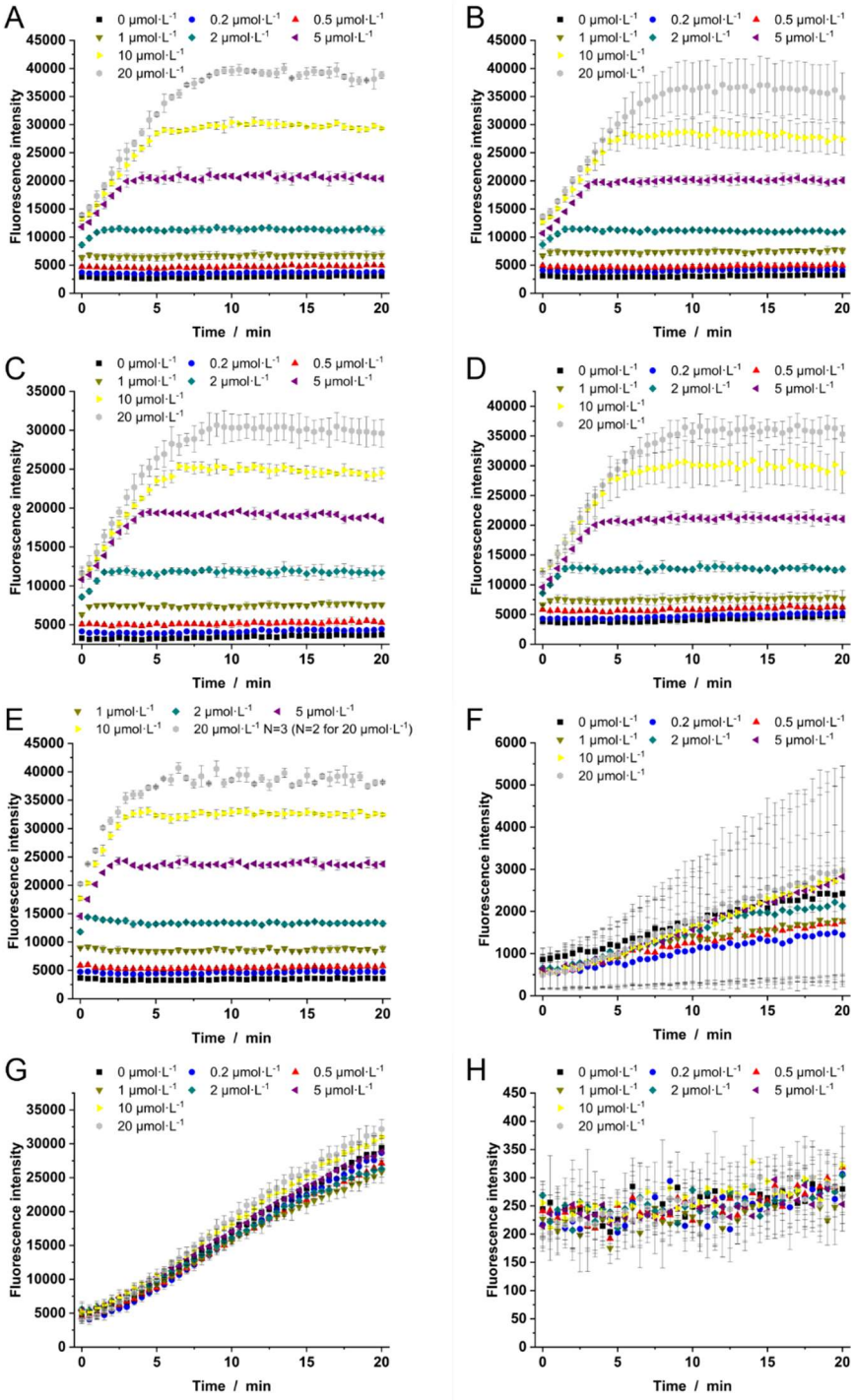

SI figure 3.4: Fluorescence measurement of kinetic curves of ADHP (50 µL stock solution, 5 mmol·L^{-1} in DMSO, 2,75 mmol/1.5 g coating solution) knife-coated in different hydrogel/solvent combinations in presence of various concentrations of H_2O_2. Foils were coated with a wet thickness of 30 µm and dried for 3 h at 37°C. Strips were laser cut and stuck to the bottom of a sticky MTP. HP-solutions and HRP-solutions (50 µL each in HEPES 0.1 mol·L^{-1}, HRP 0.875 U·mL^{-1}) were added right before the measurements. Biotek MTP-Reader: N = 3, 37 °C, $\lambda_{exc.}$ = 530-10 nm, $\lambda_{em.}$ = 555-10 nm, gain 100, bottom optic. **A:** D4 10w% EtOH/H_2O 9:1 v/v. **B:** D4 10w% ^{t}BuOH/H_2O 9:1 v/v. **C:** D4 10w% ^{i}PrOH/H_2O 9:1 v/v. **D:** D4 10w% DMF/H_2O 9:1 v/v. **E:** D640 10w% EtOH/H_2O 9:1 v/v. **F:** PVAc/CA 10w% DMF/H_2O 9:1 v/v. **G:** PVAc/CA 10w% Chon. **H:** LRPt7016 2.5w% THF/H_2O 99:1 v/v.

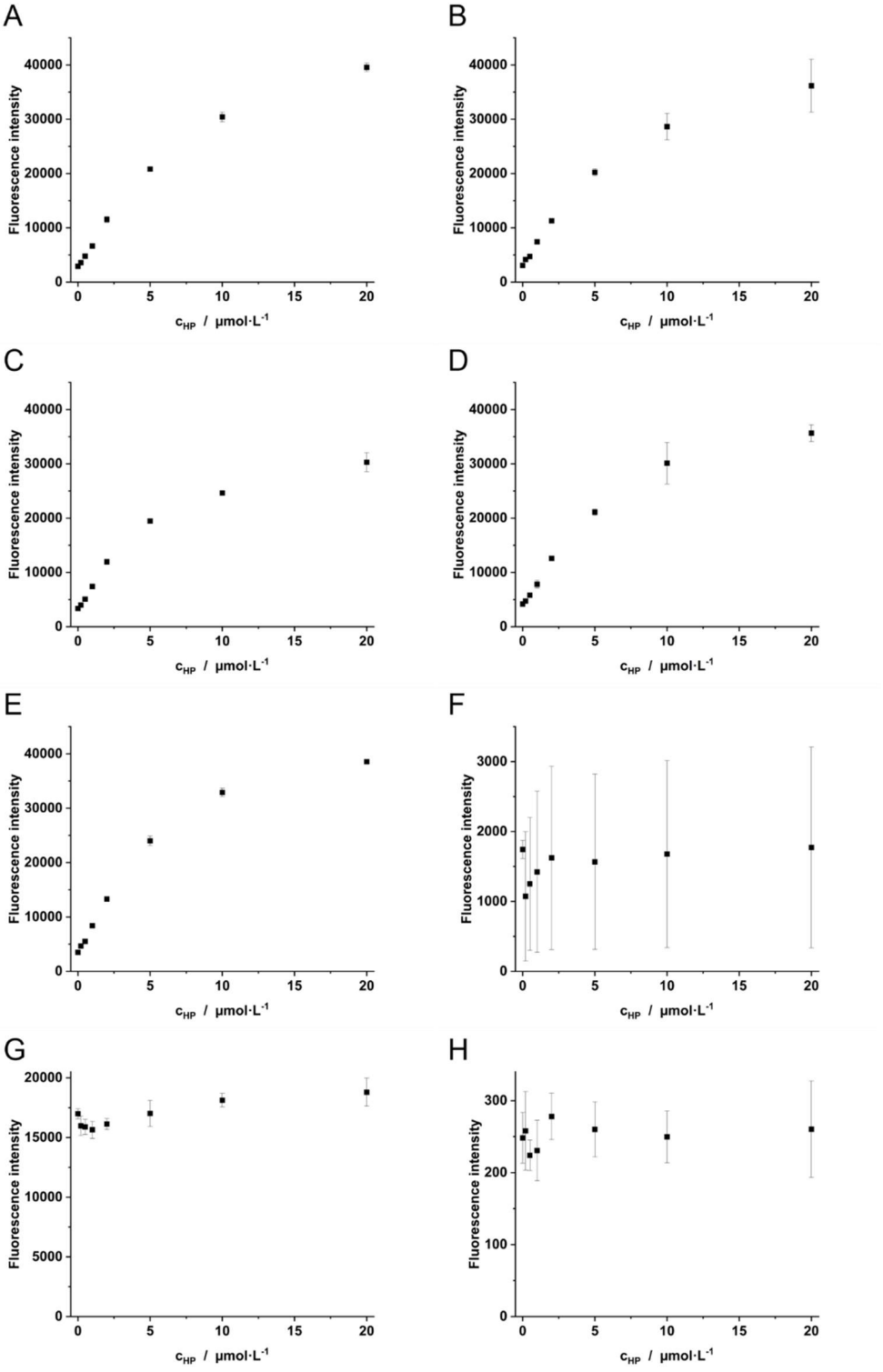

SI figure 3.5 Fluorescence measurement dose-response curves of ADHP (50 µL stock solution, 5 mmol·L^{-1} in DMSO, 2,75 mmol/1.5 g coating solution) knife-coated in different hydrogel/solvent combinations. Foils were coated with a wet thickness of 30 µm and dried for 3 h at 37°C. Strips were laser cut and stuck to the bottom of a sticky MTP. HP-solutions and HRP-solutions (50 µL each in HEPES 0.1 mol·L^{-1}, HRP 0.875 U·mL^{-1}) were added right before the measurements. Biotek MTP-Reader: N = 3, 37 °C, $\lambda_{exc.}$ = 560-10 nm, $\lambda_{em.}$ = 585-10 nm, gain 100, bottom optic. **A:** D4 10w% EtOH/H_2O 9:1 v/v. **B:** D4 10w% ^{t}BuOH/H_2O 9:1 v/v. **C:** D4 10w% ^{i}PrOH/H_2O 9:1 v/v. **D:** D4 10w% DMF/H_2O 9:1 v/v. **E:** D640 10w% EtOH/H_2O 9:1 v/v. **F:** PVAc/CA 10w% DMF/H_2O 9:1 v/v. **G:** PVAc/CA 10w% Chon. **H:** LRPt7016 2.5w% THF/H_2O 99:1 v/v.

Here, AR in D640 shows good linear correlation in the area between 0.2 – 5 µmol·L^{-1} with an LOD of 0.09 µmol·L^{-1}

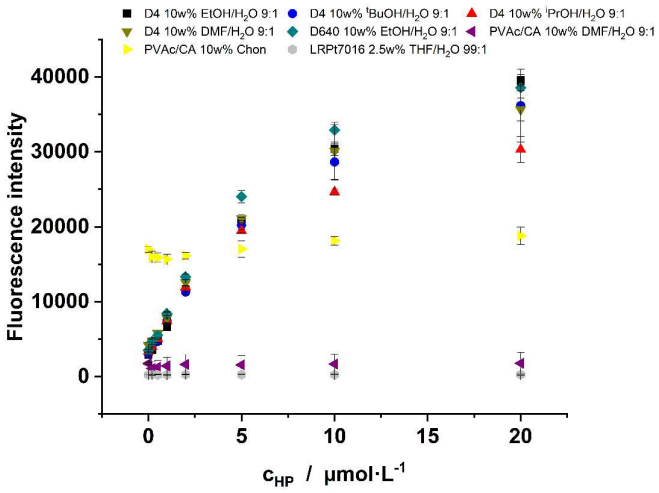

SI figure 3.6: Fluorescence measurement dose-response curves of ADHP (50 µL stock solution, 5 mmol·L^{-1} in DMSO, 2,75 mmol/1.5 g coating solution) knife-coated in different hydrogel/solvent combinations. Foils were coated with a wet thickness of 30 µm and dried for 3 h at 37°C. Strips were laser cut and stuck to the bottom of a sticky MTP. HP-solutions and HRP-solutions (50 µL each in HEPES 0.1 mol·L^{-1}, HRP 0.875 U·mL^{-1}) were added right before the measurements. Biotek MTP-Reader: N = 3 (N = 2 for D640 at 20 µmol·L^{-1}), 37 °C, $\lambda_{exc.}$ = 560-10 nm, $\lambda_{em.}$ = 585-10 nm, gain 100, bottom optic. Data points taken at 10 min.

3.8.15 membrane thickness

Too thick membranes show a reduced and slower release of ADHP.

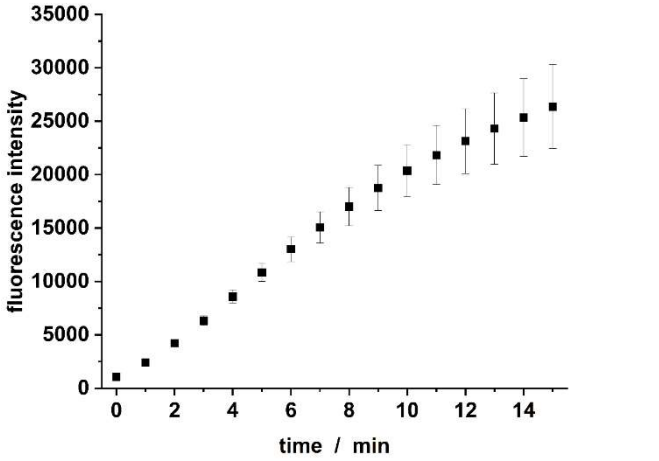

SI figure 3.7: Fluorescence measurement kinetic curves of ADHP (5 µL stock solution, 50 mmol·L^{-1} in DMSO, 2,75 mmol/1.5 g coating solution) knife-coated in different hydrogel/solvent combinations. Foils were coated with a wet thickness of 80 µm and dried for 3 h at 37°C. Strips were laser cut and stuck to the bottom of a sticky MTP. HP-solutions and HRP-solutions (50 µL each in HEPES 0.1 mol·L^{-1}, HRP 0.875 U·mL^{-1}) were added right before the measurements. Biotek MTP-Reader: N = 96, 37 °C, $\lambda_{exc.}$ = 560-10 nm, $\lambda_{em.}$ = 585-10 nm, gain 100, bottom optic.

3.8.16 HRP membrane

HRP was embedded in D640-membranes to test the co-knifecoatability of probe and enzyme. To achieve a sufficient response both in speed and signal intensity, a relatively high concentration of HRP (80 $U \cdot g^{-1}$) was necessary. Overall, the integration of HRP in D640 membranes for the fluorescent ADHP/H_2O_2 assay in the MTP showed a poor outcome both in signal intensity and cv%.

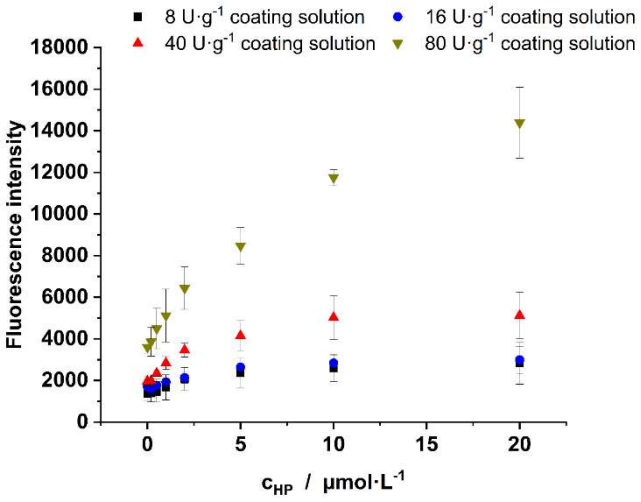

SI figure 3.8: Fluorescence dose-response curves of D640-HRP membranes with H_2O_2 and different amounts of HRP in the coating cocktail after 10 min assay time. N = 3, $\lambda_{exc.}$= 530 – 10 nm, $\lambda_{em.}$= 590 – 10 nm, 37 °C.

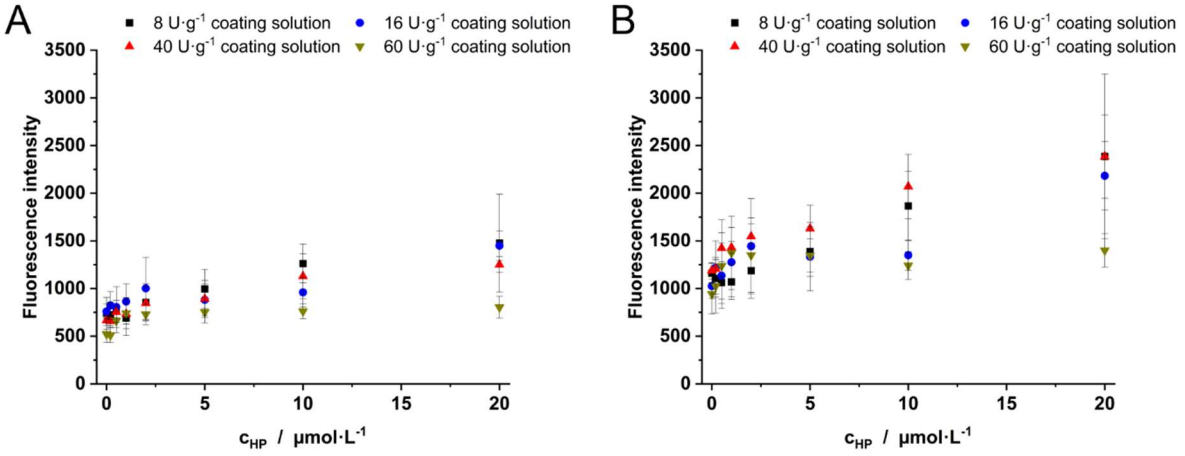

SI figure 3.9: Fluorescence dose-response curves of D640-ADHP membranes with H_2O_2 and different amounts of HRP in the coating cocktail. **A** after 10 min **B** after 20 min.

3.8.17 HRP, GOx and LOx spotting concentrations

HRP stocks with 90, 45, 22.5 and 11.25 U·mL^{-1} were spotted on ADHP membranes to determine the optimal enzyme/spot amount. DR-curves after 3 min showed the best signal for 4 spots of 22.5 U·mL^{-1} HRP. Higher concentrated HRP stocks caused a significant reduction of signal after 3 min resulting in an unreliable signal readout.

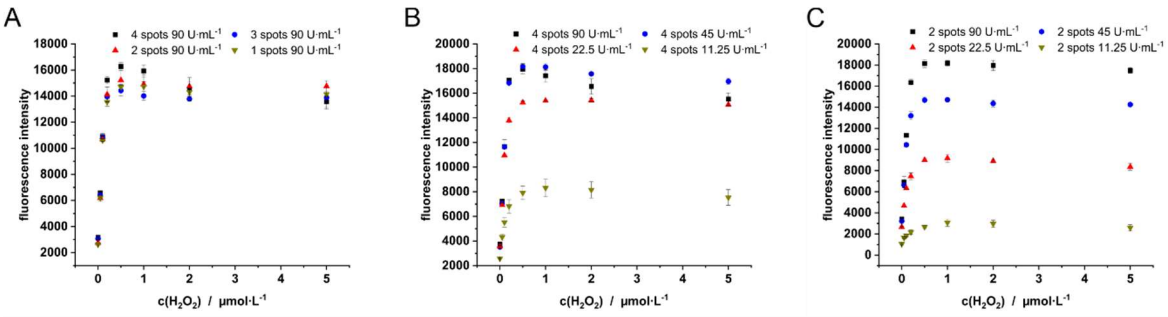

SI figure 3.10: Optimization of nanospotted HRP. Fluorescence dose-response curves of D640-ADHP membranes with H_2O_2 and different concentrations of enzyme stocks and spot number of HRP after 3 min assay time. Biotek MTP-Reader: N = 3, 37 °C, $\lambda_{exc.}$ = 560-10 nm, $\lambda_{em.}$ = 585-10 nm, gain 100, bottom optic.

4 spots (≈ 30 nL) of either GOx stocks with 0.1, 0.2, 0.5 and 1 U·mL^{-1} or LOx with 0.4, 0.6, 0.8 and 1 U·mL^{-1} were spotted on ADHP membranes with 4 HRP spots (≈ 30 nL, 22.5 U·mL^{-1}) to determine the optimal enzyme stock concentrations. DR-curves showed the best signal for 0.2 U·mL^{-1} GOx and 0.4 U·mL^{-1} LOx.

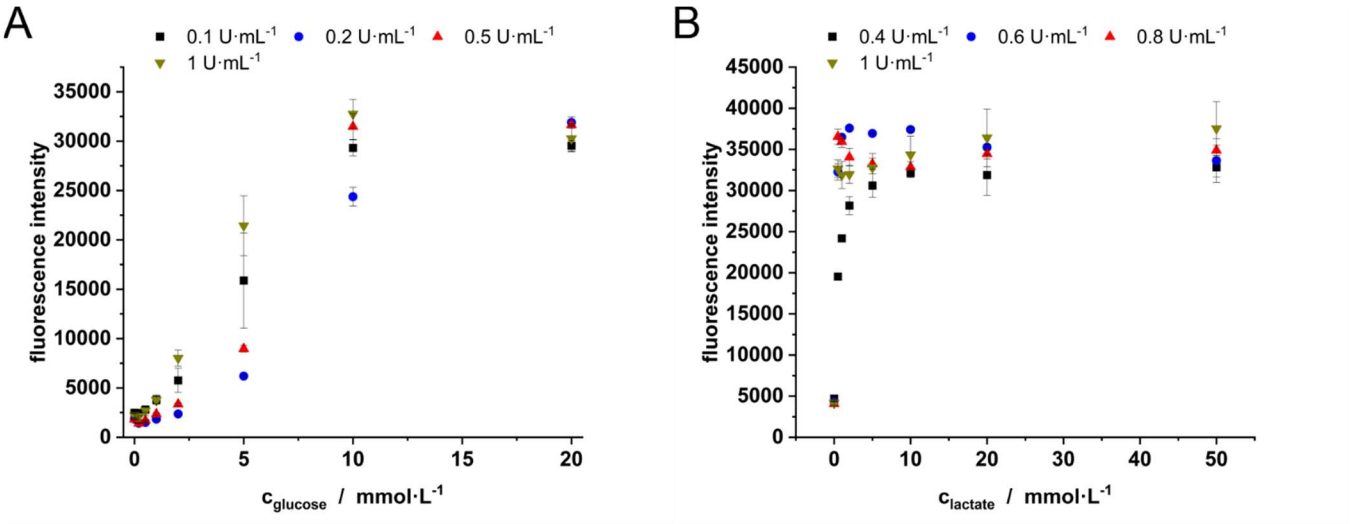

SI figure 3.11: Optimization of nanospotted GOx **A** and LOx **B**. Fluorescence dose-response curves of D640-ADHP membranes with H_2O_2 and different concentrations of GOx and LOx enzyme stocks 4 spots each and HRP (4spots 22.5 U·ml^{-1}) and spot. Biotek MTP-Reader: N = 3, 37 °C, $\lambda_{exc.}$ = 560-10 nm, $\lambda_{em.}$ = 585-10 nm, gain 100, bottom optic.

3.8.18 Cy5 PSNP membrane content

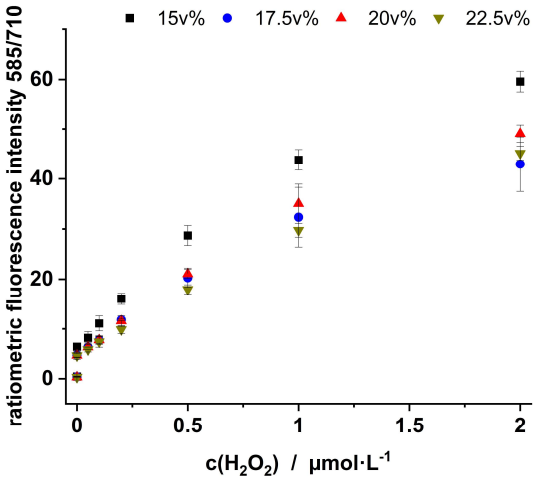

SI figure 3.12: Ratiometric dose response curves (585 nm / 710 nm) of ADHP in D640 with different contents of Cy5 PSNP stocks in the coating mixture. N = 3, 37 °C, $\lambda_{exc.}$ = 560-10 nm, $\lambda_{em.}$ = 585-10 nm, 710-10 nm, gain 100, bottom optic.

3.8.19 Stability without cryoprotectant

Hydrogel coating cocktails and the knife coating of the membranes were performed as previously reported. For the temperature-dependent stability without cryoprotectants however, a piece containing 22 strips (compare SI figure) the width of an MTP-column which could then be cut at the connecting piece were laser cut and spotted with HRP as previously described. Three of these pieces were then stored light protected, but otherwise unprotected at constant 22 °C, 4 °C and – 20 °C (N = 3 per temperature, 9 pieces with 22 strips / 198 strips in total.) A strip for each storage condition could then be separated per week, stuck to the bottom of a sticky MTP and measured in a fluorometric H_2O_2 assay with 0 µmol·L^{-1} and 0.5 µmol·L^{-1} H_2O_2 as previously described.

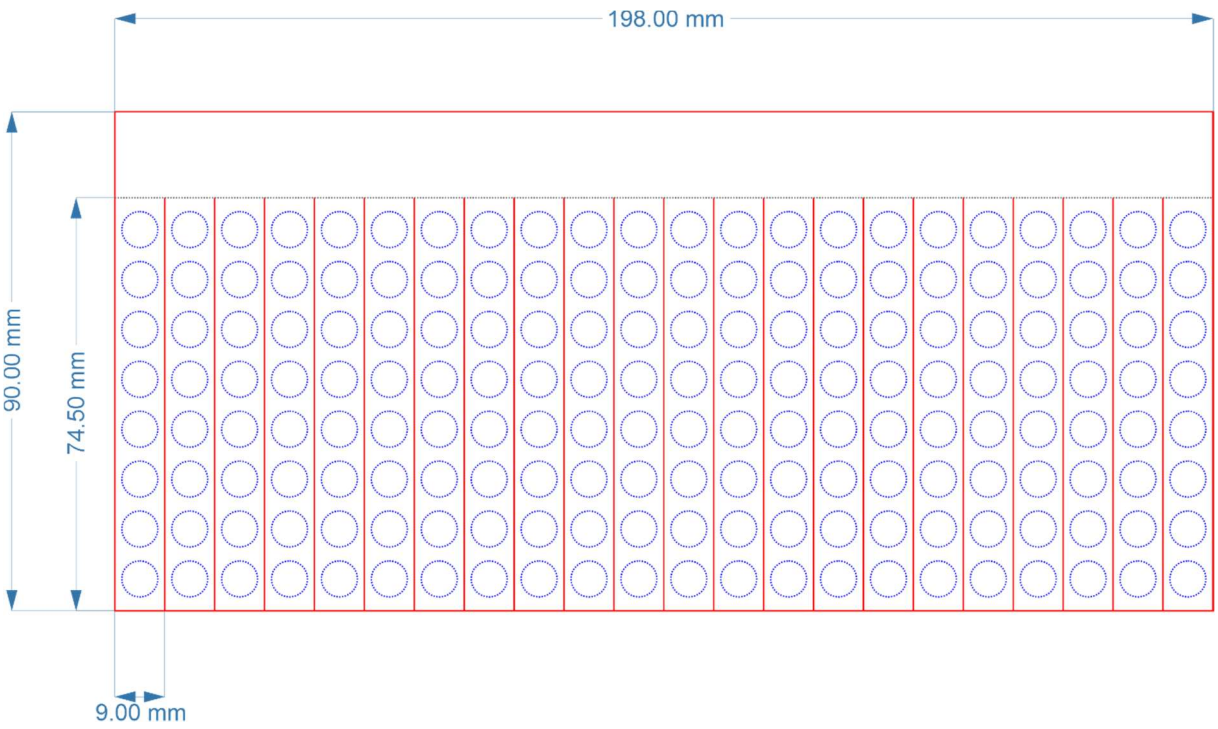

SI figure 3.13: Laser cutting template for stability strips. Red lines: laser cutting line. Indicators for the manual cutting line for strip separation (grey dotted line) and the well positions (blue dotted circles) were not laser cut and are only used here for highlighting purposes.

The stability measurements without cryoprotectant and sealing show a decrease of the fluorescence intensity with time when stored at 22 °C and – 20 °C for all concentrations, but an increase of the fluorescence intensity for the membranes stored at 4 °C. Since the response of the seemingly inactive membranes could be restored by the addition of fresh HRP, the enzyme likely degrades at 22 °C and – 20 °C.

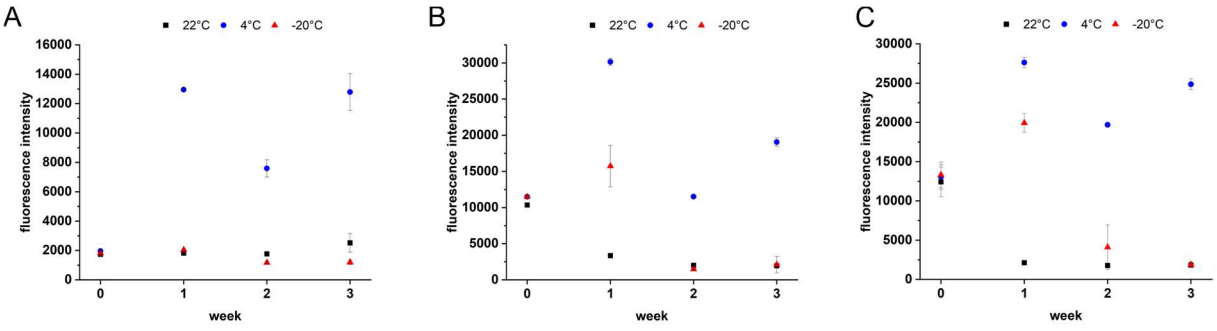

SI figure 3.14: stability measurements of ADHP in D640 spotted with HRP in PBS with 0 µmol·L^{-1} (A), 0.2 µmol·L^{-1} (B) and 0.5 µmol·L^{-1} (C) stored light protected at 22 °C (black squares), 4 °C (blue circles) and – 20 °C (red triangles). N = 2 for 0 µmol·L^{-1}, N = 3 for 0.2 µmol·L^{-1} and 0.5 µmol·L^{-1}.

The membranes of this study stored at 22 °C under the previously mentioned conditions with the inactivated enzyme could be used with fresh HRP even after 22 months of storage. This demonstrates the exceptional stability of both the

membrane and the ADHP stored inside the latter. As can be seen in SI figure 3.15 the response to H_2O_2 only takes place upon the addition of fresh HRP (black boxes), wells without fresh HRP are unresponsive (blue circles).

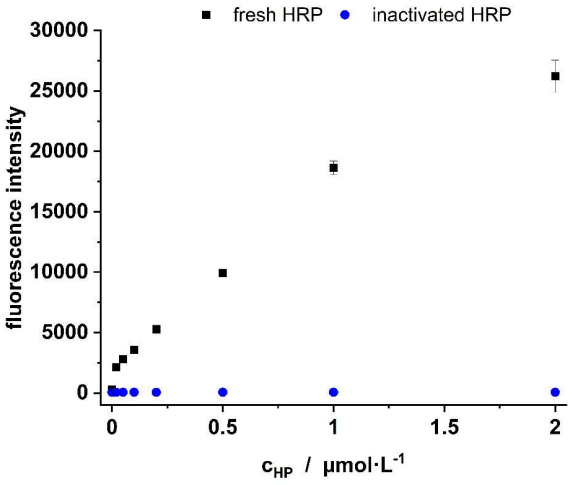

SI figure 3.15: Fluorescence dose-response curves of D640-ADHP membranes stored for 22 months at 22 °C with increasing H_2O_2 concentrations, wells without added or with inactive HRP show no concentration-dependent signal change (blue circles N = 1), whereas wells with added fresh HRP (black boxes, N = 11, 0.1 U·mL^{-1}, 5 mU per well) show a typical concentration-dependent response. T = 37°C

3.8.20 Stability study with cryoprotectants

For the stability study with cryoprotectants, five spots of HRP (22.5 U·mL^{-1}) in PBS pH 7.4, 50v% glycerol/PBS, sucrose (500 mmol·L^{-1}) and dextran (10 w% in PBS) was dispensed. The thus produced MTPs were sealed with adhesive PCR aluminum cover film after production and stored at - 20 °C until usage. Before unsealing, the microtiter plates were brought to room temperature and any condensation from the bottom and on top of the sealing cover was wiped away with a dry paper towel.

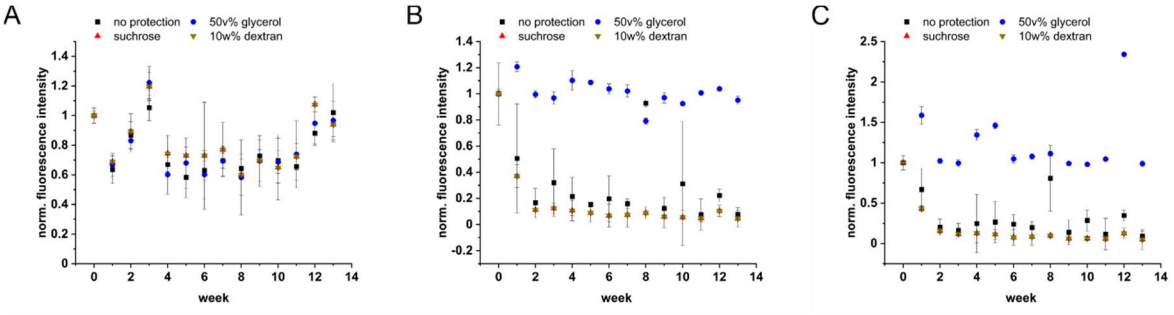

SI figure 3.16: Stability of ADHP membranes and spotted HRP with different cryoprotectants. Black boxes: no cryoprotectant, blue circles: 50 V% glycerol, red triangles: sucrose, orange triangles: 10 w% dextran. Normalized fluorescence intensity with **A** blank, **B** 0.5 µmol·L^{-1} H_2O_2 and **C** 1 µmol·L^{-1} H_2O_2. N = 3, T = 37 °C,

3.8.21 Rheology

All measured samples and water/solvent ratios showed Newtonian behavior. 22.5 v% showed a viscosity of 0.14830 ± 0.00007 Pa·s, 15 v% 0. 0.12044 ± 0.000025 Pa·s and 10 v% 0.10691 ± 0.00004 Pa·s. Based on the viscosities all used solutions were fully suited for knife coating.

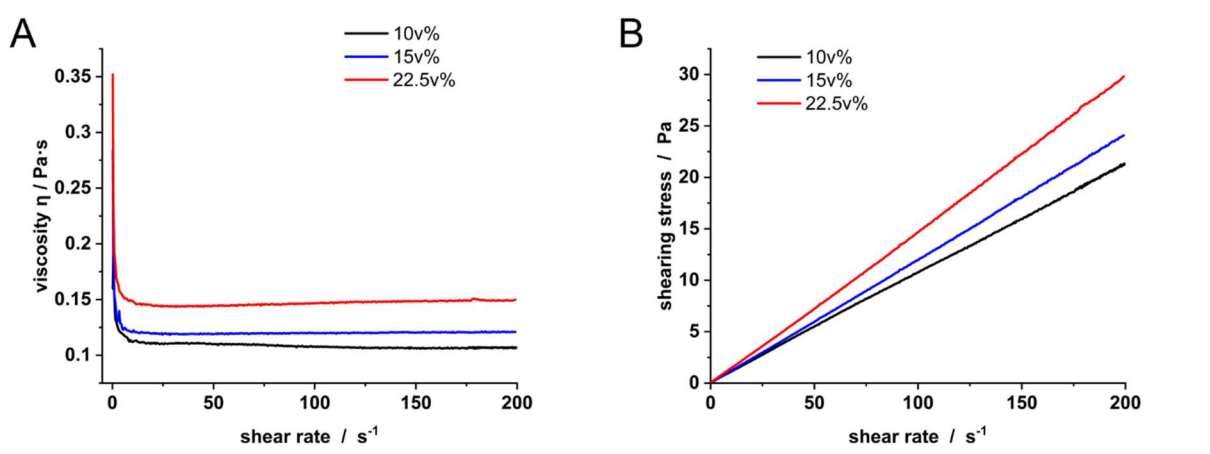

SI figure 3.17: Rheology of D640 EtOH/H_2O with different volume ratios of water in the solvent content showing Newtonian behavior. Black curves 10 v%, blue curves 15 v%, red curves 22.5 v%. **A** viscosity versus shear rate graph, **B** shearing stress versus shear rate graph.

3.8.22 Spotting Volume

Depending on the used pulse time of each valve-cycle and the applied pressure, quasi-linear increase of the spotted volume is observable with a coated NDC-M nozzle. With longer pulse time more volume is emitted. As is to be expected the difference in absolute volume emitted increases with increasing pressure.

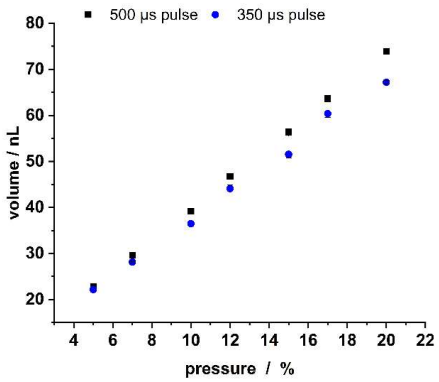

SI figure 3.18: PBS spotting volume per spot by NDC M nozzle in dependence of pressure for 500 µs (black) and 350 µs (blue) pulses and 5 Hz spotting frequency. 100 spots per run, mean and SD of 5 runs.

3.8.23 Particle characterization

The synthesized particles were received as homogenous deep blue suspension. S0982-loaded particles in a 1:100 (v/v) aqueous solution showed a main emission peak at 735 nm and a shoulder at around 690 – 700 nm under 660 nm and 560 nm excitation. The synthesized particles showed to be mainly spheres in shape with some spheroids present. The size distribution observed in the TEM micrographs agrees with the measured size distribution in the DLS with a size average of 186 nm and a PDI of 0.158. The high variance in the size species which had no adverse effect on the sensor membranes could be optimized by increasing both the number of sonication cycles and the used sonication power which also resulted in smaller particles. When incorporated into D640 hydrogel the emission peak shifts to 710 nm for both excitations at 560 nm and 660 nm.

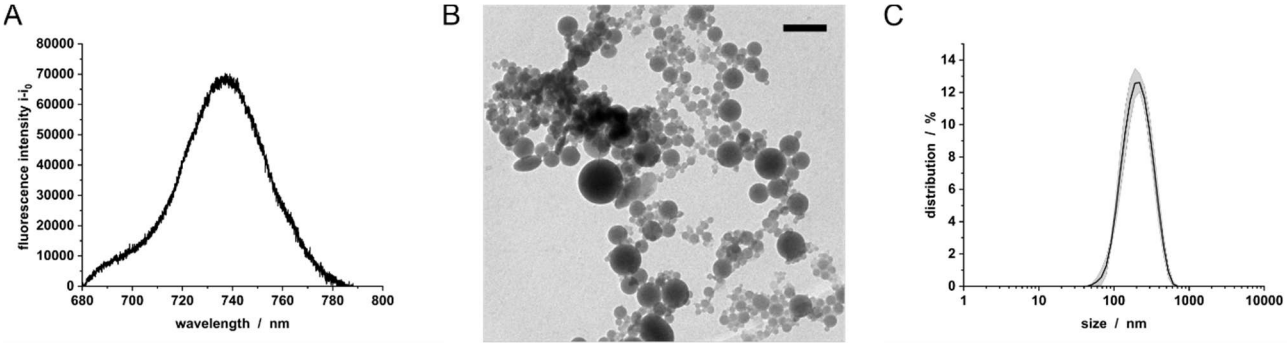

SI figure 3.19: **A** fluorescence spectrum of S0982 loaded PSNPs diluted 1:100 (v/v) in aqueous solution. Particle dye load ≈ 1 w%, $\lambda_{ex.}$ = 660 nm, em/ex bandwidth = 2 nm, 0.05 nm steps, 1 s dwell time, T =24.90 °C. **B** TEM-micrograph of dye-loaded PSNPs, size bar is 500 nm. **C** DLS size distribution of dye-loaded PSNPs used in this work, diluted 1:100, size average 186.6 nm, PDI 0.158, T = 20.0 °C

3.8.24 Material cost calculation

In a first step the material cost of a single MTP and test based on the production of six MTPs was calculated. In all cases, the costs of procurement of the used devices (knife-coater, laser cutter, nanospotter, sonicator) and the cost of labor was not considered.

SI table 3.1: List and totals of material costs per MTP and per test. The costs shown are the actual production costs per MTP and test, taking into account any necessary offcuts of coating substrate and tape as well as minimum amounts for solvent preparations based on the production of 6 MTPs. In industrial mass production, it can be assumed that material costs in general, especially the two major cost items, MTPs and Mylar, will decrease significantly.

No.	Name	Cost per pack	Pack size	Needed per Plate	Cost per plate	Needed per test	Cost per test
1	Mylar	701.89 €	12 m²	0.051 m²	2.98 €	5.3 cm²	0.031 €
2	MTP	153.65 €	40	1	3.84 €	1/96	0.040 €
3	Sticky Tape	62.02 €	50 m	0.12 m	0.15 €	≈ 1.25 mm	0.0016 €
4	Hydromed D640	180 €	453.592 g	0.1 g	0.04 €	≈ 1 mg	0.00041 €
5	ADHP	300 €	100 mg	42.97 µg	0.13 €	≈ 0.45 ng	0.0013 €
6	EtOH	21.74 €	1 L	5.9 mL	0.13 €	≈ 61 µL	0.0013 €
7	HRP	473€	25 kU	1.152 U	0.02 €	0.012 U	0.00023 €
				Sum cost per plate:	7.29 €	Sum cost per test:	0.08 €

SI table 3.2: List and totals of material costs per PSNP synthesis resulting in approx. 10 mL of particle suspension. The costs shown are the actual production costs per particle batch, including any minimum amounts for solvent preparations. In industrial mass production, it can be assumed that material costs in general, will decrease significantly.

No.	Name	Cost per pack	Pack size	Needed per batch	Cost per batch
8	S0982	55 €	0.1 g	1.729 mg	0.95 €
9	PS	205 €	1 kg	174 mg	0.036 €
10	Toluene	6.63 €	1 L	14 mL	0.093 €
11	Dialysis tubing	257 €	30 m	0.01 m	0.086 €
12	SDS	35.60€	100 g	14 mg	0.0050 €
				Sum cost per batch:	1.17 €

SI table 3.3: Material cost of PSNP per MTP and per test in dependence of the solvent volume ratio. Assuming batch volume of approx. 10 mL of particle suspension. The costs shown are the simplified costs per MTP and test, based on the production of 6 MTPs. In any case the material cost per test is well below 0.01 €

No.	V%	Needed per Plate	Cost per plate	Needed per test	Cost per test
1	10%	656 µL	0.071 €	≈ 6.8 µL	0.0007 €
2	12.5%	819 µL	0.089 €	≈ 8.5 µL	0.0009 €
3	15%	983 µL	0.11 €	≈ 10 µL	0.0011 €
4	17.5%	1147 µL	0.12 €	≈ 12 µL	0.0013 €
5	20%	1311 µL	0.14 €	≈ 14 µL	0.0015 €
6	22.5%	1344 µL	0.16 €	≈ 15 µL	0.0017 €

4 Ratiometric detection of H_2O_2 with Europium (III) Tetracycline (EuTc) as luminescent probe in thin-film sensor membranes

Abstract

A luminescent hydrogel platform technology for H_2O_2 was developed, enabling enzyme-based biosensors for the continuous monitoring of biomarkers through the lanthanide probe Europium Tetracycline (EuTc). Long-term and continuous detection remains difficult since the general challenges faced by biosensors are multiplied with the need for long measurement times and are typically due to photobleaching, signal instability in complex real samples, degradation, reversibility, and problems with interferences. Here, we advanced our previously developed enzyme-based hydrogel stacks and focused on addressing these challenges by careful selection of protective layers, the integration of ratiometric dyes, and the design of a hydrogel stack for continuous monitoring. Also, we identified 9,10-Bis(phenylethynyl)anthracene (BPEA) as an ideal reference dye since it had high photostability, excitation with the wavelength used for the EuTc probe, and minimal spectral overlap with the probe emission. It was integrated into the membrane stack through a separate cyclo-olefin copolymer (COC) layer or as BPEA loaded COC nanoparticles in a liquid assay. Choosing glucose as prominent biomarker associated with severe metabolic disease as model analyte, the general applicability of the platform technology was demonstrated in a high throughput rapid microtiter plate assay and as continuous online system. Interestingly, gamma irradiation sterilization studies suggest that this sensor system can also be used in vivo.

Keywords: H_2O_2, Hydrogen Peroxide, optical detection, optical sensors, lanthanide luminescence, EuTc

Graphical abstract

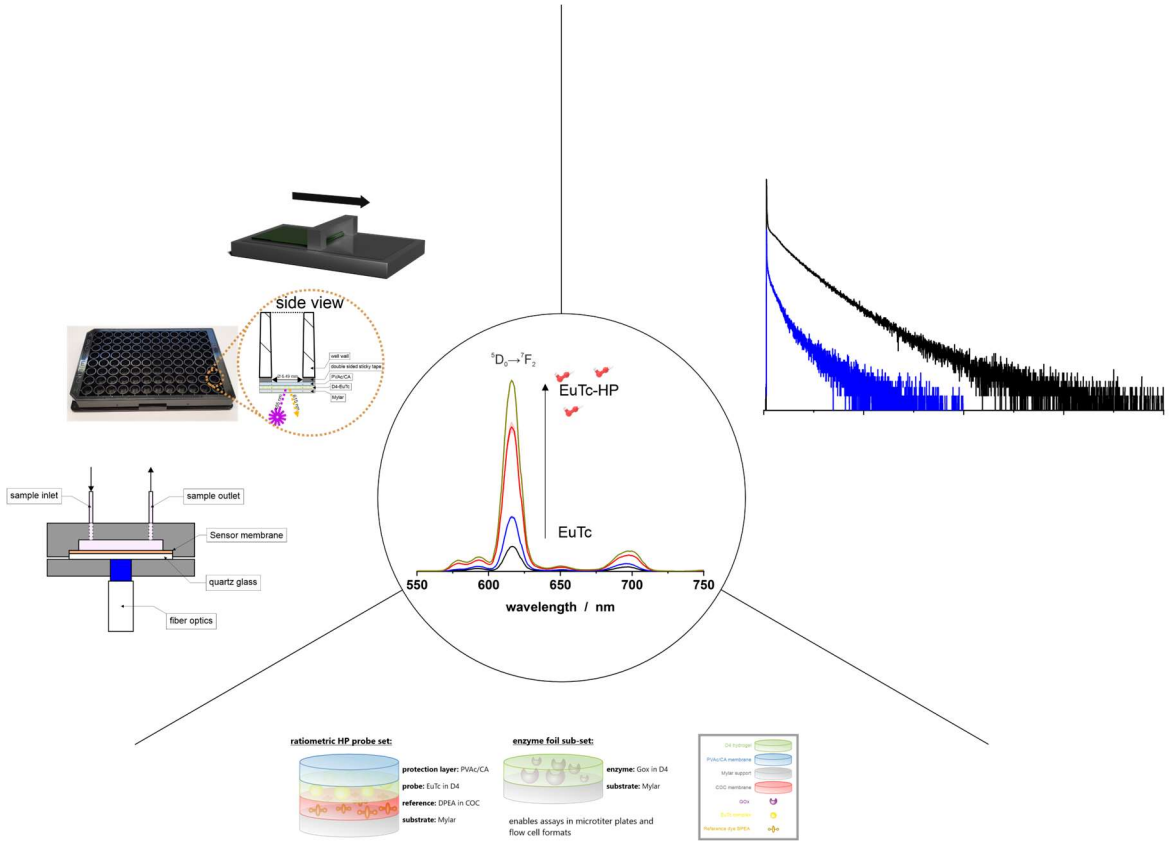

This chapter, or at least parts of it, are intended for submission but currently kept under seal due to patent claims by Terumo Cardiovascular Systems Corporation, Ann Arbor, MI 48103-9300 USA [1].

Author contributions

Most of the experimental work shown here was solely done by the author. Christina-Anna Senser and Iga Malicka collected data under supervision of the author. Some of these data sets are presented in Table 4, SI figure 4.2, SI figure 4.3 and SI figure 4.4 highlighted by an asterisk in the respective table and figure descriptions [*]. Meike Bauer (MB) and Barbara V. Grotz (BG) developed the general hydrogel membrane stack (D4//PVaC/CA) containing EuTc with the protection layer in their respective doctorate theses. Laura Deml originally discovered the effect of Hepes in the polymer cocktail during her master's thesis. Glucose oxidase and lactate oxidase discs were developed by MB. Flow cell disc size and flow speed parameter optimization was done by MB. MB, BG, Axel Duerkop (AD) and Antje J. Baeumner (AB) contributed with strategic discussions. The manuscript was written solely by the author.

4.3 Introduction

H_2O_2 is a metabolite found in numerous enzyme-catalyzed reactions, making it a particularly interesting analyte as a marker for a variety of diseases [2]. H_2O_2 is also used in a multitude of applications, as reagent, disinfectant or additive, just to name a few. For both user and product safety and for general quality control a reliable analytical method for these applications is a must [3].

Aside from being relevant as primary analyte, the availability of several H_2O_2 generating enzymes, such as glucose oxidase (GOx), lactate oxidase (LOx), galactose oxidase, cholesterol oxidase [4], tyramine oxidase [5] or monoamino oxidase type I and II [6], makes the development of a modular sensor that can reliably detect H_2O_2 as secondary analyte interesting for academia, industry and medical applications.

During heart surgeries, which already belong to one of the most dangerous surgical procedures, patients can show an increase of glucose concentration in their blood, often accompanied by increased insulin-resistance during or after [7] the operation. This can even for non-diabetic patients. This condition can be exacerbated by the administration of adrenaline or noradrenaline to counteract low blood pressure [8]. Patients that have coronary disease and at some stage might require heart surgery are generally not the healthiest individuals, often suffering from comorbidities such as obesity [9], diabetes and psychological illness, making the issue more difficult. And, with the increasing number of patients with diabetes [10], the chance of patients requiring heart surgery, but also have diabetes the number of perioperative-glucose related complications will grow in the future. Furthermore, in the recently updated Society of Critical Care Medicine Guidelines on Glycemic Control for Critically Ill Children and Adults 2024 the authors ‘suggest frequent (≤ 1 hr, continuous or near-continuous) glucose monitoring compared with monitoring at intervals greater than hourly in the management of hyperglycemia in critically ill adults on IV insulin during periods of glycemic instability’ and an intervention with insulin for patients with a blood sugar level of > 180 $mg \cdot dL^{-1}$ or 10 $mmol \cdot L^{-1}$ [11]. However, these limit values for insulin-based intervention are not entirely uncontroversial in the literature [12].

This has driven the development of a plethora of analytical approaches and probes, both electrochemical and optical [13–17].Electrochemically, the currently most reliant method is to use the glucose oxidase (GOx) and then detect the produced H_2O_2 by a Prussian blue electrode system [18]. Optically there have been several developments in the past for glucose [19]. However, a major disadvantage of many of these is the

irreversible nature of the reaction used for detection and quantification, making continuous detection a challenge. A potential workaround is the use of flow injection analysis (FIA) [20] which, coupled commonly with chemiluminescent and in fewer cases with fluorescent reagents, allows closer-meshed data collection depending on the cycle time [16,21]. Nevertheless, the appearance of truly reversible sensors is a slow and rare thing. Here, non-invasive detection based on microwaves/radio frequencies or infrared spectrometry have gained more attention in the last few years [22]. More recently, oxygen-based detection of H_2O_2, which usually depends on the quenching of either fluorescence or phosphorescence of organic dyes and metal complexes such as Platinum porphyrins or Ruthenium bipyridine and derivatives thereof [23] has seen developments [24,25]. In principle this oxygen-based detection can allow very fast response and regeneration times as the primary time-limiting factor is the diffusion trough the sensor matrix or layer. Unfortunately, these sensors rely on the catalytical degradation of H_2O_2 to O_2, which can cause issues. Furthermore, the outer structure must be as gas impermeable as possible and an additional calibration or referencing must be carried out continuously for the dissolved oxygen in the sample or the dissolved oxygen must be removed before the measurement, which in turn complicates the device design and costs response time. An option to avoid these issues is the use of innovative probes that do not require the implementation of additional catalytical steps for the detection of H_2O_2 and that do not rely on oxygen quenching. The complex Europium(III)-tetracycline (EuTc) is such a probe as it can coordinate with H_2O_2 at physiological relevant pH. This coordination leads to an increase of luminescence intensity of the $^5D_0 \rightarrow {}^7F_2$ transition of the Eu^{3+}-ion, due to the displacement of water detectable at 616 nm [26].

Apart from this enzyme- and catalyst-free possibility to detect H_2O_2, EuTc offers beneficial optical properties, such as a very large stokes shift of 211 nm, excitability with blue (405 nm) LEDs and long lifetimes in the µs range, which allows for lifetime-dependent, time resolved [27] and time-gated detection [28] reducing interference from autofluorescence and organic dyes, which usually show lifetimes in the ns range [29].

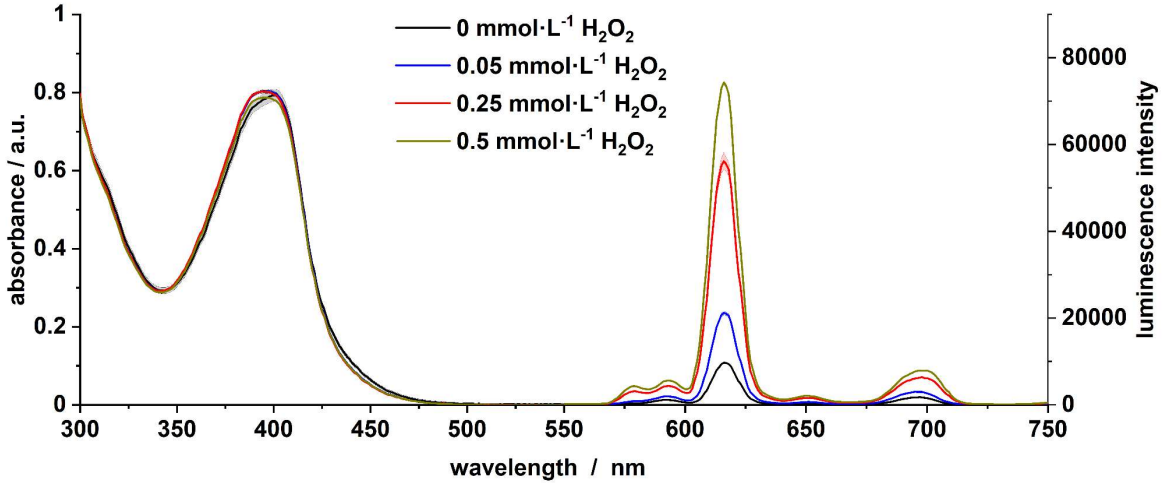

Figure 4.1: Absorbance (300 – 550 nm) and luminescence (550 - 750 nm) spectra of EuTc in Hepes at pH 7.4 showing the change in luminescence without H_2O_2 (black) and increasing concentrations of H_2O_2. Biotek plate reader, $\Lambda_{exc.}$ = 405 - 10 nm N = 12, T = 25 °C.

Furthermore, combining enzyme reactions with this H_2O_2-sensitive probe enables the development of sensors for bioanalytical applications. The probe and the enzymes, entrapped within biocompatible membranes and hydrogels, lead to optical sensors and allowed real-time flow cell measurements. Ratiometric detection was done by adding a layer containing a reference dye with suitable optical properties. This helped addressing issues like variability and instability of instrumental factors, especially for long term measurements. When combined with membranes containing glucose oxidase (GOx), the analytical scope of the sensor could be extended to detect glucose.

4.4 Materials and Methods

Extended protocols on membrane production, the used devices and all the measurements performed can be found in the SI. Bidistilled water was used for any aqueous solutions if not stated otherwise. All organic solvents used were of p.A. or better quality and used without further purification.

4.4.1 Chemicals

HydroMed D4 was supplied by AdvanSource biomaterials, Mitsubishi Chemical America Inc. (Wilmington, USA), H_2O_2-solution (34.5-36.5 %), glucose oxidase, Europium trichloride hexahydrate $EuCl_3 \cdot 6\,H_2O$ (99.9 % t.m.b.), tetracycline HCl (≥ 95 %), polyvinyl acetate (PVAc, average $M_w \approx 100\,000$), cellulose acetate (CA,

average $M_w \approx 30\,000$) was obtained from Sigma-Aldrich, Merck KGaA (Darmstadt, Germany), lactate oxidase was purchased from Sorachim SA (Lausanne, Switzerland). 9,10-Bis(phenylethynyl)anthracene (BPEA, > 98 %) was bought from TCI Deutschland GmbH (Eschborn, Germany), Topas® cyclo-olefin copolymer (COC, grade 8007) was obtained from TOPAS Advanced Polymers GmbH (Raunheim, Germany). (4-(2-hydroxyethyl)-1-piperazineethanesulfonic acid). HEPES (for biochemistry) was purchased from VWR International GmbH (Darmstadt, Germany). NaOH-solution (1 mol·L^{-1}, Titripur®) was from Merck KGaA (Darmstadt, Germany). LB broth (Miller's modification) was purchased from Alfa Aesar, Thermo Fisher Scientific Inc. (Waltham, USA).

Human plasma was thankfully received from the bloodbank of the University Hospital Regensburg.

4.4.2 Special labware

Non-sterile black bottomless 96-well MTPs were purchased from Greiner Bio-One GmbH (www.gbo.com). 3M Double-sided adhesive tape with polyester backing GPT-020F, transparent, 100 mm x 50 m, 0.202 mm was obtained from SKS GmBh (www.shop-sks.com) Biaxially oriented PET-membrane roll with a thickness of 125 µm was purchased from goodfellow GmbH (www.goodfellow.com).

4.4.3 H_2O_2 Sensor membrane stack production

Sensor membranes were produced following our previously published protocol [1]. In short, D4 hydrogel containing EuTc was knife coated on Mylar®, dried in an oven, and coated with a protective PVAc/CA layer. Hereafter described as EuTc-D4//PVAc/CA. (Figure 4.2).

4.4.4 BPEA-COC-NP synthesis

BPEA-COC-NPs were synthesized following a modified protocol form Bartoš et al. [30]. In short BPEA was dissolved in toluene together with COC. The solution was then added to an aqueous solution containing SDS. Under vigorous stirring the solutions were ultrasonicated 60 times in one-second intervals followed by one hour of stirring. This procedure was repeated four times. Afterwards the particle suspension was stirred with an open lid for 48 h to remove the organic solvent. The raw particle suspension was then dialyzed against water (800 mL) for five times over a duration of 72 h. The

particles were received as green-yellow untransparent suspension. Ratiometric H_2O_2 Sensor membrane stack production

Ratiometric H_2O_2 sensor membranes were produced following our previously published protocol [1]. In short, the ratiometric sensor membranes were produced by knife-coating and drying a layer of COC containing BPEA on Mylar® before knife-coating the D4-EuTc and PVAc/Ca membrane layers. Hereafter referred to as BPEA-COC//EuTc-D4//PVAc/CA (Figure 4.2).

4.4.6 Enzyme membrane production

Membranes containing enzymes were produced following our previously published protocol [1]. In short, D4 hydrogel containing GOwas knife coated on Mylar® and dried in an oven (Figure 4.2).

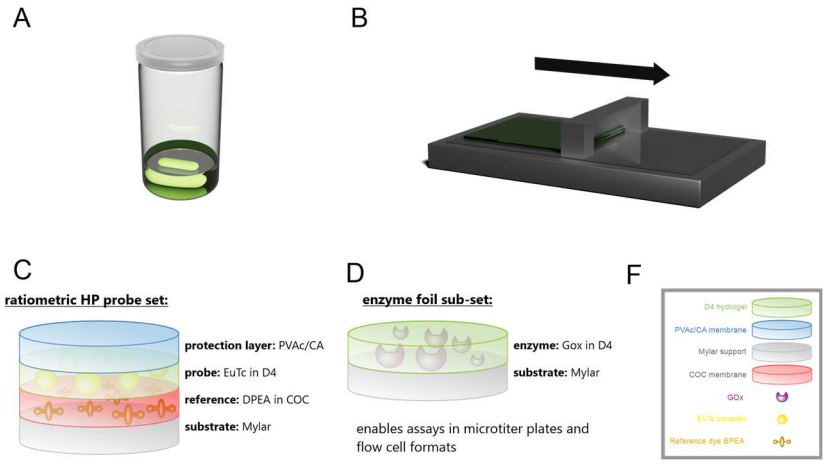

Figure 4.2: Sensor and enzyme membrane production scheme. **A** Probe, reference dye or enzyme was dissolved in a hydrogel or polymer cocktail and **B** knife coated and dried on Mylar. **C** ratiometric probe membrane stack. **D** Enzyme membrane stack. **F** component descriptions.

4.4.7 Measurement setups

MTP-based measurements were done by either punching out 6 mm discs and glueing them to the bottom of a 96-Well flat bottom MTP or by laser cutting sensor membrane and sticking it to the bottom of bottomless MTPs, as previously reported (chapter 3). For flow-cell measurements 24 mm discs were punched out and fixed in a custom-made flow cell with a rubber seal and a quartz glass disc as optical window (Figure 4.3).

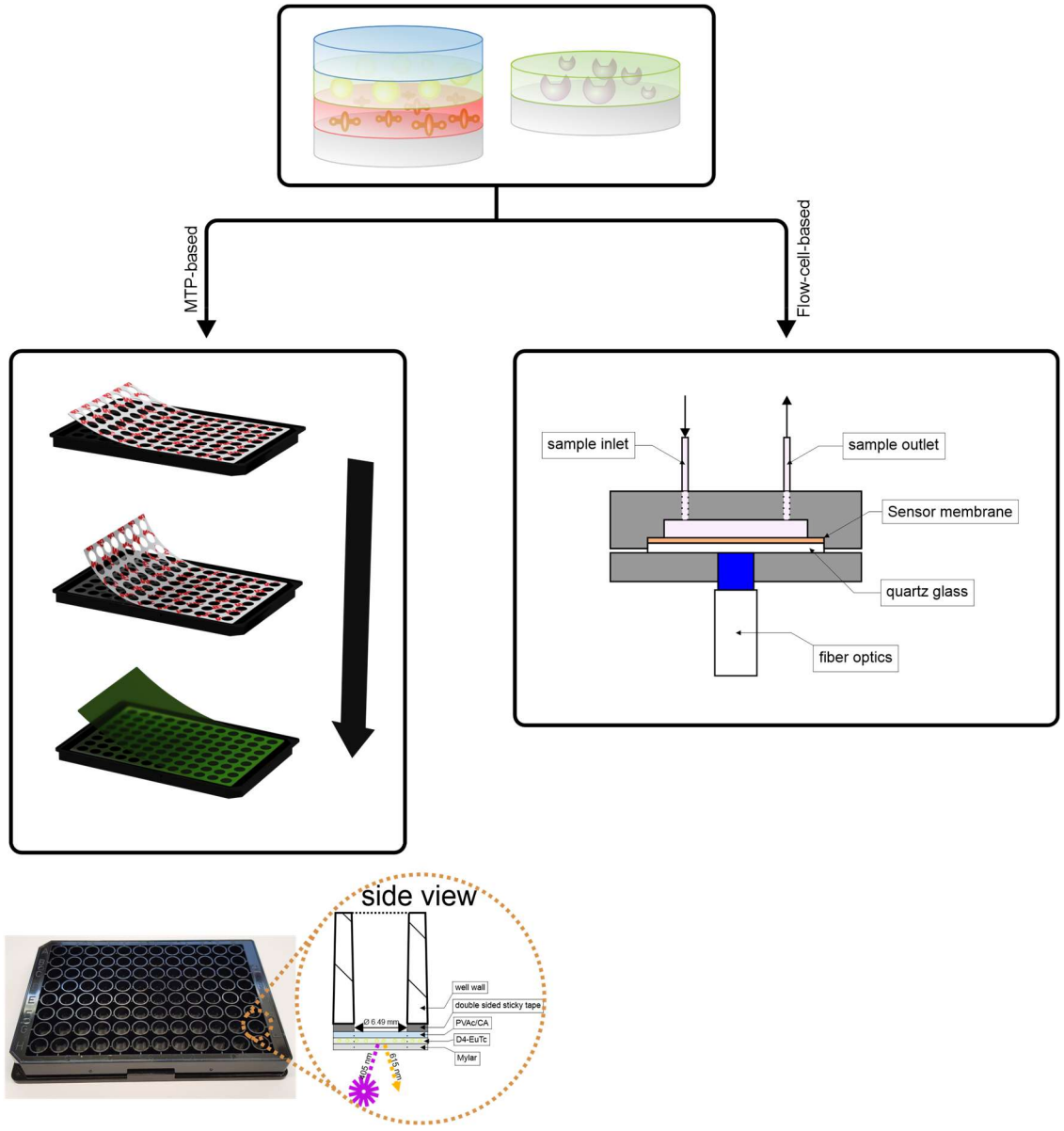

Figure 4.3: MTP and Flow cell measurement preparations

4.5 Results and discussion

On a general note: Ignoring solvent evaporation, which naturally results in a reduction of the film thickness, the layer thickness of the wet film after coating is generally lower than the setting for the knife-coating device. The actual coating thickness of the wet film depends, among other things, on temperature, the solution's viscosity, surface tension, and coating speed. Determining the thickness of the wet film with volatile solvents as used here is highly challenging if not impossible. Therefore, unless stated otherwise, the layer thicknesses mentioned in this publication refer to the set gap height of the respective knife coating device. In dried state, one can assume the volatile organic solvent to be nearly completely evaporated, which then yields a dry layer thickness reduced by about the volume factor that was initially present in the solvent mixture used for the knife-coating of the sensor cocktail. Although the sensor membranes will ultimately be implemented in a flow-cell system (hereafter referred to as "in flow"), some experiments were conducted in microtiter plates to collect a larger and statistically relevant amount of data (hereafter referred to as "MTP-based").

4.5.1 Protection membrane and initial equilibration

Moving from the liquid, buffer-based system to the hydrogel requires several adjustments. Here D4 was chosen as ideal matrix to house the complex. D4 is a polyurethane-based commercially available hydrogel that has been used for a variety of optical sensors [24,31,32].

Due to the lower optical layer thickness of the membrane, the concentration of EuTc in the film has to be increased. And, a D4 standalone membrane without an additional protection layer suffers from complex leakage and inactivation, which in turn leads to irreversible signals. Furthermore, the complex must be protected from interferents getting into the membrane and prevent blood clotting and cell adhesion. To achieve this a polyvinyl acetate/cellulose acetate (PVAc/CA) protection layer was developed by Barbara Grotz and Dr. Meike Bauer in their respective PhD theses based on a publication of Tsuchida [33], who used the polymer as matrix for an electrochemical setup do detect creatinine and creatine in serum.

However, due to the acidic pH value of D4 (≈ pH 4 - 5) and the desired measurement pH of EuTc being at pH 7.4 this protection membrane also increased the initial equilibration of the complex within the membrane due to the slower diffusion. As this limits the usability of the sensor, which is why initial equilibration should be made as

short as possible. A way of reducing this initial diffusion/equilibration time can be achieved by thinning the protection layer height. This can be done by mechanically coating a thinner film of PVAc/CA on top of the EuTc-D4 layer. Optimization with respect to the response and initial equilibration time was done using varying thicknesses of the sensor foils. With a combination of thinner protection layers for the EuTc-D4/PVAc/CA double layer shorter response times are feasible. Specifically, the equilibration time of a sensor disc with a 10 µm thick PVAc/CA protection membrane was reduced by 25 % in comparison to a sensor disc with a PVAc/CA protection 30 µm membrane (Figure 4.4).

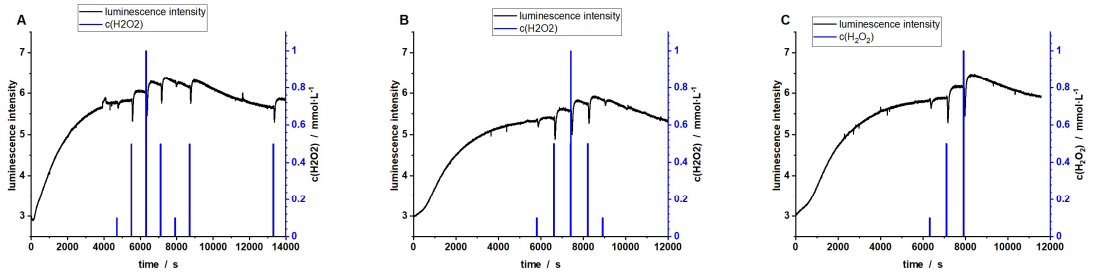

Figure 4.4: Time-resolved luminescence measurements (**black**) of unwashed 24 mm **D4-EuTc // PVAc/CA** (10-0.5//10w%) sensor discs with different wet coating thickness in the flow cell with injection times/concentrations of H_2O_2 in Hepes (**blue**). λ_{ex} = 405-8 nm λ_{em} = 615-8 nm, flow -16, running/injection buffer 0.1 M Hepes pH 7.4 (25 C). **A** 10 µm, PMT voltage: 745 V (H_2O_2 injections: 30 s 0.1 mM at 4700 s; 30 s 0.5 mM at 5500 s; 30 s 1 mM at 6300 s; 30 s 0.5 mM at 7100 s; 30 s 0.1 mM at 7903 s; 30 s 0.5 mM at 8700 s; 30 s 0.1 mM at 13300 s). **B** 20 µm, PMT voltage: 730 V (H_2O_2 injections: 30 s 0.1 mM at 5800 s; 30 s 0.5 mM at 6600 s; 30 s 1 mM at 7400 s; 30 s 0.5 mM at 8200 s; 30 s 0,1 mM at 8900 s). **C** 20 µm, PMT voltage: 735 V (H_2O_2 injections: 30 s 0.1 mM at 6300 s; 30 s 0.5 mM at 7100 s; 30 s 1 mM at 7900 s)

Presumably, even smaller protection layers would be preferrable to enhance both equilibration and response time. Unfortunately, in the context of laboratory based methods controlling the exact knife-coated membrane layer thickness is not an easy task and very difficult to reproduce [34].

Another variant which avoids the issue of having to choose smaller, thus unreliable spacers, is to reduce the concentration of polymer in the solvent. The w% of the protection layer was hereby tested with the standard 10 w%, 7.5 w%, 5 w% and 2.5 w%. With exception of the latter, all coating cocktails showed good behavior on the knife-coater and seemingly uniform layers. The cocktail with 2.5w% ran too much on the surface due to the high solvent content and was unsuitable for knife-coating, but a dip-coating or spray-coating application might be interesting. As only one viable membrane could be coated with the 2.5 w%, this dataset is only available in N = 8 in the dry state and N = 1 for the wet assay. In the dry state both the absorbance and the

emission spectra of the membranes overlap within a reasonable expectable standard deviation to the different polymer covers showing no negative impact of the relatively higher solvent during production.

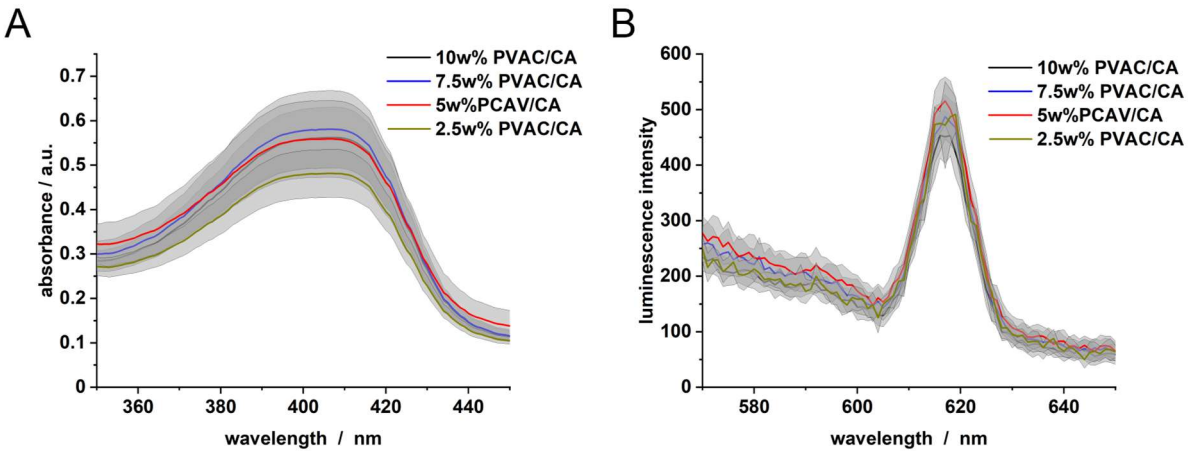

Figure 4.5: **A** Absorbance and **B** luminescence spectra of dry EuTc 0.5w%-D4//PVAc/CA (10 w%-2.5 w%) membranes with 0.1 mol·L^{-1} Hepes pH 6.5 in the aqueous part of the coating cocktail (10 v% of the 90 w. $\lambda_{exc.}$ = 405-10 nm. 25 °C, N = 24 for 10, 7.5 and 5 w% PVAC/CA, N =8 for 2.5 w% PVAC/CA. Biotek MTP gain 100, top optic, 25 °C,

As expected in the MTP assay with H_2O_2, a clear trend towards a faster response to H_2O_2 with the lower concentrated protection layers is observable. The best results regarding signal intensity, response and standard-deviation are achieved with the 5 w% PVAC/CA-protection layer as can be seen in the kinetic curve (Figure 4.7 C) and the corresponding dose-response plot (Figure 4.6). This reinforces the theory of the diffusion limitation and mechanism caused by the protection layer. Especially the 2.5 w% shows a very fast equilibration of around 5 min, but with no differentiation between the different H_2O_2 concentrations but only between buffer and H_2O_2, indicating an insufficient protection layer (Figure 4.7 D).

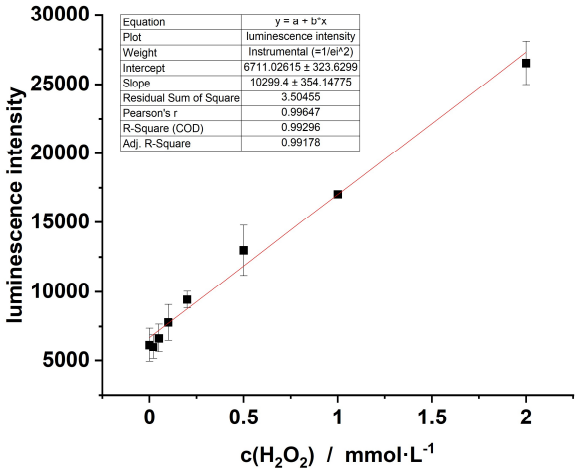

Figure 4.6: Dose-response curve with a linear fit of EuTc (0.5w%)-D4 (10 w%)-Hepes//PVAC/CA (5 w%)-membrane after 20 min assay time with H_2O_2. Biotek MTP reader λ_{exc} = 405-10 nm, λ_{em} = 615-10 nm, gain 100, top optic, 25 °C, N = 3

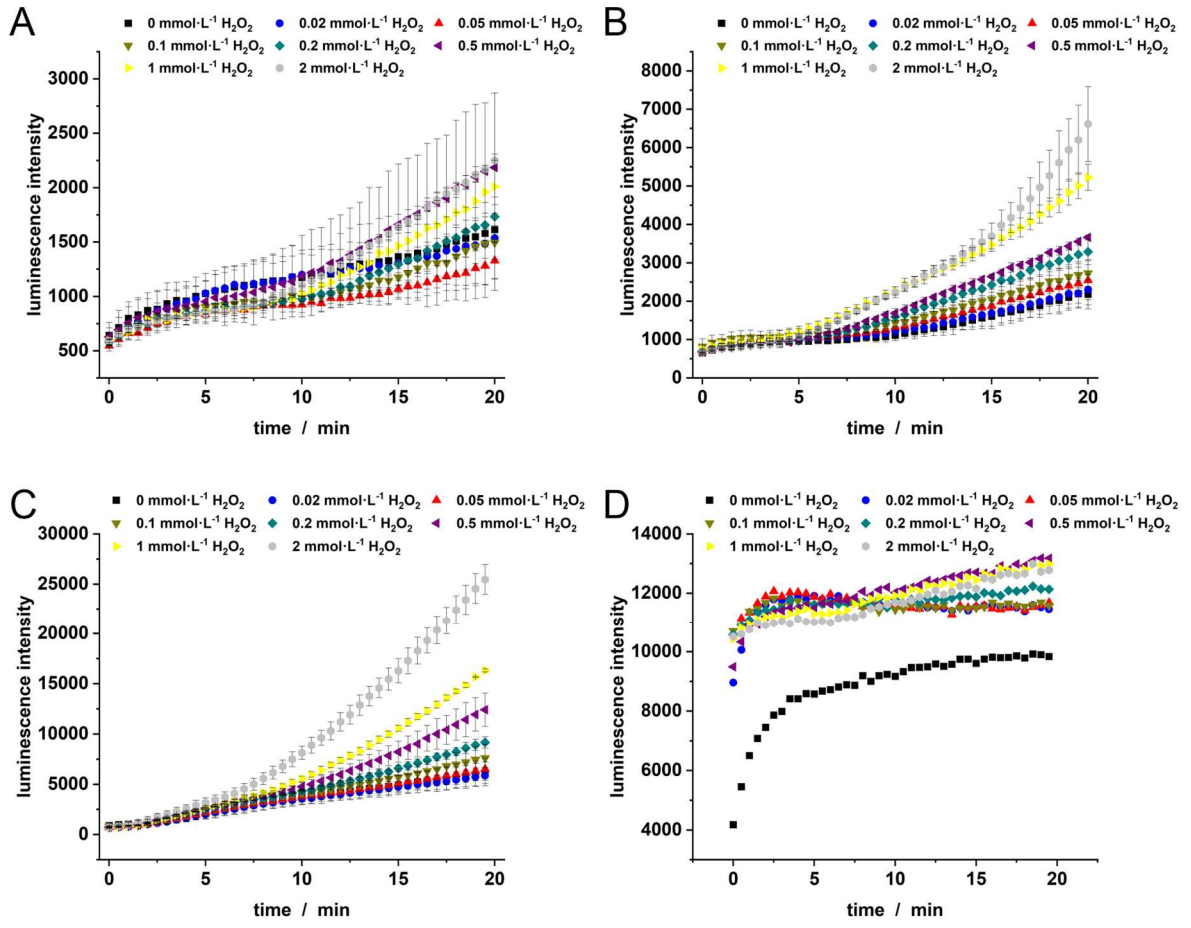

Figure 4.7: Kinetic curves of EuTc 0.5 w%-D4//PVAc/CA membranes with H_2O_2. Membranes were produced with 0.1 mol·L^{-1} Hepes pH 6.5 in the aqueous part of the coating cocktail (10 v% of the 90 w%) and varying PVAC/CA

protection layers (**A** 10 w%, **B**: 7.5 w%, **C**: 5 w%, **D**: 2.5 w%). Biotek MTP reader λ_{exc} = 405-10 nm, λ_{em} = 615-10 nm, gain 100, top optic, 25 °C, N = 3 (**A**, **B**, **C**) N = 1 (**D**)

As additive Hepes increases the pH of the coated membranes, thus reducing the initial equilibration time. D4 1 with Hepes 0.1 M pH 6.5 in the aqueous part was used to produce EuTc-D4//PVAc/CA membranes with different EuTc doping (0.1, 0.15, 0,25 & 0.5 w%). The addition of of Hepes in the aqueous part did not only reduce the observed background signal, but also allowed for the detection of the EuTc-complex in the dry membranes. Here, 0.1 w% EuTc showed the best result in regard to luminescence intensity and visibility of the emissions at lower wavelengths. The increasing absorbance indicates that there is more EuTc present in the dry membrane, but self-quenching seems to occur.

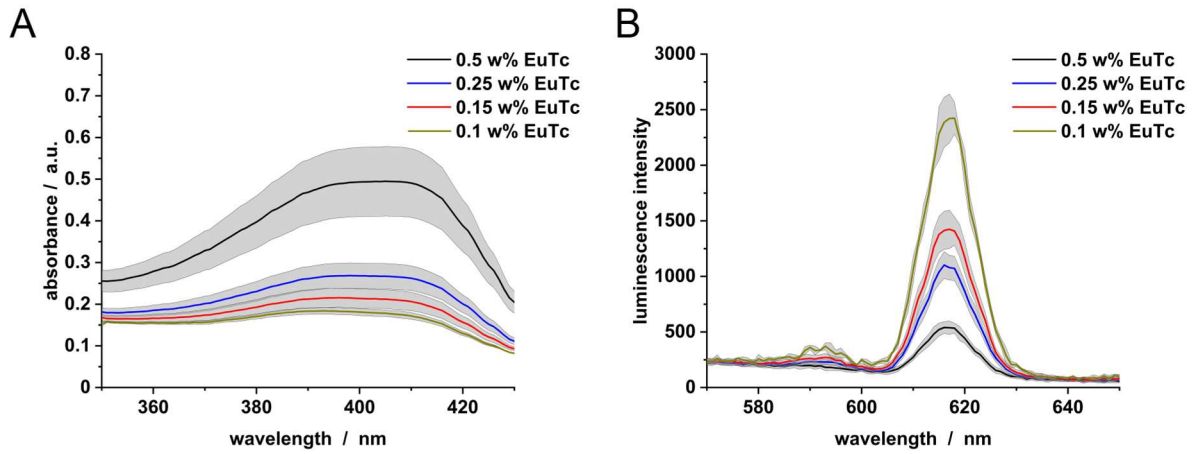

Figure 4.8: Absorbance (**A**) and luminescence (**B**) spectra of dry EuTc-D4//PVAc/CA membranes with 0.1 mol·L^{-1} Hepes pH 6.5 in the aqueous part of the coating cocktail (10 v% of the 90 w%) and varying EuTc doping. Biotek MTP reader λ_{exc} = 405-10 nm, 1 nm resolution, gain 100, top optic, 25 °C, N = 24.

In the liquid MTP assay with Hepes and H_2O_2 the membranes still show kinetic curves with a slight but noticeable gradient. Depending on the doping, the curves start to separate and increase more at the higher H_2O_2 concentrations (Figure 4.9). With 0.1 w%, for example (Figure 4.9 D), this effect occurs after approx. 5 min, but for 0.5 w% EuTc only after approx. 12 min (Figure 4.9 A). This general delay is a further indication of the retention by the protection layer. That this delayed response differs for the different doping and takes longer for higher EuTc concentrations can possibly be explained by the fact that the proportion of complex causes both structural and thus diffusion-based changes within the hydrogel on the one hand. On the other hand, as the EuTc luminescence is pH dependent, the increased amount of EuTc might take longer until fully equilibrated.

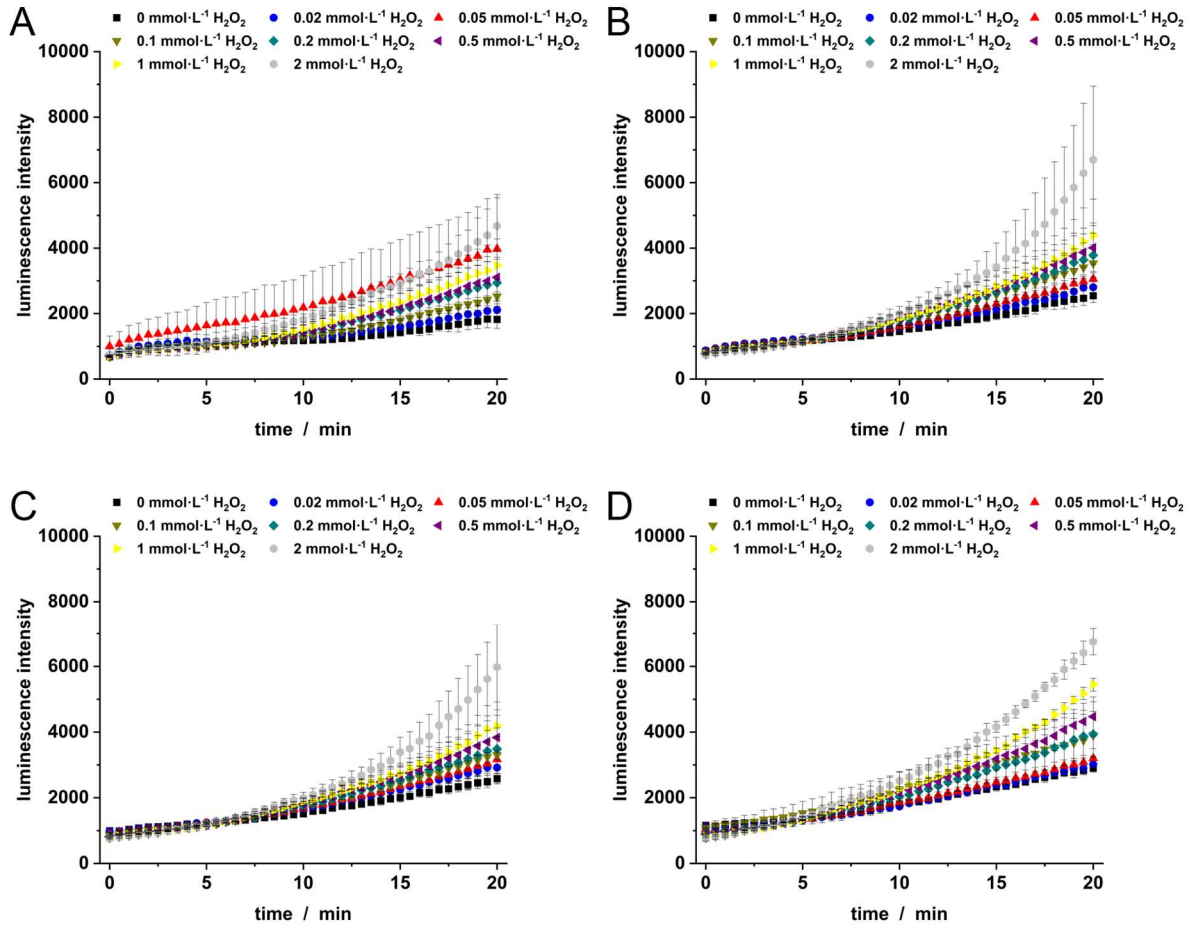

Figure 4.9: Kinetic curves of EuTc-D4//PVAc/CA membranes with H_2O_2. Membranes were produced with 0.1 mol·L^{-1} Hepes pH 6.5 in the aqueous part of the coating cocktail (10 v% of the 90 w%) and varying EuTc doping (**A** 0.5 w%, **B**: 0.25 w%, **C**: 0.15 w%, **D**: 0.1 w%). Biotek MTP reader λ_{exc} = 405-10 nm, λ_{em} = 615-10 nm, gain 100, top optic, 25 °C, N = 3

No significant difference can be observed in the dose-response plot between the individual EuTc contents except for increased standard deviation for the higher amounts. The increased standard deviations of the higher H_2O_2-concentrations, which are due to the variation in layer thickness of the different small strips from the small coater, highlight the issue of diffusion depending on the layer thickness, both protection and sensing. Especially the 0.1 w% EuTc DR can be fitted relatively well with a logistic fit, currently only leaving the standard deviations of the concentrations between 0.5 and 0.1 mmol·L^{-1} wanting. This issue might be better manageable with higher N, and more homogenous membrane (large coater) production, as the replicates are from different membranes.

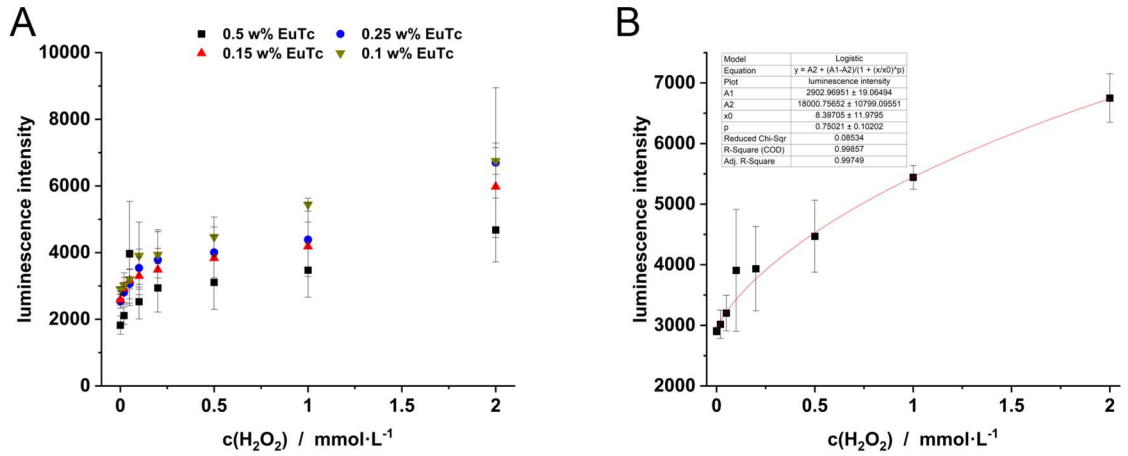

Figure 4.10: **A** Dose response curves of EuTc-D4//PVAc/CA membranes with H_2O_2 after 20 min. Membranes were produced with 0.1 mol·L^{-1} Hepes pH 6.5 in the aqueous part of the coating cocktail (10 v% of the 90 w%) and varying EuTc doping (black rectangles: 0.5 w%, blue circles: 0.25 w%, red triangles: 0.15 w%, orange triangles: 0.1 w%). $\lambda_{exc.}$ = 405-10 nm, $\lambda_{em.}$ = 615-10 nm. 25 °C, N = 3 Biotek plate reader. **B** Dose-response curve with a logistic fit of EuTc (0.1w%)-D4 (10 w%)-Hepes//PVAC/CA (10 w%)-membrane after 20 min assay time with H_2O_2. Biotek MTP reader λ_{exc} = 405-10 nm, λ_{em} = 615-10 nm, gain 100, top optic, 25 °C, N = 3.

4.5.2 Ratiometric strategy

Long-term measurements can suffer from a variety of issues such as sensory, lamp and detector drifts, photobleaching, sensor fouling or simply misalignment of the sensor in the optical pathway. For this reason, a ratiometric strategy was explored. Here, 9,10-Bis(phenylethynyl)anthracene (BPEA, Figure 4.11 A) was identified as ideal reference dye. BPEA offers several beneficial characteristics: it can be excited with 405 nm, has an excellent quantum yield of 1, a good extinction coefficient of 35400 L·mol^{-1}·cm^{-1} and shows two distinctive emission peaks at 468 nm and 500 nm in toluene [35] (Figure 4.11 B blue curve) and thus minimal overlap with the main EuTc emission at 616 nm (Figure 4.11 B red curve). With approximately 40 € per g the dye is also reasonably cheap. As the dye is very non-polar, it needs to be integrated in a polymer layer, which in turn also can protect it from water- and oxygen-based quenching [36]. For this application we chose cyclo-olefin copolymer (COC) as a perfect matrix to house the reference dye. COC shows a low birefringence, low gas and water permeability and a high transparency [37]. Furthermore, Mitsui et al. [38] could show that BPEA stored in a COC film showed a high degree of photostability, compared to pure thin films of BPEA. COC could be dissolved together with BPEA in toluene, enabling knife coating of the film.

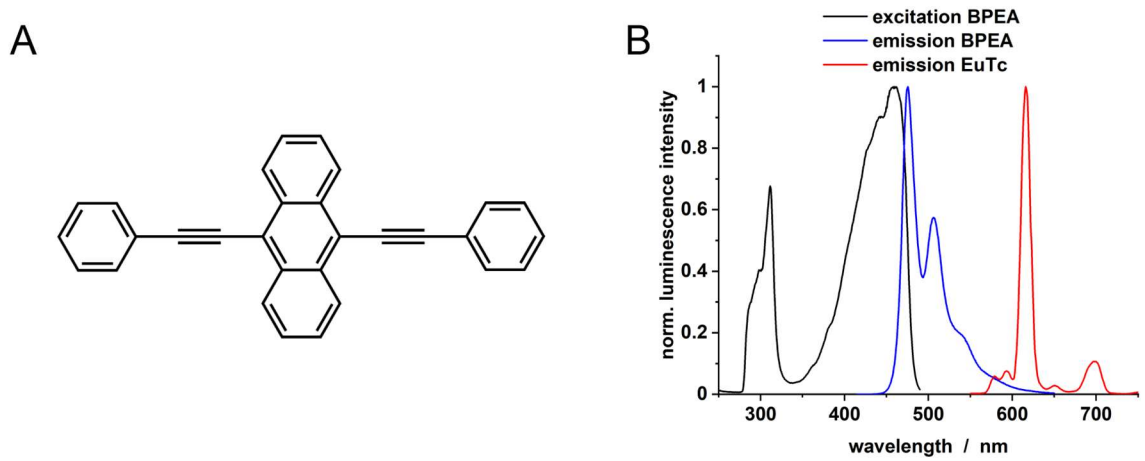

Figure 4.11: **A** Structure and **B** excitation (black curve)/fluorescence (blue curve) spectra of BPEA (2 µgL^{-1}) in toluene and luminescence spectrum of EuTc (red curve) with 0.1 mmol·L^{-1} H_2O_2 in Hepes pH 7.4. The data was divided by the respective peak maximum to normalize peak height. BPEA: Edinburgh FS5: emission spectrum λ_{exc} = 405-0.5 nm, 415 nm- 650 nm, em slit: 0.5 nm, 0.5 nm steps, 0.5 s dwell, 5 repeats; excitation spectrum: λ_{em} = 505-0.5 nm, 250 nm- 490 nm, em slit: 0.5 nm, 0.5 nm steps, 0.5 s dwell, 5 repeats. EuTc: Biotek MTP reader λ_{exc} = 405-10 nm, 550-750 nm, gain 100, top optic, 25 °C, N = 4.

4.5.3 Photostability

In order to be usable as reference, BPEA should show a high photostability in the application to minimze the baseline shift. The photostability of the reference dye was determined by irradiating BPEA in toluene (5 ng·L^{-1}) with a high-power mercury lamp for 45 min at 405-8 nm and simultaneously measuring fluorescence at 475-8 nm (Figure 4.12 B). In this photobleaching experiment the dye showed a loss of fluorescence intensity of ≈ 1 %·h^{-1} (Figure 4.12 A). This correlates with a dye loss of ≈ 50 fg·L^{-1}·h^{-1}. If one considers that the suggested main photooxidation mechanism of anthracenes is the oxidation of one of the central rings in 1, 6 position [39,40] reducing the available oxygen should also increase the photostability. When repeating the experiment, but with BPEA integrated in a COC-membrane the dye showed an increased photostability. Specifically, the loss of fluorescence intensity over a duration of 4.5 h was only ≈ 2 % and thus only half in comparison to the experiment in solution.

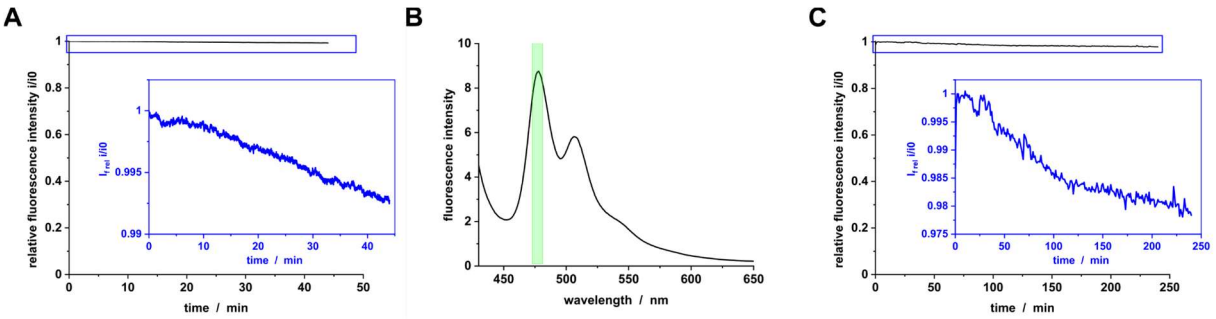

Figure 4.12: **A** Time-resolved photobleaching measurement of BPEA in toluene (5 ng·L^{-1}). λ_{ex}: 405-10 nm, the time resolution was 1 s. Including a rough estimation of the solvent evaporation and a simple graphical extrapolation of the reduction of the fluorescence intensity the overall loss of fluorescence intensity within one hour is approximately 1%. **B** fluorescence spectrum of a COC-BPEA (1.35 mg BPEA / mL coating solution) reference foil in the flow cell. The highlighted area (green) represents the bandwidth (8 nm) used for detection/photobleaching measurements. **C** (larger graph) full scale (0-1) relative (i/i_0) time-course measurement of the fluorescence of the reference foil used in **B**. The magnified area (in blue) with the Y-scale from 0.975-1.1 visualizes the photobleaching effect of the dye not visible in the main graph. The overall photobleaching after 4 h of continuous irritation was ≈2 % (I_{fmax}: 6,33→I_{Fmin} ≈6.20).

4.5.4 Flow cell detection

Looking at the flow-cell emission spectrum of a ratiometric BPEA-COC//D4-EuTc//PVAc/CA sensor disc, the peaks at 475 nm and 505 nm of the reference are visible together with the EuTc-peak at 615 nm (Figure 4.13 A). However, they are severely overlayed by a sloping background increasing towards the excitation wavelength. The observed background signal might be tetracycline not coordinated to europium [41]. Instead of unbound tetracycline, the signal could also be caused by the polymers or the hydrogel used in the membrane production. Since COC has a very low autofluorescence [42], the signal here would probably be autofluorescence of the PET substrate with 405 nm excitation. Furthermore, as the fiber sits perpendicularly on top of the quartz glass covering the sensor disc, the reflected light is also collected by the fiber. Due to the setup the light also has to travel through several layers with varying refractive indices from air to quartz glass to mylar to COC then D4, PVAc/CA then the solution in the cell and vice versa, resulting in an increased (back)scattering and reflection of the excitation. For the ratiometric detection within the flow cell 505 nm was used as reference wavelength here for the better signal intensity ratio with the probe emission at 615 nm. Considering how stable the fluorescence signal of the reference at 505 nm is over a duration of 10000 s (Figure 4.13 B blue curve) the signal seems to be independent of the solution flow in the cell and also independent from the initial swelling and equilibration of the hydrogel at the start (Figure 4.13 B red curve). This would indicate that the signal is not caused by hydrogel or non-coordinating tetracycline, as the fluorescence of the latter is pH dependent [41]. With the hydrogel

in its dried state being acidic, the pH in the matrix increases with the initial equilibration, which should also change the fluorescence of tetracycline. This would indicate that the signal was caused by the coating substrate PET. The increased noise seen here is predominantly caused by the constant 1 s interval switching of the optical grating from 615 nm to 505 nm. Nevertheless, this setup allows for the ratiometric detection of H_2O_2 based on the emission of the reference dye BPEA within the COC layer, and the probe emission of EuTc in the D4 layer. As can be seen in Figure 4.13, even with this background signal the detection - albeit primarily qualitatively - of H_2O_2 is possible.

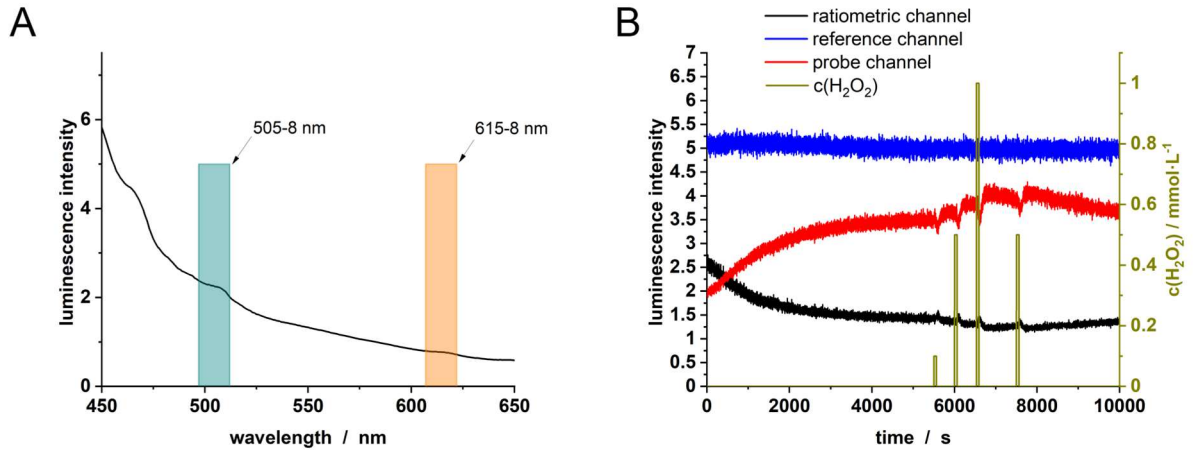

Figure 4.13: **A** Spectrum of a dry 24 mm **COC-BPEA//D4-EuTc//PVAc/CA**-disc with the respective regions of interest highlighted. **B** Ratiometric luminescence flow cell measurements of 24 mm **COC-BPEA//D4-EuTc//PVAc/CA**-discs with the ratiometric channel (**black**) the probe channel (**red**, 615-8 nm) the reference dye channel (**blue**, 505-8 nm) with the injected concentrations of hydrogen peroxide (**dark yellow**) shown with the corresponding color-coded y-axis. Settings AB2 Flow cell (**A**): λ_{exc} = 405-8 nm, λ_{em} = 505-8 nm & 615-8 nm, resolution 1 s.

The ratio between the fluorescence intensity of the reference BPEA in COC and the probe emission is also highly influenced by the respective layer thicknesses. Thicker reference layer means more reference fluorescence intensity and vice versa. An example of these differences in layer thickness that occur within a few cm of the same coated membrane is illustrated in Figure . Where one part of the membrane shows a thickness of 694.4 nm, a different part only has 525.7 nm and thus only 75.7 % the height of the thicker piece. Of course, the shown images of the membrane are two extremes that are not necessarily representative. As COC can be coated in films comparable to the used PET coating substrate, BPEA in COC could be produced as industrial film and then be used as coating substrate. This would not only eliminate an additional coating step, but also potential optical issues of the PET-COC interface and the autofluorescence of PET. Furthermore avoiding the different birefringence of PET [43] and COC might alleviate some of the spectral issues mentioned before.

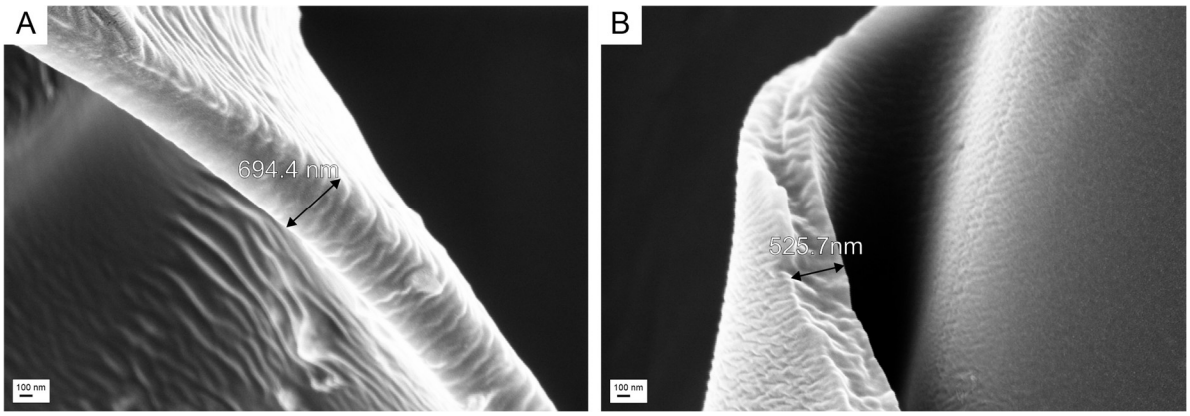

Figure 4.14: SEM-micrographs of two different tears in BPEA-COC samples allowing estimation of layer thickness. EHT = 5 kV, WD = 5.8 nm, Magnification = 50000x. the Size bars are 100 nm.

4.5.5 Different layer? Same layer!

Alternatively, BPEA can also be integrated into polystyrene (PS) or COC nanoparticles. These nanoparticles could then be added to the probe coating cocktail mixture, which makes it possible to skip an additional coating step at the cost of employing potentially harmful nanoparticles that could cause adverse effects in vivo. Here, a modified variant of the ultrasonication/emulsion polymer nanoparticle synthesis investigated by Bartos et al. [30] was used. Besides being true to its title, the synthesis was also accessible for other polymers, allowing the embedding of the reference dye in COC-nanoparticles. For the particle synthesis itself PS could easily be replaced with COC without having to adjust synthesis parameters. In the light of the specific optical properties and the lower gas permeability compared to PS, COC is the preferred polymer as matrix for the stability of BPEA. It should of course be noted that the nanoparticles can also cause scattering effects, which become worse with higher particle concentrations. To prevent this, the highest possible loading of the particles with dye must be synthesized to reduce the required quantity of particles in the membrane. However, the formation of excimers of BPEA at higher concentrations needs to be avoided. To streamline the synthesis and reduce the number of nanoparticle batches, the right order of magnitude of dye was determined by simply dissolving increasing concentrations of BPEA in toluene. As can be seen in Figure 4.15 BPEA starts to self-quench above 30 $\mu g \cdot mL^{-1}$. For the used COC with a density of 1.02 $g \cdot cm^{-3}$ and polystyrene with a density of 1.06 $g \cdot cm^{-3}$ [44] the w% should then be adjusted to about 3 w%, which in turn corresponds to 0.5 - 0.52 mg of dye in a synthesis batch (assuming a density of 1.02 $g \cdot cm^{-3}$ to maintain the mean distance between each fluorophore molecule).

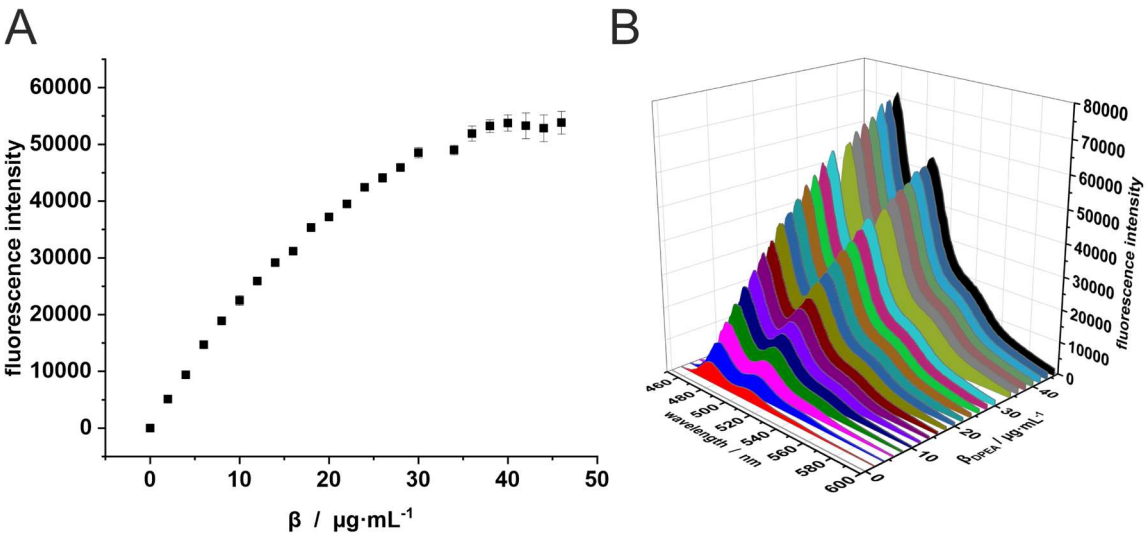

Figure 4.15: **A** mass concentration dependent fluorescence intensity of BPEA at 475 nm in toluene showing self-quenching above 30 µg·mL^{-1} Biotek MTP reader λ_{exc} = 405-10 nm, 1 nm resolution, 450-600 nm, gain 100, bottom optic, 25 °C, N = 4. **B** spectra of BPEA in toluene with increasing mass concentrations.

However, as COC only has cycloalkane and alkane moieties, BPEA will presumably not be as easily distributed as in PS, where it could π-π interact with the PS [45]. Particles made of COC could therefore not be loaded with as much BPEA as PS nanoparticles before excimer-formation was visible.

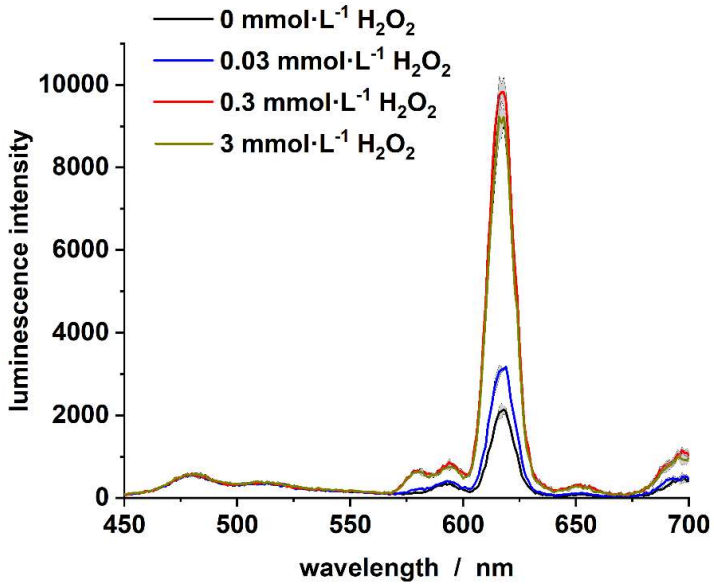

Figure 4.16: Luminescence spectra of COC-BPEA NPs with 0.23 w% dye load prediluted 1:50 and EuTc in Hepes with increasing concentrations of H_2O_2. Biotek MTP reader λ_{exc} = 405-10 nm, 1 nm resolution, 450-700 nm, gain 100, top optic, 25 °C., N = 3.

In solution best results were achieved with 1:50 predilution of 0.23 w% (and thus less than a 10th of the estimated doping) doped particle suspension. Here, no change of particle signal with changing H_2O_2 concentration, no scattering and good response of the probe up to the saturation beyond 0.3 mmol·L^{-1} H_2O_2 was possible. In a final approach these particles could be integrated in a D4 membrane along the probe dye. To avoid the previously shown background signal of PET a different coating substrate, such as a COC film, or other polymer films showing low autofluorescence [46] will have to be used in a future application.

4.5.6 Gamma sterilization study

Considering the potential application as sensor in vivo, the sensor must be sterile. However, GOx prevents sterilization by temperature or chemical means. Furthermore, chemical treatment could compromise the integrity and stability of the hydrogel layers, destroying the sensor. Therefore, sterilization with γ - rays is the method of choice. For the sterilization of the sensor foils, all three membranes were tested separately, i.e. ratiometric dye BPEA in COC, EuTc probe in D4/PVAc/CA, and glucose oxidase in D4, respectively. In principle, all polymers used can be sterilized with γ – radiation, which means no to minimal structural/matrix damage was expected. The respective membranes were exposed to approximately 12.6 kGray over a total of 66 h (irradiation time: 228893 s, Si table 4.1).

Laser-cut COC-BPEA strips were stuck to the bottom of two MTPs with double sided adhesive tape. Fluorescence measurements were performed before and after the γ-treatment. The control plate was stored light-protected at ambient conditions in a laboratory adjacent to the room containing the sterilization device. It was found that after treatment the BPEA still had more than 98% of its original fluorescence signal. Specifically, the corrected remaining fluorescence intensity (statistical outliers eliminated with Student's t-test) for the control is 1.006 ± 0.009 and 0.986 ± 0.016 for the test plate (Figure 4.17).

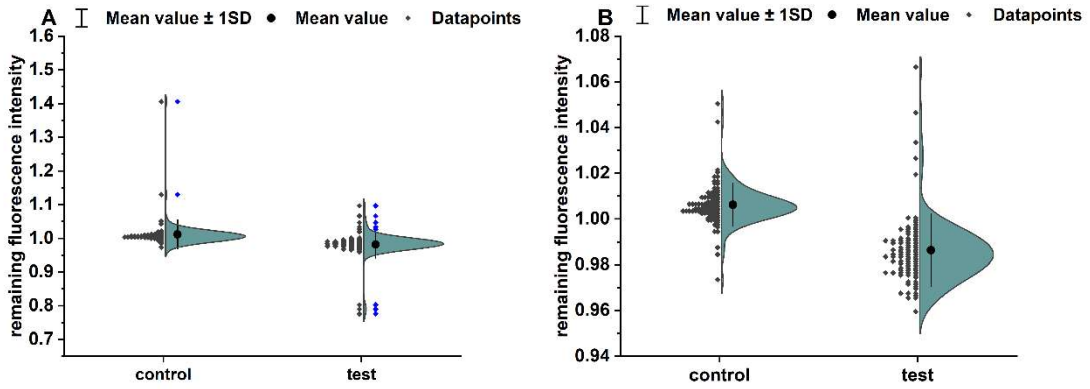

Figure 4.17: Violin box plots of COC-BPEA representing the residual fluorescence intensity ($F_{postrad}/F_{prerad}$) at 475-10 nm (λ_{exc} = 405-10 nm). Each measurement datapoint represents five averaged subsequent measurement points. (**A**) full measurement data with outliers (**blue**) included (N = 96 each). (**B**) distribution of Data with outliers removed (N = 94 control N = 90 test). The corrected remaining fluorescence intensity for the control is 1.006 ± 0.009 and 0.986 ± 0.016 for the testplate. Biotek MTP reader λ_{exc} = 405-10 nm, λ_{em} = 475-10 nm, gain 100, bottom optic, 25 °C.

MTPs with **D4-GOx** discs containing the enzyme were tested with increasing concentrations of glucose before (Figure 4.18 **A**) and after the γ-treatments (Figure 4.18 **B**) with EuTc as H_2O_2 probe in the liquid assay. The treated discs show a very comparable function after the sterilization procedure. The overall lower response of the test in comparison to the control can be explained by the two different plates and GOx membranes used. The effect is consistent for both pre- and post- irradiation.

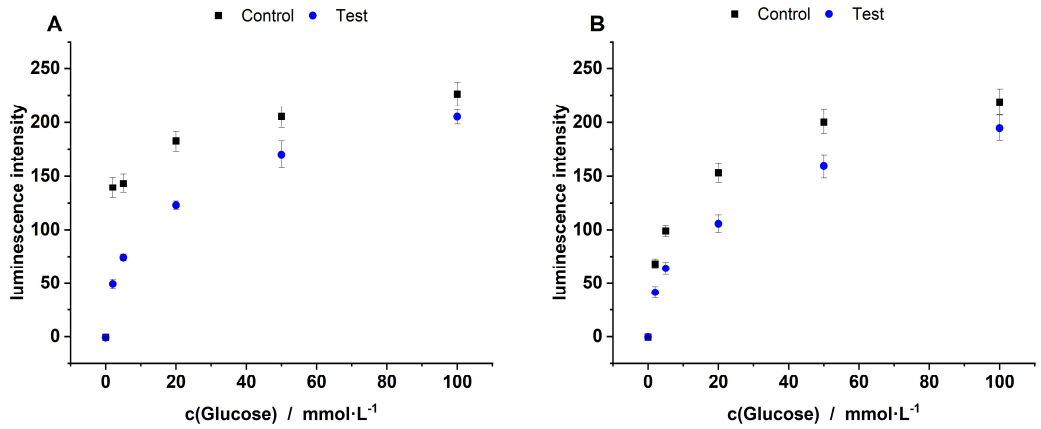

Figure 4.18: luminescence dose-response curves of GOx-D4 enzyme discs in the control- (**black**) and the test-MTP (**blue**) with EuTc as Probe in the liquid assay with increasing concentrations of glucose before (**A**) and after (**B**) the γ-treatment. Biotek MTP reader λ_{exc} = 405-10 nm, λ_{em} = 615-10 nm, gain 100, top optic, 25 °C, N = 24

MTPs with D4-EuTc//PVAc/CA discs containing the probe were tested with increasing concentrations of H_2O_2 before (Figure 4.19 A) and after the γ-treatments (Figure 4.19 B). It is observed that irradiation had a significant effect on the EuTc probe with an overall drop of the signal intensity of about 50%. Considering that the ideal storage of EuTc is below room temperature, the observed effect might be alleviated with cooling during irradiation. Furthermore, the irradiation time (66 h) will be much shorter for industrial-scale sterilization.

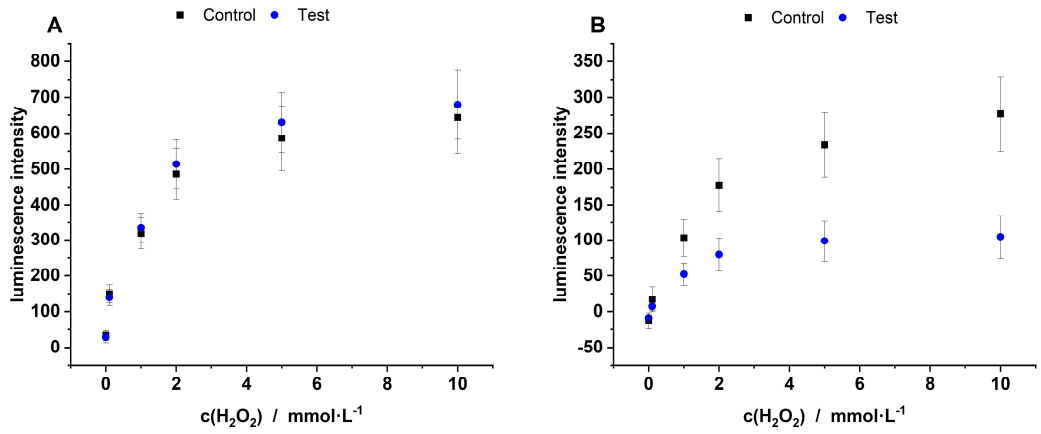

Figure 4.19: luminescence dose-response curves of EuTc in the control- (**black**) and the test-MTP (**blue**) with increasing concentrations of hydrogen peroxide before (**A**) and after (**B**) the γ-treatment. Biotek MTP reader λ_{exc} = 405-10 nm, λ_{em} = 615-10 nm, gain 100, top optic, 25 °C, N = 24

Parallel to these luminescence measurements, sterility testing with punched out foil-samples (N = 3 for each foil type investigated above) was done. Here, the used membrane discs proved to be aseptic over a duration of at least 3 months with no fungal or bacterial growth visible (SI figure 4.5).

4.5.7 Interference

To evaluate the performance of the sensor in presence of commonly encountered drugs, ions and markers, interference measurements with three concentrations (low, medium and high) for the lower limit, the upper limit and the mean of the clinical range were done. The results can be seen in Table 4 [*] and the respective graphs (SI figure 4.2 SI figure 4.3 SI figure 4.4 [*]). The sensor shows no to only very minor signal changes upon the introduction of a variety of interferents. The signal reduction for Indocyanine green and methylene blue can be rationalized by absorption of the 615 nm EuTc emission by both dyes. In that case, using a second reference EuTc-spot without enzyme that would then also show reduced emission, could help as reference. The interference caused by propofol might be a result of a coordinative interaction between EuTc and the propofol. One could think of a π-stacking mechanism with the aromatic ring systems of the tetracycline or the displacement of a water-molecule, similar to H_2O_2, considering the similarities in the signal response. Contrary to literature we observed no interference of either citrate or phosphate, which we attribute to our stacked hydrogel structure with the PVAc/CA protection layer. As the buffer contains Na and the sensor showed no interference towards $CaCl_2$, $MgCl_2$ or KCl, the reason for the quenching with NaCl is likely caused by the increased concentration of Cl^- by a factor of 20 in comparison to the other Cl^- containing salts. This is to be expected as Cl^- is a common quencher for a variety of luminophores and photocatalytic approaches [47]. However, as the response of the sensor towards NaCl was the same for all three tested concentrations and the response towards the analytes H_2O_2 and glucose was still sufficient, it is not to be expected that NaCl will have a major negative impact on continuous measurements within the physiological range as soon as the initial equilibrium is reached.

Table 4: List of tested interferents l: low concentration m: medium concentration h: high concentration and change in the luminescence signal intensity upon injection (+ + +: very strong luminescence increase; + +: strong luminescence increase; +: slight luminescence increase; o: no luminescence change; -: slight luminescence decrease; - -: strong luminescence decrease; - - -: very strong luminescence decrease). [*]

Interferent	Clinical range	Signal change
Acetylsalicylic acid / Aspirin	Single doses for grownups: 100 mg (1 x daily, anti-clotting treatment) Analgetic:300 – 1000 mg (multiple times daily) Migrane:1000 mg Daily maximum dose: 3000 mg.	l: o m: o h: o
Adrenaline /epinephrin	Dose for anaphylactic shocks 0.005 – 0.01 mg/kg BM, sometimes higher doses	l: o m: o to - h: o to -
4'-Acetaminophenon / Paracetamol	10-15 mg·kg^{-1} BM single dose, max. 60 mg/kg BM daily dose	l: o to - m: o to – h: o to -
ATP	In blood plasma ~ 1000 nmol·L^{-1}	l: o m: o h: o
Calcium Dichloride	Ca^{2+}: 2 mmol·L^{-1} in blood plasma 10-100 nmol·L^{-1} in mammalian cells 8.6-10.2 mg·dL^{-1} = **0.48-5.7** mmol·L^{-1}	l: o m: o h: o
Citrate	In blood plasma: 80-170 µmol·L^{-1}	l: o m: o h: o
2,6-Diisopropylphenol / Propofol	60 – 200 mg (for anesthetic induction)	l: -, then + + + m: -, then + + + h: -, then + + +
Dopamine	2-5 µg/kg BM/ min Very sick patients: 5 µg/kg BM/ min every 15 – 30 min stepwise by 5-10 µg·kg^{-1} BM/ min to 20-50 µg/kg BM/ min	l: o m: o h: o
Heparin (Li-salt from porcine intestine)	300 U/kg BM Bolus Patient 70 kg: 21000 U Patient 80 kg: 24000 U	l: o m: o h: o
Indocyanine-green		l: o m: - - - h: - - -
Lactate	In bloodplasma: low: <1.5 mmol·L^{-1} normal: 1.5-3 mmol·L^{-1} high: 3 mmol·L^{-1} During sport or stress: up to 25 mmol·L^{-1} (skeletal muscles) Long term: >5 mmol·L^{-1} leads to a mortality rate of 80%	l: o m: o h: o
Magnesium Dichloride	Mg^{2+}: 1 mmol·L^{-1} in blood plasma 10 mmol·L^{-1} bound in mammalian cells 0.5 mmol·L^{-1} free in mammalian cells	l: o m: o h: o
Mannitol/ Mannite	Grown-ups: 50-200 g Mannite (330-1.320 mL infusion) during 24 h prophylaxis acute kidney failure: 1-1,5 g·kg^{-1} for 1.5-4 h (30–50 mL·h^{-1}) intracranial pressure reduction 1.5-2 g·kg-1 during 30 min-1 h·z^{-1}. (Several times per day). intraocular pressure reduction during a glaucoma attack 1,5 g·kg^{-1}	l: o m: o h: o
Methylene blue	For treatment of Methemoglobinemia und diagnostic kidney function 1-2 mg/kg BM (50-100 mg kidney function)	l: - - m: - - h: - -
Phosphate	0.84 - 1.45 mmol·L^{-1}	l: o m: o h: o
Potassium Chloride	K^{+}: 4 mmol·L^{-1} in blood plasma 100 mmol·L^{-1} in heart **3.5-5** mmol·L^{-1} Hypokalemia: <2.5 mmol·L^{-1} Hyperkalemia: >6.5 mmol·L^{-1}	l: o m: o h: o
Sodium Chloride	Na^{+} 100-200 mmol·L^{-1} in blood plasma Cl^{-} 100 mmol·L^{-1} in blood plasma	l: - - m: - - h: - -

4.6 Human Plasma

After establishing the interference-performance of the sensor membranes, assays with human plasma as matrix were performed in the MTP setup (Figure 4.20). As expected, 10% plasma had minimal effect on the assay whereas 50% plasma caused quenching within the non-flow system. This reduction of luminescence intensity is likely caused by the presence of still active catalases, which reduce the amount of H_2O_2 in solution [48].

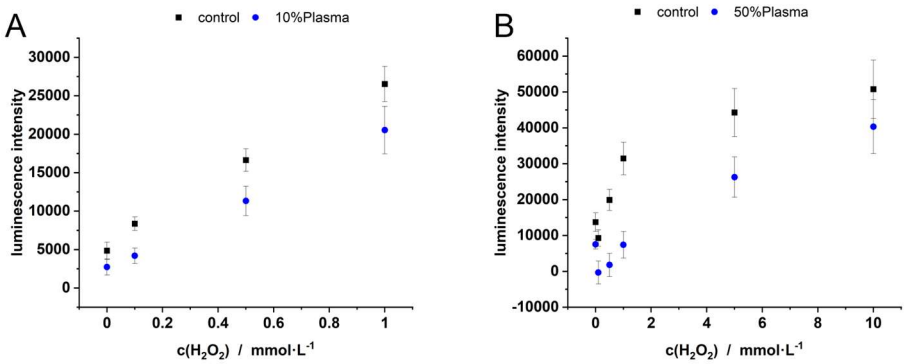

Figure 4.20: **A:** Linear range of the dose-response curves of **D4-EuTc // PVAc/CA** (50 µm wet coating thickness D4, 30 µm PVAC/CA) with Hepes buffer (pH 7.4 0.1 mol·L^{-1}) (**black**) and 10v% plasma in Hepes buffer (pH 7.4 0.1 mol·L^{-1}) (**blue**) spiked with increasing concentrations of H_2O_2 (N = 48 per curve). Foils were laser cut and stuck to the bottom of a MTP with double sided adhesive tape. Settings Biotek MTP reader λ_{exc} = 405-10 nm, λ_{em} = 615-10 nm, gain 100, bottom optic. 25°C. **B:** Normalized dose-response curves of **D4-EuTc // PVAc/CA** (50 µm wet coating thickness D4, 30 µm PVAC/CA) with Hepes buffer (pH 7.4 0.1 mol·L^{-1}) (**black**) and 50v% plasma in Hepes buffer (pH 7.4 0.1 mol·L^{-1}) (**blue**) spiked with increasing concentrations of H_2O_2 (N = 48 per curve). Biotek MTP reader λ_{exc} = 405-10 nm, λ_{em} = 615-10 nm, gain 100, bottom optic, 25 °C.

4.7 Lifetime based detection

As mentioned before, with a lifetime in the µs range, EuTc shows an extended luminescence lifetime which allows for the detection of H_2O_2, reducing the impact of interfering fluorescent species. Such lifetime-based or time-gated assays have already been developed in the past [28]. However, to this day no lifetime-based detection of EuTc in a membrane with H_2O_2 has been performed or at least published, to the author's knowledge. For this experiment a 1 cm broad D4-EuTc//PVAc/CA-membrane was set in a triangle cuvette and incubated with buffer or H_2O_2 in Hepes pH 7.4 for 15 min. Here, significant differences between the two lifetime decay curves of the initial intensity (stop condition 120 s), mean lifetime ($\langle\tau\rangle_{Hepes}$ = 22.1 ± 0.3 µs, $\langle\tau\rangle_{H2O2}$ = 51.7 ± 2.5 µs) and the length of the decay curve could be observed (Figure 4.21 A blank, B 0.1 mmol·L^{-1}). The increase of the luminescence over time with H_2O_2 is also visible in the corresponding spectra (Figure 4.21 C black curve 0 min blue curve

15 min). Due to the better spectral resolution and smaller slits used the fine structure of the $^5D_0 \rightarrow {}^7F_2$ peak is visible here even in the thin membrane. In a fiber-based setup or an MTP-integrated flow-cell these membranes could provide an interesting measurement option.

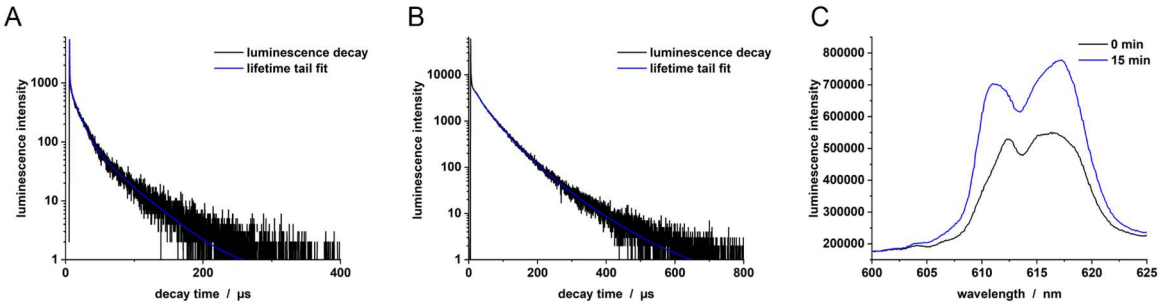

Figure 4.21: Lifetime-based detection of H_2O_2 with EuTc-D4//PVAc/CA. **A** luminescence decay curve with 0 mmol·L^{-1} H_2O_2 after 15 min incubation at 25 °C. Stop condition 120 s Fit parameters Chi^2 = 1.018 τ_1 = 0.328 ± 0.005, τ_2 = 11.230 ± 0.013, τ_3 = 44.0 ± 0.5 , ‹τ› $_{\text{amplitude-weighted}}$ = 22.1 ± 0.3 µs **B** luminescence decay curve with 0.1 mmol·L^{-1} H_2O_2 after 15 min incubation at 25 °C. Stop condition 120 s. Fit parameters Chi^2 = 0.998 τ_1 = 23.0 ± 1.1 µs, τ_2 = 49.8 ± 2.1 µs, τ_3 = 100 ± 5 µs, ‹τ› $_{\text{amplitude-weighted}}$ = 51.7 ± 2.5 µs **C** luminescence spectra of a EuTc-D4//PVAc/CA-membrane with 0.1 mmol·L^{-1} H_2O_2 directly after addition to the dry film in the cuvette and after 15 min of incubation. Edinburgh FS5: emission spectrum λ_{exc} = 405-0.75 nm, 600 nm- 625 nm, em slit: 0.75 nm, 0.1 nm steps, 1 s dwell

4.8 Conclusion and outlook

In this chapter a luminescent ratiometric hydrogel/polymer-stack based biosensor for H_2O_2 was shown. The results support the usability of the sensor membranes for both flow-cell and MTP-based measurements. Furthermore, the sensor stack shows good response in the presence of a variety of common and relevant interferents and maintains sufficient performance when using doped human plasma. While the response time in the presence of the respective analytes is almost immediate, the regeneration time will require further optimization in the future. Especially further decrease of the protection layer thickness could allow faster diffusion out of the sensor layers and thus enhance the regeneration time. Different successful strategies to reduce the initial equilibration time such as thinner protection layers and addition of buffer to the coating cocktail were demonstrated.

The chosen reference dye BPEA in its COC-layer shows an exceptional photostability, losing only 2 % of its fluorescence intensity over 4 h under continuous irradiation with a high-power mercury lamp. Both GOx and the reference BPEA in their respective layers provide excellent stability when treated with up to 12 kGy γ-radiation for sterilization. All sterilized membranes were free of bacterial or fungal growth for at least 3 months. The integration of the enzyme in a separate hydrogel stack enables a highly

adaptable and interchangeable detection platform that could also provide further customization and the broadening of the analytical scope with other H_2O_2-generating enzymes. In the flow cell setup, high background signals towards smaller wavelengths are still an issue which might be alleviated to some degree by switching the coating substrate from biaxially oriented mylar to an industrially made COC-film containing BPEA, which would reduce the number of required production steps. Alternatively, for a non-vivo application BPEA could also be integrated in COC NPs, which, showed encouraging results in liquid assays. Due to the extended lifetime of EuTc the developed EuTc-D4//PVAc/CA-membranes could also be used for luminescence lifetime detection, which eliminates several issues arising from interfering fluorescent and scattering sources.

For a better understanding of the application range further tests with more interferents, especially with commonly used opiates and heart drugs, are advisable. The integration of the presented sensor membrane technology in more advanced flow cells, microfluidic channels and shunts is feasible. Accompanied by further tweaking of the layer thickness and the superior reproducibility of industrial knife-coating devices and machines, a robust and reliable sensor platform can be envisioned in the future.

4.9 Funding

This work was partially funded by Terumo Cardiovascular.

4.10 Acknowledgements

The author thanks the blood bank team of the university hospital Regensburg, especially Marion Posset for the uncomplicated supply with human plasma and for the access to the blood irradiation device for the γ – sterilization study. Special thanks to Dr. Antonia Perju for the SEM micrographs and Christoph Bühler for the TEM micrographs. Phillip Wolf provided advice with commonly used drugs during heart surgery and the respective amounts/concentrations for which the author is very grateful.

4.11 Conflict of interest

The authors have filed a patent together with Terumo Cardiovascular Services in the subject matter and materials/design discussed in this manuscript.

4.12 References

[1] A.J. Baeumner, A. Duerkop, M. Bauer, B.V. Grotz, J.J. Galligan, L.G. Raju (WIPO Patent) WO 2024/059143 A1, 2023.

[2] Rezende F, Brandes RP, Schröder K., Detection of Hydrogen Peroxide with Fluorescent Dyes, Antioxid. Redox Signaling 6 (2018) 585–602. https://doi.org/10.1089/ars.2017.7401.

[3] J.E. Giaretta, H. Duan, F. Oveissi, S. Farajikhah, F. Dehghani, S. Naficy, Flexible Sensors for Hydrogen Peroxide Detection: A Critical Review, ACS Appl. Mater. Interfaces 14 (2022) 20491–20505. https://doi.org/10.1021/acsami.1c24727.

[4] Nóra Aányi, Teréz Barna, Tamás Emri, Márton Miskei, István Pósci, Hydrogen Peroxide Producing and Decomposing Enzymes: their Use in Biosensors and other Applications, in: J. Polaina (Ed.), Industrial enzymes: Structure, function and applications, Springer, Dordrecht, 2007, pp. 441–459.

[5] I. Sanz-Vicente, I. Rivero, L. Marcuello, M.P. Montano, S. de Marcos, J. Galbán, Portable colorimetric enzymatic disposable biosensor for histamine and simultaneous histamine/tyramine determination using a smartphone, Anal. Bioanal. Chem. 415 (2023) 1777–1786. https://doi.org/10.1007/s00216-023-04583-0.

[6] Dale E. Edmondson, Hydrogen Peroxide Produced by Mitochondrial Monoamine Oxidase Catalysis: Biological Implications, Curr. Pharm. Des. 20 (2014) 155–160. https://doi.org/10.2174/13816128113190990406.

[7] C. Kourek, M. Georgopoulou, K. Kolovou, N. Rouvali, M. Panoutsopoulou, C. Kinti, T. Soulele, D. Doubou, S. Karanikas, D. Elaiopoulos, A. Karabinis, S. Dimopoulos, Intensive Care Unit Hyperglycemia After Cardiac Surgery: Risk Factors and Clinical Outcomes, J. Cardiothorac. Vasc. Anesth. 38 (2024) 162–169. https://doi.org/10.1053/j.jvca.2023.09.022.

[8] R. Larsen, Herzchirurgie, Anästhesie und Intensivmedizin für die Fachpflege (2016) 351–370. https://doi.org/10.1007/978-3-662-50444-4_21.

[9] T.M. Powell-Wiley, P. Poirier, L.E. Burke, J.-P. Després, P. Gordon-Larsen, C.J. Lavie, S.A. Lear, C.E. Ndumele, I.J. Neeland, P. Sanders, M.-P. St-Onge, Obesity and Cardiovascular Disease: A Scientific Statement From the American Heart Association, Circulation 143 (2021) e984-e1010. https://doi.org/10.1161/CIR.0000000000000973.

[10] K.L. Ong, L.K. Stafford, S.A. McLaughlin, E.J. Boyko, S.E. Vollset, A.E. Smith, B.E. Dalton, J. Duprey, J.A. Cruz, H. Hagins, P.A. Lindstedt, A. Aali, Y.H. Abate, M.D. Abate, M. Abbasian, Z. Abbasi-Kangevari, M. Abbasi-Kangevari, S. Abd ElHafeez, R. Abd-Rabu, D.M. Abdulah, A.Y.M. Abdullah, V. Abedi, H. Abidi, R.G. Aboagye, H. Abolhassani, E. Abu-Gharbieh, A. Abu-Zaid, T.D. Adane, D.E. Adane, I.Y. Addo, O.A. Adegboye, V. Adekanmbi, A.V. Adepoju, Q.E.S. Adnani, R.F. Afolabi, G. Agarwal, Z.B. Aghdam, M. Agudelo-Botero, C.E. Aguilera Arriagada, W. Agyemang-Duah, B.O. Ahinkorah, D. Ahmad, R. Ahmad, S. Ahmad, A. Ahmad, A. Ahmadi, K. Ahmadi, A. Ahmed, A. Ahmed, L.A. Ahmed, S.A. Ahmed, M. Ajami, R.O. Akinyemi, H. Al Hamad, S.M. Al Hasan, T.M.A. AL-Ahdal, T.A. Alalwan, Z. Al-Aly, M.T. AlBataineh, J.E. Alcalde-Rabanal, S. Alemi, H. Ali, T. Alinia, S.M. Aljunid, S. Almustanyir, R.M. Al-Raddadi, N. Alvis-Guzman, F. Amare, E.K. Ameyaw, S. Amiri, G.A. Amusa, C.L. Andrei, R.M. Anjana, A. Ansar, G. Ansari, A. Ansari-Moghaddam, A.E. Anyasodor, J. Arabloo, A.Y. Aravkin, D. Areda, H. Arifin, M. Arkew, B. Armocida, J. Ärnlöv, A.A. Artamonov, J. Arulappan, R.T. Aruleba, A. Arumugam, Z. Aryan, M.T. Asemu, M. Asghari-Jafarabadi, E. Askari, D. Asmelash, T. Astell-Burt, M. Athar, S.S. Athari, M.M.W. Atout, L. Avila-Burgos, A. Awaisu, S. Azadnajafabad, D.B. B, H. Babamohamadi, M. Badar, A. Badawi, A.D. Badiye, N. Baghcheghi, N. Bagheri, S. Bagherieh, S. Bah, S. Bahadory, R. Bai, A.A. Baig, O.C. Baltatu, H.R. Baradaran, M. Barchitta, M. Bardhan, N.C. Barengo, T.W. Bärnighausen, M.T.U. Barone, F. Barone-Adesi, A. Barrow, H. Bashiri, A. Basiru, S. Basu, S. Basu, A.-M.M. Batiha, K. Batra, M.T. Bayih, N.S. Bayileyegn, A.H. Behnoush, A.B. Bekele, M.A. Belete, U.I. Belgaumi, L. Belo, D.A. Bennett, I.M. Bensenor, K. Berhe, A.Y. Berhie, S. Bhaskar, A.N. Bhat, J.S. Bhatti, B. Bikbov, F. Bilal, B.S. Bintoro, S. Bitaraf, V.R. Bitra, V. Bjegovic-Mikanovic, V. Bodolica, A. Boloor, M. Brauer, J. Brazo-Sayavera, H. Brenner, Z.A. Butt, D. Calina, L.A. Campos, I.R. Campos-Nonato, Y. Cao, C. Cao, J. Car, M. Carvalho, C.A. Castañeda-Orjuela, F. Catalá-López, E. Cerin, J. Chadwick, E.K. Chandrasekar, G.S. Chanie, J. Charan, V.K. Chattu, K. Chauhan, H.A. Cheema, E. Chekol Abebe, S. Chen, N. Cherbuin, F. Chichagi, S.B.

Chidambaram, W.C.S. Cho, S.G. Choudhari, R. Chowdhury, E.K. Chowdhury, D.-T. Chu, I.S. Chukwu, S.-C. Chung, K. Coberly, A. Columbus, D. Contreras, E. Cousin, M.H. Criqui, N. Cruz-Martins, S. Cuschieri, B. Dabo, O. Dadras, X. Dai, A.A.M. Damasceno, R. Dandona, L. Dandona, S. Das, A.M. Dascalu, N.R. Dash, M. Dashti, C.A. Dávila-Cervantes, V. de La Cruz-Góngora, G.R. Debele, K. Delpasand, F.W. Demisse, G.D. Demissie, X. Deng, E. Denova-Gutiérrez, S.V. Deo, E. Dervišević, H.D. Desai, A.T. Desale, A.M. Dessie, F. Desta, S.M.R. Dewan, S. Dey, K. Dhama, M. Dhimal, N. Diao, D. Diaz, M. Dinu, M. Diress, S. Djalalinia, L.P. Doan, D. Dongarwar, dos Santos Figueiredo, Francisco Winter, B.B. Duncan, S. Dutta, A.M. Dziedzic, H.A. Edinur, M. Ekholuenetale, T.C. Ekundayo, I.Y. Elgendy, M. Elhadi, W. El-Huneidi, O.A.A. Elmeligy, M.A. Elmonem, D. Endeshaw, H.L. Esayas, H.B. Eshetu, F. Etaee, I. Fadhil, A.F. Fagbamigbe, A. Fahim, S. Falahi, M.E.M. Faris, H. Farrokhpour, F. Farzadfar, A. Fatehizadeh, G. Fazli, X. Feng, T.Y. Ferede, F. Fischer, D. Flood, A. Forouhari, R. Foroumadi, M. Foroutan Koudehi, A.M. Gaidhane, S. Gaihre, A. Gaipov, Y. Galali, B. Ganesan, M.A. Garcia-Gordillo, R.K. Gautam, M. Gebrehiwot, K.G. Gebrekidan, T.G. Gebremeskel, L. Getacher, F. Ghadirian, S.-H. Ghamari, M. Ghasemi Nour, F. Ghassemi, M. Golechha, P. Goleij, D. Golinelli, S.V. Gopalani, H.A. Guadie, S.-Y. Guan, T.W. Gudayu, R.A. Guimarães, R.A. Guled, R. Gupta, K. Gupta, V.B. Gupta, V.K. Gupta, B. Gyawali, R. Haddadi, N.R. Hadi, T.G. Haile, R. Hajibeygi, A. Haj-Mirzaian, R. Halwani, S. Hamidi, G.J. Hankey, M.A. Hannan, S. Haque, H. Harandi, N.I. Harlianto, S.M.M. Hasan, S.S. Hasan, H. Hasani, S. Hassanipour, M.B. Hassen, J. Haubold, K. Hayat, G. Heidari, M. Heidari, K. Hessami, Y. Hiraike, R. Holla, S. Hossain, M.S. Hossain, M.-S. Hosseini, M. Hosseinzadeh, H. Hosseinzadeh, J. Huang, M.N. Huda, S. Hussain, H.-H. Huynh, B.-F. Hwang, S.E. Ibitoye, N. Ikeda, I.M. Ilic, M.D. Ilic, L.R. Inbaraj, A. Iqbal, S.M.S. Islam, R.M. Islam, N.E. Ismail, H. Iso, G. Isola, R. Itumalla, M. Iwagami, C.C.D. Iwu, I.O. Iyamu, A.N. Iyasu, L. Jacob, A. Jafarzadeh, H. Jahrami, R. Jain, C. Jaja, Z. Jamalpoor, E. Jamshidi, B. Janakiraman, K. Jayanna, S.K. Jayapal, S. Jayaram, R. Jayawardena, R. Jebai, W. Jeong, Y. Jin, M. Jokar, J.B. Jonas, N. Joseph, A. Joseph, C.E. Joshua, F. Joukar, J.J. Jozwiak, B. Kaambwa, A. Kabir, R.H. Kabthymer, V. Kadashetti, F. Kahe, R. Kalhor, H. Kandel, S.D. Karanth, I.M. Karaye, S. Karkhah, P.D. Katoto, N. Kaur, S. Kazemian, S.A. Kebede, Y.S. Khader, H. Khajuria, A. Khalaji, Khan, Moien AB, M. Khan, A. Khan, S. Khanal, M.M. Khatatbeh, A.M. Khater, S. Khateri, F. khorashadizadeh, J. Khubchandani, B.G. Kibret, M.S. Kim, R.W. Kimokoti, A. Kisa, M. Kivimäki, A.-A. Kolahi, S. Komaki, F. Kompani, H.R. Koohestani, O. Korzh, K. Kostev, N. Kothari, A. Koyanagi, K. Krishan, Y. Krishnamoorthy, B. Kuate Defo, M. Kuddus, M.A. Kuddus, R. Kumar, H. Kumar, S. Kundu, M.D. Kurniasari, A. Kuttikkattu, C. La Vecchia, T. Lallukka, B. Larijani, A.O. Larsson, K. Latief, B.K. Lawal, T.T.T. Le, T.T.B. Le, S.W.H. Lee, M. Lee, W.-C. Lee, P.H. Lee, S. Lee, S.W. Lee, S.M. Legesse, J. Lenzi, Y. Li, M.-C. Li, S.S. Lim, L.-L. Lim, X. Liu, C. Liu, C.-H. Lo, G. Lopes, S. Lorkowski, R. Lozano, G. Lucchetti, A.A. Maghazachi, P.W. Mahasha, S. Mahjoub, M.A. Mahmoud, R. Mahmoudi, M. Mahmoudimanesh, A.T. Mai, A. Majeed, P. Majma Sanaye, K.C. Makris, K. Malhotra, A.A. Malik, I. Malik, T.H. Mallhi, D.C. Malta, A.A. Mamun, B. Mansouri, H.R. Marateb, P. Mardi, S. Martini, M. Martorell, R.R. Marzo, R. Masoudi, S. Masoudi, E. Mathews, A. Maugeri, G. Mazzaglia, T. Mekonnen, M. Meshkat, T. Mestrovic, J. Miao Jonasson, T. Miazgowski, I.M. Michalek, H.N. Le Minh, G.K. Mini, J.J. Miranda, R. Mirfakhraie, E.M. Mirrakhimov, M. Mirza-Aghazadeh-Attari, A. Misganaw, K.H. Misgina, M. Mishra, B. Moazen, N.S. Mohamed, E. Mohammadi, M. Mohammadi, A. Mohammadian-Hafshejani, M. Mohammadshahi, A. Mohseni, H. Mojiri-forushani, A.H. Mokdad, S. Momtazmanesh, L. Monasta, M. Moniruzzaman, U. Mons, F. Montazeri, A. Moodi Ghalibaf, Y. Moradi, M. Moradi, M. Moradi Sarabi, N. Morovatdar, S.D. Morrison, J. Morze, E. Mossialos, E. Mostafavi, U.O. Mueller, F. Mulita, A. Mulita, E. Murillo-Zamora, K.I. Musa, J.C. Mwita, S.P. Nagaraju, M. Naghavi, F. Nainu, T.S. Nair, H.H.R. Najmuldeen, V. Nangia, S. Nargus, A.Y. Naser, H. Nassereldine, Z.S. Natto, J. Nauman, B.P. Nayak, R. Ndejjo, H. Negash, R.I. Negoi, H.T.H. Nguyen, D.H. Nguyen, P.T. Nguyen, T. van Nguyen, H.Q. Nguyen, R.K. Niazi, Y.T. Nigatu, D.N.A. Ningrum, M.A. Nizam, L.A. Nnyanzi, M. Noreen, J.J. Noubiap, O.J. Nzoputam, C.I. Nzoputam, B. Oancea, N.M. Odogwu, O.O. Odukoya, V.A. Ojha, H. Okati-Aliabad, A.P. Okekunle, O.C. Okonji, P.G. Okwute, I.I. Olufadewa, O.E. Onwujekwe, M. Ordak, A. Ortiz, U.L. Osuagwu, A. Oulhaj, M.O. Owolabi, A. Padron-Monedero, J.R. Padubidri, R. Palladino, D. Panagiotakos, S. Panda-Jonas, A. Pandey, A. Pandey, S.R. Pandi-Perumal, A.M. Pantea Stoian, S. Pardhan, T. Parekh, U. Parekh, M. Pasovic, J. Patel, J.R. Patel, U. Paudel, V.C.F. Pepito, M. Pereira, N. Perico, S. Perna, I.-R. Petcu, F.E. Petermann-Rocha, V. Podder, M.J. Postma, G. Pourali, N. Pourtaheri, E.J.S. Prates, M.M.F. Qadir, I. Qattea, P. Raee, I. Rafique, M. Rahimi, M. Rahimifard, V. Rahimi-Movaghar, M.O. Rahman, M.A. Rahman, M.H.U. Rahman, M. Rahman, M.M. Rahman, M. Rahmani, S. Rahmani, V. Rahmanian, S. Rahmawaty, N. Rahnavard, B. Rajbhandari, P. Ram, S. Ramazanu, J. Rana, N. Rancic, Ranjha, Muhammad Modassar Ali Nawaz, C.R. Rao, D. Rapaka, D.P. Rasali, S. Rashedi, V. Rashedi, A.M. Rashid, M.-M. Rashidi, Z.A. Ratan, S. Rawaf, L. Rawal, E.M.M. Redwan, G. Remuzzi, K.R.R. Rengasamy, A.M.N. Renzaho, L.F. Reyes, N. Rezaei, N. Rezaei, M. Rezaeian, H. Rezazadeh, S.M. Riahi, Y.A. Rias, M. Riaz, D. Ribeiro, M. Rodrigues, J.A.B. Rodriguez, L. Roever, P. Rohloff, G. Roshandel, A. Roustazadeh, G.M. Rwegerera, A.M.A. Saad, M.M. Saber-Ayad, S. Sabour, L. Sabzmakan, B. Saddik, E. Sadeghi, U. Saeed, S. Saeedi Moghaddam, S. Safi, S.Z. Safi, A. Saghazadeh, N. Saheb Sharif-Askari, F. Saheb Sharif-Askari, A. Sahebkar, S.S. Sahoo, H. Sahoo, K.M. Saif-Ur-Rahman, M.R. Sajid, S. Salahi, S. Salahi, M.A. Saleh, M.A. Salehi, J.A. Salomon, J. Sanabria, R.K. Sanjeev, F. Sanmarchi, M.M. Santric-Milicevic, M.A. Sarasmita, S. Sargazi, B. Sathian, T. Sathish, M. Sawhney, M.P. Schlaich, M.I. Schmidt, A. Schuermans, A.-A. Seidu, N. Senthil Kumar, S.G. Sepanlou, Y. Sethi, A. Seylani, M. Shabany, T. Shafaghat, M. Shafeghat, M. Shafie, N.S. Shah, S. Shahid, M.A. Shaikh, M. Shanawaz, M. Shannawaz, S.

Sharfaei, B.B. Shashamo, R. Shiri, A. Shittu, K.M. Shivakumar, S. Shivalli, P. Shobeiri, F. Shokri, K. Shuval, M.M. Sibhat, Silva, Luís Manuel Lopes Rodrigues, C.R. Simpson, J.A. Singh, P. Singh, S. Singh, M.S. Siraj, A.A. Skryabina, A.A.M. Sohag, H. Soleimani, S. Solikhah, M.S. Soltani-Zangbar, R. Somayaji, R.J.D. Sorensen, A.V. Starodubova, S. Sujata, M. Suleman, J. Sun, J. Sundström, R. Tabarés-Seisdedos, S.M. Tabatabaei, S.-A. Tabatabaeizadeh, M. Tabish, M. Taheri, E. Taheri, E. Taki, J.J.L. Tamuzi, K.-K. Tan, N.Y. Tat, B.T. Taye, W.A. Temesgen, M.-H. Temsah, R. Tesler, P. Thangaraju, K.R. Thankappan, R. Thapa, S. Tharwat, N. Thomas, J.H.V. Ticoalu, A. Tiyuri, M. Tonelli, M.R. Tovani-Palone, D. Trico, I. Trihandini, J.P. Tripathy, S.J. Tromans, G.M. Tsegay, A.R. Tualeka, D.G. Tufa, S. Tyrovolas, S. Ullah, E. Upadhyay, S.M. Vahabi, A.G. Vaithinathan, R. Valizadeh, K.R. van Daalen, P. Vart, S.B. Varthya, T.J. Vasankari, S. Vaziri, M.v. Verma, G.-I. Verras, D.C. Vo, B. Wagaye, Y. Waheed, Z. Wang, Y. Wang, C. Wang, F. Wang, G.T. Wassie, M.Y.W. Wei, A.H. Weldemariam, R. Westerman, N.D. Wickramasinghe, Y. Wu, R.D. Wulandari, J. Xia, H. Xiao, S. Xu, X. Xu, D.Y. Yada, L. Yang, H. Yatsuya, M. Yesiltepe, S. Yi, H.K. Yohannis, N. Yonemoto, Y. You, S.B. Zaman, N. Zamora, I. Zare, K. Zarea, A. Zarrintan, M.S. Zastrozhin, N.G. Zeru, Z.-J. Zhang, C. Zhong, J. Zhou, M. Zielińska, Y.T. Zikarg, S. Zodpey, M. Zoladl, Z. Zou, A. Zumla, Y.M.H. Zuniga, D.J. Magliano, C.J.L. Murray, S.I. Hay, T. Vos, Global, regional, and national burden of diabetes from 1990 to 2021, with projections of prevalence to 2050: a systematic analysis for the Global Burden of Disease Study 2021, Lancet 402 (2023) 203–234. https://doi.org/10.1016/S0140-6736(23)01301-6.

[11] K. Honarmand, M. Sirimaturos, E.L. Hirshberg, N.G. Bircher, M.S.D. Agus, D.L. Carpenter, C.R. Downs, E.A. Farrington, A.X. Freire, A. Grow, S.Y. Irving, J.S. Krinsley, M.J. Lanspa, M.T. Long, D. Nagpal, J.-C. Preiser, V. Srinivasan, G.E. Umpierrez, J. Jacobi, Society of Critical Care Medicine Guidelines on Glycemic Control for Critically Ill Children and Adults 2024, Crit. Care Med. (2024). https://doi.org/10.1097/CCM.0000000000006174.

[12] P.E. Marik, R. Bellomo, Stress hyperglycemia: an essential survival response!, Crit. Care 17 (2013) 305. https://doi.org/10.1186/cc12514.

[13] N. Burmistrova, O. Kolontaeva, A. Duerkop, New Nanomaterials and Luminescent Optical Sensors for Detection of Hydrogen Peroxide, Chemosensors 3 (2015) 253–273. https://doi.org/10.3390/chemosensors3040253.

[14] D.-J. Zheng, Y.-S. Yang, H.-L. Zhu, Recent progress in the development of small-molecule fluorescent probes for the detection of hydrogen peroxide, TrAC, Trends Anal. Chem. 118 (2019) 625–651. https://doi.org/10.1016/j.trac.2019.06.031.

[15] M. Moßhammer, M. Kühl, K. Koren, Possibilities and Challenges for Quantitative Optical Sensing of Hydrogen Peroxide, Chemosensors 5 (2017) 28. https://doi.org/10.3390/chemosensors5040028.

[16] J.J. Galligan, A.J. Baeumner, A. Duerkop, Recent advances and trends in optical devices and sensors for hydrogen peroxide detection, TrAC, Trends Anal. Chem. 180 (2024) 117948. https://doi.org/10.1016/j.trac.2024.117948.

[17] W. Chen, S. Cai, Q.-Q. Ren, W. Wen, Y.-D. Zhao, Recent advances in electrochemical sensing for hydrogen peroxide: a review, Analyst 137 (2012) 49–58. https://doi.org/10.1039/C1AN15738H.

[18] F. Tehrani, H. Teymourian, B. Wuerstle, J. Kavner, R. Patel, A. Furmidge, R. Aghavali, H. Hosseini-Toudeshki, C. Brown, F. Zhang, K. Mahato, Z. Li, A. Barfidokht, L. Yin, P. Warren, N. Huang, Z. Patel, P.P. Mercier, J. Wang, An integrated wearable microneedle array for the continuous monitoring of multiple biomarkers in interstitial fluid, Nat. Biomed. Eng. 6 (2022) 1214–1224. https://doi.org/10.1038/s41551-022-00887-1.

[19] M.-S. Steiner, A. Duerkop, O.S. Wolfbeis, Optical methods for sensing glucose, Chem. Soc. Rev. 40 (2011) 4805–4839. https://doi.org/10.1039/c1cs15063d.

[20] M. Trojanowicz, K. Kołacińska, Recent advances in flow injection analysis, Analyst 141 (2016) 2085–2139. https://doi.org/10.1039/C5AN02522B.

[21] M. Moßhammer, K. Koren, M. Kühl, Flow Injection Analysis with Microdialysis Probes Enable Minimally Invasive and Dynamic H2O2 Measurements, Proceedings 2 (2018). https://doi.org/10.3390/proceedings2130992.

[22] I. Ahmed, N. Jiang, X. Shao, M. Elsherif, F. Alam, A. Salih, H. Butt, A.K. Yetisen, Recent advances in optical sensors for continuous glucose monitoring, Sens. Diagn. 1 (2022) 1098–1125. https://doi.org/10.1039/D1SD00030F.

[23] O.S. Wolfbeis, Materials for fluorescence-based optical chemical sensors, J. Mater. Chem. 15 (2005) 2657. https://doi.org/10.1039/B501536G.

[24] A.Ø. Tjell, B. Jud, R. Schaller-Ammann, T. Mayr, Optical Hydrogen Peroxide Sensor for Measurements in Flow, Sens. Actuators, B (2023) 134904. https://doi.org/10.1016/j.snb.2023.134904.

[25] A.Ø. Tjell, L.-E. Meyer, B. Jud, S. Kara, T. Mayr, At-line monitoring of hydrogen peroxide released from its photocatalytic and continuous synthesis, React. Chem. Eng. 9 (2024) 777–781. https://doi.org/10.1039/D3RE00659J.

[26] S.V. Eliseeva, J.-C.G. Bünzli, Lanthanide luminescence for functional materials and bio-sciences, Chem. Soc. Rev. 39 (2010) 189–227. https://doi.org/10.1039/b905604c.

[27] L. C. Courrol, A. Monteiro, F. Silva, L. Gomes, N. Vieira, M. Gidlund, A. Figueiredo Neto, Novel fluorescent probe for low density lipoprotein, based on the enhancement of Europium emission band, Opt. Express 15 (2007) 7066–7074. https://doi.org/10.1364/OE.15.007066.

[28] W. Lei, A. Drkop, Z. Lin, M. Wu, O.S. Wolfbeis, Detection of Hydrogen Peroxide in River Water via a Microplate Luminescence Assay with Time-Resolved (?Gated?) Detection, Microchim. Acta 143 (2003) 269–274. https://doi.org/10.1007/s00604-003-0087-0.

[29] M.Y. Berezin, S. Achilefu, Fluorescence lifetime measurements and biological imaging, Chem. Rev. 110 (2010) 2641–2684. https://doi.org/10.1021/cr900343z.

[30] D. Bartoš, L. Wang, A.S. Anker, M. Rewers, O. Aalling-Frederiksen, K.M.Ø. Jensen, T.J. Sørensen, Synthesis of fluorescent polystyrene nanoparticles: a reproducible and scalable method, PeerJ Mater. Sci. 4 (2022) e22. https://doi.org/10.7717/peerj-matsci.22.

[31] L. Ding, S. Chen, W. Zhang, Y. Zhang, X. Wang, Fully Reversible Optical Sensor for Hydrogen Peroxide with Fast Response, Anal. Chem. 90 (2018) 7544–7551. https://doi.org/10.1021/acs.analchem.8b01159.

[32] M. Moßhammer, M. Strobl, M. Kühl, I. Klimant, S.M. Borisov, K. Koren, Design and Application of an Optical Sensor for Simultaneous Imaging of pH and Dissolved O2 with Low Cross-Talk, ACS Sens. 1 (2016) 681–687. https://doi.org/10.1021/acssensors.6b00071.

[33] T. Tsuchida, K. Yoda, Multi-enzyme membrane electrodes for determination of creatinine and creatine in serum, Clin. Chem. 29 (1983) 51–55. https://doi.org/10.1093/clinchem/29.1.51.

[34] M. Bauer, A. Duerkop, A.J. Baeumner, Critical review of polymer and hydrogel deposition methods for optical and electrochemical bioanalytical sensors correlated to the sensor's applicability in real samples, Anal. Bioanal. Chem. 415 (2023) 83–95. https://doi.org/10.1007/s00216-022-04363-2.

[35] I. Berlman, Handbook of florescence spectra of Aromatic Molecules, second ed., Academic Press, New York and London, 1971.

[36] X. Wang, O.S. Wolfbeis, Optical methods for sensing and imaging oxygen: materials, spectroscopies and applications, Chem. Soc. Rev. 43 (2014) 3666–3761. https://doi.org/10.1039/C4CS00039K.

[37] L. Boggioni, I. Tritto, State of the art of cyclic olefin polymers, MRS Bull. 38 (2013) 245–251. https://doi.org/10.1557/mrs.2013.53.

[38] M. Mitsui, Y. Kawano, R. Takahashi, H. Fukui, Photophysics and photostability of 9,10-bis(phenylethynyl)anthracene revealed by single-molecule spectroscopy, RSC Adv. 2 (2012) 9921. https://doi.org/10.1039/c2ra21100a.

[39] A. Viallet, J. Rouger, H. Cheradame, A. Gandini, The photooxidation of 1,4-dimethoxy-9,10-diphenyl-anthracene and the chemiluminescent decomposition of its endoperoxide, J. Photochem. 11 (1979) 129–134. https://doi.org/10.1016/0047-2670(79)80045-3.

[40] M.A. Fox, S. Olive, Photooxidation of anthracene on atmospheric particulate matter, Science 205 (1979) 582–583. https://doi.org/10.1126/science.205.4406.582.

[41] S. Schneider, M.O. Schmitt, G. Brehm, M. Reiher, P. Matousek, M. Towrie, Fluorescence kinetics of aqueous solutions of tetracycline and its complexes with Mg2+ and Ca2+, Photochem. Photobiol. Sci. (Photochemical & Photobiological Sciences) 2 (2003) 1107–1117. https://doi.org/10.1039/b304523b.

[42] D.A. Mair, E. Geiger, A.P. Pisano, J.M.J. Fréchet, F. Svec, Injection molded microfluidic chips featuring integrated interconnects, Lab Chip 6 (2006) 1346–1354. https://doi.org/10.1039/B605911B.

[43] M.I. Avadanei, D.G. Dimitriu, D.O. Dorohoi, Optical Anisotropy of Polyethylene Terephthalate Films Characterized by Spectral Means, Polymers (Basel) 16 (2024) 850. https://doi.org/10.3390/polym16060850.

[44] NIST Database, Composition of POLYSTYRENE, 2025. https://physics.nist.gov/cgi-bin/Star/compos.pl?matno=226 (accessed 7 May 2025).

[45] A. Delgado-Gonzalez, E. Garcia-Fernandez, T. Valero, M.V. Cano-Cortes, M.J. Ruedas-Rama, A. Unciti-Broceta, R.M. Sanchez-Martin, J.J. Diaz-Mochon, A. Orte, Metallofluorescent Nanoparticles for Multimodal Applications, ACS Omega 3 (2018) 144–153. https://doi.org/10.1021/acsomega.7b01984.

[46] A. Piruska, I. Nikcevic, S.H. Lee, C. Ahn, W.R. Heineman, P.A. Limbach, C.J. Seliskar, The autofluorescence of plastic materials and chips measured under laser irradiation, Lab Chip 5 (2005) 1348–1354. https://doi.org/10.1039/b508288a.

[47] C.D. Geddes, K. Apperson, J. Karolin, D.J. Birch, Chloride-sensitive fluorescent indicators, Anal. Biochem. 293 (2001) 60–66. https://doi.org/10.1006/abio.2001.5103.

[48] D. KEILIN, E.F. HARTREE, Inhibitors of Catalase Reaction, Nature 134 (1934) 933. https://doi.org/10.1038/134933b0.

4.13 Supporting Information

4.13.1 Non-measurement software

The following software instances were run on a Windows 10 Pro 64-bit-version. General data management and calculations of general nature or concerning mean values, standard deviations and error propagations were done with Excel Version 2402 (www.microsoft.com) Graph plotting, peak picking, peak analysis, particle size distribution histograms and mean particle size with standard deviation calculations were done in Origin 2024 (www.originlab.com). Graphical analysis of TEM images was performed with ImageJ version 1.53f (https://imagej.nih.gov/ij/). 3D images were designed and rendered using Blender 4.1.1 (www.blender.org). Schematics, laser cutting patterns and non-plotted graphs were designed and drawn in CorelDraw® 2023 v. 24.3.0.571 (www.coreldraw.com).

4.13.2 Instruments

Knife-coater with knife (in-house made device with adjustable film thickness in lower µm-range), K control coater K101 with a micrometer adjustable applicator “variocoater” and an aluminum vacuum bed “type B” from RK PrintCoat Instruments Ltd. (www.rkprint.com, Litlington, UK). The Coater was purchased from Coesfeld GmbH & Co KG (www.coesfeld.com, Dortmund, Germany). The applicator and the vacuum bed were purchased from Erichsen GmbH & Co. KG (www.erichsen.de).

For laser cutting sticky tape and membranes, a VLS2.30 laser cutter from Universal Laser Systems (www.ulsinc.com) with a 30 W CO_2 Laser and a 2” lens was used. In both cases, the respective substrate was placed on the template or the cutting table and fixed with masking tape if necessary.

Round sensor discs were punched out using a Berg&Schmid HK 800 toggle lever press.

All scanning electron microscopy (SEM) was performed using a Zeiss/LEO 1530, Germany with 5 - 50 kV with 5 kV by Dr. Antonia Perju. Two 6 mm circles of coated COC membranes from two different spots of the film were placed on a SEM holder. Afterwards the samples were sputtered with a gold palladium mixture. Thickness of the knife-coated polymer foil was determined with SEM images from side cuts of the materials.

All transmission electron microscopy (TEM) was performed using a 120 kV Philips cm12 microscope by Christoph Bühler. Samples were prepared by dropping 10 µL of 1.1 mg·mL^{-1} nanoparticle solutions on a carbon coated 400 mesh copper grid from Plano GmbH, Wetzlar.

Graphical analysis of the received TEM and SEM images was performed with ImageJ. For the particles. After setting the scaling of the image to the given scale bar, the color values of the TEM images were set to binary, followed by noise removal processing and, if particle silhouettes were in contact, an internal function called water shedding was processed. The Feret diameter of the particles was automatically analyzed using an image specific scaling. Size distribution and the corresponding histogram was calculated and plotted in origin. The particles mean size together with its standard deviation was calculated by a gaussian fit of the histograms.

All dynamic light scattering (DLS) of particle solutions were measured using a Zetasizer Nano ZS from Malvern Panalytical (www.malvernpanalytical.com). Particle dispersions were measured in disposable 1.5 mL semi-micro PMMA cuvettes from Brand (www.brand.de). Measurements were repeated three times, and the size distribution was calculated by the signal intensity.

MTP-based kinetic and spectral luminescence measurements were performed in a Biotek Synergy Neo2 MTP reader (www.agilent.com) with 100 µL sample per well diluted or prepared in Hepes pH 7.4. The assay was performed at 25°C and the kinetic curve was measured for 15 – 20 min. The luminescence was excited at 405 nm with a 10 nm bandwidth and measured at 615 nm with a 10 nm bandwidth for the EuTc emission and at 475 nm with a 10 nm bandwidth for the emission of the BPEA reference. Cuvette-based excitation/emission spectroscopy and lifetime detection was done in an Edinburgh Instruments FS5 spectrofluorometer.

Any shown standard deviations and variances are reported in accordance with DIN 1333.

Lifetimes were fitted with a three-component tail fit after IRF calibration.

$$R(t) = B_1 e^{\left(\frac{-t}{\tau_1}\right)} + B_2 e^{\left(\frac{-t}{\tau_2}\right)} + B_3 e^{\left(\frac{-t}{\tau_3}\right)} \quad (1)$$

Amplitude-weighted average lifetime was calculated with

$$\langle \tau \rangle = \frac{\sum B_i \tau_i^2}{\sum B_i \tau_i} \quad \textbf{2}$$

4.13.3 Irradiation experiments

Si table 4.1: γ – irradiation times. Total dose calculated with 0.553 G·s^{-1}.

No.	Date /dd.mm.yyyy	begin of exposure /hh:mm	set time /s	abort at /s	exposed for /s
1	04.02.2022	14:30	999999	999271	728
2	04.02.2022	15:30	999271	984712	14559
3	04.02.2022	19:08	984712	929759	54953
4	05.02.2022	14:40	929759	922738	7021
5	05.02.2022	13:20	922738	909601	13137
6	05.02.2022	17:10	909601	857251	52350
7	06.02.2022	07:45	857251	842388	14863
8	06.02.2022	12:15	842388	837330	5058
9	06.02.2022	14:00	837330	778143	59187
10	07.02.2022	07:00	778143	771106	7037
Total					228893
					≙12660.0 Gy

4.13.4 BPEA COC particles liquid assay

In all cases the particles showed reasonably stable signals for the duration of the kinetic measurement. With around 3 w% of doping the COC-BPEA particles show the typical decreased peak at 480 nm and the broad excimer band above 500 nm that goes well into the $^5D_0 \rightarrow {}^7F_2$ EuTc emission at 615 nm. With the 1:50 dilution (SI figure 4.1 **A**) the response of the EuTc is still relatively comparable to the control. The BPEA-COC NP batch with around 1.5 w% dye content shows the three characteristic emission peaks at 480, 510 and below 550 nm. There seems to be slight excimer formation indicated by the extended slope overlapping with the 615 nm EuTc emission. The reduction of the particle emission with increasing H_2O_2 concentration is for the 1:50 predilution (SI figure 4.1 **B**). Naturally, 2.5 w% BPEA doping also shows the excimer formation and the accompanied effects as the other particle batches with higher dye loads (SI figure 4.1 **C**).

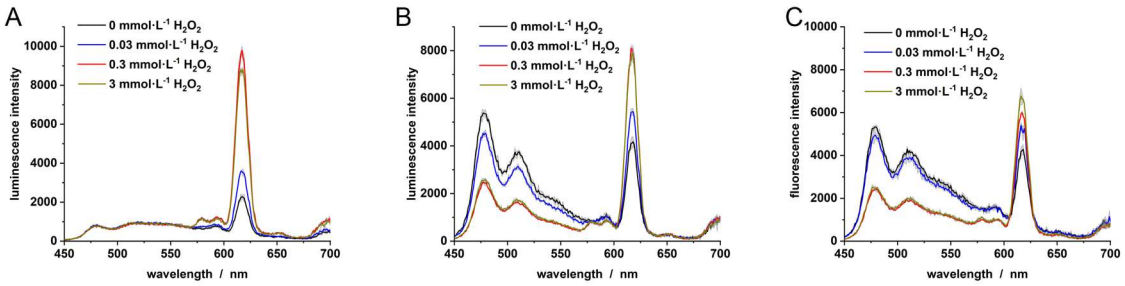

SI figure 4.1: luminescence spectra of BPEA particles prediluted 1:50 with EuTc in a liquid assay and increasing concentrations of H_2O_2. **A** 2.9 w% BPEA doping, **B** 1.5 w%, **C** 2.5 w%. Biotek MTP reader λ_{exc} = 405-10 nm, 1 nm resolution, 450-700 nm, gain 100, top optic, 25 °C., N = 3.

4.13.5 Interference time curves

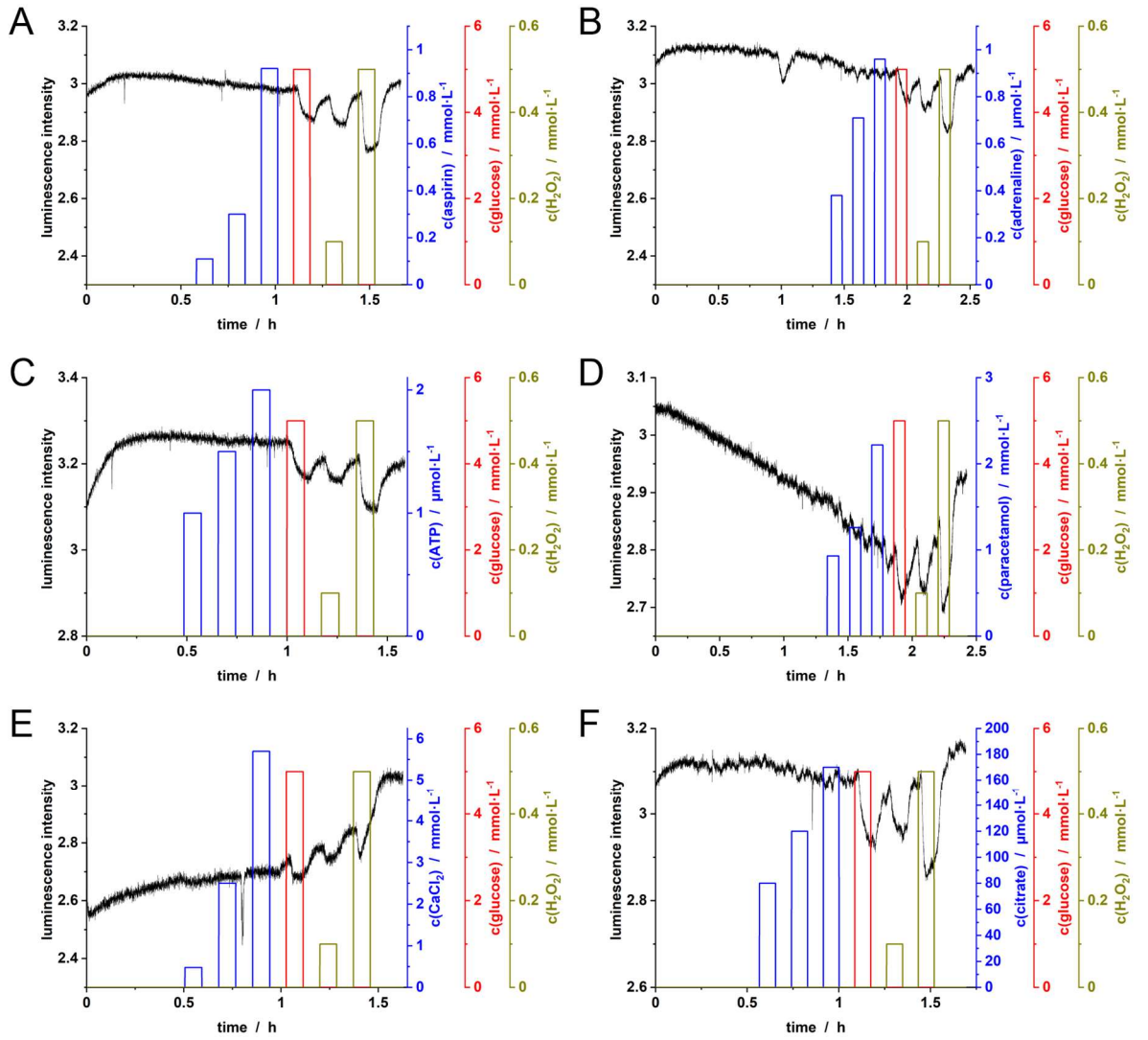

SI figure 4.2: luminescence interference time-course flow cell measurements of 12 mm **D4-EuTc//PVAc/CA**-discs with a 24 mm **D4-GOx**-ring with a 10 mm hole in the middle. The luminescence intensity is shown in **black** the injected interference concentration is given in **blue** with the corresponding color-coded y-axis, the injected concentrations of control glucose (**red**) and hydrogen peroxide (**dark yellow**) are also given with the corresponding color-coded y-axis. AB2 λ_{ex} = 405-8 nm λ_{em} = 615-8 nm, flow -16, running/injection buffer 0.1 M Hepes pH 7.4 (25 C). Interferents and settings **A**: **Acetylsalicylic acid** (ASA, aspirin), PMT voltage: 725 V; interferent injections: 5 min 0.11 mmol·L^{-1} at 0.582 h, 5 min 0.3 mmol·L^{-1} at 0.754 h, 5 min 0.92 mmol·L^{-1} at 0.925 h; glucose injection: 5 min 5 mmol·L^{-1} at 1.097 h; H_2O_2 injections: 5 min 0.1 mmol·L^{-1} at 1.269 h, 5 min 0.5 mmol·L^{-1} at 1.440 h. **B**: **Adrenaline** (epinephrin), PMT voltage: 710 V; interferent injections: 5 min 0.38 µmol·L^{-1} at 1.397 h, 5 min 0.71 µmol·L^{-1} at 1.568 h, 5 min 0.96 µmol·L^{-1} at 1.740 h; glucose injection: 5 min 5 mmol·L^{-1} at 1.911 h; H_2O_2 injections: 5 min 0.1 mmol·L^{-1} at 2.081 h, 5 min 0.5 mmol·L^{-1} at 2.255 h. **C**: **ATP**, PMT voltage: 700 V; interferent injections: 5 min 1 µmol·L^{-1} at 0.485 h, 5 min 1.5 µmol·L^{-1} at 0.656 h, 5 min 2 µmol·L^{-1} at 0.828 h; glucose injection: 5 min 5 mmol·L^{-1} at 0.999 h; H_2O_2 injections: 5 min 0.1 mmol·L^{-1} at 1.171 h, 5 min 0.5 mmol·L^{-1} at 1.345 h. **D**: **Paracetamol**, PMT voltage: 690 V; interferent injections: 5 min 0.93 mmol·L^{-1} at 1.338 h, 5 min 1.26 mmol·L^{-1} at 1.514 h, 5 min 2.22 mmol·L^{-1} at 1.685 h; glucose injection: 5 min 5 mmol·L^{-1} at 1.857 h; H_2O_2 injections: 5 min 0.1 mmol·L^{-1} at 2.807 h, 5 min 0.5 mmol·L^{-1} at 2.831 h. **E**: **$CaCl_2$**, PMT voltage: 820 V; interferent injections: 5 min 0.48 mmol·L^{-1} at 0.506 h, 5 min 2.5 mmol·L^{-1} at 0.68 h, 5 min 5.7 mmol·L^{-1} at 0.854 h; glucose injection: 5 min 5 mmol·L^{-1} at 1.027 h; H_2O_2 injections: 5 min 0.1 mmol·L^{-1} at 1.200 h, 5 min 0.5 mmol·L^{-1} at 1.372 h. **F**: **Citrate**, PMT voltage: 710 V; interferent injections: 5 min 80 µmol·L^{-1} at 0.566 h, 5 min 120 µmol·L^{-1} at 0.742 h, 5 min

170 µmol·L^{-1} at 0.915 h; glucose injection: 5 min 5 mmol·L^{-1} at 1.087 h; H_2O_2 injections: 5 min 0.1 mmol·L^{-1} at 1.260 h, 5 min 0.5 mmol·L^{-1} at 1.433 h. [*]

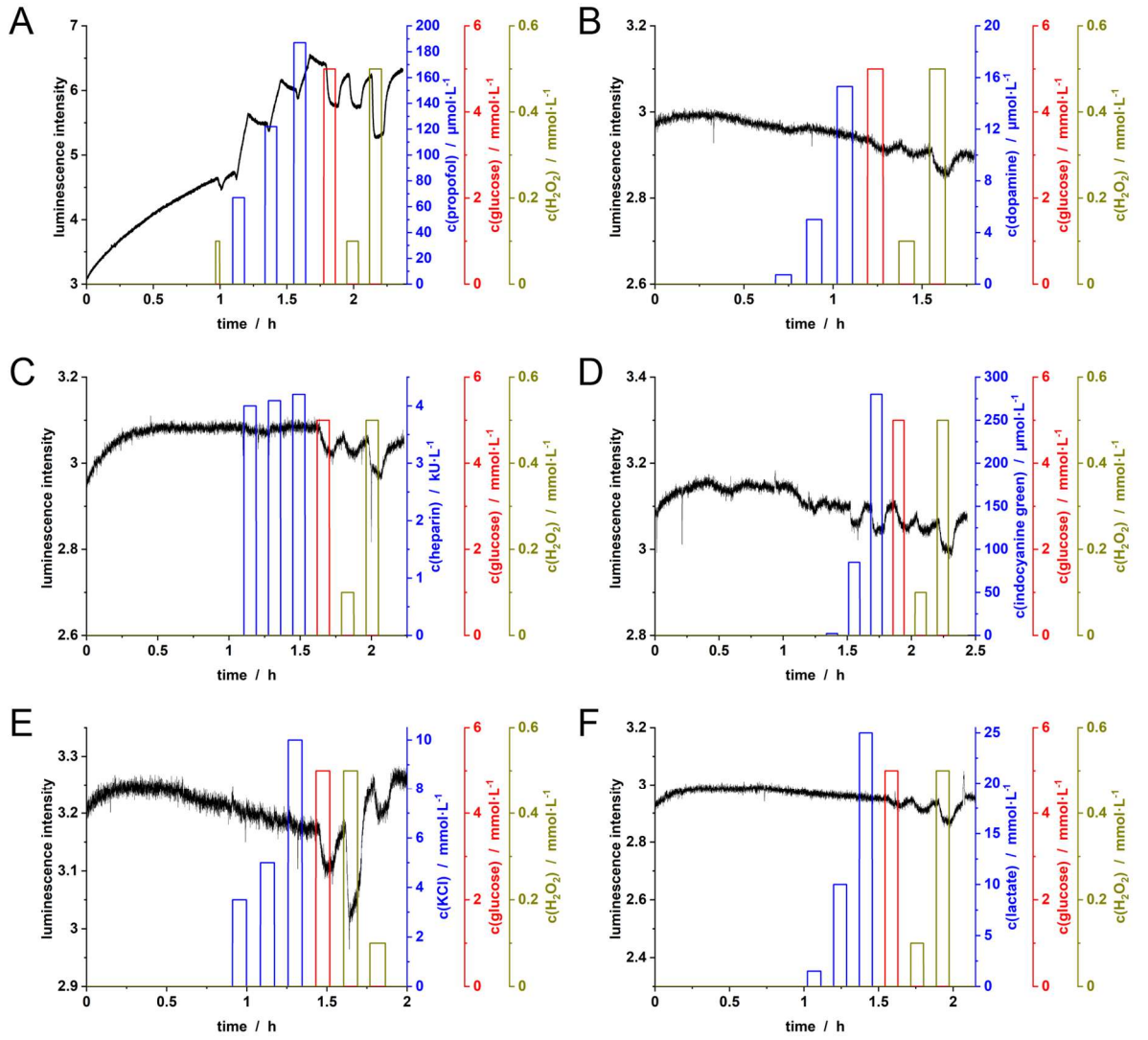

SI figure 4.**3**: luminescence interference time-course flow cell measurements of 12 mm **D4-EuTc//PVAc/CA**-discs with a 24 mm **D4-GOx**-ring with a 10 mm hole in the middle. The luminescence intensity is shown in **black** the injected interference concentration is given in **blue** with the corresponding color-coded y-axis, the injected concentrations of control glucose (**red**) and hydrogen peroxide (**dark yellow**) are also given with the corresponding color-coded y-axis. AB2 λ_{ex} = 405-8 nm λ_{em} = 615-8 nm, flow -16, running/injection buffer 0.1 M Hepes pH 7.4 (25 C). Interferents and settings **A**: **Propofol** PMT voltage: 755 V; interferent injections: 5 min 76 µmol·L^{-1} at 1.094 h, 5 min 122 µmol·L^{-1} at 1.337 h, 5 min 187 µmol·L^{-1} at 1.552 h; glucose injection: 5 min 5 mmol·L^{-1} at 1.777 h; H_2O_2 injections: 2 min 0.1 mmol·L^{-1} at 0.966 h, 5 min 0.1 mmol·L^{-1} at 1.949 h, 5 min 0.5 mmol·L^{-1} at 2.119 h. **B**: **Dopamine** PMT voltage: 705 V; interferent injections: 5 min 0.93 µmol·L^{-1} at 0.677 h, 5 min 6.23 µmol·L^{-1} at 0.851 h, 5 min 12.04 µmol·L^{-1} at 1.023 h; glucose injection: 5 min 5 mmol·L^{-1} at 1.194 h; H_2O_2 injections: 5 min 0.1 mmol·L^{-1} at 1.340 h, 5 min 0.5 mmol·L^{-1} at 1.542 h. **C**: **Heparin** PMT voltage: 705 V; interferent injections: 5 min 4 kU·L^{-1} at 1.104 h, 5 min 4.09 kU·L^{-1} at 1.276 h, 5 min 4.2 U at 1.447 h; glucose injection: 5 min 5 mmol·L^{-1} at 1.619 h; H_2O_2 injections: 5 min 0.1 mmol·L^{-1} at 1.790 h, 5 min 0.5 mmol·L^{-1} at 1.963 h. **D**: **Indocyangreen** PMT voltage700 V; interferent injections: 5 min 2.27 µmol·L^{-1} at 1.337 h, 5 min 84.93 µmol·L^{-1} at 1.510 h, 5 min 280.24 µmol·L^{-1} at 1.684 h; glucose injection: 5 min 5 mmol·L^{-1} at 1.857 h; H_2O_2 injections: 5 min 0.1 mmol·L^{-1} at 2.028 h, 5 min 0.5 mmol·L^{-1} at 2.201 h. **E**: **KCl** PMT voltage: 755 V; interferent injections: 5 min 3.5 mmol·L^{-1} at 0.911 h, 5 min 5 mmol·L^{-1} at 1.085 h, 5 min 10 mmol·L^{-1} at 1.258 h; glucose injection: 5 min 5 mmol·L^{-1} at 1.431 h; H_2O_2 injections: 5 min 0.5 mmol·L^{-1} at 1.604 h, 5 min 0.1 mmol·L^{-1} at 1.768 h. **F**: **Lactate** PMT voltage: 745 V; interferent injections: 5 min 1.5 mmol·L^{-1} at 1.022 h, 5 min 10 mmol·L^{-1} at 1.198 h, 5 min 25 mmol·L^{-1} at 1.371 h;

glucose injection: 5 min 5 mmol·L^{-1} at 1.543 h; H_2O_2 injections: 5 min 0.1 mmol·L^{-1} at 1.716 h, 5 min 0.5 mmol·L^{-1} at 1.887 h. [*]

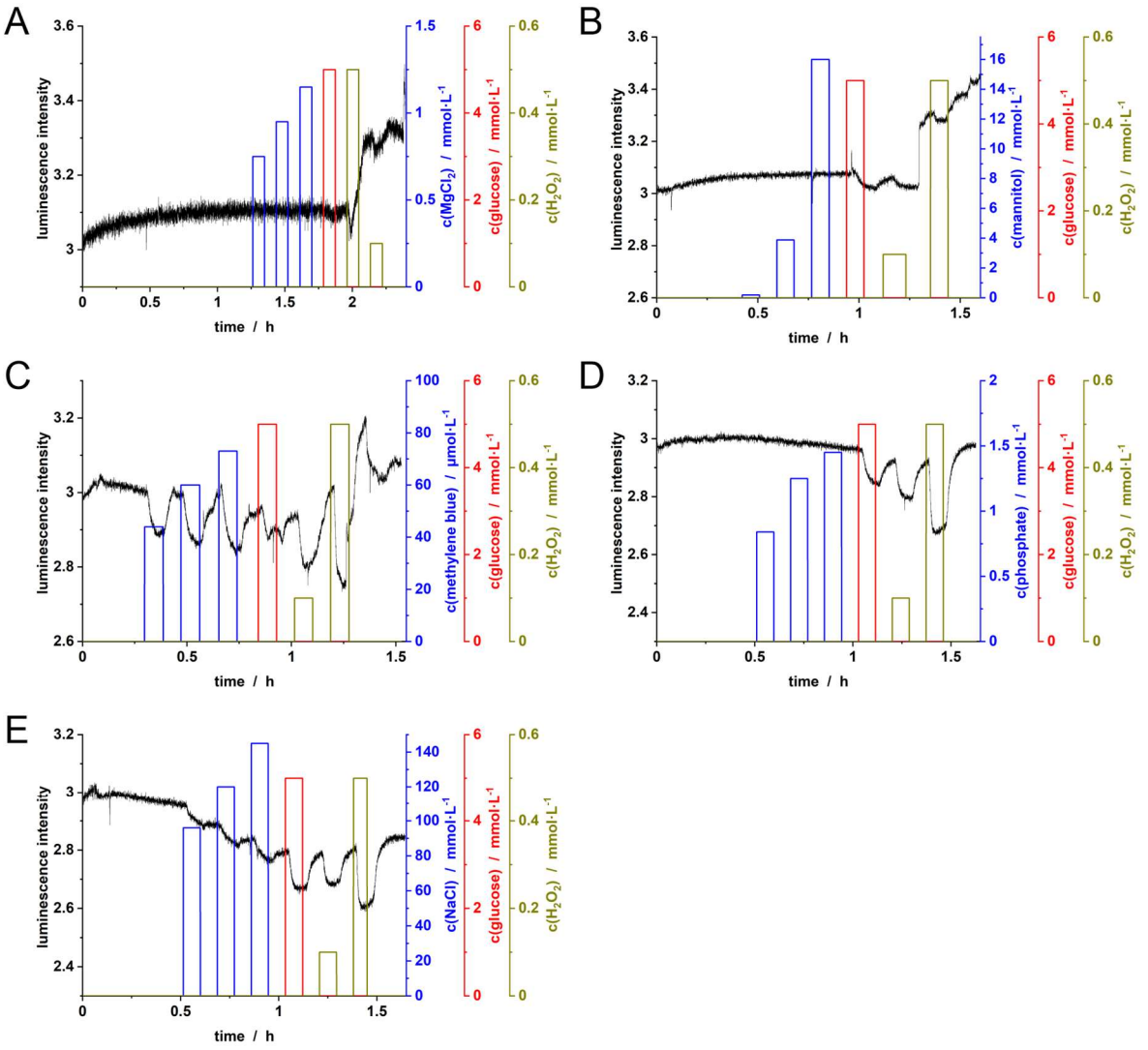

SI figure 4.**4**: Luminescence interference time-course flow cell measurements of 12 mm **D4-EuTc//PVAc/CA**-discs with a 24 mm **D4-GOx**-ring with a 10 mm hole in the middle. The luminescence intensity is shown in **black** the injected interference concentration is given in **blue** with the corresponding color-coded y-axis, the injected concentrations of control glucose (**red**) and hydrogen peroxide (**dark yellow**) are also given with the corresponding color-coded y-axis. AB2 λ_{ex} = 405-8 nm λ_{em} = 615-8 nm, flow -16, running/injection buffer 0.1 M Hepes pH 7.4 (25 C). Interferents and settings **A**: **$MgCl_2$** PMT voltage: 840 V; interferent injections: 5 min 0.75 mmol·L^{-1} at 1.262 h, 5 min 0.95 mmol·L^{-1} at 1.436 h, 5 min 1.15 mmol·L^{-1} at 1.612 h; glucose injection: 5 min 5 mmol·L^{-1} at 1.786 h; H_2O_2 injections: 5 min 0.5 mmol·L^{-1} at 1.961 h, 5 min 0.1 mmol·L^{-1} at 2.134 h. **B**: **Mannitol** PMT voltage: 720 V; interferent injections: 5 min 0.19 mmol·L^{-1} at 0.423 h, 5 min 3.88 mmol·L^{-1} at 0.594 h, 5 min 16 mmol·L^{-1} at 0.765 h; glucose injection: 5 min 5 mmol·L^{-1} at 0.938 h; H_2O_2 injections: 5 min 0.1 mmol·L^{-1} at 1.119 h, 5 min 0.5 mmol·L^{-1} at 1.353 h. **C**: **Methylene blue** PMT voltage: 705 V; interferent injections: 5 min 44 µmol·L^{-1} at 0.297 h, 5 min 60 µmol·L^{-1} at 0.471 h, 5 min 73 µmol·L^{-1} at 0.653 h; glucose injection: 5 min 5 mmol·L^{-1} at 0.841 h; H_2O_2 injections: 5 min 0.1 mmol·L^{-1} at 1.015 h, 5 min 0.5 mmol·L^{-1} at 1.188 h. **D**: **Phosphate** PMT voltage: 715 V; interferent injections: 5 min 0.84 mmol·L^{-1} at 0.510 h, 5 min 1.25 mmol·L^{-1} at 0.683 h, 5 min 1.45 mmol·L^{-1} at 0.855 h; glucose injection: 5 min 5 mmol·L^{-1} at 1.029 h; H_2O_2 injections: 5 min 0.1 mmol·L^{-1} at 1.200 h, 5 min 0.5 mmol·L^{-1} at 1.373 h. **E**: **NaCl** PMT voltage: 735 V; interferent injections: 5 min 96 mmol·L^{-1} at 0.514 h, 5 min 120 mmol·L^{-1} at 0.687 h, 5 min 145 mmol·L^{-1} at 0.860 h; glucose injection: 5 min 5 mmol·L^{-1} at 1.033 h; H_2O_2 injections: 5 min 0.1 mmol·L^{-1} at 1.208 h, 5 min 0.5 mmol·L^{-1} at 1.381 h. [*]

4.13.6 Bacterial/fungal growth

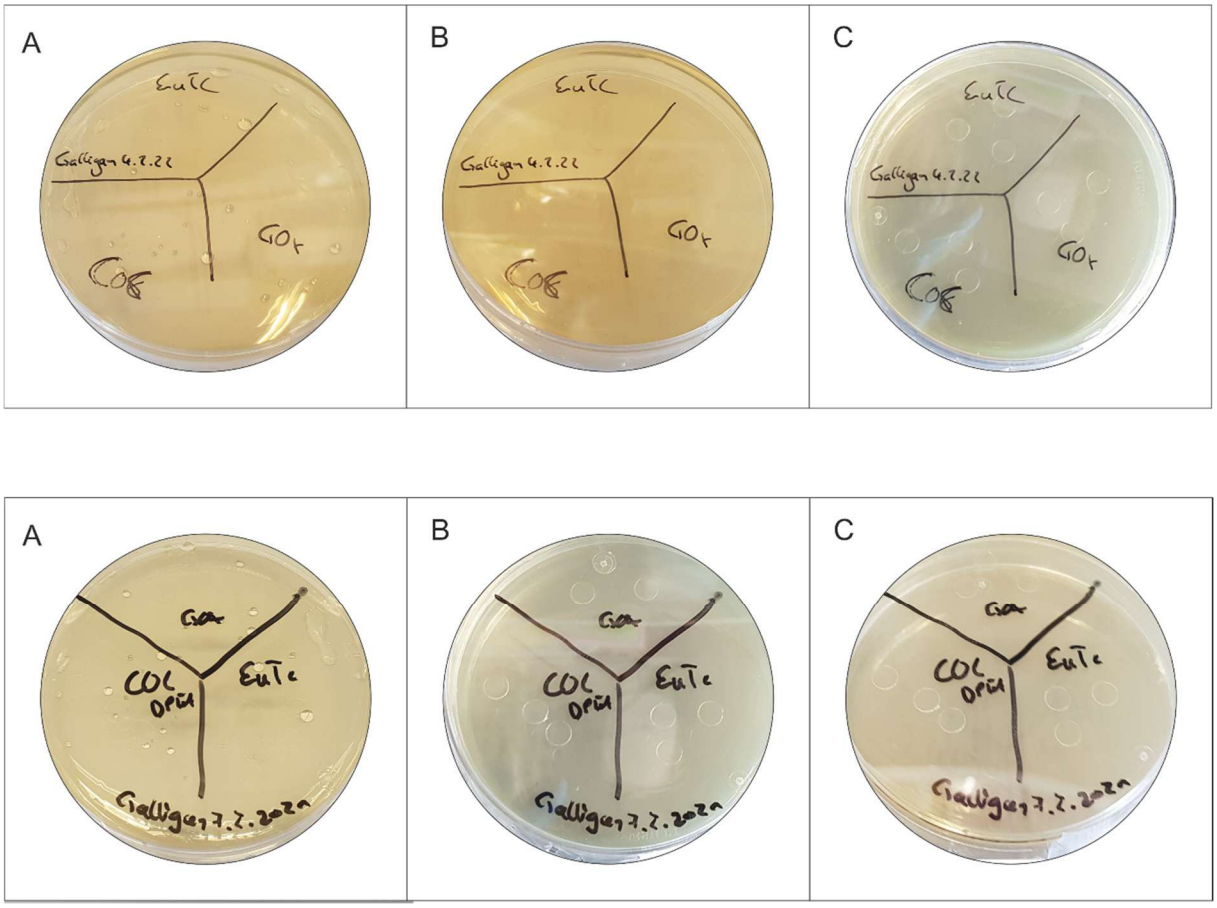

SI figure 4.5: Fungal/bacterial growth study of γ-treated membrane discs

5 Conclusion and Outlook

In the last few years, more and more versatile, better, faster, and more sensitive optical sensors and detection methods for H_2O_2 have been developed. The driving force is obvious: H_2O_2 is encountered in an abundance of applications and biochemical processes. Being the secondary analyte in a variety of enzyme-catalyzed reactions it also enables detection of important biomarkers and metabolites like glucose and lactate. However, any system currently available or published is still far from the ideal sensor. Many recently developed methods and devices strive to increase the enzyme's stability or replace the enzyme with more stable synthetic alternatives. In the context of the latter, the term enzyme mimic is often used. In many such cases, explicit mechanistic or experimental proof of the existence of a true enzyme-mimicking characteristic is lacking. In some of those cases, where there is no *real* mimicking, it is likely to be new catalysts, which are then inaccurately described as enzyme mimics. In some other cases it might be questionable whether the novel substances used are catalysts at all. Looking at the frequent and probably inaccurate use of the buzz phrase enzyme mimic in literature, a clean and fact-based (re)evaluation and (re)classification by IUPAC of the term is overdue. The last publication on this subject in pure and applied chemistry is an article by Ronald Breslow from 1990 [127] on the mimicking of transaminases and ribonucleases by attaching coenzymes to the binding part of catalysts. In the meantime, attempts are being made in literature to classify different types of mimics [128,129], but how that will be used in the future will have to be seen.

Apart from non-catalytic approaches with recognition elements such as boronate groups attached to a variety of molecules and dyes and some exceptions, the usage of classical colorimetric, chemiluminescent, and fluorescent dyes such as TMB, ABTS, Luminol, and Amplex Red™ is widespread. Considering the true plethora of probes and dyes being developed and published [29,31,32,130,131], which are *of course* superior in every way according to the authors, raises the question as to why so few sensors and detection approaches outside of cuvettes exploit this. What is unsurprising is the increased use of smartphones for easier, cheaper, and layman-friendlier detection and data evaluation. But, with the preparative effort and the need for a

complete calibration and dilution series for many of these applications, the actual simplification is modest. Furthermore, the use of smartphones is not without problems [90]. At some point standardized data reporting and benchmark experiments will have to be included in publications for true comparability and evaluation [92,94].

Semi-reversible and discontinuous approaches are focused mainly on flow injection analysis (FIA). Here, apart from some instrumental [132] and microfluidic approaches [108], novel and more efficient chemiluminescent reagents are the main innovations. The latter is hardly surprising, as the fast reaction kinetics of chemiluminescent detection [133] allows a lower cycle time. O_2-quenching of the Pt porphyrin phosphorescence following the catalytical splitting of H_2O_2 into H_2O and O_2 is currently the most advanced reversible detection approach. However, considering the susceptibility to environmental oxygen, which makes elaborate design, cell construction, and prior oxygen removal necessary, the technique is far from perfect.

In many cases, however, hydrogen peroxide is not analyzed with the discussed sensors but with commercially available assay kits. Such assay kits, as the Amplex Red™ kit, require several preparation and dilution steps. This makes any detection of H_2O_2 with such a kit a time-intensive, and therefore costly task or requires more sophisticated automation.

An approach to streamline the rapid detection of H_2O_2 and increase the sample throughput was developed and presented within the scope of this thesis in chapter 3. Here, a ready-to-use (RTU) enzymatic microtiter plate (MTP) assay with 10-acetyl-3,7-dihydroxyphenoxazine (ADHP)-loaded hydrogel membranes was developed for the fluorometric detection of H_2O_2. After screening a variety of different commercially available hydrogels and permeable polymers that do not require UV or chemical crosslinking or polymerization but only solvent evaporation, D640, a polyurethane-based hydrogel, was identified as an ideal matrix for ADHP. This commercially available hydrogel could be dissolved in a non-toxic and easy-to-handle solvent mixture of EtOH and H_2O. The possibility of storing the right amount of ADHP in such a knife-coated membrane for an assay at room temperature for at least 22 months is a true breakthrough here. In this context, the following should be particularly emphasized: No significant enhancement of the storage stability of ADHP, which is commonly stored as a stock solution in DMSO, light-protected and at – 20 °C, had been achieved since its discovery. Furthermore, the fast release mechanism of the hydrogel allowed the performance of fluorometric assays with a reaction time of only 3 min with an LOD of 0.1 µmol·L^{-1} H_2O_2. Due to the slow nonspecific oxidation of ADHP

to resorufin with HRP, previously published sensors, assay or sensing platforms using ADHP and HRP could not store the dye and the enzyme together [25].

This challenge of having to store the active dye ADHP separately from the enzyme horseradish peroxidase (HRP) was overcome by efficient separation within the MTP. To achieve this the dye was integrated in a thin hydrogel film and the enzyme was applied in small 10 - 50 nL-range drops on top of the hydrogel.

By using glycerol as a cryoprotectant, RTU MTPs were usable up to 13 weeks when stored at -20 °C without any significant loss of activity and an overall production coefficient of variance (cv) of ≈ 9 %. Without any or the wrong cryoprotectant, enzyme degradation caused the complete loss within 4 weeks. Adding nanodroplets of glucose oxidase (GOx) or lactate oxidase (LOx) enabled detection of glucose and lactate in clinically relevant ranges, with detection limits of 4 $mmol \cdot L^{-1}$ and 0.04 $mmol \cdot L^{-1}$, respectively. To compensate for membrane thickness variations, polystyrene nanoparticles (PSNPs) loaded with Cy5 dye were embedded in the hydrogel. This integration in the particles protected the reference dye from HRP-catalyzed degradation with H_2O_2 during the assay. Furthermore, with a raw material cost of only ≈ 0.08 € per well or test, the platform is already inexpensive for small-scale production.

However, the current biggest issue is the in-batch and inter-batch reproducibility of the membranes in the used research-lab-based approach. Here, more sophisticated and greater-scale industrial knife-coaters would enable both, scalable mass production and larger batch sizes. With such industrially made hydrogel films, the platform could present a powerful toolbox that could be interesting for screening and high-throughput applications in laboratories. Due to the swelling-release mechanism of the membrane, the platform could also be used to host a variety of other small probes and reagents, providing a cornerstone technology for rapid assay development based on novel and previously known probes.

Beyond single-use assays, this work also dealt with the development of continuous monitoring systems using the photoluminescent probe Europium(III) tetracycline (EuTc). In this context a dual-layer sensor membrane was developed, consisting of a D4 hydrogel layer containing the probe and a protective polyvinyl acetate/cellulose acetate (PVAc/CA) layer. As with the RTU MTP-membranes, the membranes here were coated onto a clear, biaxially oriented PET substrate. Although the protective layer effectively minimized interference from external substances and prevented leaching of the probe, it also limited diffusion and thus delayed initial equilibration. This

issue was mitigated by reducing the thickness of the protective layer through dilution and mechanical thinning, resulting in significantly faster response times. Ratiometric detection was also implemented in the continuous sensor system using 9,10-bis(phenylethynyl)anthracene (BPEA) as a reference dye. With the same excitation wavelength as EuTc, two distinctive emission bands at 475 nm and 505 nm and a slightly hidden one at approximately 530 nm with no to minimal spectral overlap, and already good photostability BPEA was chosen as the ideal reference dye candidate. In order to increase the photostability of the dye even further, BPEA was embedded in a COC-layer to prevent both photooxidation and oxygen-based fluorescence quenching. In an industrial setting, the BPEA-COC layer could be produced as thin films in larger quantities and then used as a clear and fluorescent primary coating substrate instead of the Mylar. As it stands, the reference layer is already a potent tool for keeping the reference dye protected, preventing leakage (great for in-vivo applications) and useful for proof of principle, but the additional coating step (that would not occur with an industrially made COC-BPEA coating substrate) exacerbates the reproducibility issues of layer thickness. Alternatively, BPEA-COC nanoparticles could be included directly in the probe membrane in the future. This would not only reduce the number of coating steps, but could be used to determine the layer thickness of the probe membrane as with the RTU-MTP platform. To ensure sterility without compromising enzyme activity, γ-irradiation was used as a non-thermal, non-chemical sterilization method. While BPEA and GOx in their respective layers retained excellent stability post-irradiation, EuTc in D4 exhibited a ~50% reduction in luminescence. This suggests that further optimization of irradiation parameters — such as dose, duration, and temperature — could mitigate this loss and improve overall sensor performance post sterilization. The sensor membranes demonstrated minimal interference from several common biological substances and performed well in diluted human plasma, indicating their potential for clinical applications. The long luminescence lifetime of EuTc enabled detection not only in solution but also within the membrane matrix, supporting the feasibility of continuous, in situ monitoring free from several other interfering and optical effects.

In conclusion, the thesis presents an overview of the current state of advanced optical detection possibilities for H_2O_2 and adds its own new developed findings and technologies based on versatile and useful hydrogel-based sensors and platforms. For the latter, a single-use detection platform and a reversible sensor were developed. The ratiometric RTU-platform for the rapid detection of H_2O_2 can not only be extended to quantify glucose and lactate in physiologically relevant levels, but might also house other probes, reagents and dyes in the future. The continuous sensor was optimized

with focus on the initial equilibration, a ratiometric strategy was developed, and the performance in a variety of interferents and matrices was tested. Feasibility of γ-radiation as sterilization and the possibility for lifetime-based detection could be shown.

Overall, some questions remain unanswered and will require further investigation.

For the presented MTP platform, future work should focus on:

- Scaling up to industrial-level production
- Exploring alternative cryoprotectants that are easier to dispense
- Testing additional applications and integrating new probes
- Expanding the detection range

For the reversible sensor, the following areas should be addressed:

- Incorporating dye-loaded reference particles into the probe membrane
- Reducing background signal
- Integrating the sensor into shunts and optimized flow cell systems

With these improvements the developed technologies have the potential to be very effective and powerful tools for the single-use and continuous detection of H_2O_2 and other analytes.

5.3 References

[1] R. Breslow, Enzyme mimics, Pure Appl. Chem. 62 (1990) 1859–1866. https://doi.org/10.1351/pac199062101859.

[2] E. Kuah, S. Toh, J. Yee, Q. Ma, Z. Gao, Enzyme Mimics: Advances and Applications, Chem. Eur. J. 22 (2016) 8404–8430. https://doi.org/10.1002/chem.201504394.

[3] M. Bilal, N. Khaliq, M. Ashraf, N. Hussain, Z. Baqar, J. Zdarta, T. Jesionowski, H.M.N. Iqbal, Enzyme mimic nanomaterials as nanozymes with catalytic attributes, Colloids Surf., B 221 (2023) 112950. https://doi.org/10.1016/j.colsurfb.2022.112950.

[4] D.-J. Zheng, Y.-S. Yang, H.-L. Zhu, Recent progress in the development of small-molecule fluorescent probes for the detection of hydrogen peroxide, TrAC, Trends Anal. Chem. 118 (2019) 625–651. https://doi.org/10.1016/j.trac.2019.06.031.

[5] L. Wang, X. Hou, H. Fang, X. Yang, Boronate-Based Fluorescent Probes as a Prominent Tool for H2O2 Sensing and Recognition, Curr. Med. Chem. 29 (2022) 2476–2489. https://doi.org/10.2174/0929867328666210902101642.

[6] L. Tian, H. Feng, Z. Dai, R. Zhang, Resorufin-based responsive probes for fluorescence and colorimetric analysis, J. Mater. Chem. B 9 (2021) 53–79. https://doi.org/10.1039/d0tb01628d.

[7] E. Saxon, X. Peng, Recent Advances in Hydrogen Peroxide Responsive Organoborons for Biological and Biomedical Applications, Chembiochem 23 (2022) e202100366. https://doi.org/10.1002/cbic.202100366.

[8] J. Herman, Y. Zhang, V. Castranova, S.L. Neal, Emerging technologies for optical spectral detection of reactive oxygen species, Anal. Bioanal. Chem. 410 (2018) 6079–6095. https://doi.org/10.1007/s00216-018-1233-1.

[9] G. Ross, Y. Zhao, A.J. Bosman, A. Geballa-Koukoula, H. Zhou, C.T. Elliott, M. Nielen, K. Rafferty, G. Salentijn, Best practices and current implementation of emerging smartphone-based (bio)sensors – Part 1: Data handling and ethics, TrAC, Trends Anal. Chem. 158 (2023) 116863. https://doi.org/10.1016/j.trac.2022.116863.

[10] R. Meng, Z. Yu, Q. Fu, Y. Fan, L. Fu, Z. Ding, S. Yang, Z. Cao, L. Jia, Smartphone-based colorimetric detection platform using color correction algorithms to reduce external interference, Spectrochim. Acta, Part A 316 (2024) 124350. https://doi.org/10.1016/j.saa.2024.124350.

[11] P. Cebrián, L. Pérez-Sienes, I. Sanz-Vicente, Á. López-Molinero, S. de Marcos, J. Galbán, Solving Color Reproducibility between Digital Devices: A Robust Approach of Smartphones Color Management for Chemical (Bio)Sensors, Biosensors (Basel) 12 (2022). https://doi.org/10.3390/bios12050341.

[12] M. Moßhammer, K. Koren, M. Kühl, Flow Injection Analysis with Microdialysis Probes Enable Minimally Invasive and Dynamic H2O2 Measurements, Proceedings 2 (2018). https://doi.org/10.3390/proceedings2130992.

[13] R. Gaikwad, P.R. Thangaraj, A.K. Sen, Direct and rapid measurement of hydrogen peroxide in human blood using a microfluidic device, Sci. Rep. 11 (2021) 2960. https://doi.org/10.1038/s41598-021-82623-4.

[14] L.J. Kricka, Chemiluminescent and bioluminescent techniques, Clin. Chem. (Oxford, U. K.) 37 (1991) 1472–1481. https://doi.org/10.1093/clinchem/37.9.1472.

[15] I. Sanz-Vicente, I. Rivero, L. Marcuello, M.P. Montano, S. de Marcos, J. Galbán, Portable colorimetric enzymatic disposable biosensor for histamine and simultaneous histamine/tyramine determination using a smartphone, Anal. Bioanal. Chem. 415 (2023) 1777–1786. https://doi.org/10.1007/s00216-023-04583-0.

Curriculum Vitae

Personal Data

Name	John Josef Galligan
E-Mail	john.galligan@ur.de
Date and place of birth	30.10.1995 Regensburg.

Working experience

Since 1/2025	**Research scientist,**
Fraunhofer IZI-BB	Integration of molecular probes and dyes in paper- and polymer-based detection setups. Development of microfluidic sensing layout and design. Thin-film MTP assay product development.
8/2018-3/2020	**Working Student Kit Development,**
NUMARES AG	Work in S2 und S3** Labs following BioStoffV, working with (infectious) human samples. Planning, sample preparation and execution of interference and marker experiments for NMR-diagnostics and measurements. Contact person for other departments (biostatistics, data analysis, software

development) for questions about planning and carried out measurements and experiments.

7/2016-7/2018	**Working student software development,**
NUMARES AG	Software tests and programming, database validation and managing, Production of software kits for internal testing and customers.
9/2014-8/2015	**Bundesfreiwilligendienst / Federal voluntary service**,
BRK KV Regensburg	rescue service of the Bavarian red cross

Education

Since 2/2022
University of Regensburg

Doctoral studies to obtain a doctoral degree of the natural sciences (Dr. rer. Nat.)

Thesis: *"Development of hydrogel-based ratiometric detection systems for hydrogen peroxide"* (Prof. Dr. Antje J. Baeumner)

Independent planning, coordination and implementation of the development and optimization of ratiometric luminescent hydrogel and polymer sensor and detection films; evaluation and analysis of comprehensive data; presentation of relevant research results in seminars and at conferences; supervision of practical courses, scientific bachelor and master theses,

10/2018-11/2020
University of Regensburg

M. Sc. Chemistry with focus on bioanalytical chemistry, organic chemistry and biochemistry

Master thesis: *"Raman Analysis of the Particle/Ligand interface of upconverting nanoparticles"* (Prof. Dr. Antje J. Baeumner, Dr. Thomas Hirsch)

7/2016-7/2018 *University of Regensburg*	**B. Sc. Chemistry** Bachelor thesis: *"Untersuchungen zu laser-scribed graphene Elektroden und deren Einbindung in Mikrochips"* (Prof. Dr. Antje J. Baeumner)
9/2014-8/2015 *Musikgymnasium der Regensburger Domspatzen*	**Abitur**

Voluntary Work

BRK KV Regensburg	**Wasserwacht OG Regensburg** Active member of the "Schnelle Einsatzgruppe" (SEG), Gruppenführer, Wachleiter, Motorbootführer, Dienstplaner and Fließwasserretter Since 03/2025: Stellvertretender Vorsitzender Kreiswasserwacht Regensburg sowie Ersatzdeligierter für Bezirks- und Landessitzungen
BRK KV Regensburg **COVID-Pandemic**	**COVID testing and vaccination center** Patient data management, carrying out the COVID tests and vaccination preparation.

Qualifications

Languages	**German & English** native speaker, **Latin** basics
QSM **WS 2020/2021**	Multi-day seminar for quality management

SQSS	Multi-day seminar with introduction to SQSS and statistics
Spring school GDCH	Successful participation in the “Frühjahresschule der Analytik”, division of Analytical Chemistry in the GDCh
03/2020, Aalen	

Publications, patents and presentations

A.J. Baeumner, A. Duerkop, M. Bauer, B.V. Grotz, **J.J. Galligan**, L.G. Raju (WIPO Patent) WO 2024/059143 A1, 2023.

J.J. Galligan, A.J. Baeumner, A. Duerkop, Recent advances and trends in optical devices and sensors for hydrogen peroxide detection, TrAC, Trends Anal. Chem. 180 (2024) 117948. https://doi.org/10.1016/j.trac.2024.117948.

J.J. Galligan, A.J. Baeumner, A. Duerkop, A fluorescent MTP-based Detection Platform for Hydrogen Peroxide, Glucose, and Lactate, Anal. Sens., (2025) https://doi.org/10.1002/anse.202500060

04/2024 Munich, Germany	**Analytica 2024** Poster presentation: Development of ready-to-use hydrogen peroxide, glucose and lactate sensing membranes (**J. J. Galligan**, A. Duerkop, A. J. Baeumner)
04/2023 Vienna, Austria	**ANACON 2023** Poster presentation: Development of ready-to-use hydrogen peroxide, glucose and lactate sensing membranes (**J. J. Galligan**, A. Duerkop, A. J. Baeumner)
11/2022 London, England (online)	**Sensors in Medicine** Development of Enzmye-Based Biosensors for Online Monitoring of Biomarkers with Luminescent Probe EuTc (**J. J. Galligan**, B. V. Grotz, M. Bauer, A. Duerkop, A. J. Baeumner) Awarded with 2nd poster price

Statutory declaration

I hereby declare that I have completed the dissertation presented without the impermissible help of third parties, without the use of resources other than those indicated, and that any data and concepts stemming directly or indirectly from other sources are indicated with citations to the literature.

No further persons were involved with the creation of the contents of the dissertation presented. In particular, I have not made use of the assistance of a doctoral consultant or other person in return for payment. No-one has received payment in kind either directly or indirectly for work which is associated with the content of the dissertation submitted.

The dissertation has not been submitted in the same or similar form to another examining authority, neither in Germany nor abroad.

Regensburg. 14.05.2025

John (Josef) Galligan